SCIENCE WITH BRAZILIAN DECIMETRIC ARRAY (BDA) - SOLAR PHYSICS

Hanumant S. Sawant[1], José R. Cecatto[1], Francisco C. R. Fernandes[2], and BDA Team*

[1]Divisão de Astrofísica - Instituto de Pesquisas Espaciais - INPE
Av. dos Astronautas,1758 – 12201-970, São José dos Campos - SP, Brasil
(sawant@das.inpe.br, jrc@das.inpe.br))
[2]Instituto de Pesquisa e Desenvolvimento – IP&D /UNIVAP, São José dos Campos, Brasil
(guga@univap.br)
**Participants from National and International Institutions:*
Instituto Nacional de Pesquisas Espaciais - INPE, São José dos Campos, Brasil
Departamento de Computação – DC/PUCMinas, Poços de Caldas, Brasil
Centro de Radio Astronomia e Astrofísica Mackenzie, CRAAM, Univ. Mackenzie, São Paulo, Brasil
Departamento de Engenharia e Ciência da Computação – DC/UFSCar, São Carlos, Brasil
Departamento de Física, UFSM, Santa Maria, Brasil
Indian Institute of Astrophysics – IIA, Bangalore, India
National Center of Radio Astronomy – NCRA/GMRT/TIFR, Pune, India
New Jersey Institute of Technology – NJIT, New Jersey, U.S.A.
University of California, Berkeley – UCB, Berkeley, U.S.A.

ABSTRACT

Last ten years' simultaneous X-ray and radio investigations have suggested that the acceleration of the particles or heating is occurring near photosphere where densities are around $10^9 – 10^{10}$ cm^3 this region. These densities correspond to emission in the decimetric band, and hence generated interest in the decimeter band observations. There is lack of the dedicated solar radio heliograph operating in the decimetre range. Hence development of the Brazilian Decimetric Array (BDA) operating in the frequency range has been initiated .Some of the fundamental investigations that can be carried out by BDA are: energetic transient phenomenon, coronal magnetic filed and its time evolution solar atmosphere.

INTRODUCTION

In last fifty years resolutions – frequency/energy, time and spatial - in all wavelengths have been gradually improving. Observations in radio wavelengths have significantly contributed to better understanding of the following fundamental problems in solar flares a) energy storage and its release b) site of acceleration c) acceleration/ejection and transportation of the particles. Pick et al. (1990) and Bastian et al. (1999) have reviewed these observations. What sciences can be done with radio observations was discussed well in workshop at Kyoto and is summarised in Nobeyama proceedings by (Bastian et al., 1998 a). Moreover, Bastian et al. (1999) have clearly shown the need of high spatial/time resolution solar observations in the decimeter band.

Solar flares represents explosive phenomena of the solar activity releasing energy as large as $10^{26} – 10^{32}$ ergs, either by heating of the plasma or accelerating of particles, in majority of case in chromosphere. In the impulsive phase of the flares lasting for couple of minutes particles are

accelerated up to 200 kev.

Some of these particles get trapped in the loop and travel to and from spiralling in helical orbits around the magnetic field lines generating microwave, millimetre and centimetre broad band emission by gyrosynchrotron mechanisms (Kundu, 1965). On the other hand some of these particles travel along the open magnetic field lines in the direction of the corona or in the closed magnetic field lines in the direction of the photosphere. By beam – plasma interaction these beams generate metric - decimetric type III bursts and their variants in the in meter and decimeter bands respectively. As these beams precipitates in the loop foot points of the loop they encounter high densities $\sim 10^{11}$ cm^3 and generate hard x-rays by bremsstrahlung mechanism. However it should be noted that the bursts in the decimeter band are generated mainly by the beam plasma interaction or gyrosynchrotron emission mechanisms.

Decimetric bursts have been observed since 1960 and continued in the same way up to 1970 and these observations remained to be stagnant for long time. However around 1980 for the first time Skylab observations indicated that the soft X-rays are generated in the solar atmosphere at height $\sim 2 \times 10^4$ km above the photosphere where densities are around $10^9 - 10^{10}$ cm^3 (Moore et al., 1980). Recently investigations of X-ray by Ohyama and Shibata (1998) suggested that flare processes are occurring around the above mentioned densities. Thus, suggesting that the acceleration of the particles or heating is occurring near this region. These densities correspond to emission in the decimetric band, and hence regenerated interest in the decimeter band observations.

Existing theories in 1960 – 1970 suggested that decimetric emission generated due to beam plasma interaction by the beams traveling towards the photosphere would be strongly absorbed by the strong free – free emission, which is proportional to electron density.

However, following theoretical development in the estimations of the free – free emission suggested possibility of decimetric observations above 1000 MHz:

a) Solar atmosphere is not homogeneous and contains small-scale (length) high electron density irregularities due to fibrous nature of the magnetic field. Thus estimations of the free – free emission taking into consideration irregularities in densities will substantially reduce optical depth and hence allowing escape of decimetric emission along the density gradients.
b) In addition to that if emissions were to be due to plasma emission mechanisms which are preferentially at second harmonic optical depth is further reduced by factor of 16 in comparison to that of the fundamental (Dulk, 1985).

Stähli and Benz (1987) showed that second harmonic emissions can be observed up to or more than 6000 MHz considering presence of small scale – 100km – irregularities. However fundamental emission at 1000 MHz will be strongly absorbed.

Several high resolutions decimetric spectroscopes were put into regular operation in the last decade in the frequency range of (1000- 8000) MHz. They have been summarised by (Krüger and Voight, 1999) and recently by Sawant et al 2001.There exists a very few observations of sources sizes of the decimetre type III like bursts observed by Very Large Array (VLA) (Gopalswamy et al., 1995). Observations of the active regions at few spot frequencies in the decimeter range and that of the long duration bursts are obtained by using Ovens Valley Radio heliograph and VLA. However, there is lack of radio heliograph above 1000 MHz with high time and spatial resolutions mostly dedicated for solar observations. Brazilian Decimetric Array (BDA) will fill this gap for solar observations. However BDA can be also used for non-solar observations during solar minima and at night times.

In addition to that BDA will complement observations made by Nobeyama Radio heliograph at 17 and 35 GHz (Nishio et al., 1995) Radioheliograph of Nancy (Nancy,1993), operating at 169, 327 and 408 MHz and Gauribidnur Radioheligraph operating at 40 – 150 MHz (Subramanian et al., 1994,

Ramesh et al., 1999). Combined observations of the active regions will lead to continuous investigations of the time evolution of the active regions at various altitudes. This is essential for predications of the solar activities and understanding of the fundamental problems in solar physics. Presently monitoring of the active region can be done by using is Radiolheliographs of Japan, (Nobeyama), Siberia (Siberian Solar radio Telescope- SSRT-), India (Gauribidnur), France (Nancy) and that of the USA (OVRO). However there is lack of the continuity of the observations between Europe and USA. BDA will have common time between Europe and USA thus will fill this gap, in addition to that BDA will be unique solar radioheliograph in Southern Hemisphere as shown in Figure 1.

Fig. 1 – Distributions of solar radio telescope in the world showing the importance of the position of the location of the BDA for continuos solar activity monitoring

Thus continuos monitoring of the solar activities and time evolution of active regions will lead to better prediction capabilities of the occurrences of the solar disturbances such as solar flares and coronal mass ejection - CMEs. These are the major causes of the disturbances in terrestrial magnetic fields and phenomena associated with that.

Some of the fundamental investigations that can be carried out by BDA are given below:

- ENERGETIC TRANSIENTS PHENOMENAS

Objectives

(i) Release of energy,
(ii) Acceleration of electrons and or heating of plasma.
(iii) Transportation of particles
(iv) Creation and destabilization of large scale structures

- MAGENTIC FIELDS IN THE CORONA

Objectives

(i) Estimation of coronal magnetic fields and
(ii) Time evolution of magnetic fields.

- SOLAR ATMOSPHERE

Objectives

(i) Coronal heating
(ii) Quite solar atmospheric structures.

LOCATION OF ACCELERATION REGION

In the last decade high resolutions observations in the almost all wavelengths and interpretations have lead to suggestion that the flare energy is released in space-time fragmented way (Valhos, 1994, Brown and Gary, 1994, Anastasiadis and Valhos, 1994). Also various fine structures including that of the type IIIdm bursts are observed during and prior to the impulsive phase of the flares. High resolution spectroscopic observations and their statistical investigations of the decimetric IIIdm bursts above 1000 MHz shows that their total duration is ~300 ms ,frequency range is of about 300 MHz and in majority cases, 80%, with the positive drift rates (Melendez et al., 1999). However there are a few fixed frequency observations of their positions. (Gopalswamy et al., 1995; Aschwanden et al., 1999). Bi-directional decimeric type IIIdm bursts are well related with the position of acceleration region (Aschwanden et al., 1995; Melendez et al., 1999). Thus simultaneous decimetric spectroscopic and imaging observations of BSS and BDA respectively will be able to map trajectories of the up - down going beams as shown in the Figure 2. This will enable more precise determination of the location of the acceleration region independent of density models and processes and nature of the liberation of energy to flares.

CRHOMOSPHERIC EVAPORATION

Chromospheric evaporation has been revised by Anttonucci et al. (1984 and references therein). Before the beginning flare – in pre flare phase – the turbulence in plasma of the active region begins and either it accelerate the particles and/or heat them. Hot plasma starts rising; this proccess is known as chromospheric evaporation (Sturrock et al., 1973) – though this is not a proper nomenclature. This can be inferred by broadening and blue shifts of the lines of Ca XIX and Fe XXV as observed in soft X-ray.

Until now the process of the chromospheric evaporation is investigated by observations of the soft X-ray and in H-alpha assuming the process of chromospheric evaporation is the process for transport of hot plasma. Aschwanden and Benz (1995) for the first time suggested that chromospheric evaporation could be investigated by radio observations in decimetric wavelengths generated by the beam of the electrons going down in loop and crossing up-going evaporation front. However this is just a speculation and need to be confirmed by simultaneous spectral and positional observations in radio, soft X-ray lines and H–alpha observations.

In reality, what is happening is that as hot and dense plasma rises up it creates a discontinuity in temperature and density, in the loop. Beam of the electrons moving towards the foot point of the loop interacts with this slowly upward moving “shock front” where a optical thickness is reduced due to its

temperature dependence ($\sim n \times T^{-3/2}$) allowing to escape high frequency radio emission. As the beam travels further it encounters high densities and lower temperature which increases opacity and radio emission is absorbed. Thus as the shock front moves up cut off in high frequency will be slowly decreased allowing to infer the velocity of shock front. Eventually the shock front will come in equilibrium with loop plasma and enabling escape of radio emission as shown in Figure 2. Investigations of the relative start timings of soft/hard x ray, beginning of the high frequency cut off and its drift rate will enable to determine exact parameters of the chromospheric evaporation. Simultaneous x-ray, BSS and BDA spectral/positional observations for the first time will allow to estimate the parameters of the chromospheric evaporation more accurately.

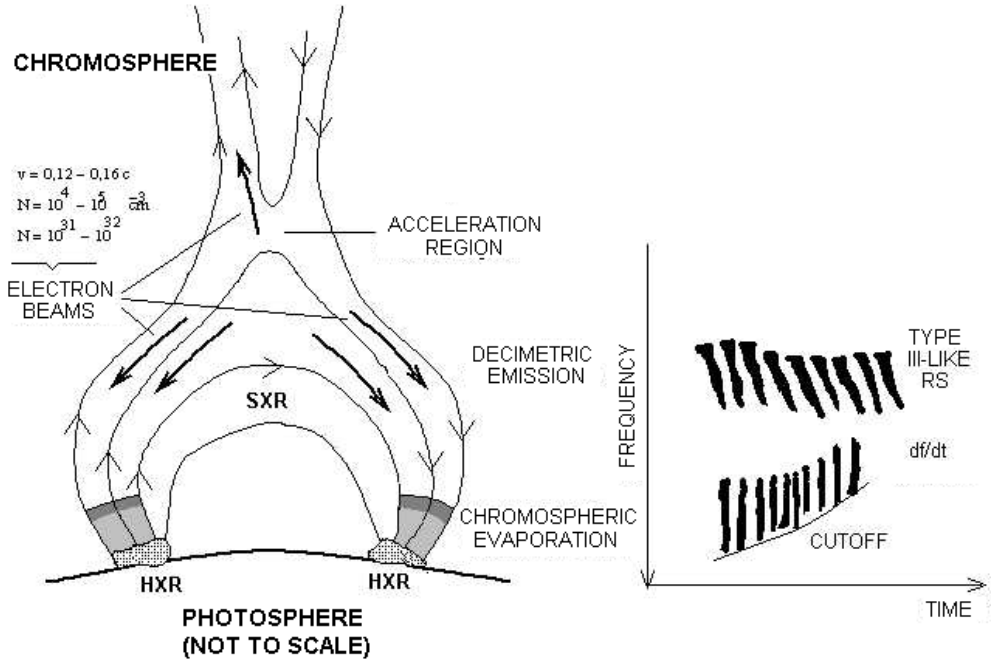

Fig. 2 - Left: A schematic representing flare scenario including the region of the acceleration, up/down going electron beams, chromospheric evaporation front and locations of soft/hard x ray sources, right: decimetric type III bursts - RS - with negative drift rates, high drift rate decimetric emission associated with chromospheric evaporation process, showing high frequency cut off and its slow drift rate associated with motion of chromospheric evaporation shock front.

MAGNETIC FIELDS OF THE ACTIVE REGIONS, ERUPTIVE COMPONENT AND CMEs

Active regions

Active regions are composed of various magnetic loops containing hot plasma. The new magnetic flux also emerges in the vicinity of these regions. They are observed routinely in optical wavelengths. However details of the magnetic field of the active regions are inferred by observations in EUV and soft X-rays.

Magnetic field at photospheric level is determined by the line observations in optical and infrared wavelengths and by extrapolation magnetic fields in the chromosphere and corona are determined. These extrapolations are sensitive to exact determination of magnetic fields at

photospheric levels which are difficult to estimate. Moreover they have been extrapolated under the assumptions that magnetic fields are force free. This assumption is a questionable. Thus determination of the magnetic fields by this technique is ambiguous.

Low frequency radio emissions of the active regions say up to 5.0 GHz is due to optically thick gyro-resonance up to 4^{th} harmonic of electron cyclotron frequency given by following equation: $f_{MHz} = 2.8 \times x\ H_{gauss.}$ This emission is originated in a thin layer of constant magnetic field. Thus high spatial resolutions observations obtained by BDA of the active regions in the frequency range of 1–5 GHz will enable to determine the magnetic fields in the corona and their height dependence.

Burst Component

In the majority of cases for the weak microwave bursts, peak frequency is around 5.0 GHz and spectra below this frequency is optically thick (Guidice and Castelli, 1975). Peak frequency is dependent upon the intensity of magnetic field and the angle of source with line of sight. Thus BDA observations of the well observed weak microwave bursts having peak around 5.0 GHz will determine the magnetic field and its time variation in the sources region.

It is well known that radio method is the unique method to determine correct magnetic fields in the corona.

Coronal Mass ejection

One of the main objectives of the on going space weather programs is to use the spectral data for the prediction of the space weather forecast by using spectral tomographic techniques (Rosa et al., 2000 and references cited therein). Coronal mass ejection has been turned out to be central point for investigations of space weather prediction and solar-terrestrial relationship programs.

Followings are the main advantages of the detection of the CMEs in radio: normally in observations of optical coronograph solar disk is occulted and hence only CMEs propagating perpendicular to line of sight are observed. However in radio observations there is no occultation of solar disk and hence CMEs on the disk can also be observed by radioheliographs. In radio CMEs can be detected in its initial stage and they can be properly identified with optical structures on the disk. Whereas in optics, they can be identified with filaments and emerging loops only after their occurrences. Sensitivity of radio observations enables to detect free – free and non-thermal emissions emitted by CMEs. Thus, increasing the chances of detentions of CMEs**.** Bastin and Gary (1997) have concluded that thermal emission of CMEs due bremssstrahlung can be detected by instruments like BDA type. Hence improving the capability of space weather prediction program by detection of CMEs in its initial phase. Program to investigate association of CMEs with active regions, current sheets and coronal holes is in progress (Srivastava et al., 1998).

Majority of solar flares occurs in an active region associated with the sunspot. However CMEs can occur outside the active regions some of them at high latitudes extending up to the poles. Thus, occupying very large volumes in comparisons to flares. It makes it difficult to distinctly separate these two eruptive events. Flares are associated with activation of eruption of filaments associated with active regions. However this is also one of the signatures of the association with CMEs. CMEs have been found to be associated with bright chromospheric patches, which can be easily detected by BDA.

CME consists of dense nucleus, surrounded by halo and front loop. Piston – shock structure normally assumed does not explain above mentioned three components of the CMEs. In many cases it has been noted that velocity of the front loop is not a super Alfvenic. Then how a CME is expanding? Kinetic energy transported by CME is normally more than a thermal energy and hence a force responsible of expansion should be of magnetic origin. However, it is not known what type of magnetic instability is responsible for activation of CME.

During the solar maxima period (2000 - 2004) it will be difficult to understand the mechanisms of launch of CME due to super positions of the multiple events and interaction among the various active regions. Thus observations in decaying phase of the solar activity will lead to a better understanding of these mechanisms, when there will be a few active regions on the disk. During the solar maxima one can observe energetic CMEs and their radio images can be investigated with simultaneous observations of X-ray obtained by SOHO and LASCO on board of SOHO satellite.

During the decay phase when BDA will be in full operation, as mentioned above, the mechanisms of launch will be better understood. Spectral data of the active regions collected during earlier years and their investigations related to the activities associated with CMEs will able to improve the capabilities of prediction of flares and CMEs. This would consequently enhance the capabilities of space the weather program, one of the main objectives of the development of BDA.

SOLAR ATMOSPHERE

Coronal heating

There exist many models for interpretations of the heating of the solar corona. BDA observations will improve the work done on the following models: resonance wave heating (Ofman et al., 1998) and an old model of Parker (1988) of “nano-flares”.

BDA observations of the some of the well observed active regions collected over a couple of years will enable determination of the magnetic fields, temperatures and their height variations in the loop which will provide the estimates of the rate of the energy deposit as a function of time and position. These are the inputs necessary for the resonant wave heating model.

In case of nano-flare model two inputs are required. One, number of small events occurring simultaneously over a wide band say from dm- mm – submm –etc. wave length. Such observations presently are not available.

The other input is energy contents of the smallest energy release events (Gary et al., 1997; Goplaswamy et al., 1995; Benz and Krucker, 1999). From our knowledge so far only one observation of tiny flares with high sensitivity has been reported by Gopalswamy et al (1994), which showed that energy content of this tiny flare was well above the canonical nano-flare value of 10^{23} ergs. The BDA can contribute. BDA can observe spatially resolved nano-flares to the limit of its sensitive in the decimer range, which will enable to determine the energy contents of the nano-flare more precisely.

Background solar radiation

Background radiation is known to be originated in a weak magnetic field by free- free emission in solar atmosphere. Microwave radiation is generated under LTE condition and in that case Plank function is valid and for microwave Rayleigh-Jeans’s approximation is valid In that case observed intensity is directly proportional to the kinetic temperature of the of the emitting sources for optically thick sources. Optical depth is proportional to $n\ T^{-3/2}$. Thus by varying frequency one can obtain the status, temperature – height, of the middle chromosphere, chromospheric and coronal transition region.

Coronal holes

Coronal holes are of interest. The efforts will be made by using long duration integrated observations to find the difference between the emissions from surroundings and from coronal holes. It is known that high velocity streams are coming from coronal holes if we can infer the position of coronal holes it will help us in identifying the possible path of propagation of these energetic streams in the solar wind. This can be used as warning to satellites, since it is known that energetic particles

may damage satellite payloads.

EMISSION MECHANISMS OF FINE STRUCTURES

Since 1970 various catalogues of the fine structures in the decimeter wavebands are published (Tarstrom and Philip, 1971; Allaart et al., 1990; Isliker and Benz, 1994). Recently, with improved instrument capabilities more and more fine structures are discovered. Many plasma instabilities leading to various mechanisms are suggested for the interpretations of these fine structures. For the first time BDA can provide positions and dimensions of these fine structures this will improve capabilities of the interpretation of these fine structures by the theoretical plasma physics community.

CORONAL ROTATION

Solar rotation has been estimated by various techniques (for recent reviews see Howard (1996). However, a clear understanding of the rotation of solar interior and exterior is still lacking. Coronal rotation is even less understood and investigated. Recently, Vats et al. (1998a) demonstrated a radio method for the determination of solar coronal rotation. Vats et al. (2001) have pursued this further by investigating the flux values at eleven radio frequencies, almost simultaneously observed, ten of which are closely spaced between 275-1755 MHz and the last one is 2.8 GHz. Using solar electron density models these emissions appear to originate in the solar corona in the heights ranging from 6 to 15 X 10^4 km above the solar photosphere.

The later study indicates that the sidereal rotation period at the highest frequency (2800 MHz), which originates from the lower corona around 6×10^4 km, is ~ 24.1 days. The sidereal rotation period decreases with height to ~ 23.7 days at lower frequency (405 MHz), which originates from ~13×10^4 km. This indicates that the solar corona rotates slightly faster at higher height. Kane et al. (2001) using the same time series however using different techniques for spectral analysis found many periodicities in the radio flux measurements.

All these investigations use the disc integrated solar flux and hence can not provide any information about the differential coronal rotation in latitude. Thus the radio maps of solar emission in the decimetric band will be useful for determining the differential rotation in latitude and will remove the ambiguities present in the above investigations which could due to the changes at various latitudes in the solar atmosphere. Moreover, Vats et al. (1998b) found that fractal dimension of solar radio emissions are minimum around 3 GHz and increases on either side of the frequencies. Hence high spatial resolution observations of the active regions of obtained by BDA in the frequency range of (1-5) GHz are more appropriate for investigations of coronal rotation and its latitude dependence.

SIMULTANEOUS X RAYS – RADIO OBSERVATIONS

X-ray observations give emission measure and the temperature diagnostics, and in the case of hard X-ray it suggests the presence of nonthermal particles. Radio observations give us similar information. However they complement each other and hence simultaneous X-ray-radio observations give more complete parameters of the sources rather than either can do alone. Efforts are made since 1970 to compare positional data in radio and in X-ray band (Kane et al., Kundu et al., 1986; Sawant et al., 1984).

YOHOKOH satellite operated until 2000 and provided for the first time the images of solar hard X-ray flares. HESSI satellite was launched in 2002 (Ramaty and Mandzhavidze, 2000) for the first time it provides high resolution X-ray images over a wide energy band ranging from 10 KeV – 10

MeV with spatial resolutions in the range of 1 to 20 arc sec. and time resolutions are of the order of 10 ms for intense flares.

HESSI will be followed by SOLAR – B (Shimizu et al., 1999) Japanese satellite to be launched in 2004. Thus there will be always some X-ray satellite providing good opportunities to compare BDA images, in all its phases of development (2007 – 2010), with hard X-ray images. Good positional accuracy, high spatial and temporal resolutions multi-wavelength (X-ray-radio) observations of BDA in the decimetre wave band, where possibly energy to flares is released, for flares will lead to better understanding of the above mentioned various fundamental problems in solar physics.

SPACE WEATHER FORECASTING

It was earlier thought that the solar fleas are responsible for the solar terrestrial relationships and perturbations caused on the earth such as failure of radio communication, of power grids and in oil/gas pipelines. In the space, various communication satellites have been damaged by excess of X-ray and energetic particle doses. Risk is further increasing with astronauts in space shuttles. Such missions will be increasing in near future to carry out various experiments on International Space Station. However recently it has become clear that CMEs also play important roles in the above mentioned problems.

Schmahl and Kundu (1997) have shown that multi-frequency observation will lead to better prediction capabilities of sunspot and irradiance .Since long it is known that 10.7-cm flux is correleted to sunspot number and area, the emission in Ly–alpha, Mg II and EUV and the total solar irradiance, which are the indicators of the solar activity. Here BDA observations at 10.7 cm can contribute significantly. Thus, forecasting community, ionospheric physicists, aeronomists. and space weather prediction community can download processed data at 2.7 GHz for their ready use. Such observations are presently lacking.

BDA has been designed to investigate fundamental problems in solar physics. Consequently it will improve the forecasting capability of solar terrestrial relationships and space weather programs. Just sitting below the galactic center it will significantly contribute to galactic extragalaxctic studies mentioned in next sections.

- BDA will provide radio images of the full Sun. It will provide the details of the active regions such as, its spectra magnetic field and its time evolution, simultaneously over selected frequencies, including 2.8 GHz, which are presently not available.
- Detection of CMEs its size, location and associated phenomena in it initial phases.

Thus observations over the period of the full solar cycle will be extremely valuable, providing groundwork necessary to make space weather forecasting a quantitative science and not just a statistical exercise.

REFERENCES

Allaart, M. A. F., van Nieuwkoop, J., Slottje, C., Sondaar, L. H., *Solar Phys.*, 130, 183, 1990.
Anastasiadias, A., Vlahos, L. *ApJ*,. 428: 819-826, 1994.
Antonucci, E., Gabriel, A. H., Dennis, B. R., *Ap.J.*, 287, 917, 1984.
Aschwanden, M. J., Benz, A. O., *ApJ.*, 438, 997, 1995.
Aschwanden, M. J., Benz, A. O., Dennis, B. R., Schwartz, R. A., *Ap.J.*, 455, 347, 1995.
Barrs, J. W. M., Van Der Bruggs, J. F., Cassae, J. L., *Proc. IEEE*, 61, 1258, 1973.
Bastian, T. S, Gary, D. E., *J. Geophys. Res.*, 102, 14031, 1997.
Bastian T., Gopalswamy N., Shibasaki K. Solar Physics with Radio Observations, Proc. of the

Nobeyama Symposium, Kyyoto, Japan, Oct.27 – 30, 1998a.
Bastian, T. S., Benz, A. O., Gary, D. E., *Ann. Rer. Astron. Astrophys.*, 36,131, 1998b.
Benz, A. O., Krucker, S., *Astron. Astrop.*, 341, 286, 1999.

Brown, J. C., Gray, N. *Space Science Reviews*, 68:93-96, 1994.
Bruggmann, G., Benz, A. O., Magun, A., Stehling, W., *Astron. Astrophys.*, 240, 506, 1990.
Christiansen W. N., Högbom J. A., Radiotelescopes, Cambridge Univ. Press, UK, 1987.
Clark, B. G., *Astron. Ap.*, 89, 377, 1980.
Cornwell, T. J., Wilkinson, P. N., *Mon. Not. Roy. Astron. Soc.*, 196, 1067, 1981.
Cornwell, T. J. in Synthesis Imaging, Proc. NRAO Summer School, Ed. Perley, R. A., Schwab, F. R., and Briddle, A. H., p109, 1986.
Cornwell T., "Very Long Baseline Interferometry and the VLBA", *ASP Conference Series* Vol. 82, Ed. J. A. Zensus, P. J. Diamond, P.J. Napier, 1995.
Dulk, G. A., *Ann. Rev. Astron. Astrophys.*, 23, 169, 1985.
Erickson, W. C., Mahoney, M. J., Erb, K., *ApJ. Supp. Series*, 50, 403, 1982.
Gabriel, E., *Solar Phys.*, 175, 207, 1997.
Gary D. E, *JGR*, 102(A7), 14.031–14.040, 1997.
Gary, D. E., Hartl, M., Shimizu, T., *ApJ.*, 477, 958, 1997.
Gonzalez, W. D., Tsuratni, B. T., McIntosh, P. J., Gonzalez, A. L. C., *JGR Lett*, 23, 2577, 1996.
Gopalswamy, N., Payne, T. E. W., Schmahl, E. J., Kundu, M. R. et al., *ApJ.*, 437, 522, 1994.
Gopalswamy, N., Raulin, J. P., Kundu, M. R., Nitta, N., Len, J. R., Herrman, R., Zarro, D., Kosugi, T., *ApJ.*, 455, 715, 1995.
Guidice, D. A., Castelli, J. P, *Sol. Phys.*, 44, 155, 1975.
Hanaoka, Y. K. et al., Nobeyama Radio Observatory Report N# 360, 35-44, 1994.
Howard, R. F., *Annual. Review Astron.Astrphysics*, 34, 75, 1996.
Isliker, H., Benz, A. O., *Astron. Astrophys. Suppl. Series*, 104, 145, 1994.
Kane R. P., Vats, H. O., Sawant H. S., *Solar Phys.*, 2001.
Kosugi, T., Makishma, K., Murakami, T., Sako, T., *Solar Phys.*, 136, 17, 1991.
Krüger, A., Voigt, W., *Solar Phys.*, 161, 393, 1995.
Kundu, M. R., Solar radio astronomy, John Wiley & Sons, Inc. 1965.
Kundu, M. R., Gergely, T. E., Kane, S. R., Sawant, H. S., *Sol. Phys.*, 103, 153, 1986.
Lüdke, E., Sawant, H. S., Subramanian, K. R., Fernandes, F. C. R., Cecatto, J. R., Rosa, R. R., Sobral, J. H. A., Swarup, G., Gonzalez, W. D., Moron, C. E., Mucheroni, M. L., *Geofisica Internacional*, 39 (1), 147-152, 2000.
Nobeyama Radio Observatory Report n. 360. Hanaoka, Y. et al., *Proc. Kofu Symposium*, 1994.
Melendez, J. L., Sawant H. S., Fernandes, F. C. R., Benz, A. O., *Solar Phys.*, 187, 77, 1999.
Moore, R. et al., in Sturrock, P. A., Ed. Solar flares: a monograph from Skylab Solar Workshop II. Report of NASA Skylab Workshop on Solar flares. Boulder, Colorado University Press, p341, 1980.
Moron, C. E., Ribeiro, J. R. P., Saito, J. H., Sawant, H. S., Rosa, R. R., *Proc. SBAC-PAD'2000* 12th Sysmposium on Computer Architecture and High Performance Computing, pg. 313, 2000.
Mucheroni, M. L., Saito, J.H., Machado, G., Rosa, R. R., Sawant, H. S., Moron, C. E., *Proc. SBAC-PAD'2000* 12th Sysmposium on Computer Architecture and High Performance Computing, pg 175, 2000.
Nancy Radio Heliograph group, *Adv. Spac. Res.*, 13(9), 411, 1993.
Nakajima, H. et al., Nobeyama Radio Observatory Report, 339, 1993.
Nakajima, H. et al., *Proc. IEEE*, 82(5), 1994.

Narayan, R., Nityananda R., *Ann. Rev. Astron. Ap.*, 24, 127, 1986.
Nishio, M. Nakajima, H., Enome, S., Kofu Symposium, 19, 1995.
Nityananda, R.; Narayan, T., *Astron. Astrophy.*, 3, 319, 1982.
Ofman, L., Klimchuk, J. A., Davila, J. M., *ApJ.*, 493, 474, 1998.
Ohyama M., Shibata K., *ApJ*., 499, 934
Parker, E. N., *ApJ.*, 330, 474, 1988.
Pearson T. J., Readhead A. C. S., *Ann. Rev. Astron. Astrophys.*, 22, 97, 1984.
Pick, M., Klein, K. L., Trottet, G., *Ap.J. Suppl. Series*, 73, 165, 1990.
Ramaty R., Mandzhavida, N., Astronomical Society of the Pacific Conference Series Vol. 206, 2000.
Ramesh, R., Subramanian, K.R., Sundrajan, M.S. and Sastry, Ch.V., *Solar Phys.*, 181, 444, 1998.
Rhode, U., Digital Phase Lockeded Loops, Theory and Applications, John Wiley & sons, 1982.
Rosa, R. R., Sawant, H. S., Valdivia, J. A., Sharma, A. S., *Adv. Space Res.*, 20, 233, 1997.
Rosa, R. R., Sawant. H. S., Ramos, F. M., Sharma, S., Valdivia, J. A., *Geofisica International*, 1999.
Rosa, R. R., Sawant, H. S., Costa Junior, R. A., Ramos, F. M., Cecatto, J. R., Fernandes, F. C. R., Mascarenhas, N., Saito, J. H., Moron, C. E., Mucheroni, M. L., *ASP Conference Series*, 206, 293-296, 2000.
Sawant, H. S., Gergely, T. E., Kundu, M. R., *Sol. Phys.*, 77, 249, 1982.
Sawant, H. S., Kane, S. R., Kundu, M. R. and Gergely, T. E., In Proc. of STIP Symp., Maynooth, Ireland, 113-118, 1984.
Sawant, H. S., Lattari, C. J. B., Benz, A. O., Dennis, B. R. *Sol. Phys*., 130, 57, 1990.
Sawant, H. S., Sobral, J. H. A, Fernandes, F. C. R., Cecatto, J. R., Day, W. R. G., Neri, J. A. C. F., Alonso, E. M. B., Moraes, A., Adv. Space Res., 17(4/5), 385, 1996.
Sawant, H. S., Subramanian, K. R., Faria, C. Fernandes, F. C. R., Sobral, J. H. A., Cecatto, J. R., Rosa, R. R., Vats, H. O., J. A. C. F. Neri, E. M. B. Alonso, F. P. V. Mesquita, V. A. Portezani, A. R. F. Martinon, Solar Phys., 167, 2001.
Sawant, H. S., Subramanian, K. R., Lüdke, E., Sobral, J. H. A., Swarup, G., Fernandes, F. C. R., Rosa, R. R., Gonzalez, W. D., Cecatto, J. R., *Adv. Space Res.*, 25(9), 1809, 2000b.
Schmahl, E., Kundu, M. R., in Synoptic Solar Physics, ASP Conf. Ser., 1997.
Schwab F., *Proc. S.P.I.E.*, 231, 18, 1980.
Schwartz, U. J., *Astronomy and Astrophysics*, 65, 345, 1978.
Smith, D. F., Benz, A. O., *Solar Phys.*, 131, 351, 1991.
Srivastava, N., Gonzalez, W. D., Sawant, H. S., *Adv. Space Res.*, 20(12), 2355, 1998.
Stähli, M., Benz, A. O., *Astron. Astrophys.*, 175, 271, 1987.
Sturrock, P.A., Symp. on high energy phenomena in the Sun (NASA/GSFC Rept), 1973.
Subramanian, K.R., Sundarajan, M.S., Ramesh, R. and Sastry, Ch.V., STEP GBSC news, 4, 13, 1994.
Shumizu, T. et al., NRO Report No. 479, 459, 1999.
Swarup, G., *Indian Journal of Radio and Space Physics*, 43, 31, 1990.
Tarnstrom G. L., Philip, K. W. Scientifi Report, Univ. Alaska, UAG R-217, 1971.
Thompson, A. R., Clark, B. C., Wade, C. M., Napier, P. J., *ApJ. Supp. Series*, 44, 151, 1980.
Vats et al., *Solar Phys.*, 181, 351, 1998a.
Vats et al., *Earth, Moon and Planets*, 76, 141, 1998b.
Vats, H. O., Cecatto, J. R., Mehta, M., Sawant, H. S., Neri, J. A. C. F., *ApJ. Lett.*, 2001.
VanVleck, J. K., Middleton, D., *Proc. IEEE*, 54(1), 2, 1966.
Vlahos, L. *Space Science Reviews*, 68, 39-50, 1994.
Weinreb, S., MIT Technical Report, 412, 1963.
Zirin, H., Baumert, B. M., Hurford, G. J., *ApJ.*, 370, 779, 1991.

HARDWARE & SOFTWARE FOR BDA TRACKING SYSTEM

Abhay Joshi and Abhijit Dandekar

Intelligent Motion Technology Pvt.Ltd. S. No 100/5 Ambegaon Pune 411046
Phone no: +91 20 24318121, 24318122 Fax +91 20 24318124
(abhay@intelmotion.com; abhijit@intelmotion.com)

ABSTRACT

Second phase of the BDA will consists of array of 26 antennas located 300m away from control room. Intelligent Motion Technology Pvt. Ltd., Pune (India) is providing a control system & software for this system. In the abstract we have described main features of Hardware and Software used in the system. Antennas are controlled through motion controllers connected to Ethernet port. System Control software will be operated from a computer stationed in control room. Computer communicates to each motion controller through Ethernet port.

HARDWARE DETAILS

Block diagram

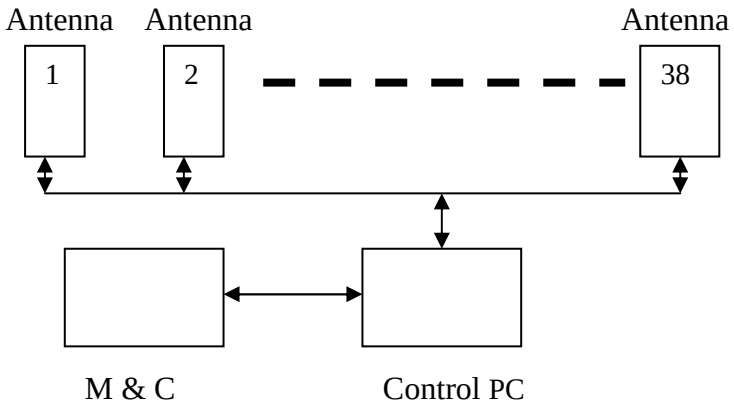

Fig. 1 - Overall Block Diagram.

This is overall block diagram of the BDA. In this each antenna is connected to the control PC via Ethernet. Each antenna is equipped with two drives for driving AZ & EL axes & one motion controller to control the axis motion. Control room PC will get the look-up table from Monitor & control PC. This lookup table contains the data of AZ angle & elevation angle with respect to time. The Servo software will download the required AZ & EL position to selected antennas respect to time.

Block Diagram of single Antenna

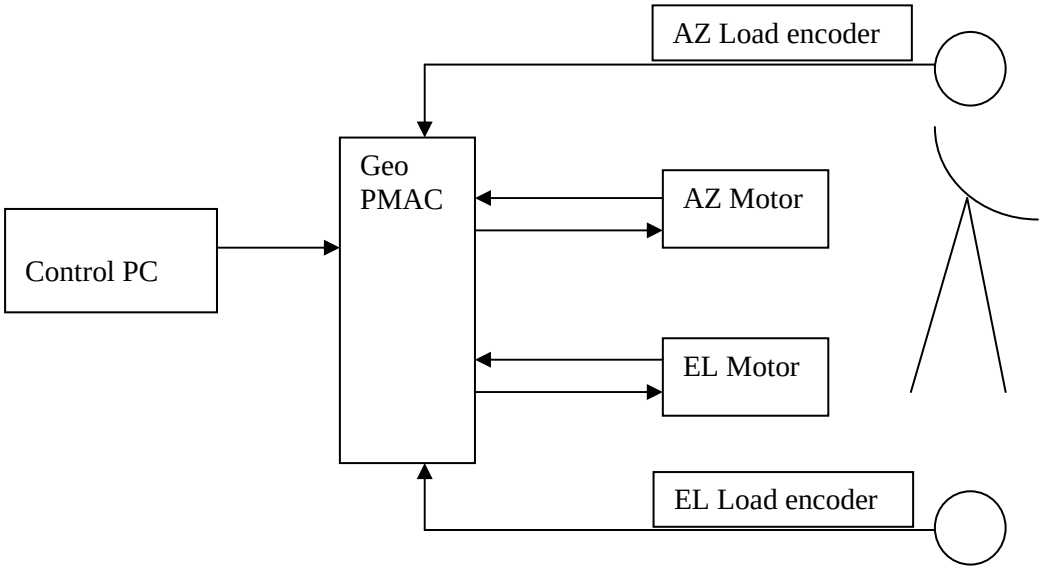

Fig. 2 - Block Diagram of single antenna.

Block Diagram Description

One antenna consists of AZ & EL axis. This AZ & EL axis are driven by Servo motors through gear box. To drive the motors we need two amplifiers or drives. To control the motion of AZ & EL as per time we require some motion controller. We have selected GEO PMAC. This GEO PMAC is powerful state of art controller with built in drives. GEO PMAC communicates with Control PC on Ethernet Port.

We need two load encoders to close the position loop. These load encoders are to read the exact position of the antenna. There are two ways to read the antenna position; one method is to use encoder or resolver on the motor. So with some gear ratio calculations we can display the antenna angle. In this method we cannot get exact reading because of exact gear ratio value & backlash in the gears. To avoid this load encoders are used.

During first phase installation & in last two years we have learnt many things. We have changed the hardware in second phase so that all these problems can be avoided.

Difference between First Phase & second Phase

In the first phase only 5 antennas were controller. The communication bus was RS 485. Looking at the third phase distances & communication speed of RS485 we decided to change the communication from RS485 to Ethernet. In third phase the longest antenna can be communicated via Ethernet by fiber optic link.

In the first phase antenna pointing was done with the help of resolver on the motor & load encoder reading was compared with the required reading. In second phase, position loop is closed on the load encoder.

The load encoder resolution in first phase was sufficient for 4 min of arc accuracy. Now this

resolution of load encoder is increased by 4 times to get better accuracy.

The brake operation feedback was not considered in the first phase. In second phase we have used brake protection modules. Because of this antenna will stop in case of brake failure.

Features of GEO PMAC Controller

Geo PAMC is a very powerful standalone controller with built in drives. It can communicate on USB & Ethernet.With dual feedback facility we can close the loop on load encoder.Built-in safety features like following error, max acceleration limit, max velocity limit, Software limits, Hardware limits etc. can be used to protect antenna structure. Different types of feedbacks can be interfaced like

Resolver, Absolute encoder, incremental etc. Very fast Servo update rate; which is 440 micro seconds. Linear, circular interpolation can be done. Maximum 256 motion programs can be saved. It has 36 bit position range.

Geo PMAC is available with single axis & two axis models. We have selected the two axis module which is working on 230 v AC 50 Hz supply. With this we can eliminate two drives from the first phase configuration.

Built-in drive is protected with following faults.

- Over voltage
- Under Voltage
- Over Current
- Over temperature
- Short Circuit

Features of Baldor Make Servo Motors

To drive AZ & EL axis we have selected Baldor make servo motor. Motor specifications are same as motors used in phase 1. Baldor Model No is BSM 90 C 2250DA. Following are the specifications.

- Stall Torque - 5.2 Nm
- Cont. current - 2.51 amps
- Peak Torque - 15.6 Nm
- Peak Current - 6.3 amp
- Rated Speed - 1200 rpm
- Feedback - Resolver
- Brake Supply - 24 V
- Thermal Protection - @155^{o} C
- Oil Seal - At shaft end.

Some protections are provided. In first phase it was found that water is going inside from the shaft. So oil seal is added in this model. Motor is with built-in thermal contact. This contact will operate when motor temperature goes beyond 155^{o} C. This thermal contact is connected to controller input.

Homing

This Homing term is related to referencing of the antenna. When we power on the antenna we have to move the antenna to home position. This home position is nothing but the known degree of AZ & EL. This can be done with the help of limit switch. This Homing operation is required as we have

used the incremental encoder on the load side. During initial setting of the antenna we have to find out the AZ & EL degrees at this limit switch. After each power on we have to do the homing operation. Once this is done the reference position is valid up-to next power fail. This can be avoided either by using absolute encoders or by UPS power supply to controller.

Error Budget

As we are closing the loop on load encoder we will get the required accuracy. But it is necessary to find out the error budget. We have used 10000 PPR load encoder.

For one rotation of AZ/EL will get 10000 X 4 counts in controller

360^{o} = 40000 counts

1 encoder count = 360/40000

= 0.009 deg (0.54 min of arc)

Tuning of the system will decide the accuracy of the system. In worst case even if we do the tuning of the system in 4 counts, the accuracy will be 0.036 deg (2 min of arc).

Protections

Protections from Lightning: In first phase heavy lightning is observed at BDA site. Due to this some component failure is observed. This failure is mainly of 232 to 485 converter. Another component which is mounted outside is load encoder. This can be failed during lightning. To avoid this failure we have suggested lightning arresters / surge protection devices. We have suggested model no. D-UFB-V24/S-DSUB 9/SB-B

Brake protection: As discussed in previous sections we have observed the brake failure in first phase. To avoid this we have developed Brake protection module. This module will sense the current flowing through brake. Because of any reason if current stops flowing, immediately antenna will stop its motion indicating brake failure message on GUI.

SOFTWARE DETAILS

Tracking software is loaded on Servo control PC. This software will communicate with all selected antenna. This software is developed under VB.net platform. once we open the software the Main screen will get open.

On Main Screen five command buttons are provides.
Communication: this command button will open screen for communication.
Homing: This command button will open screen for homing.
Manual: This command button will open screen for manual mode movement.
Tracking: This command button will open screen for tracking mode.
Settings: This command button will open screen for settings.

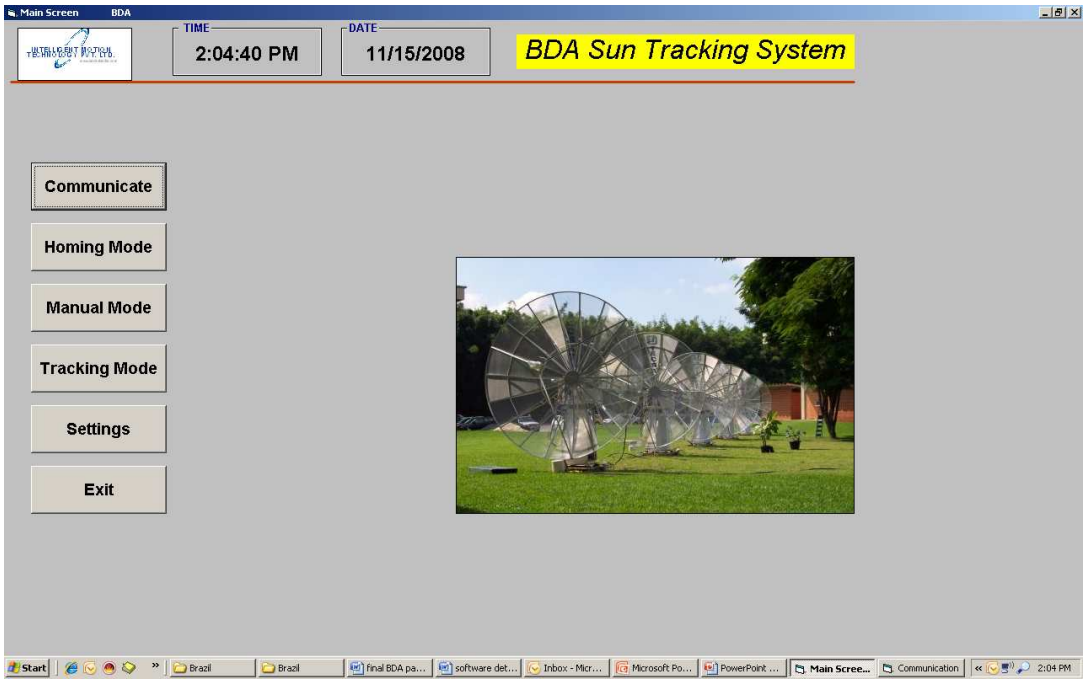

Communication Screen

Following figure shows the proposed version of the program screen.

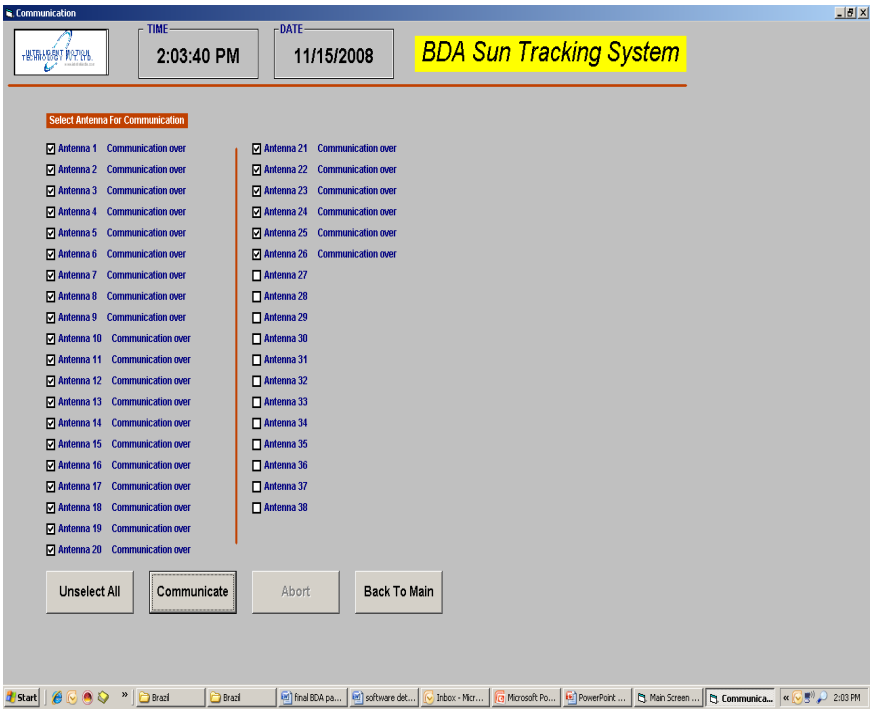

This screen will show the entire forty antennas. User can select the required antenna for

communication. If we select 5 antennas for communication; all other screens will show 5 selected antennas only. This software will work for 1 antenna to 38 antennas.

After selecting antenna user have to click on *Communicate* button to start communication. After successful communication *Back to main* button will appear on screen. User can abort the communication with *Abort* button.

Homing screen

Following figure shows the proposed version of the screen which is used for homing for all the selected antennas.

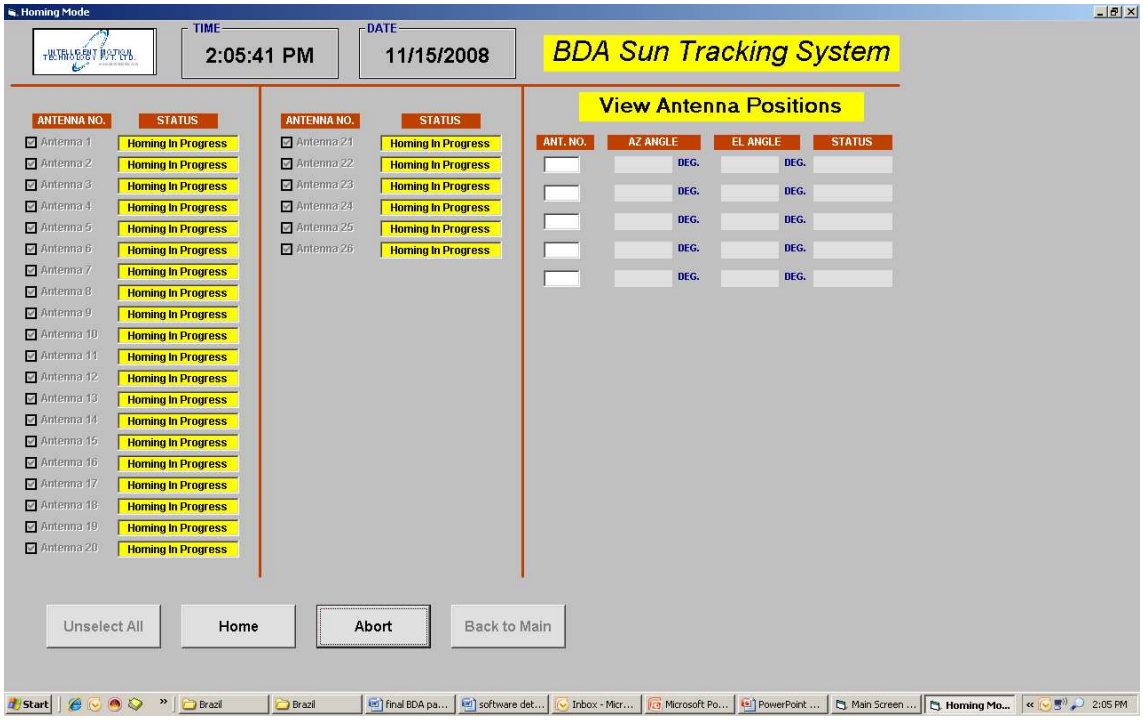

Homing screen will show only those antennas; which user has selected for communication. Select all antennas with Select All button. Click on Home command button. Homing of all antennas will start at a time.

One status window is provided in front of antenna no. this window will show following messages.

Homing required

Homing in process

Homing Over

Fault.

All messages will get displayed with different colors. If any fault occur during homing; Antenna will stop moving & status window will show FAULT message with red color.

User can view the positions of the antenna in right side of the screen. User can view five antennas positions at a time. To view position user has to enter the antenna no in the window provided.

Once homing is over user can select tracking by going to main screen.

Tracking Screen

Following figure shows the proposed version of the screen which is used for Tracking operations.

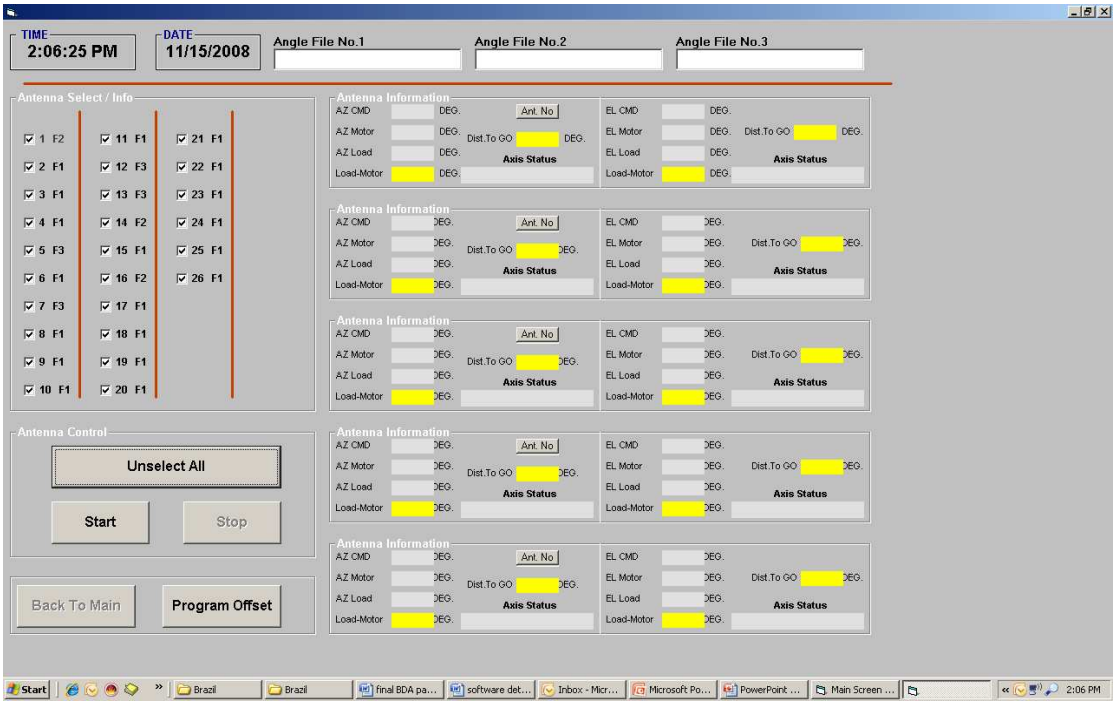

This screen is mainly used for tracking purpose. On left side of the screen Antenna Select/Info screen is provided. With this user can select the antenna for tracking. User can select the tracking source . Beside the antenna no. User has to click on F1 & select the source. Tracking can be done for three different sources.Once tracking is on; all selected antennas will glow with green color. If there is some fault antenna no. will glow with red color. During tracking user can deselect a particular antenna to stop the tracking.

User can view the positions of 5 antennas at a time. In each position window, user has to enter the antenna no.

Position window will show following Information:

- AZ & EL command value
- AZ & EL motor encoder value
- AZ & EL Load encoder value
- Distance to go for AZ & EL - this is nothing but the difference between commanded & actual angle
- Load-Motor for AZ & EL - this is nothing but the difference between load encoder & motor encoder.
- Axis status for AZ & EL

To stop the tracking for all antennas user has to click on STOP command button. There is other

way to stop the antenna; program will check for the end time. This end time is entered by user on tracking screen.

During tracking user can enter the program offset for each antenna by selecting the program offset screen. This offset will not get stored in file. This offset is the difference between predicted & actual.

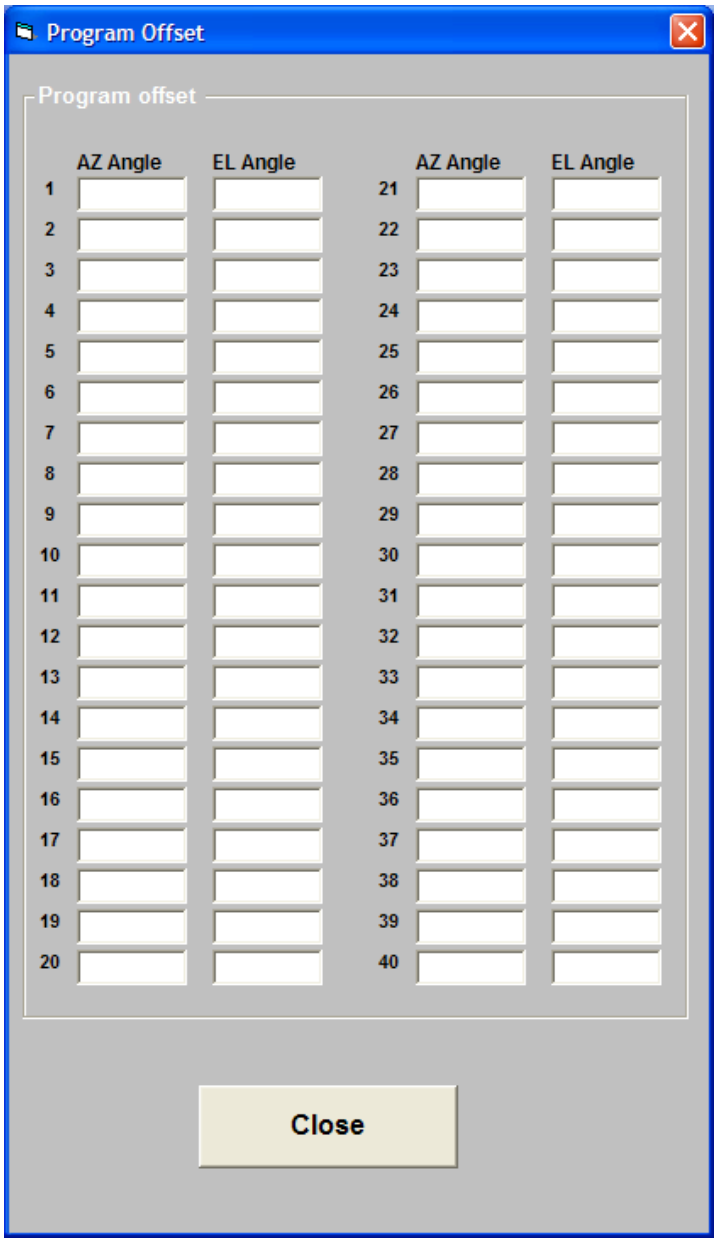

Manual Mode screen

Following figure shows the proposed version of the screen which is used for Manual Mode operation.

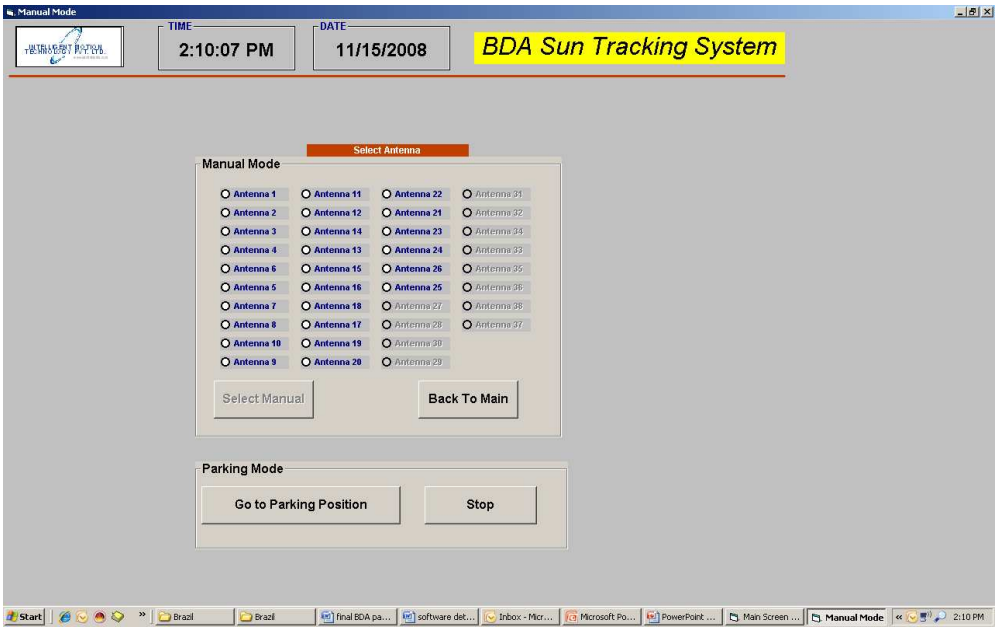

Once manual mode is selected this basic screen will get displayed. This screen is only to select antenna for manual movement. At a time only one antenna can be selected for manual movement. After the tracking all selected antenna can be moved to Parking position. The parking position angle is common for all antennas. This angle can be defined in setting mode.

Once antenna is selected & SELECT MANUAL button is clicked; another screen gets open.

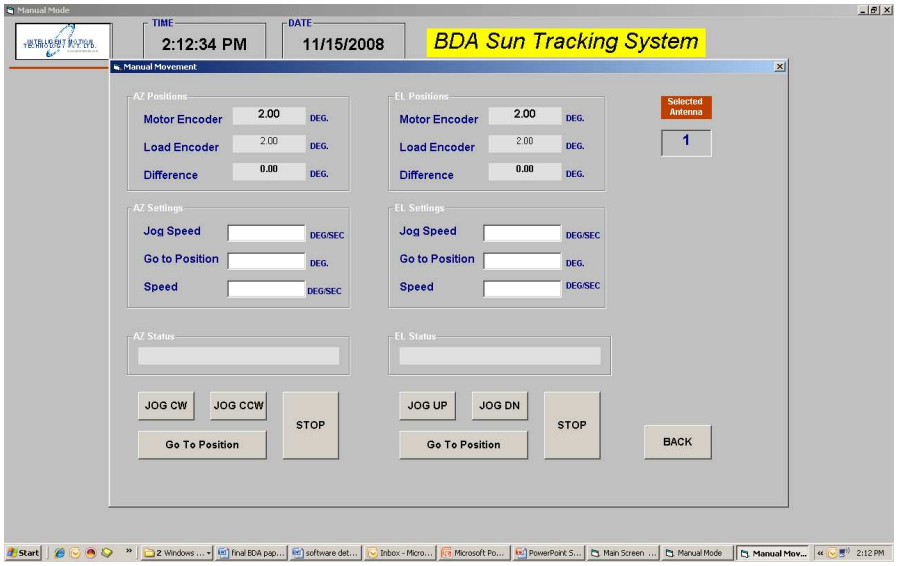

This screen will display the selected antenna no. In manual mode Jogging of AZ & EL axis is possible. This jogging speed can be entered in the window.

User can enter per defined Position for AZ & EL. During this mode antenna will reach to

defined position. Speed for this can be entered in settings window.

Screen for Setting antenna offsets

These offsets are nothing but the antenna mounting offsets. This value can be different for different antenna.

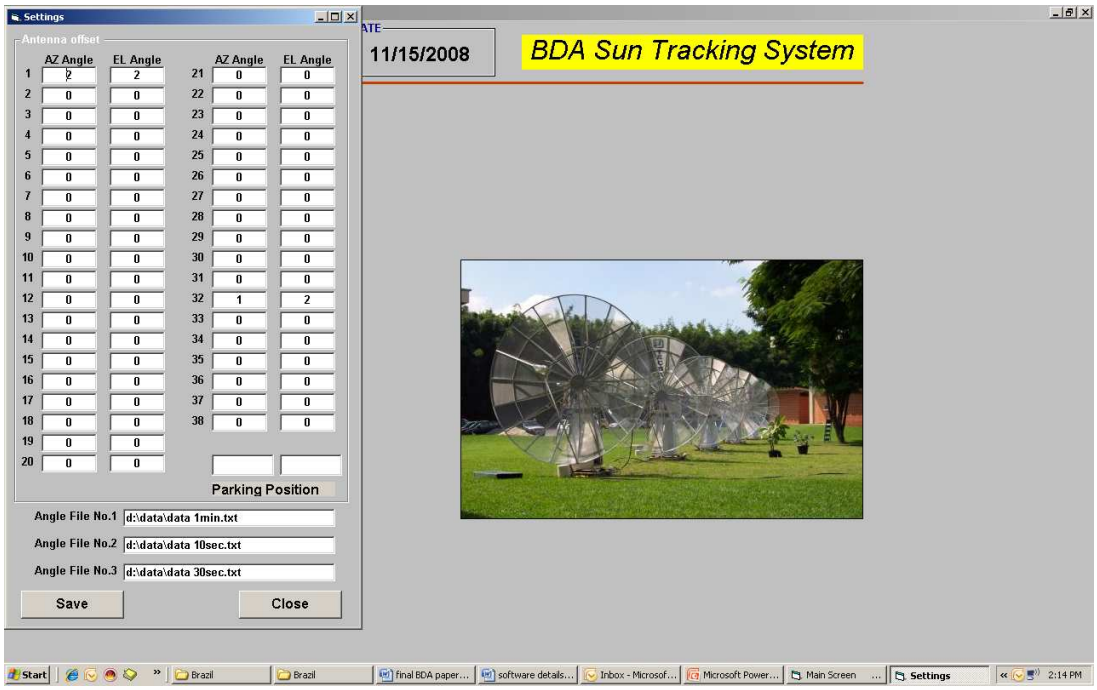

These values can be changes during tracking also. After entering the value, user has to save these values with save command button. All values are stored in one text file. Angle data files for different sources can be stored anywhere in the PC. User has to define the full path in the setting window.

Data Log & Event Log

Once tracking gets started; software will start data logging & event logging. This logged data will get saved in one file automatically. Event data will get saved in different file. Both the files will get saved with date.

CONCLUSION

With this state of art tracking system, the tracking of the BDA antenna will be accurate & without any fault. For details of the BDA project see Sawant et al. (2008)

REFERENCES

Sawant, H. S. et al., INPE, 2008.

Proceedings of the Brazilian Decimetric Array Workshop
São José dos Campos, Brazil - July 28 – August 1, 2008

DIGITAL CORRELATOR SYSTEM FOR BRAZILIAN DECIMETRIC ARRAY (BDA)

Solar Radio Astronomy Group*

Solar Radio Astronomy Group
Indian Institute of Astrophysics
Koramangala, Bangalore – 560034, India

* Talk presented by K. R. Subramanian

ABSTRACT

The basic principles of a digital correlator system are explained. A 30 channel one bit digital correlator system for the Brazilian Decimetric Array (phase I) and 1500 channel system for BDA (phase II) are described.

INTRODUCTION

Correlation means dependence, or the extent to which one thing depends on another. For example the pressure of steam in a boiler depends very much on the rate of fuel burning. In terms of signals, we say that correlation is a measure of the way in which one signal depends on another, or the way in which one part of the signal depends on another part of the signal. Radio interferometer system measures the complex cross – correlation function (fringe pattern) of the output of a pair of antennas (i, j). This quantity is defined as $R_{ij}(\tau) = \langle V_i(t)\, V_j(t+\tau) \rangle$ where the brackets indicate time average. The cross correlation function is related to the visibility function $V = |V| \exp(i\varphi(sky))$ by $R_{ij}(\tau) = A\,|V|\,\Delta f \cos(2\pi\,\Delta f\,\tau(g) - \varphi(sky))$ where A is the collecting area of the antenna, Δf is the IF bandwidth, $\tau(g)$ is the geometrical delay and $\varphi(sky)$ is the phase due to the source. This is a real function of the delay and can be estimated by a simple correlator. By Fourier transforming the visibility function the source brightness distribution can be obtained. The basic observables in the complex visibilities are: amplitude and phase as functions of baseline, time, and frequency. If Vi (t) and Vj (t) are narrow band signals centered at ν with a bandwidth of $\Delta\nu << \nu$, then $R_{ij}(\tau)$ is nearly sinusoidal with a period of $1/\nu$. At a given frequency, all we can know about the signal is contained in two numbers: the real and the imaginary part, or the amplitude and the phase. For measuring the amplitude and phase of the correlator output signal, 2 correlators are used one which multiplies the signal directly and another one with a 90 degree phase shift network. ie the output is Hilbert transform of the input. The 90 degree phase shift can be also effected by feeding the signal to 2 mixers with LOs in phase quadrature or by using a 90 degree hybrid at the output of the final IF filter. The combination of two correlators and the quadature network is called a Complex correlator. The 2 kinds of correlators are XF and FX. In the FX correlator then signals are Fourier transformed and then multiplied. In the case of XF correlator, the signals are multiplied and then Fourier transformed.

PRINCIPLES OF A DIGITAL CORRELATOR SYSTEM

Digital correlator

Modern correlators are implemented digitally because digital operations are precisely defined and repeatable. Analog circuitry is subject to environmental conditions such as temperature and humidity. Digital circuits can be exactly replicated at low cost when many identical elements are needed. For long baseline (> 10 km for connected elements and 1000 Km for VLBI and wide bandwidths) only digital delay can be used. Accuracy of the delay depends on the accuracy of the timing pulse and long delays with Pico second accuracy can be achieved digitally. No distortion of the signal other than calculable effects of quantization occurs. Correlations with wide dynamic range are easily implemented digitally.

Quantization

The digital correlator must first convert the analog signals to digital form. This requires sampling which converts continuous time signal V(t) to as discrete – time sequence of its samples{V(kt), k= 0,1,….} and quantizing which converts a continuous variable to one of a finite set of values. This combination of a sampling and quantizing device is called digitizer. The signal can be sampled and quantized or quantized and sampled. The samples of a continuous time (analog) signal have a continuous amplitude range. These signals are approximated to the nearest pre –fixed level in the case of digital correlator. This approximation of the signal to the nearest level is known as *Quantization.* The quantized digital samples are applied to an encoder. The encoder responds to each of the samples by generating a unique identifiable binary pulse pattern. The combination of the quantizer and the encoder is called an A/D converter. The quantization processes introduces an error which is the difference between the input signal m(t) and the quantized signal mq (t). This error is called quantization noise by Qe (t) = m(t) - mq(t). Quantization adds noise to the signal and therefore the S/N ratio decreases. For quantization to n bits, the amplitude range of the signal is divided into 2n discrete levels, and each sample is quantized to the nearest bit level.

Sampling

A band – limited signal is a signal f(t) which has no spectral components beyond a frequency B Hz. i.e. F(s) = 0 for $|s| > 2\pi B$. The sampling theorem states that a real signal f(t) which is band limited to B Hz can be reconstructed with out error from samples taken uniformly at a rate 2B samples per second. This minimum sampling frequency 2B Hz is called the Nyquist rate or Nyquist frequency. In the synthesis telescope we are interested in the cross correlation function of 2 signals that are jointly obey Gaussian random process. For Gaussian noise signals, VanVleck (1966) showed that quantizing can be carried out to the extreme of recording merely the sign of the samples. The penalty paid for deleting the amplitude information in such one –bit correlator (Weinreb 1963) is loss of sensitivity by a factor 2/Π relative to a continuous or analog correlator The advantage of one – bit sampling is that it is immune to variations in the input level thus eliminating the need for tight control of the correlator inputs. In a one – bit correlator, the samples are represented by a normalized values ± 1.

The estimate of the normalized one – bit correlation function is

$$\rho 1 (n \Delta t) = \{Kc(n) – Ka(n)\}/K \qquad (1)$$

where Kc (n) is the number of polarity coincidence and Ka(n) is the number of anticoincidence observed in K products

$$\text{Since } K = \{Kc(n) + Ka(n)\} \quad (2)$$

Therefore $\rho 1 (n \Delta t) = [1 - 2 (Ka(n)/K] = [2(Kc(n)/K) - 1]$

For a continuous correlation is generated using the Van Vleck (1966) relationship

$$\rho = \sin [(\Pi/2) \rho 1] \quad (3)$$

The S/N ratio can be improved by sampling the signal at a rate > than the Nyquist rate.

Walsh switching

There can be DC offset in the comparator where the input analog signal is digitized. In a one – bit correlator the out put is 1 or 0 if the input analog signal is above or below the zero level of the comparator. In practice the zero level may not be perfect.

Due to this the out put of the comparator will be affected and there will be spurious correlations at the out put of the correlator which will affect the dynamic range of the synthesized images. Phase switching was used in earlier interferometers to remove the background. In correlator system of multiplications, phase switching is useful to remove small offsets in correlator outputs that can result from imperfections in circuit operations or from spurious signals. The latter are difficult to be removed from any complicated receiving systems. Such signals at levels too low level to detect by common test procedures can be strong enough to produce unwanted components in the output. Cross coupling of the signals between cables and circuits in the field also give cross talks. The 180 degree switching cycle is used to remove spurious signals that are correlated between antennas and introduced after the phase switch. Therefore switching is most effective if it is done as early as possible in the signal path. The demodulation of the phase switch is done by changing the sign of the data after sampling by adding and subtracting in the correlator accumulation hardware. After demodulation, the spurious signals will be modulated with the inverse of the switching and the signals before the phase switch (the desired sky signal) will not be modulated. If the switching functions has been chosen so that their product integrates to zero (functions are orthogonal) the correlator will remove the spurious signals as forms products and integrates.

Walsh switching period for different antenna are integral fraction of the integration time, the cross talks get averaged to zero as they are correlated half of the time + ve ly and other half – ve ly. Using the same Walsh functions (Beaucahmp, 1975), this switching sequence is subsequently, removed at the output of the sampler, thereby eliminating the errors due to DC offsets in the A/D converter. Unwanted signals get averaged to zero only of it s amplitude is constant over a Walsh cycle. The effective removal of the unwanted cross terms depends on the ratio of the time difference between the on and OFF states of the switching pulse periods of the pulse. In the case of BDA the average value of the periods of the Walsh function is 100 msec and 10 microseconds in the time gap between the ON and OFF states of the switching pulse. The level of cross talk will be down by $10\log [(10 \times 10^{6}) / (100 \times 10^{-3})]$ is ~ 40 dB.

Total Power measurements

In a one bit correlator, the output of the quantizer is either high or low with no information on the absolute strength of the signal (like in correlator systems with an ALC loop), as only the sign of the input waveform is retained. Thus one – bit correlator measures the normalized correlation coefficient. The out put of a one – bit correlator is proportional to the ratio between the power of the correlated and the sum of the correlated and uncorrelated signal fed at the input. If Ts and Tb are the

source and background brightness temperatures then the input to the correlator is Ts/ (Ts + Tb).The output of an analog correlator is proportional to the power of the input signal is proportional to Ts In order to get the above correlation coefficient from a one – bit digital correlator receiver, the total power received by the antenna i.e. (Ts + Tb) has to be measured separately and multiplied with the measured correlation coefficient ρm. The conventional techniques to measure the strength of the signal requires square – law detectors, A/D converter etc and it will be difficult to synchronize the data collection with the correlation data. The following method (Uday Shankar, 1986) uses the one – bit correlator itself to measure the total power assuming that the input is a Gaussian signal which is true in the case of radio astronomical signals. The signal is digitized to one – bit according to if the signal voltage is > Vth then the comparator output is 1. If the signal voltage is < Vth then the comparator output is 0. This signal is correlated with 0 and measure the correlation coefficient ρ It can be shown that $\rho = \text{erf}(Vth / \sqrt{2}\,\sigma)$, from which the value of σ can be determined for a particular value of Vth the value of σ was calculated from the measured correlation coefficient ρ. for input noise signals of various peak to peak values. The tests were repeated for different values of Vth. It was found that for Vth of ~ 50 mv, the out put was linear in the range of 150 – 200 mv for the BDA correlator system.

BDA CORRELATOR SYSTEMS

In Phase I of BDA at Caucheria Paulista, (Sawant et al, 2007) the IF signals from 5 antennas on a East – West baseline were correlated in to get one – dimensional brightness distribution of the Sun at 1.6 GHz with a maximum baseline of 216 m. The IF signals at 70 MHz at the base of the antennas were Walsh switched and taken to the receiver building and split into in an quadrature phase and down converted into base band signals with a bandwidth of 2.5 MHz. The IF signals are first quantized using an A/D 790 comparator (a sign comparator). When the signal is above zero the output is 1 and below zero the out put is 0. The quantized signal is then sampled in a D flip flop (74LS74). The clock is at 5 MHz and the output also at 5 MHz. The sampling is done at the edge of the sampling clock. The quantized and sampled signal is then Walsh demodulated in an EXOR 74LS86. Walsh is derived from the basic clock. The signal is 180 deg phase switched when the Walsh signal is 1, the signal is inverted i.e. made 0 phase i.e. demodulated. The quantized and sampled and Walsh demodulated signal is delayed through a shift register 74LS164. The delay will be selected through a computer control. The necessary delay will be introduced under the control of a computer to a maximum value of 2.8 microseconds in steps of 0.1 microseconds. The delay system will be helpful to carry out observations of sources located even at 75 deg from zenith by applying corrections for the geometrical delays suffered by different antennas. The signals then enter the correlator system. There are 15 independent correlations and are

1X2 2X3 3X4 4X5 5X6
1X3 2X4 3X5 4X6
1X4 2X5 3X6
1X5 2X6
1X6

In order to get quadrature correlations a 30 channel correlator was built using 8 chips primarily designed for the Nobeyama radio heliograph. These are custom built double side band (DSB) chips using CMOS gate array technology. Each chip is composed of 4 complex correlator units. The functional diagram of the chip is shown in the figure 1, where C and S are the cosine and sine IF signal corresponding to each antenna. Detailed testing of the correlator is given in Ramesh (1998).

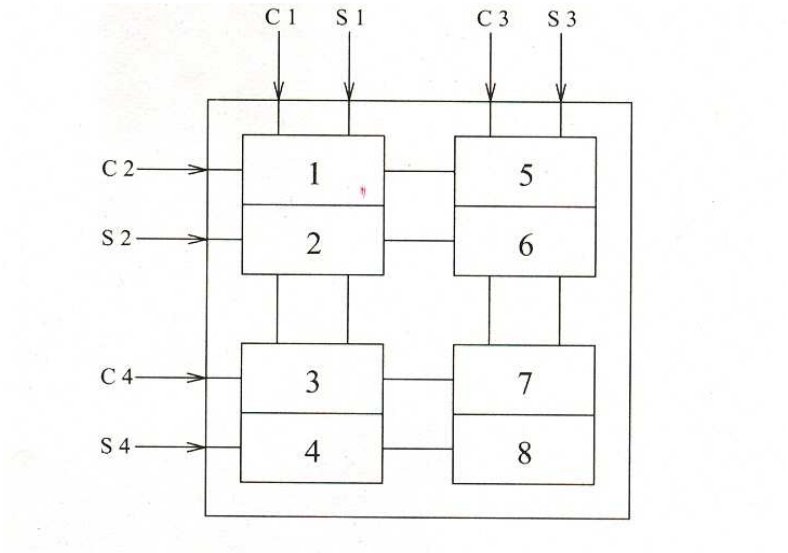

Fig. 1 - Functional diagram of the correlator chip.

The out put of correaltor 1 (cosine correlator) is

$$C1 \times C2 + S1 \times S2$$

and the output of the correaltor 2 (sine correlator) is

$$C1 \times S2 + S1 \underline{\times} C2$$

where $\times$ and $\underline{\times}$ means Ex –or and Ex – nor operations. Total power from 2 antennas is measured using the correlator. The outputs are written into 2 memory banks and read into a PC every 53 seconds. The correlator is interfaced to a PC using an I/O card with 2 FRC connectors. Software for acquisition and storage in ASCII format has been written in C language. The specifications of the BDA (phase I) correlator system is given in Table 1.

Table 1 – Specifications of the BDA (phase I) correlator system

No of inputs	6 Complex
IF Signal bandwidth	2.5 MHz
No of channels	30 Complex + 2 Total power
Sampling frequency	5 MHz
Delay range	Delay step 0.2 microseconds
Sampling type:	1 bit
Integration time	~ 104 msec

The system was used for making 1-D images of the Sun at 1.6 GHz. Figure 2 shows the East _West brightness distribution of the Sun at 1.6 GHz on 11 December 2004, around 15:00 UT.

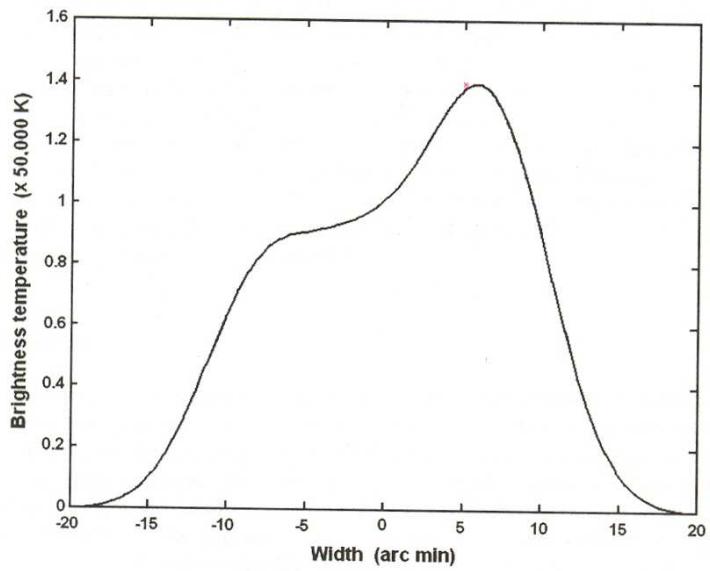

Fig. 2. - zE East _West brightness distribution of the Sun at 1.6 GHz on 11 December 2004, around 15:00 UT. The off line integration time used is 1.6 seconds. Solar East is to the left.

In the final phase of the BDA there will be 38 antennas. The IF signal at 70 MHz from the base of each dish antenna will be phase switched and brought to the receiver room via coaxial cables. The signal will be split into in phase 0 deg and quadrature phase 90 deg using a power splitter and down converted into base band signal 0 – 5 MHz by mixing with a LO at 70 MHz. For the 38 antenna of the BDA there will be 76 (38 in phase and 38 quadrature) IF signals as inputs to the digital correlator. A 1500 Channel correlator will be built with collaboration with industry. The specifications are given in Table 2.

Table 2 – Specifications of 1500 Channel correlator - FPGA based

IF bandwidth	6 MHz
Sampling frequency	12 MHz
Delay range	steps 0.08 microsecond to 1 microseconds (100 steps) (set by computer)
Sampling type:	1 bit

CONCLUSIONS

The principle of the working of a digital correaltor system was explained. Terms like quantization, sampling, Walsh switching, one bit correlation etc were described. A 30 channel one bit digital correlator system for the Brazilian Decimetric array (phase I) system for was described

ACKENOWELDEGMENTS

I would like to thank the funding authorities, FAPSEP, for their financial support to attend the BDA workshop.

REFERENCES

Beaucahmp, K.G., Walsh functions and their applications, Academic Press, 1975.
Ramesh, R., PhD. Thesis Bangalore University, 1998.
Sawant, H. S. et al., *Solar Phys.*, 242, 213, 2007.
Uday Shankar, N., PhD Thesis, Bangalore University, 1986.
Van Vleck, J. H., Middleton, D. *Proc. IEEE*, 54(1), 2, 1966.
Weinreb, S., *MIT Res. Lab Rep.* 312, 1963.

Proceedings of the Brazilian Decimetric Array Workshop
São José dos Campos, Brazil - July 28 – August 1, 2008

DEVELOPMENT OF THE BRAZILIAN FPGA CORRELATOR

Cesar Strauss, Alan B. Cassiano, Hanumant S. Sawant

Divisão de Astrofísica - Instituto de Pesquisas Espaciais - INPE
Av. dos Astronautas,1758 – 12227-010, São José dos Campos - SP, Brasil
(cstrauss@cea.inpe.br; alan@das.inpe.br; sawant@das.inpe.br)

ABSTRACT

The design is for an complex cross-correlator for 6 antennas with 3-level quantization and 5MHz sample rate, including an Walsh function generator and delay lines. This will be integrated in a 400k gate FPGA. The input is the sine and cosine signals from 6 antennas, coming from the digitizer. The output is 15 complex correlations and 6 total-power measurements, which are read by the computer each 104 ms. The digitizer has 3-level window comparators for each antenna, with adjustable threshold levels.

Key-words: correlator, FPGA

INTRODUCTION

A correlator system has to analyze a great quantity of data in real time. Up to recently, this task was left to special-purpose integrated circuits. However, with advances on field-programmable gate arrays (FPGA), it has become possible to implement a correlator in one or more FPGAs (Parsons, 2008). The main advantages are that the FPGA is easily found for purchase, relatively cheap, and can be reprogrammed to increase bandwidth, include polarization, improve the precision of the delay tracking, etc.

Parsons (2008) describes a correlator architecture capable of obtaining the correlations as a function of frequency. In the "FX correlator", a Fourier transform (F) is done for each antenna, in real time, before the correlations (X) are done.

Equivalently, in the "XF correlator", the correlations (X) are made before their Fourier transform (F) are done. However, this method does not apply as well when the number of antennas is large, due to the great increase in simultaneous Fourier transforms to be done.

On the other hand, the system built by Ramesh (2006), with custom correlator chips, does not separate the correlations in frequency. Given the complexity and cost of implementing the real-time Fast Fourier Transform in FPGA, we choose to sacrifice the spectral output at this stage, and implement this simpler system in a single FPGA.

THE CORRELATOR SYSTEM

In the BDA, the 70 MHz I.F. signal from each antenna is split by a hybrid microwave component into sine and cosine signals, which are mixed into baseband signals. These form the inputs to the correlator.

The digitizer

The task of the digitizer is analog-to-digital conversion. It is possible to minimize the computing power of the correlator design by using as few levels as possible, and accepting the increase in digitizing noise. While two levels are enough for solar observation, our three-level design has advantages for weaker sources.

As seen on Figure 1, the baseband signal is fed to two high speed comparators, which together define the three digitizer levels: negative, zero and positive. The digital-to-analog converters supply the reference levels that are adjusted periodically to maintain the optimal balance between the levels. The op-amps buffer and invert the positive-only output of the converters. The total-power information is derived by considering the current reference level and measuring the residual imbalance between the levels.

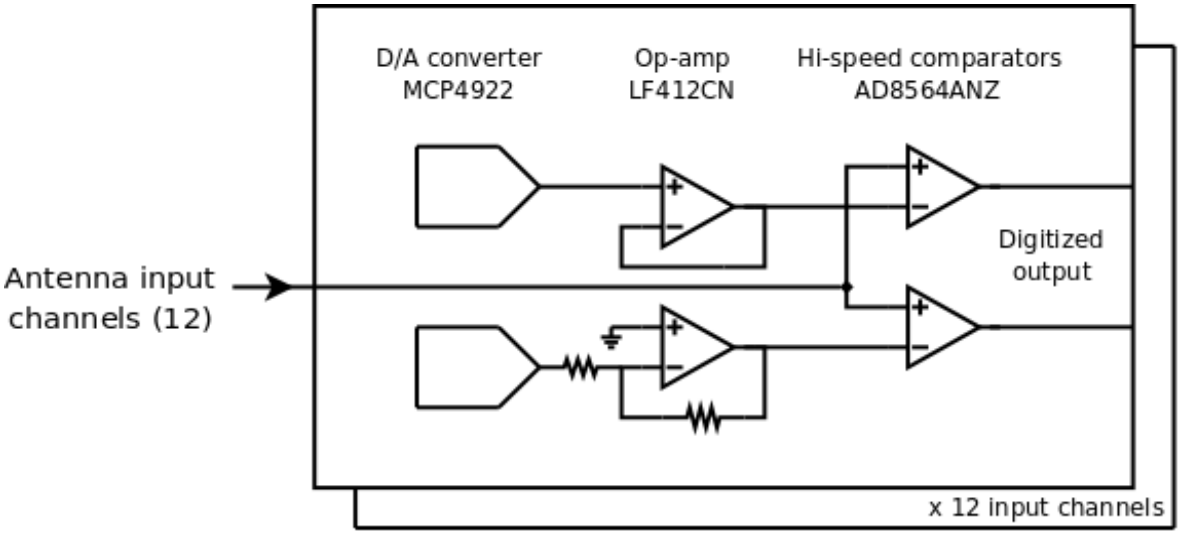

Fig. 1 – Simplified design for a three-level digitizer with automatic level adjustment.

A first batch of prototype digitizer boards were manufactured and are currently undergoing testing.

The FPGA

A commercial FPGA board was acquired from AVNET (DS-KIT-3SLC400) which has a XC3S400 Spartan-3 FPGA, several I/O ports and USB communication. The digitizer connects to the I/O ports while the USB port interfaces to the acquisition computer.

The FPGA was programmed in the Verilog language, implementing a complex correlator circuit based on Ramesh (2006), as shown in Figure 2. One full 3-level complex correlator circuit occupied 72 FPGA slices, or 2% of our 3500-slice FPGA. Six antennas means (6*5)/2=15 correlations, which gives 15*72=1080 slices, well within budget. The Walsh function generator and delay lines (Ramesh, 2006) will also be implemented within the same FPGA.

The design was successfully verified with synthetic data.

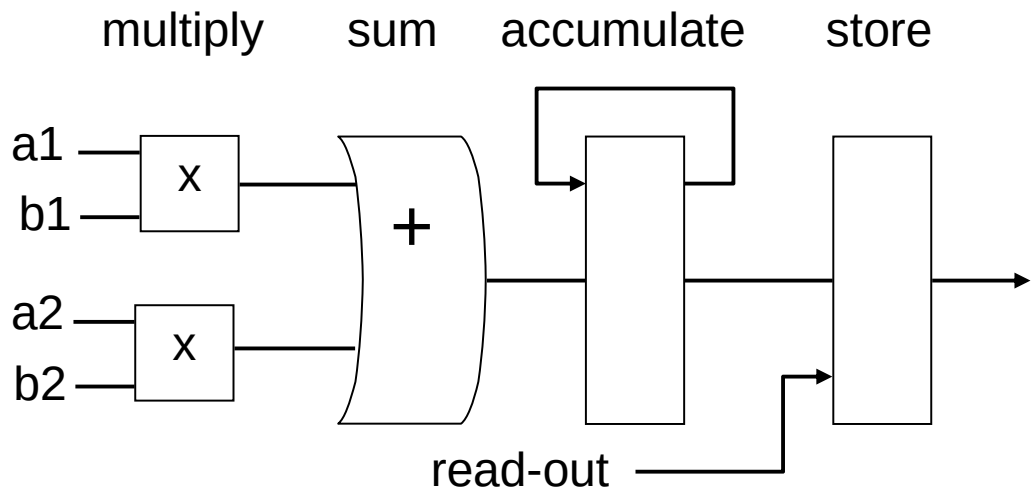

Fig. 2 – Design of a correlator cell. The inputs are the cosine and sine signals from a pair of antennas.

The data acquisition software

In contrast to the current refresh rate of around 50 seconds, we expect to be able to refresh the display at the full rate of 100 ms. This is due to the new correlator design, which continuously outputs data, and the increased speed of new PCs, which gives no chance of data loss.

CONCLUSION

FPGA technology has evolved to the point of replacing custom integrated circuits in highly parallel real-time applications. This results in lowering costs, as these components are available commercially. Given the simple circuit of Ramesh (2006) and the small bandwidths as in the BDA, even a small and cheap ($200) FPGA board is found to be sufficient for 6 antennas.

REFERENCES

Parsons A., Backer D., Siemion A., et al., *Publications of the Astronomical Society of the Pacific*, *120*, 1207-1221, 2008.

Ramesh R., Sundara Rajan M.S., Sastry Ch.V., *Experimental Astronomy*, *21*, 31-40, 2006.

Proceedings of the Brazilian Decimetric Array Workshop
São José dos Campos, Brazil - July 28 – August 1, 2008

ALTERNATIVE BDA CORRELATION SYSTEMS: FPGA VERSUS SOFTWARE CORRELATION

Gustavo Poli, José H. Saito

Departamento de Computação - Universidade Federal de São Carlos
Rodovia Washington Luis, Km 235 – São Carlos-SP
(saito@dc.ufscar.br, gustavo_silva@dc.ufscar.br)

ABSTRACT

This work is concerned to an analysis of the use of alternative BDA Correlation Systems implementations. The first one is the FPGA (Field Programmable Gate Array) system, using commercial platforms of reconfigurable chips, in this case a Virtex-II Pro (XC2VP30) of Xilinx Company. The second alternative is the software correlation. In this case, a software development platform, explicitly the GPU (Graphic Processing Unit) processor, with multiple cores driven by very high memory bandwidth, is analyzed. The results showed the viability of this type of device as a massively parallel data processing tool, and that smaller the granularity of the parallel processing, and the independence of the processing, better is its performance.

INTRODUCTION

In the BDA correlations, all the interferometer pairs formed by the 39 antennas are measured using one-bit correlators which can be assembled with digital logics, that yields greater stability than analog correlators. In order to obtain all possible multiplications between the 39 antennas, n(n-1)/2 = 741 complex correlations are calculated. At the implementation of the BDA correlators in the phase I, it was used the chips designed for the Nobeyama radioheliograph, Japan (Ramesh, 1998). There, each chip is composed by 4 complex correlator units, which corresponds to 2x2 combinations of antennas, and each unit consists of there 4-bit- parallel Ex-OR circuits, one 4-bit- parallel Ex-NOR circuit, two addition circuits, two integration circuits, a latch, and a multiplexer circuit. It can be noted that in the 22-bit counter used for integration, only the 16 MSBs (most significant bits) are read out with the 6 LSBs (least significant bits) being truncated inside the chip.

The complex correlation of one interferometer pair is obtained as a cosine correlation and sine correlation. Considering that an antenna *i* provides cosine signal, Ci, and sine signal, Si, the output of the cosine correlator is C1(+)C2 + S1(+)S2, and the output of the sine correlator is C1(+)S2+S1(.)C2 where (+) represents the Ex-OR operation and (.) represents the Ex-NOR operation, when we consider the antennas 1 and 2.

In the BDA case, the correlator system may be comprised by 8 boards, each one with 16 correlator chips. At the end of each integration period (about 145 ms), the correlated data from each of these 128 correlators in one board is written into a memory unit. This operation goes on synchronously in all 8 boards. The process of reading correlated data from each chip and writing into the memory unit goes on until we reach 256 integration cycles. At the same time, the data which was written into

another memory unit during earlier 256 integration cycles will be read into a computer. At the end of 256 integration cycles, the operations of the memory units are exchanged.

In the other side, reconfigurable electronic components have been introduced since 1980's, becoming more and more attractive to many applications. A FPGA is a semiconductor device containing programmable logic components called logic blocks, and can be programmed to perform the function of basic logic gates such as AND, and XOR, or more complex combinational functions such as decoders or mathematical functions. In most FPGA's, the logic blocks also include memory elements, which may be simple flip-flops or more complete blocks of memory. The inherent parallelism of the logic resources on a FPGA allows for considerable compute throughput even at low clock rate. The current generation of FPGAs can implement around a hundred single precision floating point units, all of which can compute a result in a single clock cycle. The flexibility of the FPGA allows for even higher performance by trading off precision and range in the number format for an increased number of parallel arithmetic units. The adoption of FPGAs in high performance computing is currently limited by the complexity of FPGA's design compared to the conventional software and the extremely long turn-around times of current design tools, where some hours wait is necessary after even minor changes to the source code.

The first part of this work is concerned to an analysis of the use of alternative BDA Correlation Systems implementations, using commercial platforms of reconfigurable chips, in this case a Virtex-II Pro (XC2VP30) of Xilinx Company. with 13969 Slices, 80 × 46 Array Size, 136 Multiplier Blocks, 2448 Kb RAM per block and 2 PowerPC RISC Cores. For the development it is used the ISE 9.2 environment and VHDL as the programming language of the correlation circuit. As it is expected the results are similar to the first implementation for the BDA correlation system, using Nobeyama radioheliograph correlation chip.

The second part is concerned to the software correlation. In this case, a software development platform, explicitly the GPU (Graphic Processing Unit) processor, with multiple cores driven by very high memory bandwidth, is analyzed.

The following sections are concerned to the description of these two alternative implementations, and the conclusions.

FPGA CORRELATION DEVELOPMENT

In this section it is described the FPGA application development system used to the BDA correlation development. The XUP (*Xilinx University Program*) Virtex-II Pro (XILINX, 2006) platform provides advanced resources to the development of reconfigurable applications, which consists of high performance FPGA, XC2VP30, with a high quantity of components that can be used to create complex systems. It follows the main elements of the platform: Virtex-II Pro FPGA with two PowerPCs 405 cores; 512Mb de (DDR) SDRAM; USB connections and interface to FPGA reconfiguration and data store; 10/100 Ethernet network interface; RS-232 DB9 serial port; 2 serial ports PS-2; 4 LEDs conected to Virtex II I/O pins; 4 *switches* connected to Virtex II I/O pins; 5 buttons connected to Virtex II I/O pins; AC-97 audio *CODEC*; XSGA video output with 1200 x 1600 resolution at 70 Hz; and 3 ATA serial port, with 100 MHz clock system, and 75 MHz SATA clock.

The Virtex-II Pro platform provides several configuration methods. The configuration data can be originated from the platform Flash PROM, from a compact-flash memory card, or from a external configuration by a USB or parallel port.

The applications development can be realized using the WEBPack ISE 9.2, the free tool environment from Xilinx, which consists of a set of tools, as Xilinx Plataform Studio (XPS). In this environment the programs are described using ANSI C language and specific libraries to access the

protocol IEEE 802.3 to send data from host computer to the FPGA. All environment is realized on Linux 64-bits operation system (Ubuntu 7.10).

SOFTWARE CORRELATION DEVELOPMENT

Recently, we are attending to a huge evolution on the development of high performance computing platforms. Among these platforms, the GPU (Graphics Processing Units) has evolved into an absolute computing workhorse, with multiple cores driven by very high memory bandwidth. Today's GPUs offer incredible resources for both graphics and non-graphics processing. One of the main reasons is the fact that GPU is specialized to compute-intensive, highly parallel computation – exactly what graphics rendering is about – and therefore is designed such that more transistors are devoted to data processing rather than data catching and flow control. The internal pipelined processing fashion makes the GPU's suitable for stream processing. Furthermore, GPU's speed grows much faster than the famous Moore's law for CPU's, that is, 2.4 times/year versus 2 times per 18 months. Moreover, a GPU usually contains multiple (typically 4 or 8) parallel pipelines and is indeed a SIMD processor. Another important feature of most contemporary GPUs is their programmability of the partial or full graphics pipeline, thanks to the introduction of vertex shaders and pixel shaders in DirextX-8. The powerfulness of SIMD operation and programmability of GPU's have motivated an active research area of using GPU for non-graphics oriented operations such as numerical computations like basic linear algebra subprograms (BLAS) (Harris, 2003) and image/volume processing (Larsen and McAllister, 2001; Rumpf and Strzodka, 2001; Thompson, Hahn, and Oskin, 2002; Colantoni, Boukala, and Rugna, 2003; Moreland and Angel, 2003; Hopf and Ertl, 2000). In Larsen and McAllister (2001), the authors presented a technique for multiplying large matrices quickly using the graphics hardware of a PC. Strzodka and Rumpf have implemented numerical schemes solving parabolic differential equations fully in graphics hardware [5]. Chris Thompson et al. introduced a programming framework of using modern graphics architectures for general purpose computing using GPU (Thompson, Hahn, and Oskin, 2002). In Colantoni, Boukala, and Rugna, 2003), the authors tested five color image processing algorithms using the latest programmability feature available in DirectX-9 compatible GPUs. Performing FFT on GPU was reported by Doggett et al. in Moreland and Angel (2003). Wavelet decomposition and reconstruction was implemented on modern OpenGL capable graphics hardware (Hopf and Ertl, 2000).

For the development of this non-graphic application on GPU it was used CUDA (Compute Unified Device Architecture) as API (Application Programming Interface) between the CPU and the GPU, from GeForce 8800 GTX from NVIDIA, with 128 ALU's. CUDA is a new hardware and software environment for issuing and managing computations on the GPU as a data-parallel computing device without the need of mapping a graphics API. The operating system's multitasking mechanism is responsible for managing the access to the GPU by several CUDA and graphics applications running concurrently.

The objective of this work is to use GPU as an alternative correlation system, and compare the result with the FPGA correlation system. For this, it was developed the application using NVIDIA GeForce 8800 GTX, with 128 processing unit cores.

The CUDA Toolkit target a class of applications whose control part runs as a process on a general purpose computer, and which use an NVIDA GPU as coprocessor for accelerating SIMD parallel jobs. Such jobs are 'self-contained', in the sense that they can be executed and computed by a batch of GPU threads entirely without intervention by the 'host' (CPU) process, thereby gaining optimal benefit from parallel graphics hardware.

Dispatching GPU jobs by the host process is supported by the CUDA Toolkit in the form of remote procedure calling. The GPU code is implemented as a collection of functions in a language that is essentially 'C', but with some annotations of distinguishing them from host code, plus annotations for distinguishing different types of data memory that exists on the GPU. Such functions may have parameters, and they can be 'called' using a syntax that is very similar to regular C function calling, but slightly extended for being able to specify the matrix of GPU threads that must execute the 'called' function. During its life time, the host process may dispatch many parallel GPU tasks.

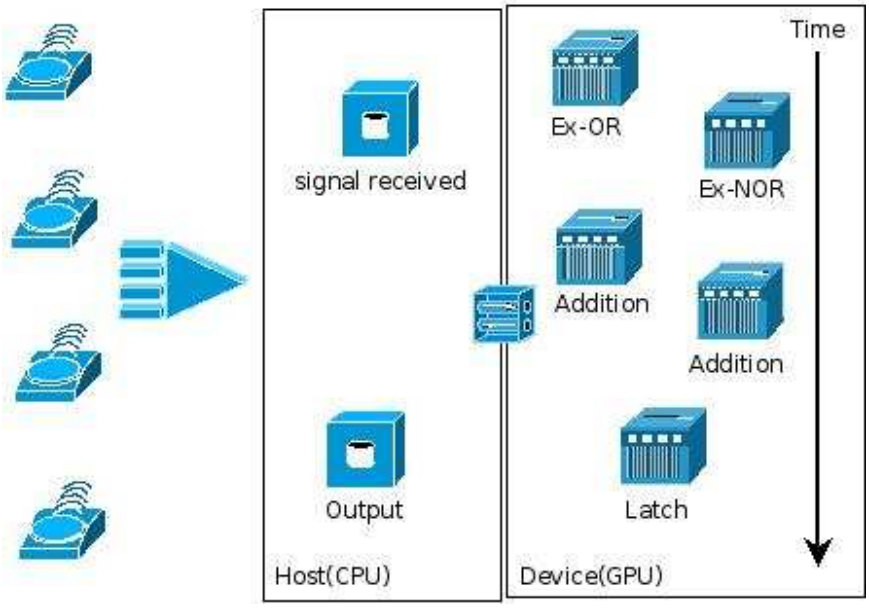

Fig. 1 - GPU/CUDA Software correlation diagram.

This work implements the software correlation to the BDA signals as shown in Figure 1. As the signals are received by the host CPU, it is buffered, until 10 sequential samples are achieved, corresponding to 29.640 antenna signals of 741 interferometers of BDA. When the buffered data is been processed at the GPU, the CPU must be receiving the subsequent signals from the antennas. The GPU processing uses two buffers Ex-OR and Ex-NOR, to compute these correlations in parallel, followed by the latching process to the Output buffer, at the CPU, to complete the process. The processing time in the GPU was 1.6 ms for 29,640 elements (741 x 4 in 10 times), but it can be increased using new versions of GPU.

CONCLUSIONS

It was implemented a subset of the correlation system using the Virtex II Pro platform of FPGA, and preliminary results showed its performance to the application, close to the Nobeyama radioheliograph correlator chip. The results of the use of GPU, showed the feasibility of the software correlation with this processing device, as a massively parallel data processing tool, and that smaller the granularity of the parallel processing, and the independence of the processing, better is its performance.

REFERENCES

Ramesh, R., PhD. Thesis, Bangalore University, 1998.

XILINX. *Xilinx University Program Virtex-II Pro Development System - Hardware Reference Manual*. [S.l.], Março 2006.

Harris, M., http://www.cs.unc.edu/~harrism/gpgpu, 2003.

Larsen E. S., McAllister, D. K. *Proc. IEEE Supercomputing*, 55, 2001.

Rumpf, M., Strzodka, R., *Proc. ICIP*, 3, 1103–1106, 2001.

Thompson, C. J., Hahn, S., Oskin, M., *Proc. ACM/IEEE MICRO*-35, 306–317, 2002.

Colantoni, P., Boukala, N., Rugna, J. D., *8th Int. Fall Workshop: Vision Modeling and Visualization*, Munich, Germany, 2003.

Moreland K., Angel, E., *Proc. SIGGRAPH/Eurographics Workshop Graphics Hardware*, 112–119, 2003.

Hopf, M., Ertl, T., *Proc. EG/IEEE TCVG Symp. Visualization*, 93–103, 2000.

BRAZILIAN DECIMETRIC ARRAY CONFIGURATION IN A NUTSHELL

Cláudio Faria[1], Stephan Stephany[2], Hanumant S. Sawant[3]

[1]Depto. de Computação – Pontifícia Universidade Católica de Minas Gerais - PUCMinas
Poços de Caldas-MG, Brasil
(cfaria@pucpcaldas.br)
[2]Lab. Associado de Computação e Matemática Aplicada - Instituto de Pesquisas Espaciais - INPE
Av. dos Astronautas,1758 – 12201-970, São José dos Campos-SP, Brasil
(stephan@lac.inpe.br)
[3]Divisão de Astrofísica - Instituto de Pesquisas Espaciais - INPE
Av. dos Astronautas,1758 – 12201-970, São José dos Campos-SP, Brasil
(sawant@das.inpe.br)

ABSTRACT

Here we present the proposed configuration for the second phase of the BDA, Brazilian Decimetric Array. The corresponding u-v coverage and synthesized beam are also presented as well as results obtained employing simulated solar images from the Nobeyama data.

INTRODUCTION

The final proposed configuration of the antenna array for the Brazilian Decimetric Array (BDA) is T-shaped. Phase I comprehended the BDA prototype, a line-array composed of the first 5 antennas that is already operational (Sawant et al, 2007). In phase II, 21 antennas will be added to existing ones forming a T-shaped array. Finally, in phase III, other 4 antennas will be added in each arm of the T. These latter antennas will be placed starting at a distance of 250 m from the central antenna of the array following the concept of a "fat T". A former random 26-antenna configuration was proposed (Faria et al., 2005), but abandoned, since the available terrain allows to employ a T-shaped configuration that presents good and more redundant coverage in the u-v plane. For instance, a Y-shaped configuration was not possible due to the terrain restrictions.

In the following section we describe the u-v coverage and synthesized beam for the 26-antenna BDA phase II T-shaped configuration, as well as results obtained for this configuration employing solar images from the Nobeyama data.

ANTENNAS CONFIGURATION FOR BRAZILIAN DECIMETRIC ARRAY - PHASE II

The main characteristics of the array are given in Table 1.

Table 1 - Principal Characteristics of BDA

Number of Antennas	26
Frequencies	1.2 – 1.7, 2.7 and 5.6 GHz
Time Resolution	~100 ms
Diameter of Antennas	4 m
Angular Resolution	~2.8', ~1.4' e ~0.8'
Maximum baseline	252 m
Minimum baseline	9 m
Field of View	40'
Sensibility (at 5.6 GHz with $\Delta t = 1$ s)	~ 360 Jy/beam (Sun) ~ 2170 mJy/beam (other sources)

PROPOSED CONFIGURATION FOR BDA PHASE II

In the first phase of the BDA project, named PBDA (Prototype of BDA), an east-west five-element interferometer was developed and installed at INPE, using 4-meter diameter parabolic dishes with alt-azimuth mount and complete tracking capability. PBDA operates in the frequency range of 1.2–1.7 GHz. In BDA phase II, it is planned to lay out new 17 antennas over the distance of 252 meters in the East-West direction and another 9 antennas over a distance of 162 meters in the North-South direction forming a T-shaped array (Faria et al., 2004a; Faria et al., 2004b). Figure 1 shows the array configuration suggested for BDA phase II.

The configuration presents a dense array near the intersection of the "T", with spacing of 9 meters between adjacent antennas. In each arm of the "T" this spacing is increased to 18 and 36 meters after the fourth and seventh antennas respectively.

Figure 2a shows the *UV coverage* and Figure 2b, the synthesized beam obtained with this configuration at the frequency of 1.4 GHz.

The one-dimensional profile is presented in Figures 3 and 4 for 1.4 and 2.8 GHz respectively. The gratting lobes are ~80 arc minutes from main lobe.

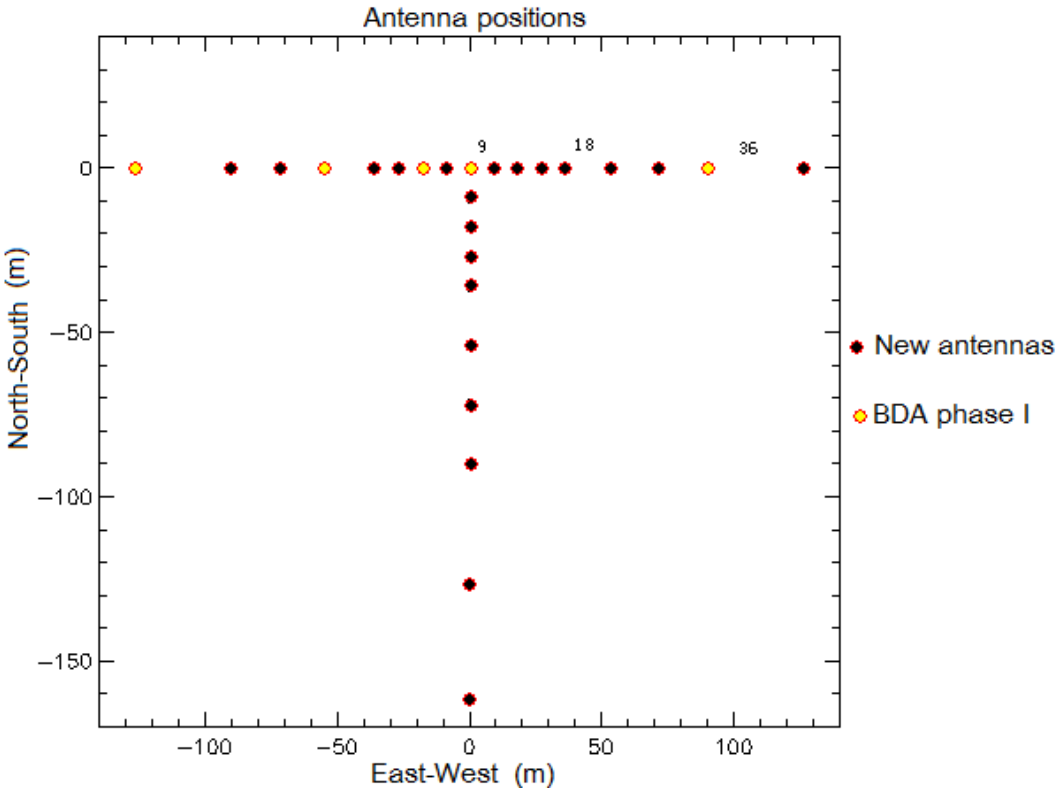

Fig. 1 – Antennas configuration for BDA phase II. The antennas in light colors represent the current configuration (BDA phase I).

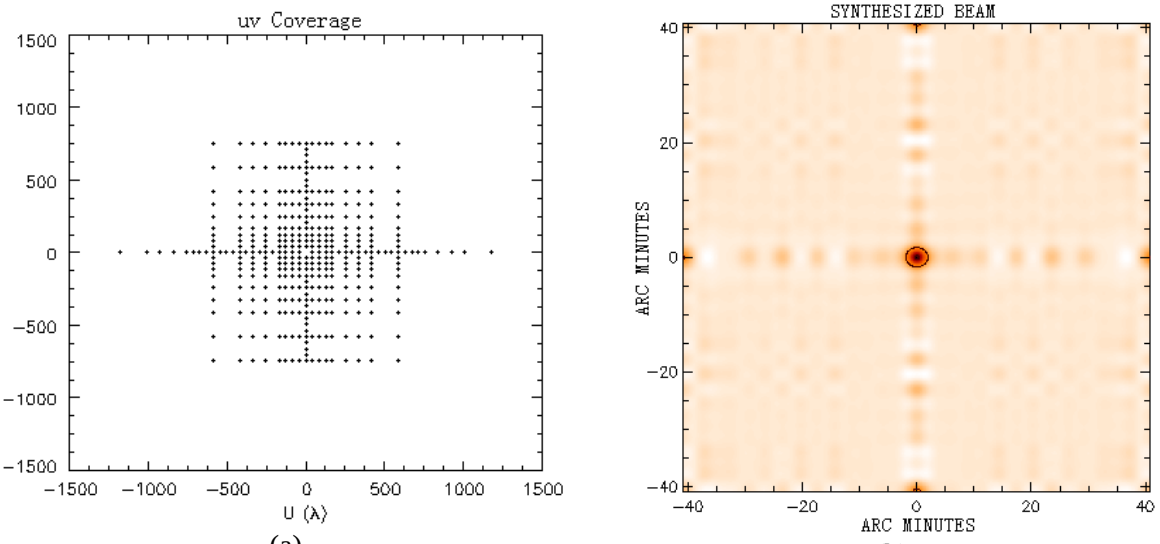

(a) (b)

Fig. 2 - Resulting *uv* coverage (a) and synthesized beam (b) obtained with the proposed configuration.

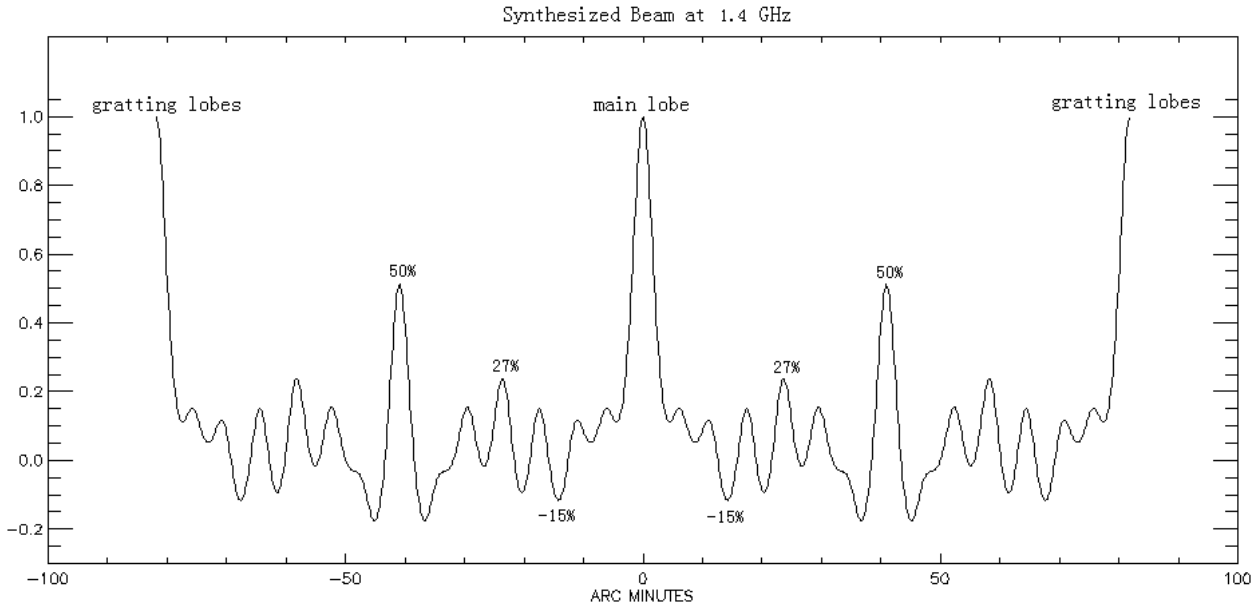

First gratting lobe at 82 arcminutes

Maximum side lobe on the 40 arc min = 27% of main lobe

Minimun side lobe within 40 arc min = - 15 % of main lobe

Fig. 3 – One-dimensional profile of the BDA phase II at 1.4 GHz.

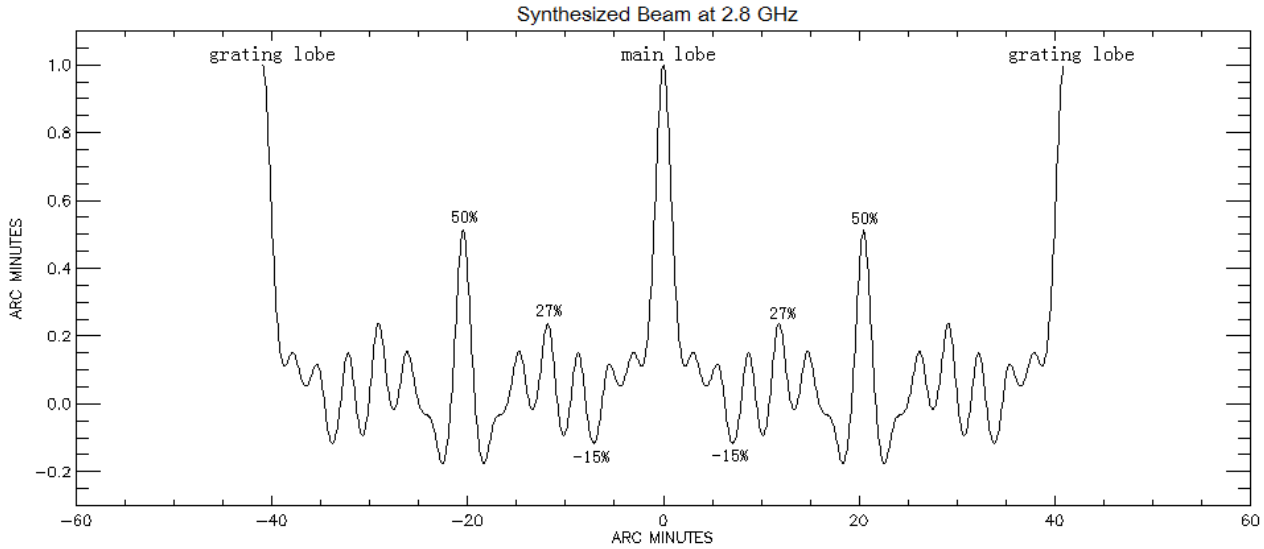

First gratting lobe at 41 arcminutes

Maximum side lobe on the 40 arc min = 27% of main lobe

Minimun side lobe within 40 arc min = - 15 % of main lobe

Fig. 4 – One-dimensional profile of the BDA phase II at 2.8 GHz.

SIMULATION

In order to investigate the quality of the *uv* coverage of the BDA configuration on the radio imaging of the Sun, a simulation was performed using a Sun image synthesized by the Nobeyama Radio Heliograph at 1.7 GHz as a model of the source (Figure 5a). In this simulation, the position of the Sun is assumed at the zenith and the observation frequency is 1.4 GHz. The corresponding dirty image is showed in Figure 5b. The visibility data is assumed full calibrated.

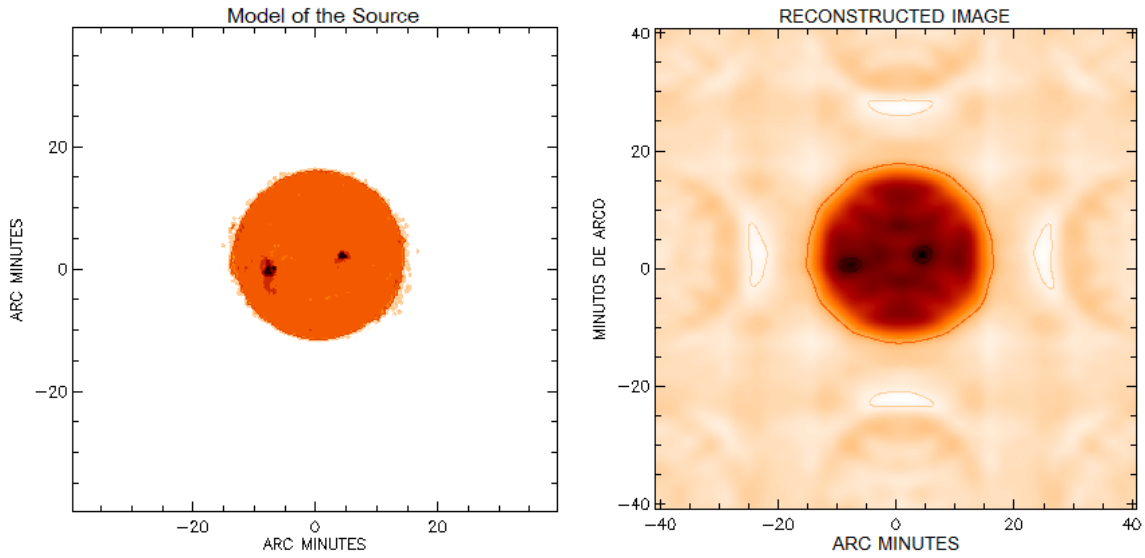

(a) (b)

Fig. 5 - a) Image of Solar disc obtained from Nobeyama Radio Heliograph at 17 GHz that was used as a model of the Sun; (b) dirty image obtained with BDA configuration presented in Fig. 1.

ACKNOWLEDGEMENTS

Authors thank FAPESP for the approval of grants that supported the development of the BDA project (06/55883-0).

REFERENCES

Sawant, H. S., Ramesh, R., Cecatto, J. R., Faria, C., Fernandes, F. C. R., Rosa, R. R., Andrade, M. C., Stephany, S., Cividanes, L. B. T., Miranda, C. A. I., Botti, L. C. L., Vilas Boas, J. W. S., Saito, J. H., Moron, C. E., Mascarenhas, N. D. D., *Solar Phys*., 242, 213-220, 2007.

Faria, C., Stephany, S., Sawant, H. S., Proc. of the 5th ICIPE. Leeds, Inglaterra : Leeds University Press, 1, 1-10, 2005.

Faria, C., Sawant, H. S., Neri, J. A. C. F., Stephany, S., Ramesh, R., Subramanian, K. R., Ananthkrjshnan, S., Rao, A. P., Sirothia, S. K., Proc. of the VII COLAGE, 1. 67-67, 2004a.

Faria, C., Stephany, S., Sawant, H. S., In: Workshop dos Cursos de Computação Aplicada do INPE, 4. (WORCAP), 2004b, São José dos Campos. *Anais.* São José dos Campos: INPE, 2004. CD-ROM, On-line. Disponível em: <http://urlib.net/lac.inpe.br/worcap/2004/10.05.21.49>. Acesso em: 24 mar. 2009.

Proceedings of the Brazilian Decimetric Array Workshop
São José dos Campos, Brazil - July 28 – August 1, 2008

WIDE FIELD IMAGING WITH THE BDA

A. Pramesh Rao

National Centre for Radio Astrophysics (TIFR)
Pune University Campus
Ganeshkhind, Pune 411007, INDIA

ABSTRACT

Imaging the sky with better sensitivity and resolution is the mainstay of all astronomy. While radio maps of the sky do exist at various radio frequencies, astronomers continue to image the sky for various reasons -the improved capabilities of the new instruments, improved analysis and imaging software, variability of the sources in the sky and new questions generated by our improved understanding of the physics of sources. The availability of images of large sources or regions of the sky is a valuable tool in these days of multi wavelength studies of astronomical sources. While the Northern sky has been well studied at radio wavelengths by a variety of modern radio telescopes, the study of the sky south of declinations of -45 degrees has been relatively limited, though a number of new telescopes are being planned. While many of the interesting objects have been imaged with the Australia Telescope, the BDA with its large field of view and better short spacing coverage would do a better job at mapping the extended diffuse features. An all sky survey at 5.8 GHz going down to a few milli Janskies, the southern equivalent of the NVSS catalog would be a valuable contribution and would generate interesting science when combined with the Molongolo survey at 843MHz and surveys at different bands. The wide field of view and good short spacing coverage of the BDA can be used for relatively new areas of research like detection and study of transient radio sources, magnetic fields in the ISM by studying filamentary structures seen in polarization, etc. Some of these projects, along with the science drivers and the effort involved will be discussed.

The construction of a new telescope is expected to produce a flurry of scientific activity and since every new telescope is generally built to fill a niche and address some specific question better than any previous telescope. The niche of the Brazilian Decameter Array (BDA) is solar physics where there is a need for a dedicated, high resolution radio telescope at decameter wavelengths to complement the various planned telescopes at other wavelengths. However, since the sun is up in the sky only during the day and radio telescopes can operate twenty four hours, it is of interest to examine what else it can do after the sunset. This is of special interest if the telescope has to used by astronomers outside the solar community.

The primary purpose of a radio telescope is to image sky as efficiently as possible so that the entire sky can be mapped, within the geographical constraints of the instrument, as rapidly as possible. For this the BDA is well since it is designed to image the sun which is large and variable on short time scales. All high resolution radio telescopes around the world are earth rotation aperture synthesis telescopes that consist of an array of single dishes with complex electronic backends that form N(N-

1)/2 pairwise interferometers between the N elements in the array. In modern synthesis arrays N can be large (27 for the VLA[1], 30 for the GMRT[2], 26 for the BDA and even larger values for various proposed radio telescopes). Each interferometer pair measures one spatial fourier component of the patch of sky seen by the individual antennas and as the earth rotates, the geometry of the array with respect to the source changes, leading the same interferometer pair to measure different fourier components. At the end of a full synthesis (observing a source from rise to set) a synthesis radio telescope upwards of a few hundred thousands fourier components (visibilities) and forming an image of the field of view of the telescope consists of fourier inversion on a computer of the observed visibilities and complex image processing to remove artifacts caused by the incomplete measurement of the fourier space and possible errors in calibrating the observed data.

The properties of the telescope that are of direct concern to the astronomer are:

1. its sensitivity which is a function of N, the size of the antennas, the bandwidth and quality of the electronics and the integration time;
2. its angular resolution which is inversely proportional to the longest baseline;
3. its field of view which is inversely proportional to the size of the individual elements of the array;
4. its speed for imaging to a given sensitivity which depends on the array configuration (one dimensional versus two dimensional arrays);
5. the ease of analysing data from from the instrument.

Ideally, the astronomer would like all these quantities to be high, but this is not easily achieved since many of them are contradictory. For instance, increasing antenna sizes to increase the sensitivity leads to leads to smaller fields of view. Increasing the bandwidth increases the complexity of the electronics and the analysis. Increasing the angular resolution and field of view in two dimensional arrays leads to complexities due to the breakdown in the simple fourier relationship between the observed visibilities and the image of the sky. Any radiotelescope has to optimise these various parameters to maximise its impact.

In trying to examine what science can be done with a telescope, its performance has to be compared with existing and planned instruments. From the point of view of an astronomer, the Brazilian Decameter Array has both strengths and weaknesses. The strengths are its large field of view for a telescope in its frequency range, its two dimesional configuration that provides good instantaneous u-v coverage, the relative ease of data analysis since it is unlikely to be affected by w-term and ionospheric problems and its access to the entire southern sky which has till recently been relatively understudied in radio astronomy since most of the radio telescopes are in the northern hemisphere and can see only down to declinations of 45 degrees south. At present, the only major synthesis radiotelescopes that can study the sky south of 50 degrees declination are the Australia telescopes and the Molongolo Radio Telescopes, both of which are east-west arrays. The weaknesses are its relatively poor sensitivity since it was designed for studying the sun which is very bright, its poor angular resolution, its limited bandwidth and the fact that a number of radiotelescopes are being built or planned in the southern hemisphere which could be competitors to the BDA.

The southern sky has a number of unique objects that have yielded interesting results whenever they are observed. The center of our galaxy with all its associated objects, many of which vary with time, is almost overhead for the BDA. The Magellenic clouds, our nearest neighbour galaxies are also easily accessible to the BDA.

Given its large field field of view, any observation of these regions by the BDA would cover a very large number of individual objects which increases the probability of discovering interesting objects. There are also many interesting and unique extended extragalactic sources in the southern sky

like Centaurus-A, Pictor-A and Fornax-A which would benefit from high quality low resolution images since most of the modern synthesis radiotelescopes have limited fields of view and poor short spacing coverage of the fourier plane. Combining the BDA data with existing high resolution data and redoing the imaging analysis would generate high quality images that could provide interesting insight on the physical processes in the source. The same is true of the galactic center complex and the various extended supernova remnants and HII regions like 40Doradus that lie in the southern galactic plane.

Besides imaging individual sources, a project to map the southern sky down to a flux limit of a few milliJanskys should be undertaken by the BDA since it will be very sensitive to low surface brightness objects that are often missed in high resolution studies. The Sydney University Molonglo Sky Survey (SUMSS)[2] has surveyed the southern sky at 843MHz with a resolution of 50". A BDA survey at 5.6 GHz would have a similar resolution and would yield valuable scientific results by identifying interesting object by studying the radio spectra between these two frequencies. Many interesting objects that are often ignored as not reliable when they are near survey limits, get studied when they are detected independently in a different study. An all sky survey would consume a lot of telescope time and would also involve large volumes of data and analysis. Such a survey should be undertaken only after the instrument is reasonably debugged and astronomer are confident of undertaking the effort. A major limitation of the BDA for such studies is its relatively poor sensitivity, because of which the time required for the survey could become prohibitive. One hour observation with the BDA Phase III will produce images with noise of 3 milliJansky rms enabling detection of sources stronger than 10 milliJansky. Increasing the bandwidth of the BDA by a factor of 10, which is not too difficult with today technology would increase the sensitivity by a factor of 3 and bring the observing time for the survey to acceptable values.

One of the most active areas in astronomy is the study of transient and variable sources which are seen in all wavelengths bands - gamma rays, X-rays, optical and radio.

The prototype for such objects is the sun which shows variability in all wavelength bands and at all time scales, from millisecond bursts to secular variations over years. With modern telescopes, variable sources are detected from all distances, ranging from the edge of the universe (gamma ray bursts), through objects at extragalactic distances like active galactic nuclei and supernovae, to galactic objects like Xray binaries, optical variable and flare stars and radio pulsars and transients. A proper understanding of the nature of any source requires studying its properties in the different wavelength bands which is often a challenge since it requires coordinated observations from different telescopes across the world and in space, which is often difficult to arrange at short notice during the short life of a transient source. Every observatory routinely gets hundreds of requests for observations of a newly discovered transient but only a few can be handled given the various other planned observations at the observatory. This is a field that is growing and the BDA would benefit from participating in this area of research since many of these transients are within the sensitivity range of the BDA. Even when not detected, the upper limits set by the BDA would provide useful constraints while modeling the sources.

However, acting as a service facility and adding one or two points in somebody else's project is no doubt, a useful scientific activity, it is not very glamorous and would not excite younger astronomers. More exciting would be to discover new transient sources, initiate observations at different observatories and carry out the modeling and interpretation of the sources. This could be achieved by regularly monitoring interesting fields in the sky where the density of stars and hence the probability of detecting such transients is high. Possible regions to monitor are the galactic center region, the Magellenic clouds and regions at galactic longitude 90/270 degrees. A program to routinely monitor a few selected fields in such regions, combined with near real time analysis of the data, would

enable detection of new transients and would trigger the associated follow up activity. For this, the contacts developed by acting as a radio facility to users in other wavelength bands would come in handy.

Astronomy is evolving rapidly and new areas of research keep cropping up. The filamentary structures seen in polarization by the Westerbork Radio Telescope, which are believed to be due to structure in the foreground rotation measure screen is one example. A new telescope brings in new people and new perspectives which generally leads to a period of enhanced scientific activity.

REFERENCES

Thompson A. R., Clark, B. G, Wade, C. M., Napier, P. J., *ApJ Supp*, 44, 151, 1980.

Swarup, G., Ananthakrishnan, S., Kapahi, V. K., Rao, A. P., Subrahmanya, C. R., Kulkarni, V. K., *Current Science*, 90, 95, 1991.

Bock, D. C.-J., Large, M. I., Sadler, E. M., *Astron. J*, 1578, 117, 1999.

Proceedings of the Brazilian Decimetric Array Workshop
São José dos Campos, Brazil - July 28 – August 1, 2008

PROTOTYPE OF BDA PHASE STABILIZATION SYSTEM

Mário C. P. Almeida, Alan B. Cassiano, Lúcia E. Q. V. Alves, Hanumant S. Sawant

Instituto de Pesquisas Espaciais - INPE
Av. dos Astronautas,1758 – 12201-970, São José dos Campos-SP, Brasil

ABSTRACT

This paper describes the Prototype of BDA phase stabilization system. The stabilization system provides attenuation of factors larger than 10 for high frequency temperature perturbations in the cable and electronics box and can provide great stabilization of phase delays in the system. The results of the tests performed showed the maximum rate of change of temperature was of about 1^{o}C/hour.

INTRODUCTION

The BDA – Brazilian Decimetric Array is a radio-telescope formed by an array of antennas dedicated to the study of Solar Physics. Individual antennas are provided with a LNA (Low Noise Amplifier) amplifier and a double conversion receiver along with the electronics for tracking and control movement of the antennas. The reference frequency signal to the receivers local oscillators is generated centrally and is distributed to the receivers through coaxial cables at 10 MHz frequency. Using PLL (Phase-Locked Loop) circuits the individual receivers generate their necessary LO frequencies signals. The down converter signals, at 70 MHz, corresponding to the received signal for the individual antennas, are them transmitted, through coaxial cables to the analyzing circuitry in the control room.

Figure 1 shows the simplified block diagram of the receiving section of BDA.

Due to the large dimensions of the array (some hundred meters) and to its components being located far apart and exposed to the sun, different operating temperatures and difference temperature variations are expected to occur during observations. Temperature variations may cause differential delay variations in the signal transmitted in the cables and also cause differential delay variations in the receiver electronics. Also, due to long distance between the antennas and the long lengths of the cables, the relative phase between the signals coming from different antennas can be totally masked by the temperature induced drifts.

STABILIZATION TECHNIQUES

Several different stabilization techniques are simultaneously employed to cope with temperature induced phase instabilities: temperature compensation of phase delay variations, thermal insulation, and temperature stabilization.

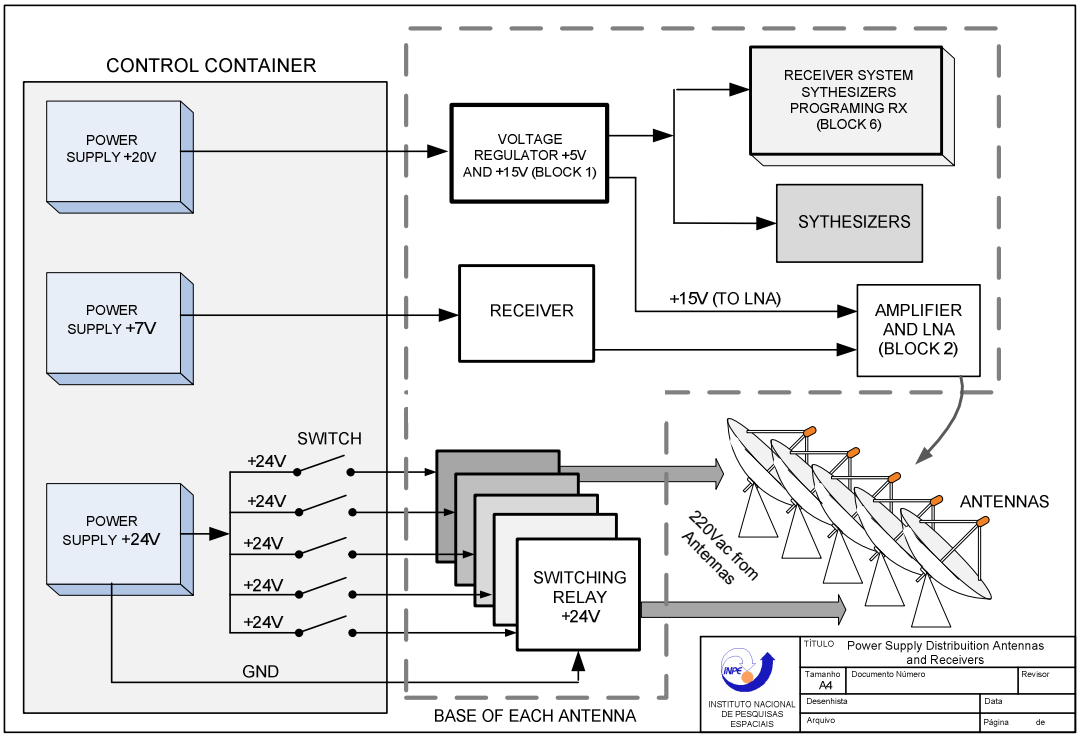

Figure 1 - BDA's receiving section simplified block diagram

TEMPERATURE COMPENSATION OF PHASE DELAYS

Propagation speed in coaxial cables is heavily dependent on its temperature. Given the large differences in the distances between the antennas and the analyzing circuitry room, the temperature induced differential phase shifts between cables can be very large, even if using phase-stable cable.
A simple technique is used to compensate for such differential delays among different cables. The technique consists is cutting, to the same electrical length, all cables carrying the same type of signal from different antennas, regardless of the distance between the antenna the and analyzing circuitry room. All cables are cut to the same length of the longest cable, the remaining length of cable being kept at the same temperature as the used length. Assuming the cables are from the same manufacturer and have the same temperature coefficient of the propagation speed, the differential delays among the different cables are compensated for any temperature variation because the delays will track equally among them.

As an illustration of this, measurements of phase delays were carried-out for a length of 48 meter of the cable type intended to be used in the BDA (coaxial RGC 213 manufactured by Datalink Telecomunicação).

Phase delay measurements taken using an HP8510 Network Analyzer and a climatic chamber are presented in the Figure 2.

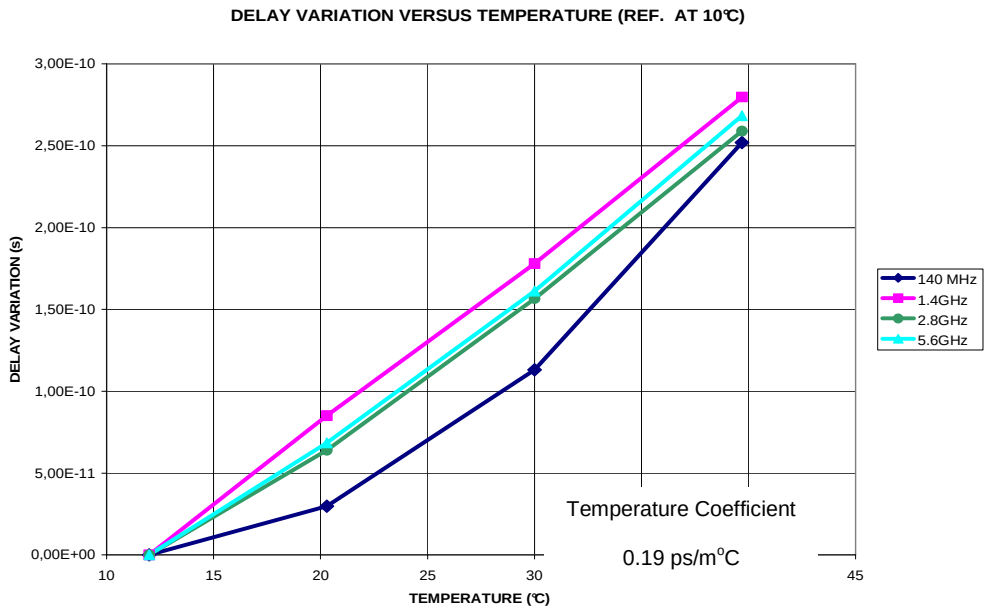

Fig. 2 - Phase delay measurements for cable datalink RGC213.

THERMAL INSULATION

Temperature compensation technique of cutting the individual cable to the same electrical length is not enough to assure delays stability if the temperature change seen by the cables is large. So, in order to reduce the temperature changes in the cables, the cables are buried at 1.0 meter depth. It was determined by tests that the temperature variations at this depth is only a very small fraction of the ambient temperature variations, this effect being caused by the high thermal impedance of the soil, i. e., high mass and low thermal conductivity.

The cable lengths that are not used, because they come from an antenna distant from the control room, are coiled and kept at the basement floor of the control room. The basement is also built underground, has thick walls, no windows and no parts above the surface. The cable bundle comes directly from the underground conducts to inside the basement floor.

Figure 3 shows actual ground temperature measurements, at different depths, performed at the site of the BDA during a period of one month. The graph shows that the temperature variation, at a depth of 1.0 m, during a period of one hour is negligible. The one-day period noise, clearly visible in the measurements taken at 0.5 m and 1.0 m, is caused by interference on the measurement system from the condensation prevention heater turn-on/turn-off during night-time.

GEOTHERMAL COUPLING

There are parts of the system that, despite being built identical, are difficult to compensated and difficult to insulate from the environment temperature changes because they must be installed above ground due to required maintenance, etc. These are the receiver box, the LNA amplifier and the interconnecting cables. Those parts are difficult to stabilize because they have low thermal inertia and are exposed to the atmosphere and to the sun. The temperature stability of those parts are assured by

insulating them from the environment by using insulation foam material and coupling them to the thermally stable ground temperature by a geothermal heat exchanger using air as a heat transport fluid.

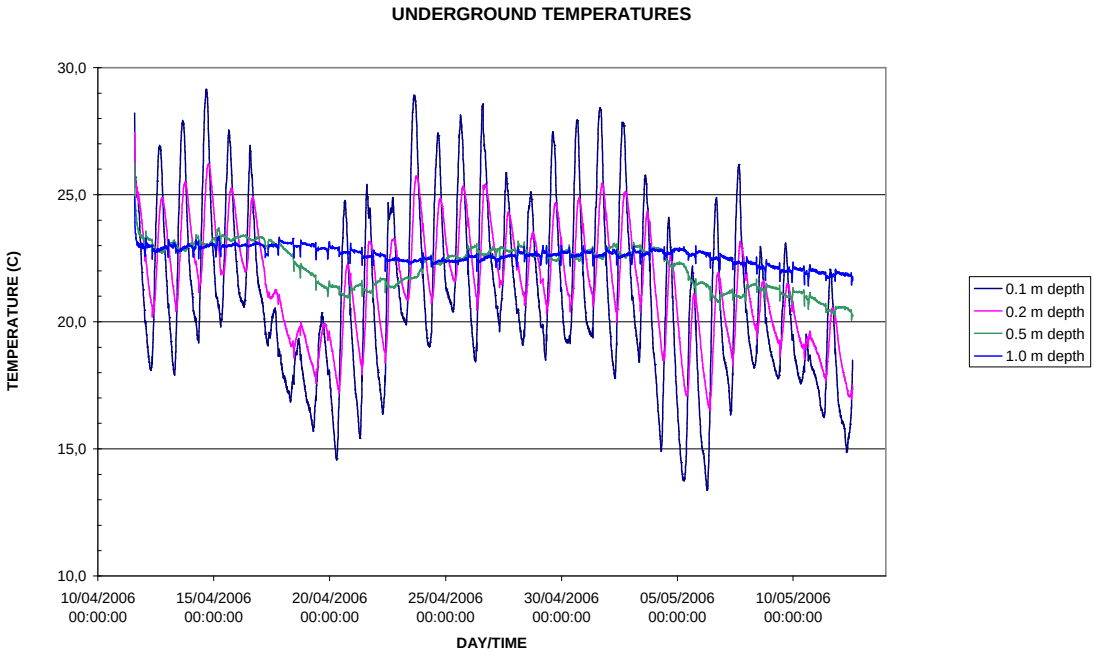

Fig. 3 - Actual temperature monitoring at different depths.

PROTOTYPE OF BDA PHASE STABILIZATION SYSTEM

Description

Instead of starting taking measurements of ground thermal conductivity, thermal capacity, etc, for the proper dimensioning of the stabilization system, it was decided to build a prototype of the system in one antenna and, after some tests, adjust its characteristics (insulation thickness, air speed, etc) to meet our requirements. It was agreed that this could save time in the development of the system.

The prototype design is of a closed type, i.e., the same air is used to transport the heat to/from the antenna system and the underground heat exchanger. This would prevent condensation inside the system caused by the prevalent high humidity conditions at the site, which would occur if an open system was used.

Several difficulties have arisen during the search of the necessary material for building the prototype. The most difficult problem to solve was to find an adequate air blower. It was found that it is possible to find in the market several types of axial flow blowers with several different sizes and capacities but, radial flow blower, the most adequate for the prototype, could be found only in a very small number of different capacities. The prototype was built only using commercial available parts. Coaxial cables are running inside regular electrical conduits and are thermally insulated using closed cell polyethylene foam tubing used in hot water system for residential buildings. Thermal insulation is improved by the use of aluminized adhesive tape. The receiver electronics is installed inside a rigid

PVC box insulated with polystyrene foam. The air blower case and the LNA box were insulated using closed cell synthetic rubber foam (Armaflex). The use of different materials for different applications was required because some materials are only available in rigid sheets, inappropriate to insulate boxes of cylindrical or irregular shapes.

The underground heat exchanger was built using thin walled 40 mm diameter rigid PVC piping commonly used for residential sewer system. The underground heat exchanger has a total length of 12 m and was buried at 1.0 m depth. No action was taken to improve the heat conductivity of the soil in the region of the heat exchanger. The total length of the external (above ground) system is about of the length of the underground heat exchanger. Considering the soil temperature absolutely stable, it is foreseen that the attenuation of the external temperature variations must be in direct proportion to the ratio between the internal-to-external thermal resistance and the internal-to-soil thermal resistance. Figure 4 presents a sketch of the heat exchanger and piping system.

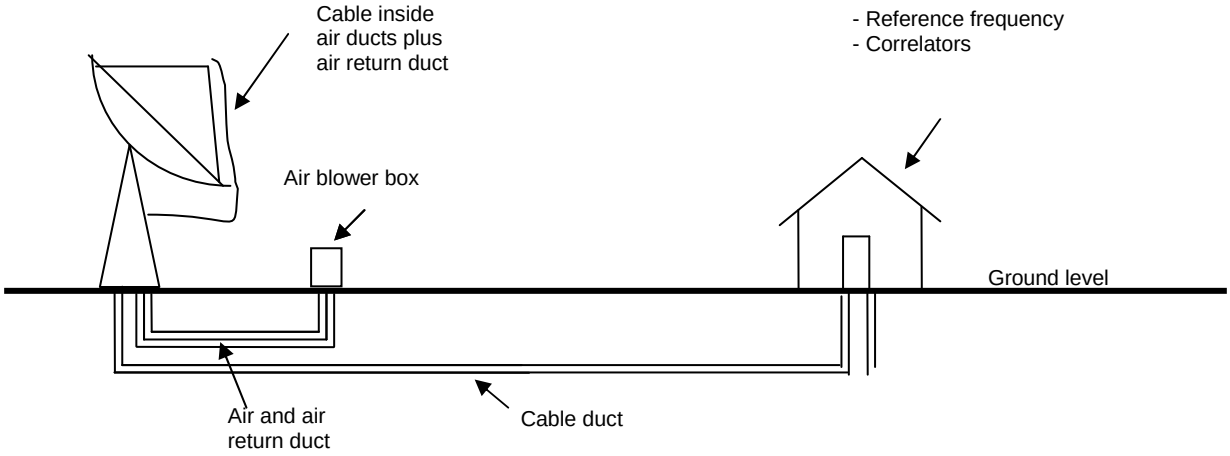

Fig. 4 - Sketch of the heat exchanger and piping system.

EXPERIMENTAL RESULTS

Test of July 16th, 2008

The test performed in July 16th, 2008, was done before the planned configuration for the prototype had been fully completed. There were some lengths of piping not insulated with polyethylene foam, aluminized film was not applied over the thermal insulation, and the blower motor was not thermally insulated from the blower. Figure 5 shows the temperature evolution during the test.

It can be seen from the graph that the internal temperature was closer to the external temperature than to the soil temperature. This effect is caused by poor thermal insulation in the above ground system parts. Some filtering of the external variations can be seen due to higher thermal impedance of the system. It is clearly visible that the internal temperature was rising with a rate greater than the external temperature. This effect was probably caused by the heating introduced by the blower motor. Another test was planned after the system thermal insulation was improved.

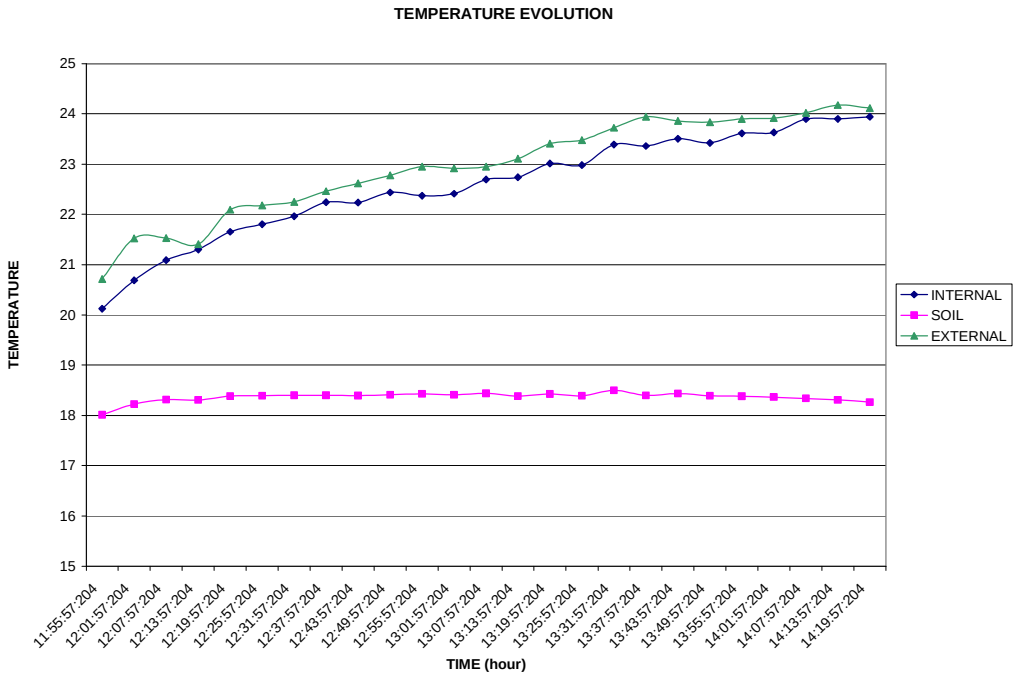

Fig. 5 - Temperature evolution during the first test.

Test of July 25th, 2008

The second test was done after better insulation of the external piping, the installation of aluminized adhesive tape over the expose piping and the better insulation between the electric motor and the blower. Measurements taken during the second test are presented in the Figure 6.

The results of the second test show that is much better uncoupling of the external environment temperature and the internal system. The maximum rate of change of temperature was of about 1^{o}C/hour.

CONCLUSION

Measurements taken without any stabilization system, presented in Figure 7, show that temperature variation of more than 10^{o}C/hour can occur. The stabilization system provides attenuation of factors larger than 10 for high frequency temperature perturbations in the cable and electronics box and can provide great stabilization of phase delays in the system. It is planned to carry-out measurements of the phase variations caused by the observed temperature variations to verify if upgrades are still required in the prototype.

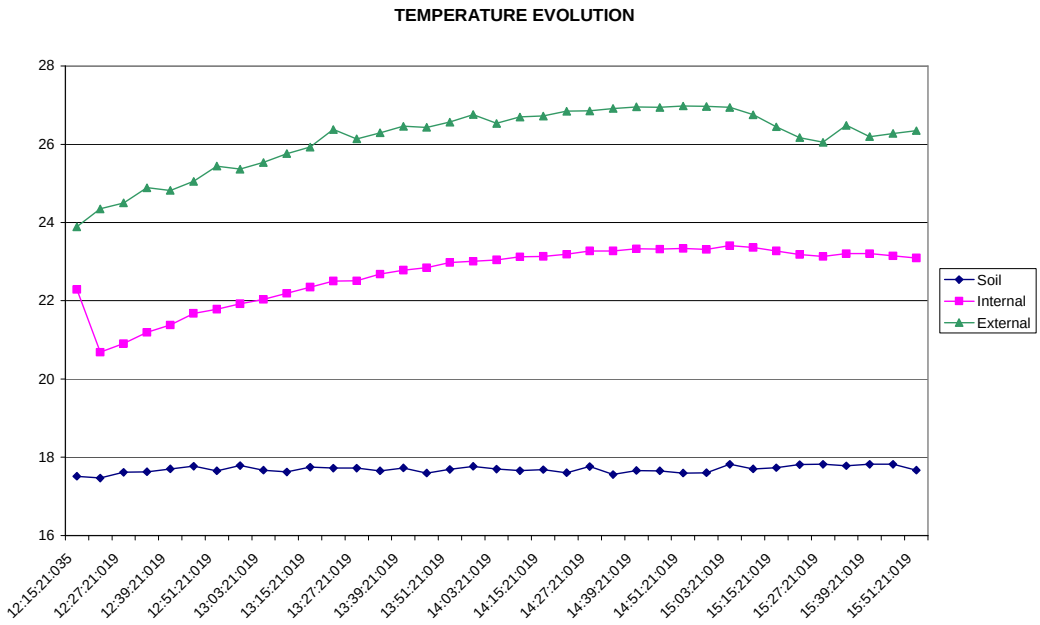

Fig. 6 - Temperature evolution during the second test.

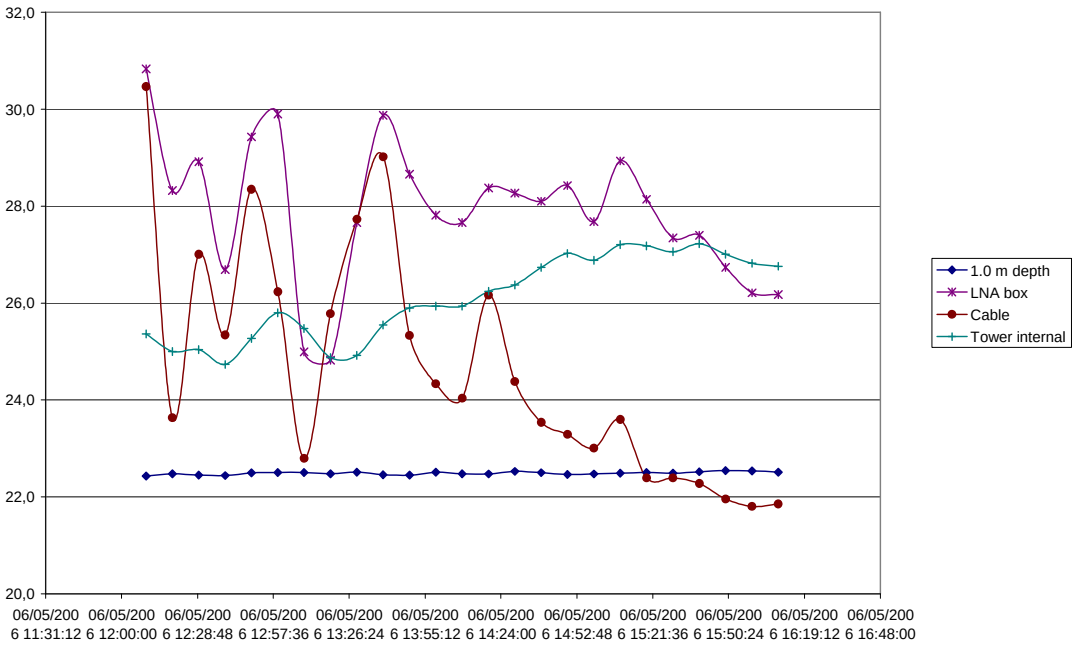

Fig. 7 - Temperature measurements without stabilization system.

REFERENCES

ALMA Memo No. 131 - Gain and Phase Stabilities of Some Components Used in the BIMA Array - B. Frye, R. Forster, J. Lugten, L. Mundy, R. Plambeck, D. Thornton, and J. Welch.

ALMA Memo 314 - Underground Temperature Fluctuations and Water Drainage and Water Drainage at Chajnantor - Laura A. Snyder, Simon J. E. Radford, and Mark A. Holdaway - National Radio Astronomy Observatory, Tucson.

ATA Memo No. 27 - Notes on Delay and Phase Tracking for the ATA - Larry R. D'Addario - 2001 May 09.

Test report of cable Datalink RGC 213.

1D SUN BRIGHTNESS PROFILE USING BDA DATA

José R. Cecatto and Maria C. Andrade

Divisão de Astrofísica - Instituto de Pesquisas Espaciais - INPE
Av. dos Astronautas,1758 – 12227-010, São José dos Campos-SP, Brasil
(jrc@das.inpe.br, con@das.inpe.br)

ABSTRACT

The process to generate images from the raw data involves several steps: editing, calibration, deconvolution and cleaning. In order to generate one-dimensional brightness temperature map of the Sun in a snapshot mode, we have developed an alpha version of a computational code, making use of the ten baselines available for the Prototype of the Brazilian Decimetric Array (PBDA) five element array operating in transit mode. The code based on simple assumptions and a standard method was developed in the Matlab environment. Description of the method, assumptions and parameters applied on the code development are described. One-dimensional brightness temperature map of the Sun will be presented using raw data of five element array and that of the calibrator sources.

Key-words: 1D imaging, BDA, brightness

INTRODUCTION

It is well known since the beginnings of radio interferometry that the brightness distribution of a target source in principle can be obtained applying a Fourier Transform to the measured visibility data. However, it is not so simple and both the element primary beam pattern and sampling in the uv-plane, due to the array configuration, must be taken into account during the process of reducing data as purpose to produce an acceptable quality image. Generally, the primary beam pattern is not known analytically and then must be determined empirically. Also, geometry of the array configuration together the source position in the sky permit us to know in detail the sampling in the uv-plane as well as geometric delay. In addition, noise must be taken into account for the recorded data. The basic equation, Eq. (1), is given by (Thompson et al., 1994):

$$I^D(l,m) \equiv \int_{-\infty}^{\infty}\int_{-\infty}^{\infty} S(u,v)V'(u,v)e^{2\pi i(ul+vm)}\,dl\,dm \qquad (1)$$

S is the (u,v) sampling function, V' the observed visibility data which has intrinsic noise, and $I^D(l,m)$ is known as "dirty image" due to the artifacts which are generated by the limited discrete sampling and gaps in the uv-plane of the array. As the Fourier Transform cannot be analytically represented it must be numerically approximated. This can be done either by "Direct Fourier Transform - DFT" or by interpolating the data onto a rectangular grid and after that apply the "Fast Fourier Transform - FFT" algorithm (Taylor et al., 2003). In this work we choose the FFT method. Also, due to the array design

at regular spacings a natural weighting is assumed.

To recover *I(l,m)*, i.e. the recovered "clean image" from $I^D(l,m)$ either a model with determined parameters, or a non-parametric approach must be used. By a practical point of view two algorithms have been applied during last four decades. CLEAN and Maximum Entropy (MEM) methods are the most traditional and widely used to produce a "clean image" since the "dirty image". Each one has its own advantages and drawbacks (Taylor et al., 2003) discussed below. We know that recently improved versions of the traditional algorithms and hybrid ones have been applied to the interferometric data showing better results in comparison to the algorithms used before (Wakker and Schwarz, 1998). However, several additional aspects must be considered to implement any other method than CLEAN which we used on the code. CLEAN is basically an empirical method which produces a brightness distribution image of a source from raw data and calibration, although its criterious noise analysis is not available yet (Högbom, 1974; Taylor et al., 2003).

Also, the five antenna array (PBDA) is a prototype put into operation to engineering and operational tests in actual conditions of severe weather in open field. Details of PBDA are given in Sawant et al. (2007).

In this work, we present a computational code development and generation as a purpose to produce 1D Sun brightness profiles using the BDA prototype East-West 5-element array data. It is the alpha version based on the pure CLEAN algorithm (Högbom, 1974). Preliminary results of its application to PBDA data are also presented. Also, a discussion about these first results to guide either future developments or alternatives is described.

TRADITIONAL ALGORITMS APPLIED TO GENERATION OF INTERFEROMETRIC IMAGES

We know the brightness distribution of a target source can in principle be obtained by the inverse Fourier transform of the measured visibility function. By this method a "dirty" image is produced which requires further processing. The additional processing must take into account for the primary beam pattern of each antenna (assuming all antennas are identical), sampling function in the uv-plane, and the calibration of interferometric data using calibrator sources, e.g. Cygnus-A.

1- CLEAN – The CLEAN method was first noticed by 1974 (Högbom, 1974). Roughly, it is an empirical method that represents emission components by δ-functions. Initially, maximum intensity is identified in the image as the strongest compact emission component. About 10% of that component with a Gaussian fit is removed from the image. After this the strongest component is compared with the rms noise level in the image. In case both are about at the same level the "cleaning" process is stopped and the "clean" image is restored. This constitutes the first cycle of "CLEAN". In case, the emission components present in the image are stronger than noise a new cycle of "cleaning" runs iteratively. This process keep running until the last component in the image is at the rms noise level. Then, all components removed are restored and the final image is produced. As "CLEAN" is modeling compact sources is dedicated to image either point or compact sources. Despite of that three conditions are required as to provide good quality images. First, the beam must be symmetric; second, the beam must be positive definite or semi-positive definite; and the last, there must be no spatial frequencies present in the dirty image which are not also present in the dirty beam.

2- MEM – Maximum Entropy Method is an analytic method (Frieden, 1972; Frieden and Burke, 1972). In this case, the image selected is that which fits the data, to within the noise level, and also has maximum entropy. Here, entropy can be defined by the expression (Taylor et al., 2003) given in Eq. (2):

$$\mathrm{H} = -\sum_k I_k \ln \frac{I_k}{M_k e} \tag{2}$$

where M_k is the "default" image to allow a priori information to be used. A "default" image is assumed as model. Then, a priori information is used based on data constrained to the fact that the fit, χ^2, of the predicted visibility to that observed, be close to the expected value given by Eq. (3):

$$\chi^2 = \sum_k \frac{\left|V(u_k, v_k) - V'(u_k, v_k)\right|}{\sigma^2_{V(u_k, v_k)}} \tag{3}$$

Maximizing H with the constraint that χ^2 be equal to expected value leads to an image which fits the long spacings extremely well (better than 1σ) since that a predicted value for the zero-spacing flux density is provided by the user (Cornwell and Evans, 1985).

COMPUTATIONAL CODE DEVELOPMENT

The computational code development was based on simplified hypothesis and assumptions as a purpose the alpha version be available in a relatively short time. Actual version is a crude code which requires several additional improvements. However, first and preliminary results could be obtained and give us information about the interferometer functioning, quality of data, and subside to plan either a further code improvement or necessity of new code development.

The hypothesis on which the computational code is based are the following:

1- Application of the closure phase method provides the best phase calibration;
2- Observations of the Sun on transit mode are able to generate a sufficiently high S/N ratio on the data recorded;
3- Snapshot mode permits us to produce an image of a strong source like the Sun;
4- The phase gains do not change during a sample of data;
5- No solar activity is noticed during the acquisition of sample data used to generate the image;
6- Any interference signal which could deprove the data quality is completely mitigated by the Walsh switching put at the back-end before the correlator inputs;
7- Last significant digit on data bring no useful information about measured visibilities and is excluded from raw data through the edition data process;
8- Instrumental phase components keep constant during the data recording and cause no disturbance relevant to a deproval of data quality;
9- Pure CLEAN method gives us good results;
10- Amplitude is normalized to the maximum measured value on the smaller baselines and scaled with the daily solar flux measured by solar patrols. No absolute amplitude calibration is done because the absence of a strong source with a comparative flux level as the Sun.

By the other side, taking into account for all the limitations relative to available time, experience and practice on interferomety and computer code development for interferometry, as starting point we based on the following assumptions:

I. The most important is phase calibration. Absolute amplitude calibration is not applied to this version of the code;
II. A modular architecture of the code is the best approach. Each module executes a determined task or run a specific function. The assembling of all modules integrate the computational code generated;

III. Correction for the slope and shift of the fringes from zero mean are required and applied to the data (mean of the first and last 200 points and straight line fit). This is part of the editing data processing;
IV. Due to array design the final antennas configuration is approximately at regular spacings. This permitted us to develop a code whose sampling is based on a natural weighting;
V. Time evolution of baseline amplitudes can well be fitted by Gaussian profiles. The maximum of each Gaussian gives us amplitude maxima for all baselines;
VI. Corrupted fringe patterns, amplitude profiles, and unstable phases are criteria used to edit data and exclude baselines which have compromised data.
VII. The Single Value Decomposition function available in the MatLab environment is able to apply the "closure phase" method (Jennison, 1958; Rogstad, 1968; Readhead and Wilkinson, 1978; Pearson and Readhead, 1984) and find a good and valid solution for the calibrated phases.

With those hypothesis and assumptions on mind we start the code development on a relatively flexible and available computational environment (MatLab) which had the most of functions necessary for the code generation. The software was planned on a main code and several modules with pieces of code which correspond each one to a specific function or task. The only usage of the main code is to establish a hierarchy and organize all the modules required. Then, the code is composed of one main code and eleven modules. Some few modules execute more complex tasks. For instance, those modules which perform the "closure phase" as well as the one executing the deconvolution and "cleaning" make use of fundamental functions and correspond to relatively complex tasks required. Despite the code be responsible for the execution of functions and tasks, it is interactive with the user. In this sense, the user is totally responsible for the inputs of parameters as well as to define the choices requested by the code based on all available information about the instrument, observational process, and target source.

It has to be mentioned that some of the most widely used software packages to perform the tasks of edition, calibration, deconvolution and imaging of interferometric data are AIPS, MIRIAD, CLIC and CASA. There are some packages of restricted usage, for instance, NEWSTAR and FESTIVAL. For details on these refer to the internet.

APPLICATION TO THE BDA PROTOTYPE DATA AND PRELIMINARY RESULTS

To test the functionality and validate the code developed and generated we selected a small sample of PBDA data. Besides, the application of the code to actual data recorded by the prototype permit us to check the interferometer is working properly or not. Doing this way, we could verify the best results are obtained for three of the five shortest baselines of the array (1×2, 2×3, and 1×3), and therefore these are used systematically to obtain any 1D brightness profiles using PBDA data. Particularly, we selected one sample of relatively old data as well as one sample of more recent and good quality data. The results of the code application to PBDA data are shown on Figures 1 and 2 jointly to EUV and X-ray data for comparison. Figure 1 (top) shows the 1400 MHz 1D brightness distribution of the Sun on 10th Sept., 2007 at 17UT. EUV, 175 Å (EIT-SOHO) solar map for same day is also shown (bottom). Figure 2 exhibits the 1600 MHz 1D brightness distribution of the Sun for 11th Dec. 2004 at 15UT (bottom). Also, is exhibited (top) East-West one-dimensional soft X-ray image of the solar corona for the same day and time. The original 2D image was integrated along latitude to allow us a comparison.

It has to be taken into consideration that these are results of the alpha version code applied to data of three baselines of the array. Then, the excessively smooth profiles obtained are mainly due to these reasons. However, as mentioned above, the array is limited to five antennas and the processing

of any sample of data using additional baselines resulted in unreasonable 1D profiles in comparison to data on other spectral bands, e.g., EUV and X-ray.

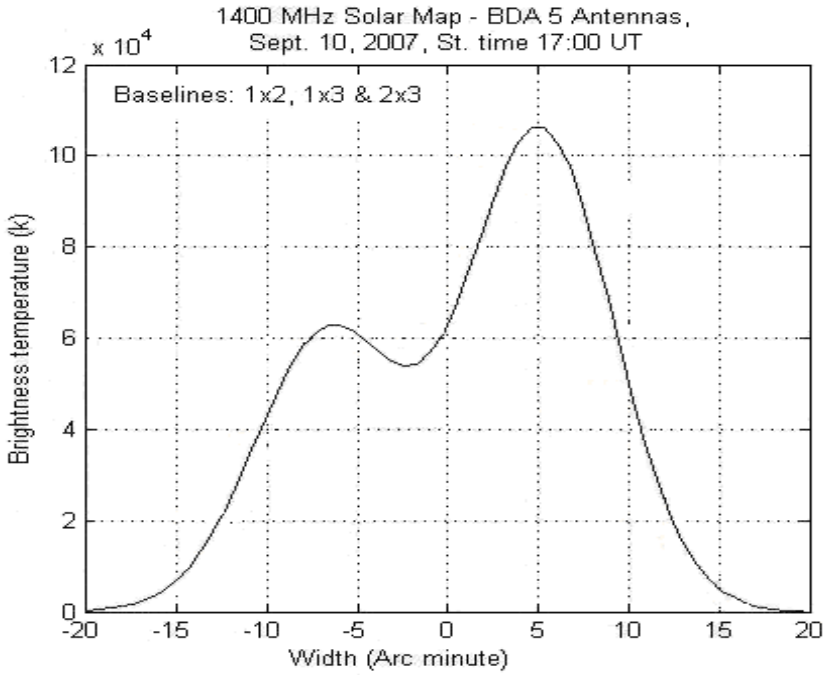

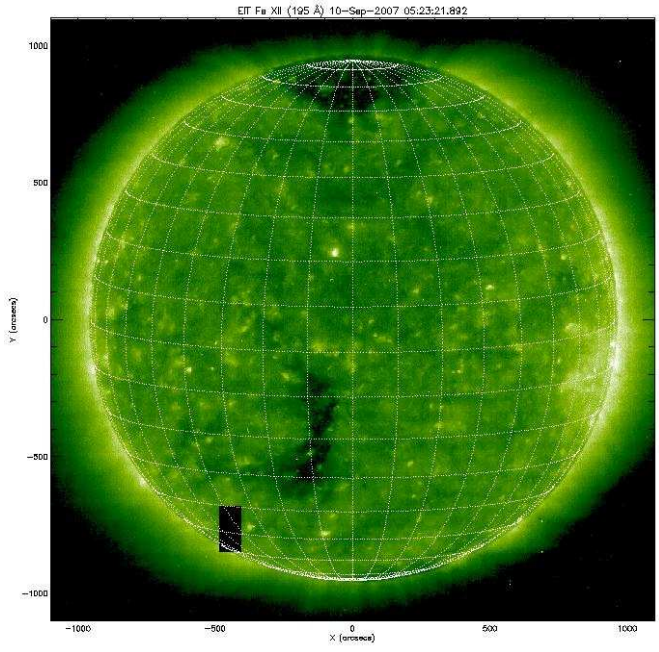

Fig. 1 – (Top) One-dimensional 1400 MHz brightness distribution of the Sun obtained on 10th Sept. 2007 at 17 UT, using 5-antennas BDA Prototype. (Bottom) EUV (175 Å) image of the solar corona on 10th Sept. 2007 at ~ 5:30 UT, obtained from EIT experiment on board SOHO satellite.

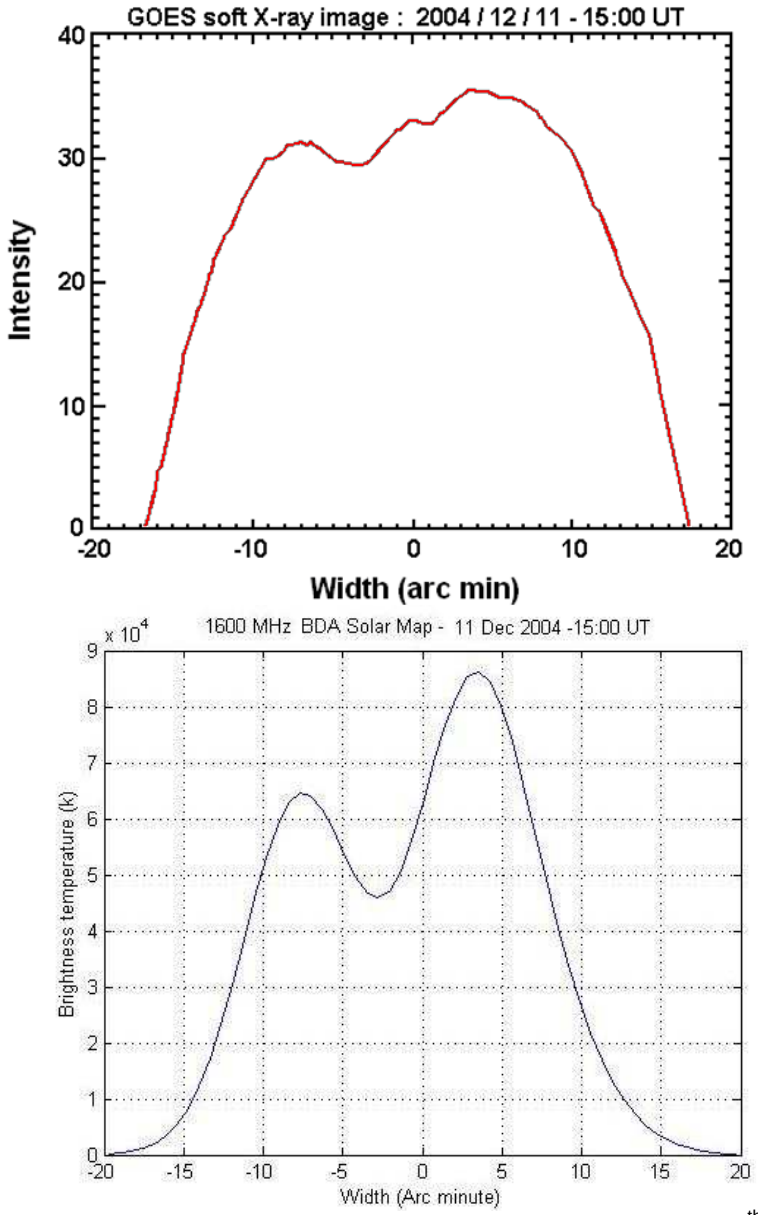

Fig. 2 – (Top) East-West one-dimensional soft X-ray image of the solar corona on 11th Dec. 2004 at 15 UT. Original two-dimensional image was integrated along the latitude (North-South direction) to permits a comparison with the radio brightness distribution obtained from BDA 1600 MHz observations (Sawant et al., 2007). (Bottom) One-dimensional 1600 MHz brightness distribution of the Sun obtained on 11th Dec. 2004 at 15 UT, using 5-antennas BDA Prototype.

DISCUSSIONS

Based on the results obtained by the application of the computational code developed some considerations must be done. First, in the code was implemented the empirical and simple algorithm

CLEAN due to the limited experience of developers on computation for interferometry. Despite this, at least a preliminary and operational code could be generated even though based on the most simple and traditional algorithm.

Second, the five element array was designed exclusively to perform engineering and operational tests of the several systems and sub-systems in the actual operation conditions at open land subjected to weather conditions as well as eventual interference signals. Although some results showing the proper performance of the interferometer could be obtained, those are not for scientific purpose due to the limited number of useful baselines with good data, 3.

The last, generated code is the first version only – alpha – supported by various hypothesis and assumptions. From this point there are at least two choices. To go ahead with the code development upgranding to a modern algorithm in a more sophisticated and complete code which attends the requirements of the BDA. The other choice is to adapt the data acquisition and formatting as a purpose the freely available Packages, e.g. AIPS, can be used to perform the reducing data to generate the interferometric images.

ACKNOWLEDGMENTS

We acknowledge FAPESP by the grant (06/55883-0) as a purpose of financial support to the second phase development of Brazilian Decimetric Array (BDA). Also, thanks are due to Dr. R. Ramesh, from IIAp, and Dr. S. Sirothia, from NCRA, from whom valuable discussions and informations were obtained which collaborated to the code development.

REFERENCES

Baars, J. W. M., Genzel, R., Pauliny-Toth, I. I. K., Witzel, A., *A&A*, 61, 99-106, 1977.
Cornwell, T. J., Evans, K. F., *A&A*, 143, 77-83, 1985.
Frieden, B. R., *J. Opt. Soc. Am.*, 62, 511-518, 1972.
Frieden, B. R., Burke, J. J. *J. Opt. Soc. Am.*, 62, 1202-1210, 1972.
Högbom, J. A., *A&A Suppl.*, 15, 417-420, 1974.
Jennison, R. C. *MNRAS***,** 118, 276, 1958.
Pearson, T. J., Readhead, A. C. S., *Ann. Rev. A&A*, 22, 97-130, 1984
Readhead, A. C. S., Wilkinson, P. N. *ApJ*, 223, 25-36, 1978.
Rogstad, D. H., *Applied Optics IP*, 7, 585, 1968.
Sawant, H. S. et al., *Solar Phys.*, 242:213-220, 2007.
Taylor, G. B., Carilli, C. L., Perley, R. A., *Astron. Soc. Pacific - Conf. Series*, Vol. 180, 2003.
Thompson, A. R., Moran, J. M., Swenson Jr., G. W., Krieger Publishing Co. Malabar, Florida, USA, 1994.
Wakker, B. P., Schwarz, U. J., *IAU Colloquium 131 ASP Conf. Series*, Vol. 19, 268, 1998.
Zirin, H., Baumert, B. M., Hurford, G. J., *ApJ.*, 370, 779-783, 1991.

SESSION 2 - RADIOASTRONOMY INSTRUMENTATION

Proceedings of the Brazilian Decimetric Array Workshop
São José dos Campos, Brazil - July 28 – August 1, 2008

HIGHLIGHTS OF RADIOASTRONOMY IN BRAZIL FOR THE LAST THREE DECADES

Zulema Abraham

Instituto Astronômico e Geofísico, USP

ABSTRACT

The development of radioastronomy in Brazil is strongly related to the installation of the 14 m Itapetinga radiotelescope, which operates in the frequency range 20-50 GHz. In the decade of 1970, it was crucial for the discovery of many southern hemisphere strong H_2O and SiO maser sources and to the follow up of their variable emission. It also resulted in the first detection of maser sources in external galaxies. The continuum thermal and non-thermal emission from galactic sources and from Active Galactic Nuclei were also studied, for which tracking and data acquisition techniques were developed, to overcome the limitations imposed by the fast changing sky contribution, typical at these frequencies. The Itapetinga radiotelescope participated in several VLBI campaigns related to the study of the changing structure of AGN cores, using the MARK II data acquisition system; the increase in the north-south baseline allowed the study of several equatorial sources with an almost circular beam.

SCIENCE WITH THE ITAPETINGA RADIOTELESCOPE

Since this workshop is dedicated specially to instrumental work, I will emphasize the improvements made to the Itapetinga radiotelescope, especially concerning its tracking facilities and data acquisition systems, which allowed most of the scientific work done during the last 30 years, which I will also discuss. The 13.7 m Itapetinga radiotelescope became available for radioastronomical work around 1973. It was the first radome enclosed radiotelescope build by ESSCO Corporation, and a large controversy arouse regarding its use for radioastronomy. Nowadays, similar radiotelescopes are used around the world (Finland, Spain, Korea, China, etc).

THE SCIENTIFIC CHALLENGE

Extragalactic Radioastronomy

During the decade of 1970, astronomers were discussing the nature of the recently discovered QSRs (Quasi Stellar Radiosources), specially their galactic or extragalactic nature (Hoyle et al., 1966; Rees, 1967; Jones and Burbridge, 1973; Burbridge, 1979). The main argument in favor of their galactic origin was the very high intrinsic luminosity that would result if they were at extragalactic distances.

The nature of the radio emission had been already attributed to incoherent synchrotron emission of a non thermal population of relativistic electrons rotating around the magnetic field lines (Alvén and Herlofson, 1950; Shklovsky, 1953). Soon after its association of QSRs with optical, high

redshifted objects, it was discovered that its flux density varied in timescales of months (Dent, 1965; Scholomitskii, 1965), Variability put constrains to the actual size of the emitting object: $l < 2ct_v\ (1+z)$, which allowed the calculation of the brightness temperatures, which needed to be $T_B > 10^{12}$ K, to avoid the Compton catastrophe. To explain the existence of sources with $T_B > 10^{12}$ K, Rees (1966) postulated the relativistic expansion of the emitting source. In this case, the time t_v, in the observer frame, must be multiplied by the Doppler factor δ of the relativistic expansion, which can be large, increasing in the same proportion the actual size of the emitting source $l < 2ct_v\ \delta(1+z)$.

The spectra of quasars soon extended up to 90 GHz, and presented different shapes. In some cases the spectra resembled that of the external regions of radiogalaxies, with the flux density decreasing with frequency as a power law. Other presented a canonical spectrum, decaying at both sides of a central frequency, also as power laws. However, a large portion of the spectra presented flat spectra, which would require a very specific combination of magnetic field and electron density distribution laws to be produced, this requirement was called the “cosmic conspiracy” (Cotton et al., 1980).

The decade of 1970 was dedicated to data collection. In Brazil, the recently inaugurated Itapetinga radiotelescope , with a radome enclosed 13.7 m dish, operated initially at 22 GHz and later on also at 30 and 43 GHz; it was used by Kaufmann et al. (1974) to obtain the brightness distribution of the central region of the nearest radiogalaxy NGC5128, also known as Centaurus A. Variability studies of this source in timescales of days and months showed some quiescent periods (Fogarty and Schuch, 1975), and others with variability in different timescales (Kaufmann et al., 1977; Kaufmann and Raffaelli, 1979).

Due to its proximity, Centaurus A appears as a powerful source. Quasars, on the other hand, even being intrinsically brighter, are so far away that their flux density is very low. This fact, together with the high contribution of the earth atmosphere, results in a very small signal to noise ratio and prevents the detection of a large part of them. The scheme used for these observations was beam switching, in which the signal introduced by the source and the sky in one horn is subtracted from the contribution of the sky, measured by another horn, at an offset of about 20’ in azimuth. The switching was made at a rate of about 100 Hz and the horn that observed the source switched periodically every minute (ON-ON). This method, which in principle eliminates the contribution of the atmosphere, can cause large errors in the measured flux, due to small difference of gain between the horns, inhomogeneities in the atmospheric emission and in the radome transmission. To eliminate these problems, several new observational methods were introduced in Itapetinga, involving changes in the tracking and data acquisition systems (Abraham, 1989). First, the interval in the ON-ON switching were reduced from 1 minute to 20 seconds, afterwards the ON-OFF synchronous method was introduced, intended to cancel the contribution of possible standing waves produced in the radome structure. Finally, the method of SCANS was introduced, in which the radiotelescope scans the sky with an amplitude, direction and duration fixed by the observer, passing in front of the source in the middle of the scan. This method resulted more reliable, because it allows visualizing a point source as a Gaussian at the center of the scan, with half power width equal to the beam width HPBW. Latter, a method was developed, using a noise source and a room temperature load, to compensate the atmospheric absorption even in the presence of a wet radome, which allowed variability studies, even when the source was visible during the night (Abraham and Kokubun, 1992).

The development of these observational techniques allowed the extension of the spectra of southern hemisphere QSRs to 22 and 43 GHz. They were, at that time, the highest frequencies used systematically (except for a few isolated measurements at 90 GHz). Initially, research was limited to the determination of the spectra of a sample of objects, which resulted to have either canonical,

decreasing power law or flat shapes (Medeiros, 1981). Comparison with spectra obtained at other epochs, extracted from the literature, show that some of them, classified as flat, had presented variations, which converted them, at least at high frequencies, in canonical, so that the phenomenological classification of QSRs lost its validity (Abraham, Medeiros & Kaufmann, 1984). Studies of variability using the scanning method started in 1980 and extends up to the present (Abraham, Medeiros and Kaufmann, 1984; Botti and Abraham, 1988; Tornikoski et al., 1993; 1996).

The existence of very small sources in the cores of quasars was confirmed by the first measurements made with VLBI (Very long Baseline Interferometry, which provided mas resolution. This technique involves two or more radiotelescopes, without any physical connection, separated by hundreds or thousands of kilometers. Besides finding unresolved sources, with sizes smaller than 1 pc, complex sources were discovered, with their structure changing with time. Two of the strongest quasars at radio wavelengths, 3C273 and 3C279, were modeled by the simplest two component model, but structural variations indicated that the the components were separating with superluminal velocities (Whitney et al., 1971; Cohen et al., 1971). These velocities are easy to explain through special relativity, if the emission arises in a jet, with relativistic bulk motion, which forms a small angle with the line of sight.

The temporal evolution of the superluminal components show that their flux density decreases as they separate from the core; in a few cases it first increases when the component is very close to the core, and afterwards it decreases, showing that the source became optically thin. As the components separate from the core, new components are formed. It is believed that the process involves the formation of shock waves, which propagate along the jet. The electrons are first accelerated, and afterwards they lose energy, first by the synchrotron process and afterwards by the inverse Compton and adiabatic expansion (Marsher and Gear, 1985). From the point of vies of single dish observations, the birth of a new component can be seen as a flare, starting at high frequencies (optical and infrared), and propagating to millimeter and radio wavelengths. Observations of variability at 22 and 43 GHz made at Itapetinga allowed the identification of several peaks in the light curves of 3C273 with the formation of new components in the parsec scale jet, detected with VLBI techniques (Abraham and Botti, 1990).

A Mark II VLBI data acquisition system was built in Brazil through a CNPq-NSF agreement, involving Itapetinga and Hystack observatories, and a 10.7 GHz was provided by CALTECH. The participation of Itapetinga in the interferometric observations was very important because it improved the north-south coverage of the u-v plane, especially important for equatorial sources, The first observations of 3C273 were performed in 1984 (Biretta et al., 1985), and repeated several times afterwards, including 3C279. These are the only two strong enough objects that can be observed with good signal to noise ratio. Otherwise, the integration time is limited by the stability of the rubidium atomic clock; the appropriate hydrogen maser clock was, by that time, too expensive for the Brazilian budget. When the VLBI acquisition system changed to MARK III, it also became too expensive, especially the magnetic tape storage system, and the observations were discontinued. The advent of the VLBA was also a factor in this decision, since it somehow provides a better coverage of the north-south baselines.

Here, there seem to be an appropriate place to comment on the difficulties of radioastronomy in Itapetinga during the first decades of operation, not only for the low budget, but also because of market protection, meaning that the acquisition of imported equipment, even computers was very difficult, and sometimes impossible. When these restrictions were lifted, the problem became the opposite, foreign countries, especially the USA, did not allow exportation of high technology, for security reasons.

Despite the observational difficulties, important theoretical work was inspired in the VLBI and

single dish variability studies. Interferometric studies along the years showed that the velocities and position angles in the plane of the sky of the different superluminal components remain constant for each component, but can vary by a large amount between components, (Carrara et al., 1993; Abraham et al., 1996). This behavior was attributed to jet precession and applied successfully to several objects: 2C279, 3C273, OJ287, 3C345, 3C120, BL Lac (Abraham and Carrara, 1998; Abraham and Romero, 1999; Abraham, 2000; Caproni and Abraham, 2004a; 2004b). The origin of the precession could be either a black hole system), with an accretion disk not coincident with the plane of the orbit (Romero et al., 2000), or the Bardeen-Peterson effect, produced by the misalignment between the relativistic jet and spin axis of a Kerr black hole (Caproni, Mosquera-Cuesta and Abraham, 2004; 2006a; 2006b; 2007).

Galactic radioastronomy

The decade of 1970 was also important for galactic radioastronomy. Surveys of the galactic plane were made at 408 MHz and 5 GHz, which allowed the classification of the sources in thermal HII regions and non-thermal synchrotron sources (Goss and Shaver, 1970; Shaver and Goss, 1970). These surveys are very important, because many of these regions are not visible at optical wavelengths because of the high extinction. At the same time, H and He recombination lines, representing the transitions between high quantum number states, were observed in the direction of HII regions, and the source distances determined using kinematic methods (Wilson et al., 1970). However, the detection of maser emission in transitions of molecules like OH, H_2O and SiO, was probably the principal discovery of that epoch (McGee et al., 1965; Cheung et al., 1969; Thaddeus et al., 1974). Itapetinga was specially equipped for maser observations, first with the 22 GHz receiver, appropriate for the water maser transition and latter at 43 GHz, for several transitions of the SiO molecule. Several unknown water sources associated with star forming regions and late stars were detected (Kaufmann et al., 1974; 1976; 1977; Scalise and Braz ,1980; Braz and Scalise, 1982). The SiO J=1-0 (v=3 transition was observed for the first time at Itapetinga at several late type supergiants detected (Scalise and Lépine, 1978; Lépine, Scalise and Le Squeren, 1978). The receivers were room temperature superheterodyne systems with a multichannel spectrograph consisting of 45 channels with 100 kHz bandwidth (about 1.3 km s^{-1} velocity resolution at 22 GHz). Weak sources were observed with a cryogenic H maser receiver lent by Haystack, in costly campaigns, since the He cooling system was not closed. Here again, we must emphasize the lack in Brazil of competitive receivers, which were lent by foreign observatories because of their interest in the new southern hemisphere discoveries. Besides new galactic masers we must emphasize the discovery of the first water vapor megamaser, in the galaxy NGC4959 (dos Santos and Lépine, 1979), in the Large Magellanic Cloud (Scalise, Gahm and Sandell, 1981) and the strongly polarized maser in Orion (Abraham et al., 1981; Abraham, Vilas Boas and del Ciampo, 1986; Vilas Boas and Abraham, 1988; Abraham and Vilas Boas, 1996).

In the decade of 1990, a close cycle cryogenic receiver, operating at 22-24 GHz, was acquired from NRAO though a FAPESP grant, which allowed the observation of the NH_3 transitions (Vilas Boas and Abraham, 2000; Caproni, Abraham and Vilas Boas, 2000). The H66α recombination line was also detected towards HII regions, and evidences of non-LTE conditions discovered in some of them; they must be produced in the very high density gas present in ultra-compact regions (Celoni, 1997).

The recent advances in infrared astronomy, with the construction of very sensitive imaging cameras, showed the existence of very young stellar clusters still embedded in their parent molecular cloud, as already predicted by the presence of far infrared IRAS point sources, with colors of ultra-

compact HII regions (Wood and Churchwell, 1989) and molecular line emission from high density gas (Bromfman, Nyman and May, 1996). Most of the radio continuum surveys have angular resolution of the order of 4' (Goss and Shaver, 1970; Shaver and Goss, 1970; Haynes, Caswell and Simons, 1978; Griffith and Wright, 1993; Condon, Broderick and Seielstad, 1989; 1991), which is not enough to study individual clusters, or very high resolution (obtained with interferometers, eg. Walsh et al., 1998), in which case only the very compact sources are detected. Itapetinga's 43 GHz detector has a HPBW of about 2', and turned out to be an intermediate tool to detect the embedded HII regions (Barres de Almeida, 2006).

FINAL REMARKS

Radioastronomy in Brazil had a difficult development; it suffered first from difficulties in the acquisition of competitive equipment, due to market protection, first in Brazil and afterwards in the rest of the world. It suffered also, especially in the last decade, for the lack of engineers in the technical staff of Itapetinga. It suffered finally of the hot and humid tropical weather that makes difficult to eliminate atmospheric emission at cm and mm wavelengths. However, the scientific work that can be done with the radiotelescope is still large: we have the whole galaxy to be mapped at 22 and 43 GHz, H recombination lines to be observed at wavelengths at which non-LTE effect can be large, and high density molecular clouds that can be map in the NH_3 and CS transitions.

REFERENCES

Abraham, Z., Cohen, N. L., Opher, R., Raffelli, J. C., Zisk, S. H., *A&A*, 100, L10, 1981.
Abraham, Z., Vilas Boas, J. W. S., Del Ciampo, L. F., *A&A*, 167, 311, 1986.
Abraham, Z., Vilas Boas, J. W. S., *A&A*, 290, 956, 1994.
Abraham, Z., Botti, L. C. L., in "Parsec-Scale Radio Jets", ed. J. A. Zensus e T. J. Pearson, Cambridge Univ. Press, p 226, 1990.
Abraham, Z., Carrara, E. A., Zensus, J. A., Unwin, S. C., *A&A* Supp. 115, 543, 1996.
Abraham, Z., Carrara, E. A., *ApJ*, 496, 172, 1998.
Abraham, Z., Kaufmann, P., Botti, L. C. L., *AJ*, 87, 532, 1982.
Abraham, Z., Medeiros, J. R., Kaufmann, P., *AJ*, 89, 200, 1984.
Abraham, Z., Tese de Livre Docência, IAG, USP, 1989.
Abraham, Z., Kokubun, F., *A&A*, 257, 831, 1992.
Abraham, Z., Romero, G. E., *A&A*, 344, 61, 1999.
Allvén, H. Herlofson, *N. Phys. Rev.*, 78, 616, 1950.
Barres de Almeida, U., PhD Thesis, University of São Paulo, 2006.
Biretta, J. A., Cohen, M. H., Hardebeck, H. E., et al., *ApJ*, 292, L5, 1985.
Botti, L. C. L., Abraham, Z., *AJ*, 96, 465, 1988.
Braz, M. A., Scalise, E., *A&A*, 107, 272, 1982.
Bromfman, L., Nyman, L-A., May, J., *A&ASS*, 115, 81, 1996.
Burbridge, G. R., *Nature*, 282, 451, 1979.
Caproni, A., Abraham, Z., Vilas Boas, J. W. S., *A&A*, 361, 685, 2000.
Caproni, A., Abraham, Z., *ApJ*, 602, 625, 2004a.
Caproni, A., Abraham, Z., *MNRAS*, 349, 1218, 2004b.
Caproni, A., Mosquera Cuesta, H. J., Abraham, Z., *ApJ*, 616, L99, 2004.
Caproni, A., Abraham, Z., Mosquera Cuesta, H. J., *ApJ*, 638, 120, 2006a.
Caproni, A., Livio, M, Abraham, Z., Mosquera Cuesta, H. J., *ApJ*, 653, 112, 2006b.

Caproni, A., Abraham, Z., Livio, M., Mosquera Cuesta, H. J., *MNRAS*, 379, 135, 2007.
Carrara, E. A., Abraham, Z., Unwin, S. C., Zensus, J. A., *A&A* 279, 83, 1993.
Celoni, L., PhD Thesis, University of São Paulo, 1997.
Cheung, A. C., Rank, D. M., Townes, C. H., Thornton, D.D., Welch, W. J., *Nature*, 221, 626, 1969.
Cohen, M. H., et al. 1971.
Cohen, M. H., Zensus, J. A., Biretta, J. A. et al., *ApJ*, 315, L89, 1987.
Condon, J. J., Broderick, J. J., Seielstad, G. A., *AJ*, 97, 1064, 1989.
Condon, J. J., Broderick, J. J., Seielstad, G. A., *AJ*, 1022041, 1991.
Cotton, W. D., Wittels, J. J., Shapiro, I. I., Marcaide, J. M., Owen, F. N., Owen, F. N., Spangler, S. R., Rius, A., Angulo, C., Clark, T. A., Knight, C. A., *ApJ*, 238, L123, 1980.
Dent, W. A., *Science*, 148, 1458, 1965.
Goss, W. M., Shaver, P. A., *AuJP*A, 14, 77, 1970.
Griffith, M. R. , Wright, A. E., *AJ*, 105, 1666, 1993.
Haynes, R. F., Caswell, J. L., Simons, I. W. J., *A&A*, 213, 148, 1978.
Hoyle, F., Burbridge, G., Sargent, W., *Nature*, 209, 731, 1966.
Jones, T. W., Burbridge, G. R., *ApJ*, 186, 791, 1973.
Kaufmann, P., Fogarty, W. G., Scalise, E., Schaal, R. E., *AJ*, 79, 933, 1974.
Kaufmann, P., Scalise, E., Marques dos Santos, P., Fogarty, W. G., *MNRAS*, 169, 15P, 1974.
Kaufmann, P., Gammon, R. H., Ibanez, A. L., Lépine, J. R. D., Marques dos Santos, P., Paes de Barros, M. H., Scalise, E., Schaal, R. E., Zisk, S. H., Carter, J. C., *Nature*, 260, 306, 1976.
Kaufmann, P., Scalise, E., Schaal, R. E., Gammon, R. H., Zisk, S., *AJ*, 82, 577, 1977.
Kaufmann, P., Marques dos Santos, P., Raffaelli, J. C., Scalise Jr., E., *Nature*, 269, 311, 1977.
Kaufmann, P., Raffaelli, J. C., *MNRAS*, 187, 23P, 1979.
Lépine, J. R. D., Scalise, E., Le Squeren, A. M., *ApJ*, 225, 869, 1978.
McGee, R. X., Robinson, B. J., Gardner, F. F., Bolton, J. G., *Nature*, 208, 1193, 1965.
Marscher, A. P., Gear, W. K., *ApJ*, 298, 114, 1985.
Medeiros, J. R., Dissertação de Mestrado, ON, 1981.
Rees, M. J., *Nature*, 211, 468, 1966.
Rees, M. J., *MNRAS*, 135, 345, 1967.
Romero, G. E., Chajet, L., Abraham, Z., Fan, J. H., *A&A*, 360, 57, 2000.
Scalise, E., Lépine, J. R. D., *A&A*, 65, L7, 1978.
Scalise, E., Braz, M. A., *A&A*, 85, 149, 1980.
Scalise, E., Gahm, G. F., Sandell, G., *A&A*, 104, 166, 1981.
Scalise, E., Braz, M. A., *Nature*, 290, 36, 1982.
Shaver, P. A., Goss, W. M., *AuJPA*, 14. 77, 1970.
Shklovsky, I. S., *Dokl. Akad. Nauk SSSR*, 90, 983, 1953.
Sholomitskii, G. B., *Sov. Astron*., 9, 516, 1965.
Thaddeus, P., Mather, J., Davis, J. H., Blair, G. N., *ApJ*, 192, 33, 1974.
Tornikoski, M., Valtaoja, E., Terasranta, H., Kotilainan, J., Lainela, M., Botti, L. C. L., *AJ*, 105, 1680, 1993.
Tornikoski, M., Valtaoja, E., Terasranta, H., et al., *A&A Supp.* 116, 157, 1996.
Vilas Boas, J. W. S., Abraham, Z., *A&A*, 204, 239, 1988.
Vilas Boas, J. W. S., Abraham, Z., *A&A*, 355, 1115, 2000.
Walsh, A. J., Burton, M. G., Hyland, A. R., Robinson, G., *MNRAS*, 301, 640, 1998.
Whitney, A. R., Shapiro, I. I., Roberson, D. S., Knight, C. A., Clark, T. A., Goldstein, R. M., Marandino, G. E., Vandenberg, N. R., *Science*, 173, 225, 1971.
Wilson, T. L., Mezger, P. G., Gardner, F. F., Milne, D. K., *A&A*, 6, 364, 1970.

Wood, D. O. S., Churchwell, E., *ApJ*, 340, 265, 1989.

Proceedings of the Brazilian Decimetric Array Workshop
São José dos Campos, Brazil - July 28 – August 1, 2008

CHINESE SPECTRAL RADIOHELIOGRAPH: SYSTEM OVERVIEW AND ARRAY DESIGN

Wei Wang[1], Yihua Yan[1], Jian Zhang[2], Fei Liu[1], Zhijun Chen[1], Guoshu Ji[1], Yujiang Dou[1], Linjie Chen[1], Junbo He[1]

[1]National Astronomical Observatories, Chinese Academy of Sciences,
Rd. Datun A20, Chaoyang Dist. Beijing 100012, China
(wwang@bao.ac.cn, yyh@bao.ac.cn)
[2]Beijing University,
Rd. Yiheyuan 5, Haidian Dist. Beijing 100871, China

ABSTRACT

This paper describes specifications and current progress on CSRH project. Also, receive system includes antenna, optical fiber, analog receiver and correlator is introduced. Furthermore, array design for CSRH project has been performed from early 2004, and we consider several configurations, such as T shape, Y shape and others, and choose spiral shape array finally. Some simulated results on array design are also presented in this paper.

Key-words: Radioheliograph, system design, array design

INTRODUCTION

Imaging spectroscopy over centimeter and decimetric wavelength range are important for addressing fundamental problems of energy release, particle acceleration and particle transport (Bastian et al., 1998). Therefore a new instrument capable of true imaging spectroscopy, with high temporal, spatial, and spectral resolutions is required to meet this end (Gary & Keller, 2004). The Chinese solar physics community had long been wishing to build a radioheliograph. Some pre-studies were carried out on proposals for radioheliograph in either centimeter-band (Hu et al., 1984) or millimeter-band (Fu et al., 1997), but none of these had been implemented. Following these lines, it was suggested to build a Chinese Spectral Radioheliograph (CSRH) in the decimetric to centimeter-wave range with a limited budget in the next few years (Yan et al., 2004). A prototype study of 2-element interferometer has been built and tested for overall design. The site survey for the CSRH array is carried out and a radio quiet region in Inner Mongolia of China appears promising.

CSRH SYSTEM OVERVIEW

In order to understand the coronal dynamics, there is a strong need to have high spatial, temporal and spectral resolutions in radio observations with CSRH or FASR (Bastian, 2003; Vilmer, 2006). The proposed specifications for the CSRH, as driven by scientific requirements, are shown in Table 1 (Yan et al., 2004).

The CSRH project is composed of two phase-phase I (400 MHz-2 GHz) and phase II (2 GHz-15 GHz). The block diagram of phase I is shown in Figure 1.

Table 1 - The specifications of CSRH

Frequency Range	0.4 - 15 GHz (λ:75 – 2 cm)
Frequency Resolution	64 or 128 chan (I: 0.4-2 GHz)
	32 or 64 chan (II: 2-15 GHz)
Spatial Resolution	1.3″- 50″
Temporal Resolution	<100 ms (0.4-15 GHz)
Dynamic Range	30 db (snapshot)
Polarizations	Dual circular L, R
Array	(40×4.5 m + 60×2 m) parabolic antennas
Lmax	3 km
Field of view	0.6° – 7°

PROTOTYPE EXPERIMENTS OF CSRH

A prototype study of two elements has been carried out for overall design since 2004 at Miyun radio observation station of NAOC. The prototype system includes two 4.5m antennas, LNA (Low Noise Amplifier), Optical transmitter, Optical fiber, optical receiver, radio frequency receiver and digital correlator receiver.

The two antennas are in the E-W direction and the baseline is 7.986 m. The left- and right-handed circular polarization signals are received by ANSERLIN (Annular Sector, Radiating-Line) feed in 1.2-1.8 GHz range mounted at the prime focus of each dish. LNA is connected to left-handed circular polarization port of feed. Optical transmitter and LNA are installed in a front-end box. The optical signal from each antenna is transmitted to the observation building located at a distance of 150 m from antennas through a 200 m long, phase-stable optical fiber. The amplified RF signal is mixed with two local oscillator signals, then down-converted to a single sideband IF signal (10-200 MHz). These signals are digitized using an 8bits, 400 Msps digitizier, and then pass through a digital filter bank. These digital signals were recorded in disk after A/D conversion so that we can process them in different ways (such as different bits quantization, frequency channelization method, Wang et. al., 2006). Also, we can prove the result of correlator by processing the recorded data. The signals from the two channels pass through delay lines and correlated with one-bit, two-level quantization. In delay adjustment unit, we have simultaneous 64 delay channel outputs within ± 80 ns shift in order to analyze the results.

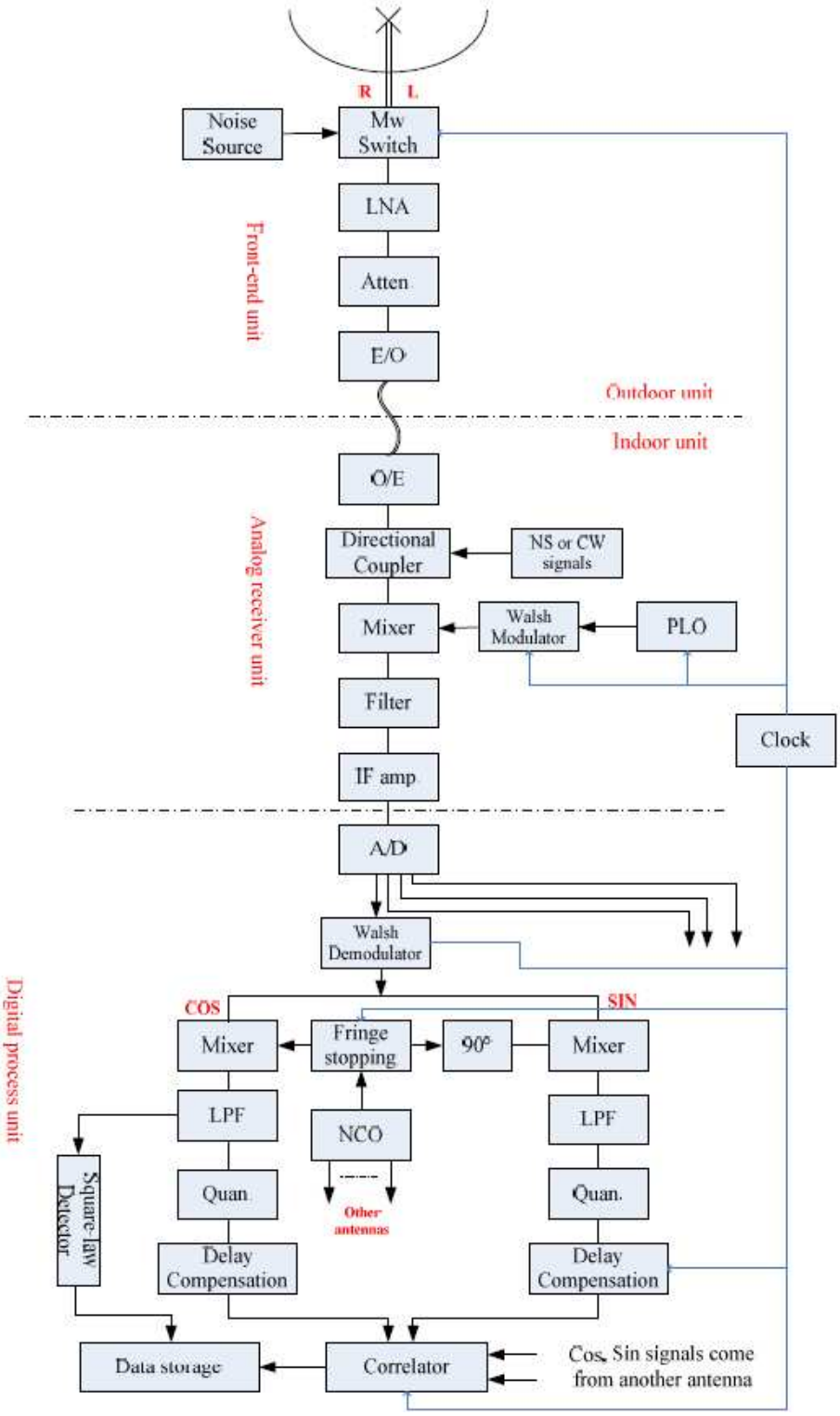

Fig. 1 - Block diagram of CSRH phase I.

Observational results

Observation of weather satellite: Before observing the sun, observation of weather satellite was carried out at Miyun station (longitude 116.977° E, latitude 40.558° N) during July 2005. The observing frequency was 1687.5 MHz, and bandwidth was 5 MHz. The first fringe was obtained by observation of satellite. We obtained very good correlated coefficient (>0.9) because the signal came from satellite is strong, compact enough and the satellite can be treated as a point source. This result corresponded well with theoretical analysis.

Observation of the quiet sun: We performed two days observation of the quiet sun using CSRH prototype system. The sun was tracked from 4:59 UT to 7:49 UT on July 7 2005, and observed data was recorded per 10 minutes. The other observation started at 1:45 UT and ended at 5:00 UT on July 8 2005, data was recorded per 5minutes. Observed fringe obtained in the sun observation was shown in Figure 2.

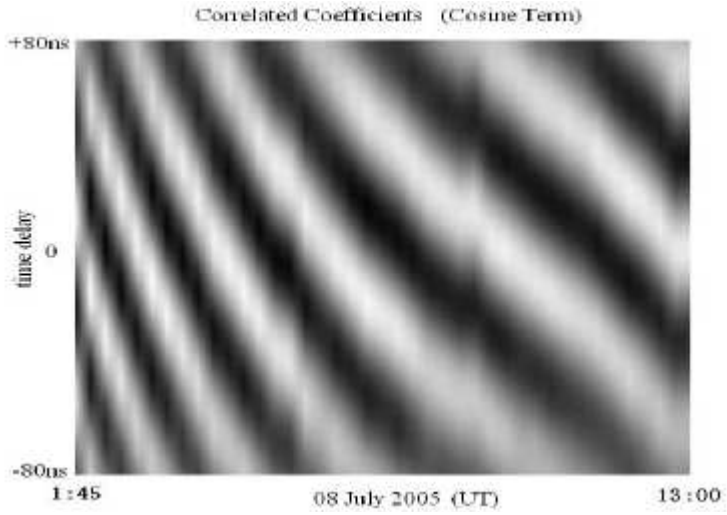

Fig. 2 - Observed fringe variation in 64 channels at a cadence of ~5 min with 8 m short baseline.

Generally, the quiet sun can be assumed as a uniformly bright disk in radio astronomy. Therefore, Fourier transform of uniform disk, which can be named as visibilities in interferometry, can be computed.

So, we computed the visibilities as the theoretical value to estimate observation of the sun with 2-element interferometer. In CSRH prototype experiments, correlated coefficients we observed is about 0.6~0.7. This value is in good agreement with the theoretical values.

As we all know that phase error is more important than amplitude error in modern interferometers, and phase errors are the dominant cause of poor imaging (Perley, 1989). Also, phase error is hard to estimate in CSRH prototype system although we took observation of satellite as calibration data to correct system error.

If the sun is quiet in our observed duration, the difference between phase center of the 2-element interferometer and center of the sun is dominant cause of phase error. Furthermore, antenna position errors and pointing error must be considered in these experiments.

So, theoretical phase can be calculated according to observing time, observing site, source position if the errors (include antenna position error and pointing error) were assumed. Also, phase of

visibilities can be derived from observed data. The difference between theoretical phase and observed phase is shown in Figure 3.

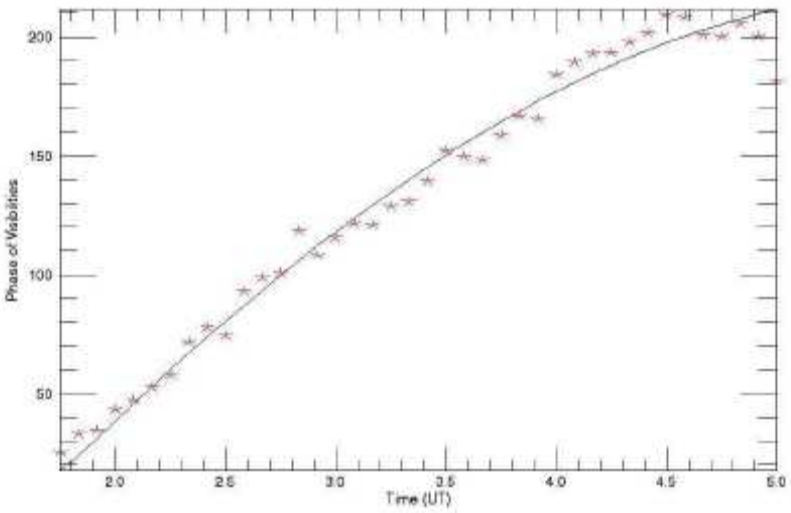

Fig. 3 - the phase change of visibility versus time deduced from observed data (star symbols) and the theoretic curve (the solid line) on 8 July 2005.

ARRAY DESIGN

As we all know that the method of aperture synthesis is based on sampling the visibilities function with separate telescopes distributed in the u-v plane. Imaging simulations clearly show that the exact distribution of antennas dose strongly affect imaging quality. For CSRH project, because of the limited antennas, we have to receive a small quantity of u-v sample points in the u-v plane, and even worse in snapshot. To obtain high quality radio imaging, an appropriate array configuration is necessary. So we do some work on array design for CSRH project from early 2004.

Because of the terrains constrain of observation site, we have compared four array design plans - “T”, “Y”, irregular, and spiral configuration, and without circular and triangle configuration. The irregular configuration in this paper based on the Boone’s algorithm. The fourth configuration is self-similar logarithmic spiral geometry, and Conway listed its advantages (Conway, 1999).

For the four configurations, we have simulated u-v data with abstract Fourier plane distribution. Base on scientific demands and engineering implement, we compared and analyzed above four configurations and chose the spiral configuration finally. The antenna position of spiral array is shown in left panel in Figure 4 and its dirty beam is shown in right panel.

Furthermore, some simulation observation for CSRH has already been carried out. We built a solar model based on solar image observed by SOHO/EIT. Then we simulated that phase I of CSRH observed the solar model at different time with different frequencies. The dirty image is cleaned by CLEAN arithmetic and Maximal Entropy Method. The source model and cleaned image by MEM are shown in Figure 5.

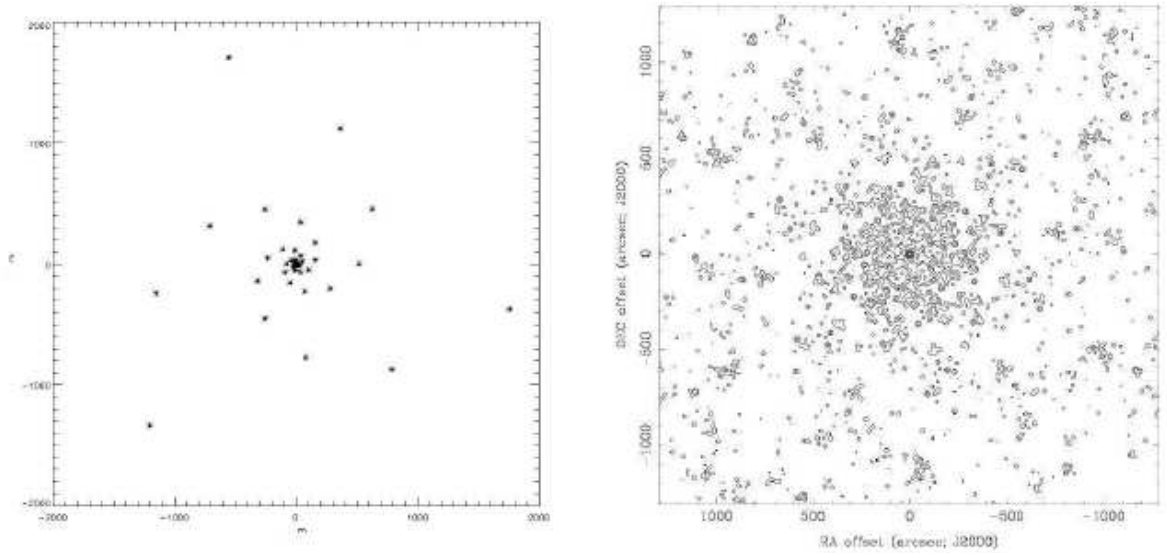

Fig. 4 - Antenna position and dirty beam.
Contours, 0.05, 0.1, 0.2, 0.3, 0.4, 0.5, 0.6, 0.7, 0.8, 0.9

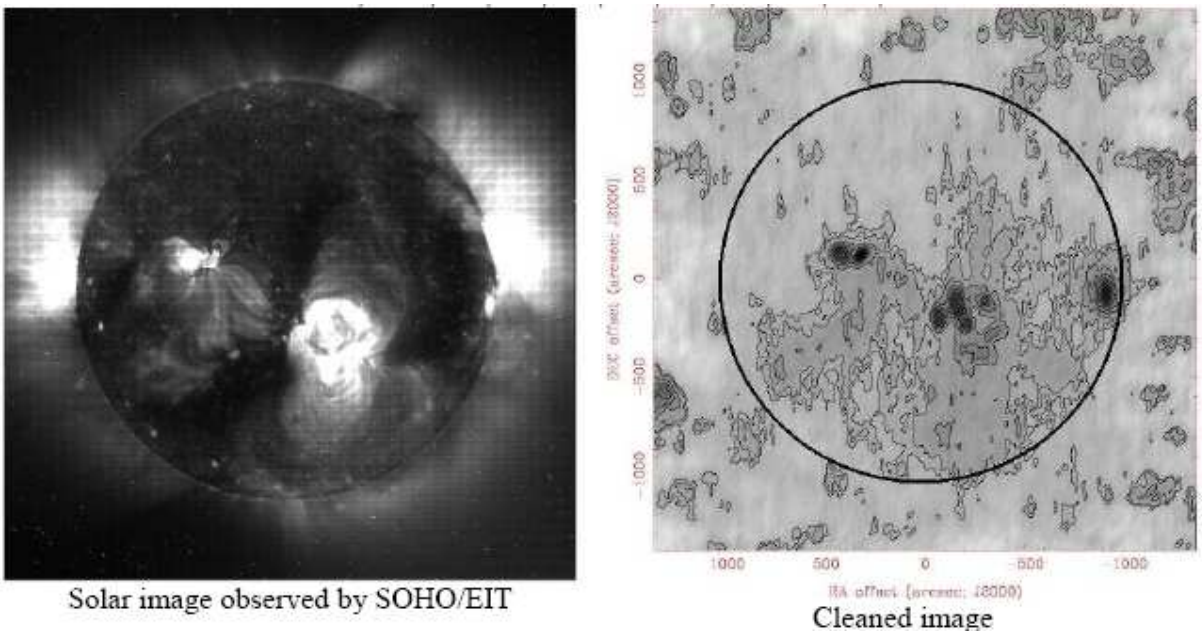

Fig. 5 - Source model and simulation observation.
Contours, 0.05, 0.1, 0.2, 0.3, 0.4, 0.5, 0.6, 0.7, 0.8, 0.9

SUMMARY

A radio heliograph with high temporal, spectral and spatial resolutions has been proposed. The key technology studies include array design for CSRH have been conducted. Furthermore, we believe CSRH and BDA will play important roles in solar physics and space weather studies.

ACKNOWLEDGEMENT

This work was supported by the National Basic Research Program of the MOST (Grant Nos. G2000078403 & 2006CB806301) and CAS-NSFC Key Project (Grant No. 10778605).

REFERENCES

Bastian T., Benz A., Dary D., *Ann. Rev. Astron. & Astrophys.*, 36, 131, 1998.

Bastian T., *Proc. SPIE*, 4853, 98, 2003.

Conway, J. "A Comparison of Zoom Array with Circular and Spiral Symmetry", MMA Memo 260, 1999.

Fu, Q., Xu Z., Qin Z., et al., *Astrophysics Report, Publ. Beij. Astron. Obs*., 30, 71, 1997.

Gary, D.E., Keller, C.U. *Solar and Space Weather Radiophysics* (Dordrechet: Kluwer) 2004.

Hu, C. M., Fu, Q., Li, S. D., et al., *ACTA Astrophysica Sinica*, 4(4), 340, 1984.

Perley, R.A., Schwab F.R., and Bridle A.H., "*Synthesis imaging in radio astronomy*", 1989, Astronomical Society of the Pacific Conference Series, 6, 477-500, 1989.

Vilmer, N. *Solar Activity: Progress and Prospects – 3rd French-Chinese Meeting on Solar Physics*, eds. C. Fang, B. Schmieder, M. Ding (Nanjing: Nanjing Univ Press), 2006.

Wang, W., Yan, Y., Zhang, J., et al., *Astronomical Research & Technology Publ. Nation. Astron. Obs. China*, 3(2), 128, 2006.

Yan, Y., J. Zhang, G. Huang, et al. in Proc. 2004 Asia-Pacific Radio Science Conference, Qingdao, China, eds. Tang, K. & Liu D. (Beijing: IEEE), 391, 2004.

CHINESE SPECTRAL RADIOHELIOGRAPH: CURRENT INVESTIGATION IN DIGITAL RECEIVER AND CONTROL SYSTEM

Wei Wang[1], Fei Liu[1], Yihua Yan[1], Jian Zhang[2] , Linjie Chen[1], Junbo He[1], Zhijun Chen[1] Guoshu Ji[1], Yujiang Dou[1]

[1]National Astronomical Observatories, Chinese Academy of Sciences,
Rd. Datun A20, Chaoyang Dist. Beijing 100012, China
(wwang@bao.ac.cn, yyh@bao.ac.cn)
[2]Beijing University,
Rd. Yiheyuan 5, Haidian Dist. Beijing 100871, China

ABSTRACT

In this paper, I will introduce several reasonable design of digital receiver and control subsystem in CSRH project. For digital receiver it seems reachable to get high resolution correlation result in both time domain and frequency domain by employing high sampling rate ADC (~1 GHz) and polyphase filter bank. By combining with FFT, frequencies in which we are interested could be synthesized and the bandwidth of certain frequency can be set flexibly as well. Another design is from traditional heterodyne and complex quadrature mixing, as a result, correlation results are in time domain. Control subsystem in CSRH is designed based on distributed control network.

Key-words: Radioheliograph, digital receiver, control system

INTRODUCTION

CSRH project is proposed for a dedicated solar radio synthesis array with high temporal, high space and high frequency resolution (Yan et al.), whose frequency coverage is from 400 MHz to 15 GHz. The first phase of CSRH project, which includes 40 antennas (400 MHz ~ 2 GHz), is under investigation and exploration. This paper will show two main parts of CSRH-I project — digital receiver design and control subsystem design.

PRIMITIVE DIGITAL RECEIVER DESIGN

CSRH primitive digital receiver design is based on heterodyne and complex quadrature mixing. 400 MHz is processed one time (e. g. instantaneous IF bandwidth output from analog receiver). In this case 1 GHz ADC over sampling is employed by the rule of Nyquist sampling theory. The complete specifications of digital receiver are listed in Table 1.

Table 1 Specification of digital receiver

A/D Sampling Frequency	1 Gsps, 8 bit
Instantaneous IF bandwidth	~400 MHz
Channel bandwidth	2, 4, 5, 6, 8, 10 MHz (-3 dB)
System time resolution	≤ 100 ms
Delay compensation accuracy	≤ 1 ns
Delay compensation range	0-10 us

Figure 1 shows the whole process of digital signal processing and correlation. To satisfy the requirements of flexible configuration of frequency being observed, numerical control oscillator is used to mix with signal from ADC to produce desired frequency. Fringe rotation is added up to the mixer. During observation channel bandwidth is supposed to be reconfigured, which is able to be implemented by reloading LPF coefficients stored in RAM in advance. 1-bit correlation is considered in primitive design but we are thinking over 2-bit or multi bit correlation now since in modern FPGA more hardware resource can be got than before.

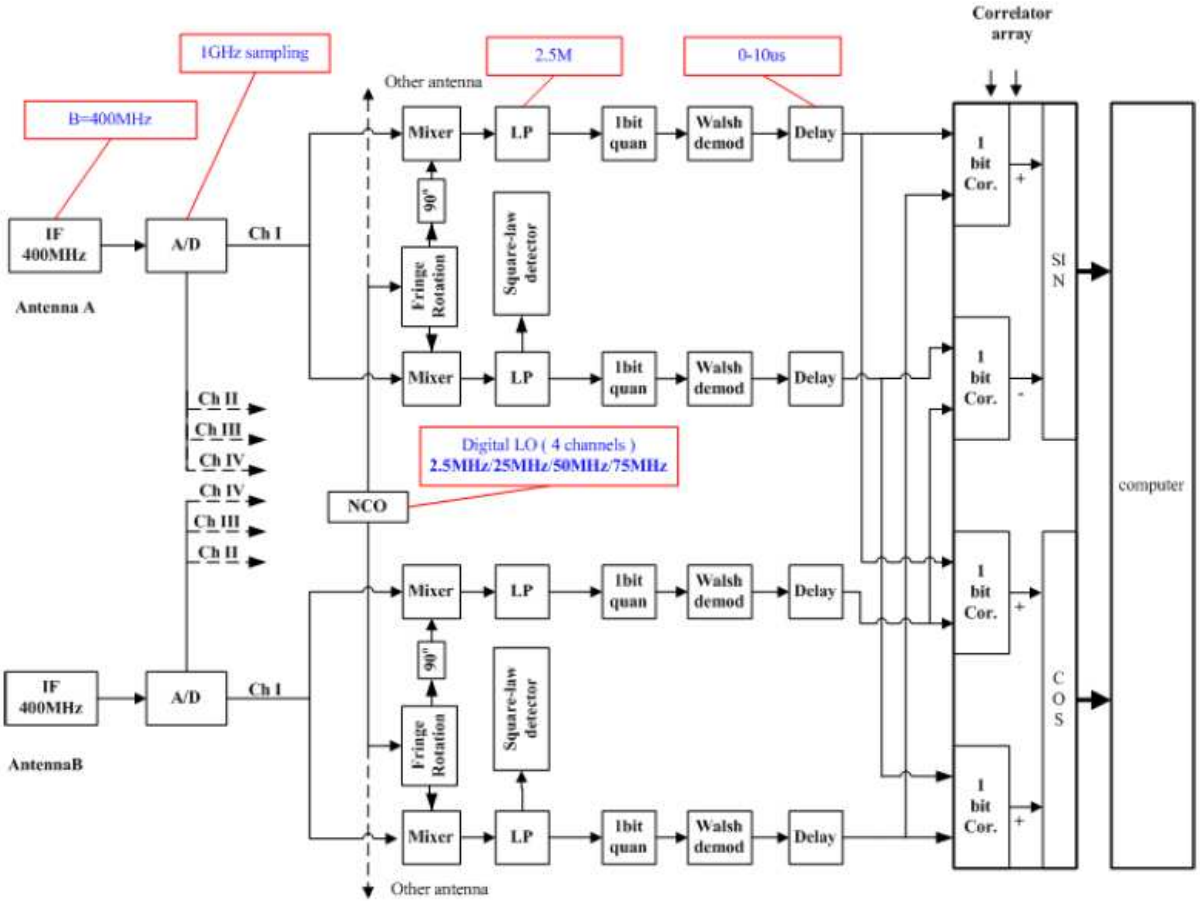

Fig. 1 - Primitive digital receiver principle block diagram (Chen et al.).

POSSIBLE STRATEGY IN DIGITAL CORRELATOR

In the mean time spectrum correlator design (in current case, it is FX) is considered as well. Compared with primitive digital receiver design, FX correlator can be implemented by polyphase LPF and FFT, which can produce lots of desired frequencies in one cycle. In addition, different channel bandwidth is achieved by frequency synthesizing after FFT. Figure 2 shows the FX correlation.

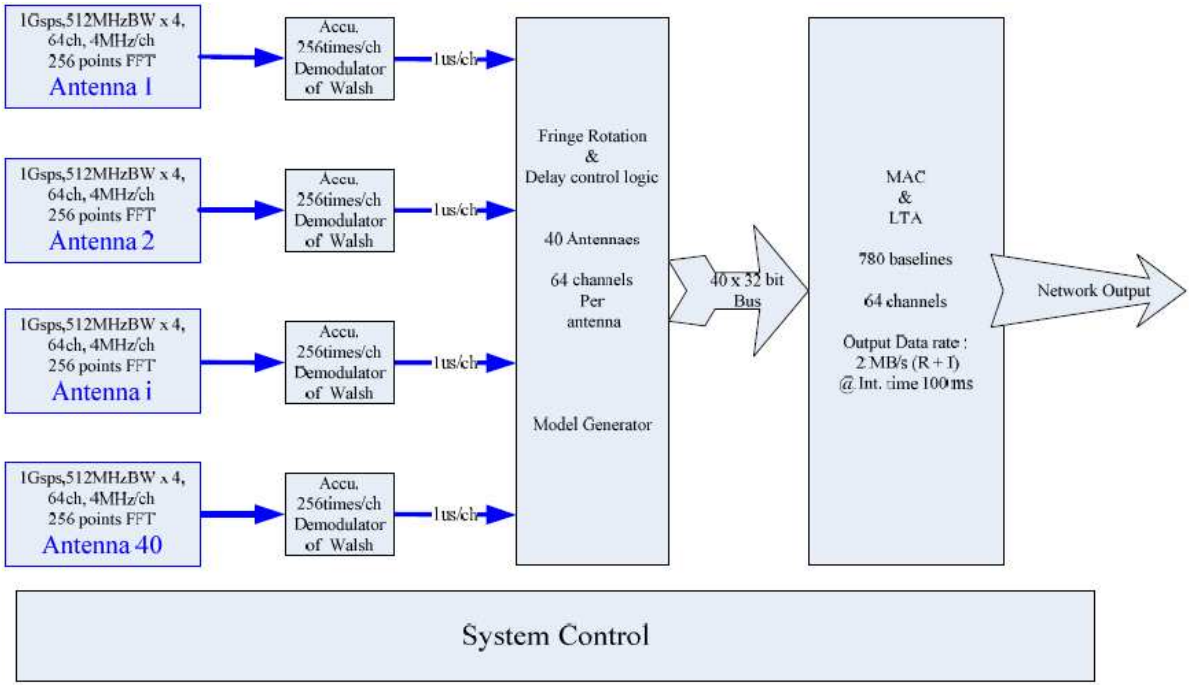

Fig. 2 - FX correlator block principle block diagram (Zhang et al.).

MONITOR AND CONTROL SUBSYSTEM

CSRH monitor and control subsystem is divided into two parts — 40 sets of antenna & front-ends and all devices indoor. For antenna & front-ends control, different embedded units run the individual control task in all antenna terminals. They are connected with central control computer by standard communication network. The possible connection method is point to point so far because different embedded units are not supposed to exchange information, and the possible communication network is Ethernet whose merits and faults are analyzed (Liu). Synchronizing control is required for all antenna tracking and polarization switching. For CSRH low frequency array (400 MHz ~ 2 GHz), max tracking error is ~ 9’ which is not a problem in synchronization. The key point is polarization switching in real time (e. g. every 3 ms). So we need to synchronize the local clock (on antenna terminal) with central clock carefully. The antenna & front-end control block diagram is shown in Figure 3. Clock for synchronization is transferred up and distributed to every antenna terminal.

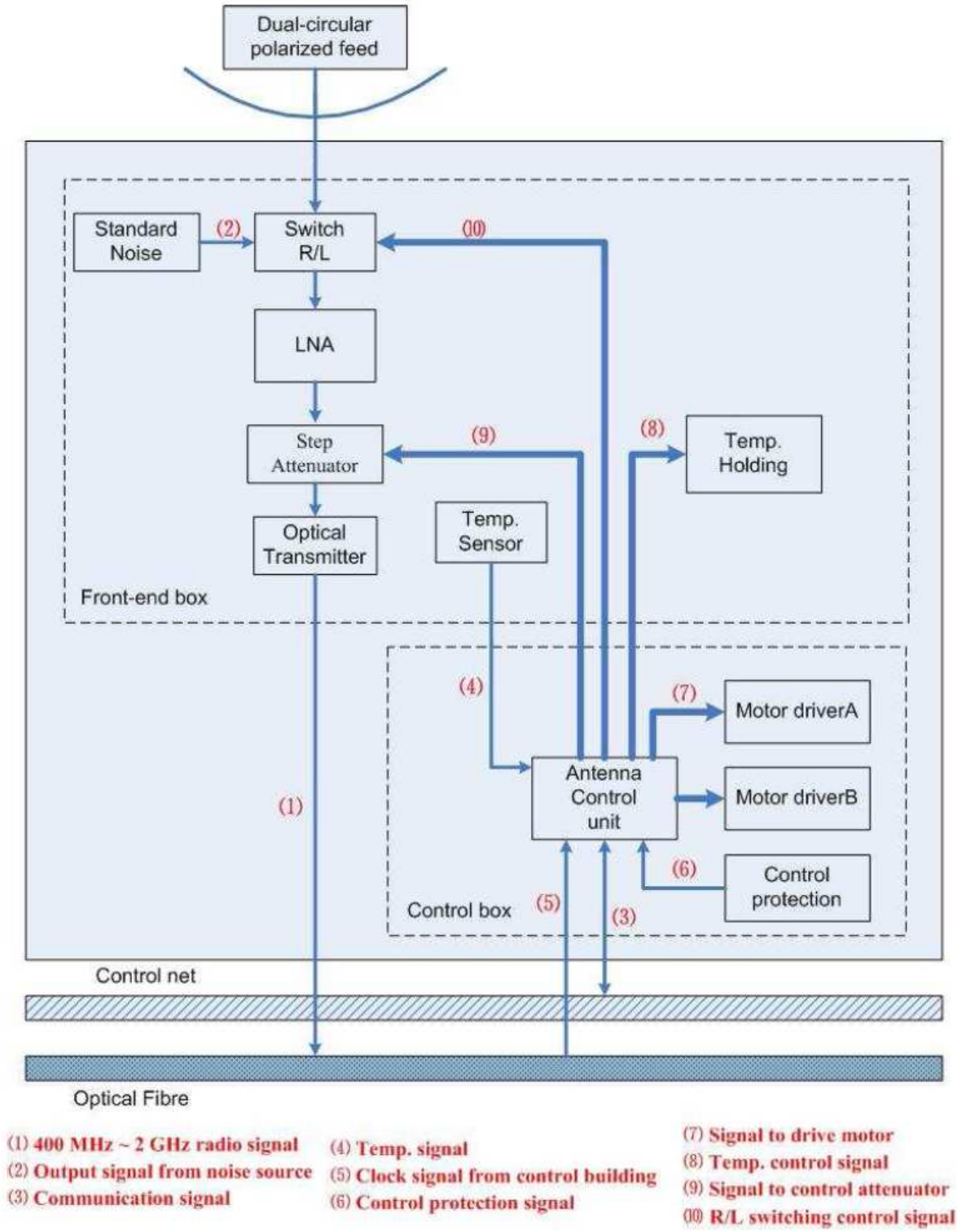

Fig. 3 - Antenna & front-end control block diagram.

SUMMARY

We present two methods to implement digital receiver in this paper. The primitive design is based on LPF banks, heterodyne and complex quadrature mixing. The other is FX correlator which is based on polyphase filter bank combining with FFT. Both methods are being evaluated now to not only satisfy system demands but can be implemented in low cost and high performance. We are also developing a prototype of monitor & control subsystem for CSRH.

Furthermore, we believe CSRH and BDA will play important roles in solar physics and space weather studies.

ACKNOWLEDGEMENTS

This work was supported by the National Basic Research Program of the MOST (Grant Nos. G2000078403 & 2006CB806301) and CAS-NSFC Key Project (Grant No. 10778605).

REFERENCES

Yan Y. et al., *Astronomical research & technology*, 3(2), 93-97, 2006. (in Chinese).

Yan, Y., Zhang, J., Huang, G. et al. in *Proc. 2004 Asia-Pacific Radio Science Conference*, Qingdao, China, eds.Tang, K. and Liu, D. (Beijing: IEEE), 391, 2004.

Chen L. et al., *Astronomical research & technology.* (accepted, in Chinese).

Zhang X. et al. (for discussion, in Chinese)

Liu F., PHD thesis. (in Chinese)

Perley, R. A., Schwab, F. R., Bridle, A. H., *Astronomical Society of the Pacific Conference Series*, 6, 477-500, 1989.

Proceedings of the Brazilian Decimetric Array Workshop
São José dos Campos, Brazil - July 28 – August 1, 2008

CURRENT STATUS OF FASR, AND COLLABORATION WITH BDA

Dale E. Gary

Center for Solar-Terrestrial Research
New Jersey Institute of Technology, Newark, NJ 07102

ABSTRACT

The Frequency Agile Solar Radiotelescope (FASR) design is now firmly established, and the project has been formally proposed to U.S. funding agencies. The broad range of science to be done with this major solar-dedicated radio facility is discussed. The details of the design and current status of the project are also given. The proposed site near Big Pine, California means that there should be excellent overlap in daily observing between the Brazilian Decimetric Array and FASR. Observations by the BDA below 2.5 GHz should be especially useful for collaborative studies.

INTRODUCTION

The Frequency Agile Solar Radiotelescope (FASR—Bastian, 2003; Gary, 2003) has now been formally proposed to US funding agencies (National Science Foundation), and its design has been finalized to the extent that its operation can now be envisioned in some detail. The original plan for the array called for of order 60-100 antennas in each of three arrays, each dedicated to different parts of the 0.05-21 GHz frequency range to be covered by FASR. The estimated cost of the full project was about $50 M. The funding opportunity that we have proposed for carries a lower funding cap of $25 M, which has forced a significant re-scope of the project. I give a brief history of the trade-offs that were necessary to reach the current design within the cost cap of $25 M. Having established the current design, I then revisit the science goals and list the expected performance of the re-scoped array for realization of these goals. All of the main science goals will be achieved with the rescoped array, and we are enthusiastic about FASR's impact on our understanding of the main problems in solar physics.

One of the impacts of the funding constraint is the decision to focus resources on the high-frequency (2-21 GHz) frequency range. The result is that the proposed FASR instrument calls for 15, rather than the original 80, antennas in the decimetric (300-3000 MHz) frequency range. This makes the Brazilian Decimetric Array (BDA) even more crucial to the success of FASR, by providing additional information about solar bursts observed by both instruments simultaneously. Such observations are made possible by the large overlap in observing time range for the two instruments.

ORIGINAL FASR DESIGN

The original FASR design called for three overlapping frequency ranges (0.05-0.35 GHz, 0.3-3 GHz, and 2-21 GHz) to be covered by three different receiving element designs, called FASR C, B and A, respectively. The numbers of antennas envisioned for each array were 60, 80 and 100 in the

three arrays C, B and A, with the FASR C elements being log-periodic dipoles, fat dipoles, or similar, FASR B consisting of 6 m dishes, and FASR A consisting of 2 m dishes. The total cost of the instrument was expected to be around $50 M, and included a 100-antenna correlator that would be time shared among the three arrays.

RE-SCOPED FASR DESIGN

The funding opportunity that we have responded to has a funding cap of $25 M for the entire project, with a funding profile of roughly $5 M/year. An assumed start in early 2009 will result in completion of the facility in 2013. The factor-of-two decrease from the originally assumed funding means that a re-scope of the instrument is necessary. By judicious choice of re-scope options, the FASR team has ensured that FASR will address all of its original science goals with an acceptable reduction in range of measurable quantities and speed of measurement. Table 1 lists the parameters of the re-scoped design, where the main change from the original design is in the number of antennas and in the number of simultaneously correlated antennas, with a small subsequent hit on the time required to complete a frequency-correlation cycle. The cost savings is realized partially by decreasing the number of antennas, which of course scales as N, but even more by the decrease in the size of the correlator, which scales roughly as N^2.

Table 1 - FASR Parameters.

Angular resolution	20/νGHz arcsec
Frequency range	50 MHz – 21 GHz
Number data channels	2 (RCP + LCP)
Total instantaneous BW	2 x 500 MHz
Frequency resolution	1% or 5 MHz
Time resolution	**A** (2-21 GHz): [snapshot 1 s] **B** (0.3-2.8 GHz): 1 s **C** (50-350 MHz): 0.2 s
Polarization parameters	IQ/UV
Number antennas	**A** (2-21 GHz): **B** (0.3-3 GHz): **C** (50-350 MHz): 15
Antennas correlated per integration cycle	30
Size antennas	**A** (2-21 GHz): 2 m **B** (0.3-3 GHz): 6 m **C** (50-350 MHz): LPDA
Array size	2.9 km EW x 3.8 km NS
Absolute positions	1 arcsec
Absolute flux calibration	<10%

As shown in Table 1, the re-scoped design calls for 45 FASR A antennas, and 15 each of FASR B and C elements. The correlator will be designed to correlate 30 antennas at once, doing three correlation cycles of the FASR A antennas, and using a fourth correlation cycle to correlate both FASR B and C arrays simultaneously. For example, if we separate the 45 FASR A antennas into 3

groups of 15 antennas, referred to as A1, A2 and A3, then the four correlation cycles will correlate group A1 with A2, group A1 with A3, group A2 with A3, and then B and C simultaneously. Since the correlator handles 500 MHz at one time, to cover the FASR B 0.3-3 GHz range requires 6 separate tunings. To cover the FASR A range (2-21 GHz) requires 38 tunings. The design calls for 20 ms data samples, for which the entire set of frequency- correlation cycles can be done in 3 s, although full-spectrum imaging in A array can be done in 1 s, and in B array in 0.5 s, while C array is fully sampled once every 0.1 s. In this way, a solar- science-relevant temporal cadence is maintained for all three frequency ranges so that the science goals are satisfied.

SCIENCE WITH FASR

The FASR science goals are largely unchanged with the re-scoped array. The science case for FASR was made in the book *Solar and Space Weather Radiophysics* (Gary and Keller, 2004). Although some imaging capabilities are compromised or will be made less often, the image quality, spectral, and temporal resolutions are sufficient to answer the science questions. The four main science areas are

1. The Nature and Evolution of Coronal Magnetic Fields
2. The Physics of Flares
3. The Drivers of Space Weather
4. The Physics of the Quiet Sun

All of these science goals target measurement of magnetic fields in one form or another, as the heretofore largely invisible driver of the Sun's activity and atmospheric structure. FASR will for the first time provide sufficient spatial, spectral, and temporal resolution to allow the use of magnetic field diagnostics on a regular basis, and in a wide range of phenomena, including active regions, flares, CMEs and even quiet regions.

The FASR A array will provide the key observations for areas 1 and 2, above, and hence the re-scope ensures enough antennas (45) to retain all of the key science involving that area. Snapshot imaging with FASR A will be extremely good, to allow imaging of rapidly varying solar bursts. From inversion or forward modeling of the resulting spatially resolved spectra, magnetic fields will be determined precisely in and around flaring loops. These spectra also supply diagnostics of other plasma and particle parameters, such as temperature, density, numbers of high-energy electrons, electron energy spectra, and pitch angle.

With a small amount of Earth rotation synthesis (e.g. over 0.5-1 hour), active region magnetic fields will be measured in exquisite detail via their gyroresonance emission, making FASR into a coronal magnetograph. This will provide a standard data product for comparison and extension of photospheric field extrapolations.

FASR A will also image the CME precursor environment, eruption phenomena, and perhaps some CMEs themselves that emit at higher frequencies. FASR B, on the other hand, will be working in the same frequency range as BDA and will help to open this frequency range to imaging observations for the first time (e.g. review by Bastian et al., 1998). In this frequency range, solar bursts occur in a bewildering variety, and are expected to illuminate the very regions where magnetic reconnection takes place - the phenomenon that is responsible for explosive release of magnetic energy, and for restructuring the corona. Finally, FASR C will image bursts in the metric range, providing information on the location and propagation of electron beams and shocks.

Perhaps the most exciting aspect of FASR is that it provides images at all of these frequencies at

once, to give a simultaneous, perfectly registered view of the flare, eruptive phenomena, associated bursts, and all of their consequences, with quantitative diagnostics. This panoramic view of solar activity will revolutionize our understanding of the Sun.

COLLABORATION WITH THE BRAZILIAN DECIMETRIC ARRAY

Within the frequency range covered by FASR, the decimetric range is perhaps the most exciting. This range has been almost completely unexplored with spatial resolution, while the many observations with spectrographs have shown an extremely rich and fertile ground for studying flare energy release and plasma physics. The BDA will also exploit this frequency range, and as such will be at the forefront of progress in this area of solar physics. Because of the FASR re-scope, the number of antennas (15) - and hence its imaging capability - will be limited. The BDA can fill in this gap by fielding a larger number of antennas, potentially providing a higher dynamic range for following the weaker and more complex emissions that would be invisible to FASR.

Given the fact that FASR and BDA will enjoy a significant amount of overlapping observation time (being at similar longitudes), there are ample possibilities for combining the strengths of the two instruments. This includes both observations and cross calibration. For example, a burst seen simultaneously by both instruments at the same frequency can be compared quantitatively to ensure that both instruments obtain consistent results. Any calibration differences will be readily apparent, and the cause can be discovered and corrected. At most times of the year, BDA will also extend FASR's observation time, and vice versa, since BDA will acquire the Sun before it rises at the OVRO site, and FASR observations will continue for a time after the Sun sets for BDA. Thus, there are several ways in which BDA and FASR observations in the decimeter band will enrich each other.

CONCLUSION

The FASR project will soon be underway, with construction occurring in parallel with the BDA development. It is important that these two efforts be coordinated to some extent, to maximize the value of the future collaboration. FASR will revolutionize our understanding of the Sun by providing the most complete view of the radio window that we can design. BDA will extend FASR's capability in the important decimetric part of that window, which has heretofore been largely unexplored. New discoveries await, and both instruments will be at the forefront of a new era in solar physics research.

REFERENCES

Bastian, T. S., Proc. SPIE, 4852, 98, 2003.
Bastian, T. S., Benz, A. O., Gary, D. E., *Ann.Rev. Astron. Astrophys.*, 36, 131, 1998.
Gary, D. E., *J. Korean Astron. Soc.*, 36, 135, 2003.
Gary, D. E., Keller, C. U., Springer, *Astrophysics and Space Science Library*, vol. 314, 2004.

Proceedings of the Brazilian Decimetric Array Workshop
São José dos Campos, Brazil - July 28 – August 1, 2008

INTERFEROMETERS, USERS AND SCIENCE - THE SOFTWARE LINK

Gordon Hurford

Space Sciences Laboratory
University of California, Berkeley, CA, USA 94720

ABSTRACT

A sometimes under-emphasized element in the development of new observing facilities tools is the software. While often representing 5 to 20% of the cost of a new system, it can easily be taken for granted in the planning and construction until relatively late in the development program. This talk will review the role and character of interferometer software required to vet the hardware, meet the needs of the user community and in shaping the character of the science that a new facility can achieve. The talk will be illustrated with the experience of RHESSI (which does Fourier transform solar imaging in hard x-rays and gamma-rays), and the plans for FASR (the Frequency-Agile Solar Radiotelescope), and will attempt to relate these experiences to the BDA.

INTRODUCTION

The purpose of this talk is to review the role and character of interferometer software in vetting the hardware, in meeting the needs of the user community and in shaping the character of the science that a new facility can achieve. I will begin with some general software considerations as they relate to solar facilities, illustrate these considerations with RHESSI and FASR and then suggest how they might be relevant to the BDA. The treatment will be very general, and much of what I will say is quite mundane, and for this I apologize in advance. If, however, there are bits that are controversial, then perhaps this will provide the basis for useful discussions.

GENERAL CONSIDERATIONS

Software provides the interface between an interferometer's hardware and its users. As such the software and hardware have comparable impacts on the ultimate success of a facility. It represents a growing fraction of the cost of modern facilities, often more than 20% of the total facility cost. Despite this, software is sometimes taken for granted in the planning and implementation of a program and not given much attention in planning until relatively late.

The role of software has some additional implications; its development provides an excellent way to involve students; its development can provide an effective vehicle for involving remote collaborators. In the longer term, upgrading the software provides a powerful and cost-effective way to upgrade the performance and capabilities of an instrument.

BROAD FACTORS AFFECTING SOFTWARE DESIGN

In designing the software for a solar interferometer, there are several rather basic questions which much be considered.

"What are the goals of the facility?" There are many possibilities here: to support technology development, either locally or globally; to provide a tool for educating students; to act a prototype for a future facility; to provide observational support to other instrumentation; to provide a significant advance in capability of previous similar instruments; to provide synoptic data in support of solar activity forecasting or nowcasting; to be an exploratory instrument operating in a previously unexploited observational domain. The relative importance of these and other possible goals for a given facility has profound effects on how its software should be designed.

What type of operation is planned for the interferometer? Will it be operated for a few times or for many years to come? Will it be user-controlled with a series of custom observing programs or in a standardized way? Will there be professional operators, by the users themselves or is it fully-automated?

Who are the users? Are they students (perhaps inexperienced, but eager to learn and contribute)? Are they hands-on scientists with broad experience in the field? Are they scientists in closely-related fields with interest in the data but limited time to learn the observing or data reduction techniques? Are they members of other science communities, who are interested in only the final results?

There are many 'customers' who will be using the software, each with their own needs and preferences. For example the operators, who interact with the control software need real-time feedback on broad aspects of array performance and in some cases, in the current state of solar activity. The engineering staff needs to have effective access to data for failure identication and to evaluate quantitative aspects of array performance. The science staff needs to be able to effectively edit and calibrate the data, evaluate the more subtle aspects of array performance and generate the data products upon which the subsequent science is based. The external community not only needs access to the final calibrated data products (e.g. light curves, images and/or spectra), but also to the metadata that serves as an index to what is available. For this community, convenience is critical.

For the data analysis software, the anticipated data volume and processing requirements are of course fundamental factors. The anticipated RFI environment and atmospheric attenuation can also be important. Less obvious is the question of whether the analysis will be done by full-time or 'guest' analysts and what is the 'style' of the analysis. This can range from case-by-case custom reduction to routine procedures to fully-automated pipelines.

What are the programming resources available? The experience and language-familiarity of the software team is obviously a factor here as is of course, the available time, budget and computing hardware. Also relevant is whether the software development is to be subcontracted to a commercial concern, or be done by in-house software professionals, by done by scientists or by students.

Almost all of the possibilities suggested above could be illustrated by one or more existing or planned facilities. I'll illustrate this with two current examples of solar facilities.

RHESSI

The Reuven Ramaty High Energy Solar Spectroscopic Imager (RHESSI) is a NASA small explorer mission launched in 2002, that provides high spatial and spectral resolution observations of x-rays and gamma-rays in solar flares. Why is it relevant to an interferometer workshop? First, like the solar program of the BDA, its observation program is directed to transient phenomena rather than a variety of fixed targets. Like an interferometer, it uses indirect imaging techniques (as opposed to

pixelated detectors in a focal plane) and so requires image reconstruction. In fact its image reconstruction is the precise mathematical analog to that required to convert interferometer data to images.

RHESSI is an exploratory instrument, doing the first imaging spectroscopy at x-ray energies and the first solar gamma-ray imaging. As such, many of parameters of its targets (e.g. size scales) and some of its current uses (e.g. a search for axions) were not foreseen. Although there are many in the solar community who are keenly interested in the data, there was and is a very limited population of those that combine knowledge of both high-energy solar x-rays and the image reconstruction techniques.

RHESSI's data volume was moderate by current standards (1.8 GBytes/day) but its handling still required some consideration since over 6+ years this has built to ~4 Terabytes. The character of the data provided both special problems and opportunities. The transmitted data was based on the arrival time and energy of each detected photon. This provided the opportunity to choose the 'exposure time', field of view, imaging parameters, energy range and resolution when the data were analyzed in response to the event and objectives under study rather than at the design phase. While this flexibility has magnified the effectiveness of the data, it has provided users with an unfamiliar array of decisions. It also implied that almost all science analyses start from level-0 (raw) data, rather than from higher-level data products. Figure 1 shows the overall operations and data flow.

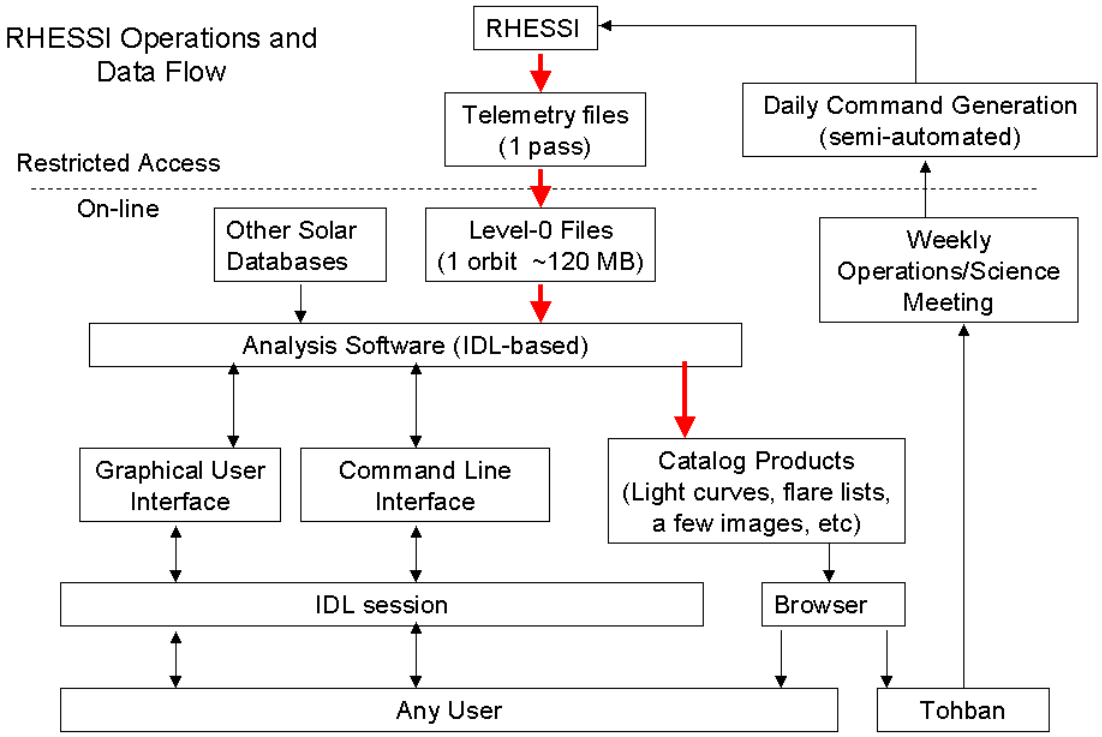

Fig. 1 - RHESSI Data Flow.

FASR

FASR is a proposed interferometer that represents quantum step forward in terms of its combination of radio imaging and frequency coverage. Its parameters are shown in Table 1.

The primary challenges here are threefold – first, as with RHESSI, the majority of the user community has little experience with the techniques required to analyze the data; second the RFI environment is an important factor, and third, the data volume and processing requirements are rather substantial. For example the output of the correlator is ~500 Mbytes/second (~25 Tbytes/day) which is to be reduced to an archival data volume of ~50 Gbytes/day. Figure 2 illustrates the current approach towards addressing this task.

Table 1 – FASR Parameters

Angular resolution	$20/\nu_{GHz}$ arcsec
Frequency range	50 MHz – 21 GHz
Number data channels	2 (RCP + LCP)
Total instantaneous BW	2 x 500 MHz
Frequency resolution	1% or 5 MHz
Time resolution	**A** (2-21 GHz): 3 s [snapshot 1 s] **B** (0.3-2.8 GHz): 1 s **C** (50-350 MHz): 0.2 s
Polarization parameters	IQ/UV
Number antennas	**A** (2-21 GHz): 45 **B** (0.3-3 GHz): 15 **C** (50-350 MHz): 15
Antennas correlated per integration cycle	30
Size antennas	**A** (2-21 GHz): 2 m **B** (0.3-3 GHz): 6 m **C** (50-350 MHz): LPDA
Array size	2.9 km EW x 3.8 km NS
Absolute positions	1 arcsec
Absolute flux calibration	<10%

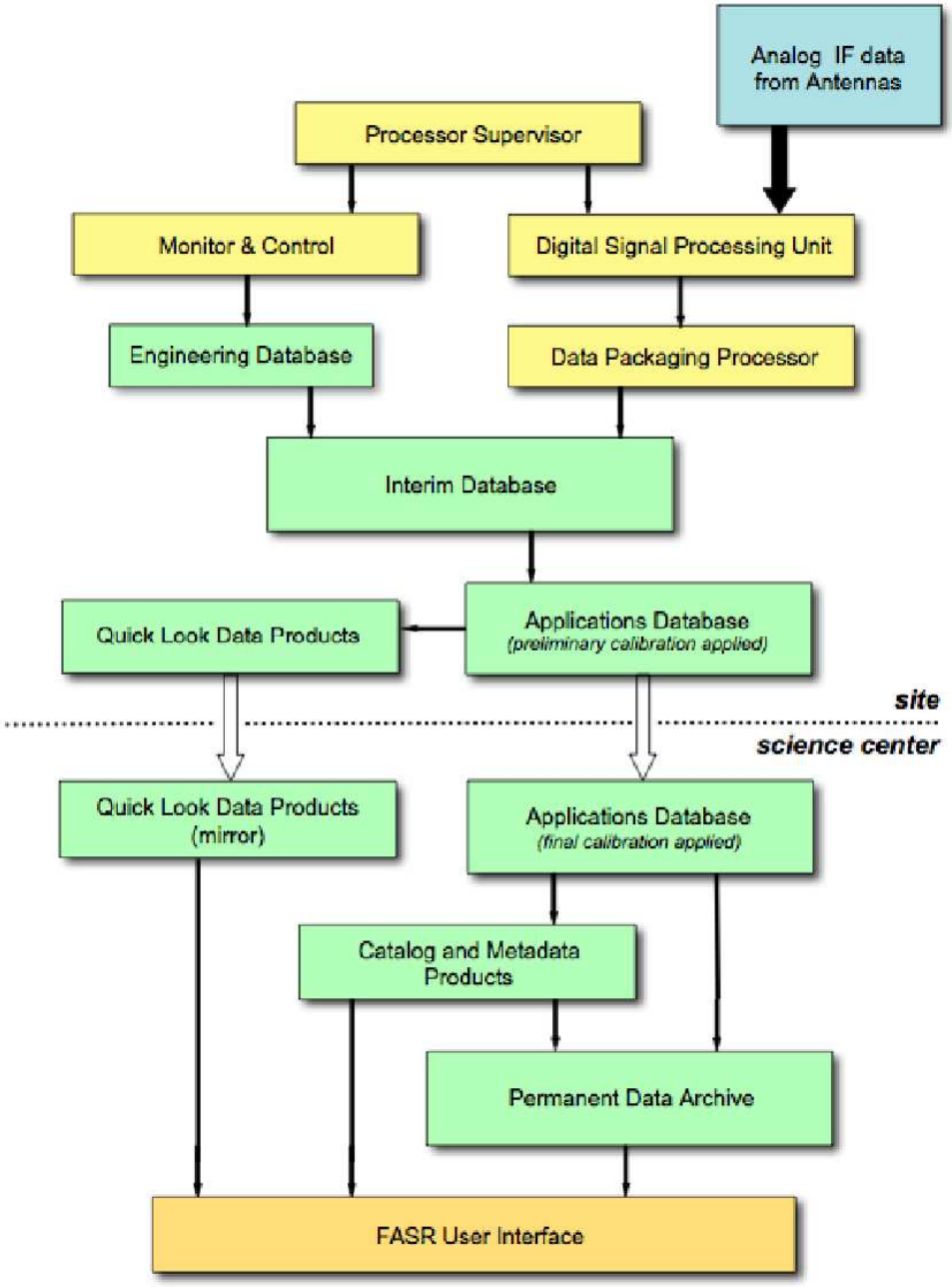

Fig. 2 - FASR Data Flow.

APPLICATION TO THE BDA

To illustrate how these considerations might be applicable to the BDA, let me take the risky step of reviewing some of the BDA's potential impacts. I'll ask your forgiveness in advance for my mis-state the case.

At the national (Brazilian) level, the BDA is providing an excellent vehicle for developing technology infrastructure. It also provides a rich resource for student training and involvement in engineering, astronomy and software. As this meeting illustrates, it encourages international scientific and technical collaboration. Through the joint study of specific events, it will also provide the basis for effective access to internationally sources of other solar data

On a worldwide level, the BDA will provide high-sensitivity radio coverage of solar activity in a distinct (and under-represented) longitude range. It can provide burst positions and flux values valuable for joint interpretation with other data. Continuous operation would provide a new synoptic database for solar activity.

SOFTWARE IMPLICATIONS FOR THE BDA

What do such potential impacts have to do with software design?

Maximizing the impact on technology development requires effective, quantitative feedback on array performance (e.g. phase stability). Maximizing its impact in the broader technical and general communities can be helped by the BDA website and by public outreach programs.

Student involvement, for example in software design, requires choosing software approaches that encourage contributions and adaptation, rather than the direct adoption of existing legacy packages which, in some cases, can present a formidable barrier to modification.

The exploitation of the BDA's longitude advantage would be aided if plans called for daily operation. That in turn has implications for the desirability of automation of both the control and analysis software.

Possible application to synoptic monitoring of solar activity, would also require a program of daily observations, but it would also place demands on the robustness and speed of routine data product generation.

To exploit its capability for burst position measurements, considerable effort in phase stability and calibration protocols are required.

Finally, to exploit its role in the international solar community, it is a fact of life that any modern facility must provide access to calibrated data products to non-specialists that is both convenient and timely.

REFERENCES

Lin, R. P. et al., *Solar Phys.*, 210, 3, 2002.

Bastian, T. S., in Solar and Space Weather Radiophysics, D. E. Gary and C. U. Keller, eds. Kluwer, p47, 2004.

SESSION 3 - SOLAR INVESTIGATIONS

Proceedings of the Brazilian Decimetric Array Workshop
São José dos Campos, Brazil - July 28 – August 1, 2008

SOLAR SCIENCE WITH THE BRAZILIAN DECIMETRIC ARRAY

Natchimuthukonar Gopalswamy

NASA Goddard Space Flight Center,
Greenbelt, MD 20771, USA

ABSTRACT

The Brazilian Decimetric Array (BDA) is a unique solar dedicated radio imager operating at short wavelengths probing the corona where most of the phenomena of heliospheric consequence originate. Currently, the Very Large Array (VLA) is the only instrument in the American continents that observes the Sun in this wavelength range, but it is not a solar dedicated instrument. The Siberian Solar Radio Telescope operates at a single frequency (5.7 GHz). BDA has wide open the radio window in the frequency range 1-6 GHz with an important band at 2.8 GHz not used by the VLA. Radio images obtained by BDA correspond to the region where flux ropes form and propagate into the interplanetary medium carrying nonthermal electrons. These images provide important information on the physical state of the eruptive structures and the post-eruption arcades left behind in the corona. The BDA with its wide field of view will be well-suited for observing prominences and filaments, which are the core structures of coronal mass ejections. The BDA can also observe the other source of space weather, viz., coronal holes, which produce high speed streams and geomagnetic storms. This paper provides an overview of these important issues that will be addressed by BDA.

INTRODUCTION

Coronal mass ejections (CMEs) and coronal holes are two large-scale structures of the Sun that seriously affect the space environment of Earth. CMEs drive shocks, accelerate particles, and produce geomagnetic storms. Coronal holes accelerate high speed solar wind that collide with slow solar wind to form corototating interaction regions (CIRs), which also produce geomagnetic storms and lead to electron acceleration in the magnetosphere. CMEs have been extensively studied since their discovery in the early 1970s (Tousey, 1973) primarily using white light coronagraphic data. Coronagraphs detect the Thomson-scattered photospheric light which is about a million times weaker than the direct photospheric light. To detect such a weak signal, the coronagraphs employ an occulting disk to block the direct sunlight which causes some restrictions on the observability of CMEs: (i) the occulting disk blocks an area larger than the solar disk, so we miss information on where the CMEs are rooted on the Sun, (ii) because of the occulting disk, CMEs occurring on the disk (Earth-directed) are not very well observed, and (iii) the Thomson-scattered signal is strongest when the CME is in the plane of the sky and hence produces a biased sample of CMEs. In the past, information on the near surface manifestations of CMEs could be obtained mainly from Hα spectroheliograms which show eruptive prominences and two-ribbon flares. We now know that both of these phenomena provide only partial information on CMEs; we need multiwavelength observations to get a complete picture of the CME

onset and early evolution. Microwave, EUV, and X-ray observations of CMEs can be very useful for this purpose because they do not have the limitation of occulting disks and they can observe eruptions at any longitude. Plasmas of different temperatures are involved in these eruptions and one has to use instruments sensitive to a wide range of temperatures (a few thousand K for prominences to several MK for flares). CMEs produce the most dramatic space weather effects. CIRs are also important because they are more frequent and produce effects different from those of CMEs. In this paper, we show that the Brazilian Decimetric Array (BDA) can make crucial information on both CMEs and coronal holes.

CORONAL MASS EJECTIONS

CMEs are multithermal plasmas typically consisting of a frontal structure, a cavity, and a prominence core (see e.g., Hundhausen, 1997). When the CMEs erupt, they leave behind post-eruption arcades also known as flare loops. During the eruption, electrons are accelerated, which result in intense nonthermal microwave emission. While the nonthermal microwave emission gives information on the magnetic properties of the post-flare loops, the thermal emission gives information on the CME structures. Here we focus on the CME observations. The frontal structure and the filament cavity are coronal features optically thin at microwave frequencies. On the other hand the prominence core is very dense and relatively cool and hence optically thick in microwaves. The arcade formation is a hot coronal structure but of much higher density.

The observability of CME substructures in microwaves can be assessed using the simple formula for free-free optical depth (Gopalswamy, 1999):

$$t_{ff} = \alpha \int n^2 f^{-2} T^{-3/2}\, dl, \qquad (1)$$

where $\alpha \sim 0.2$ for $T > 10^4$ and ~ 0.08 for $T < 10^4$, n = electron density, f = observing frequency and T = electron temperature. $\int n^2\, dl$ is the emission measure of the structure we are interested in, dl being the elemental length along the line of sight. Let us evaluate the optical depth for various substructures.

The frontal structure and cavity

The typical temperature and density of the frontal structure are 2 MK and $\sim 10^8$ cm^{-3} respectively, so at an observing frequency of 5.6 GHz, one needs a line of sight depth of 4×10^{13} cm (~ 3 AU) to make the CME optically thick. If we use a realistic thickness of ~ 1 solar radius, equation (1) gives an optical depth of 1.6×10^{-3} and the frontal structure will be at a brightness temperature of only 3142 K. The same argument applies to the cavity which is of similar size and lower density and hence the contribution will be still smaller. It must be noted that at meter wavelengths, the conditions are more favorable. At 50 MHz, a CME of 1 solar radius thickness will be optically thick and can be readily observed. Such CMEs were observed by radioheliographs at Clark Lake (Gopalswamy and Kundu, 1992; 1993b) and Culgoora (Sheridan et al., 1978). A simulation study by Bastian and Gary (1997) on the detectability of CMEs in microwaves resulted in a similar conclusion.

The prominence core

The cool dense prominence has a large opacity in microwaves: for typical temperature (~ 8000 K) and density ($\sim 10^{10\text{-}11}$ cm^{-3}), the prominence core becomes optically thick even for a small line of sight depth of 0.3 km. Hence the prominence core can be readily observed by BDA at 5.6 GHz, similar

to what is observed at 17 GHz (Hanaoka et al., 1994; Gopalswamy et al., 1996; 1997a; Gopalswamy and Hanaoka, 1998; Gopalswamy, Hanaoka and Hudson, 1999b). Since the corona is optically thin and contributes very little to the microwave brightness temperature, it results in a "cold sky" in microwaves. A prominence observed against the cold sky appears as a bright structure, very similar to a prominence in Hα. The brightness temperature is typically ~ 8000 K in microwaves. During eruptive events, the prominence can expand and drain considerably and can become optically thin as shown by Fujiki (1999). Because of the inverse-square frequency dependence of the free-free opacity, the prominence can easily become optically thin at higher frequencies (Irimajiri et al., 1995), although it can remain optically thick at lower frequencies such as 17 GHz. At 5.6 GHz, the prominence will remain optically thick even at greater distances from the Sun, and hence can be readily tracked by BDA. Figure 1 shows a bright eruptive prominence observed by the Siberian Solar Radio Telescope at 5.7 GHz, a frequency used by the BDA.

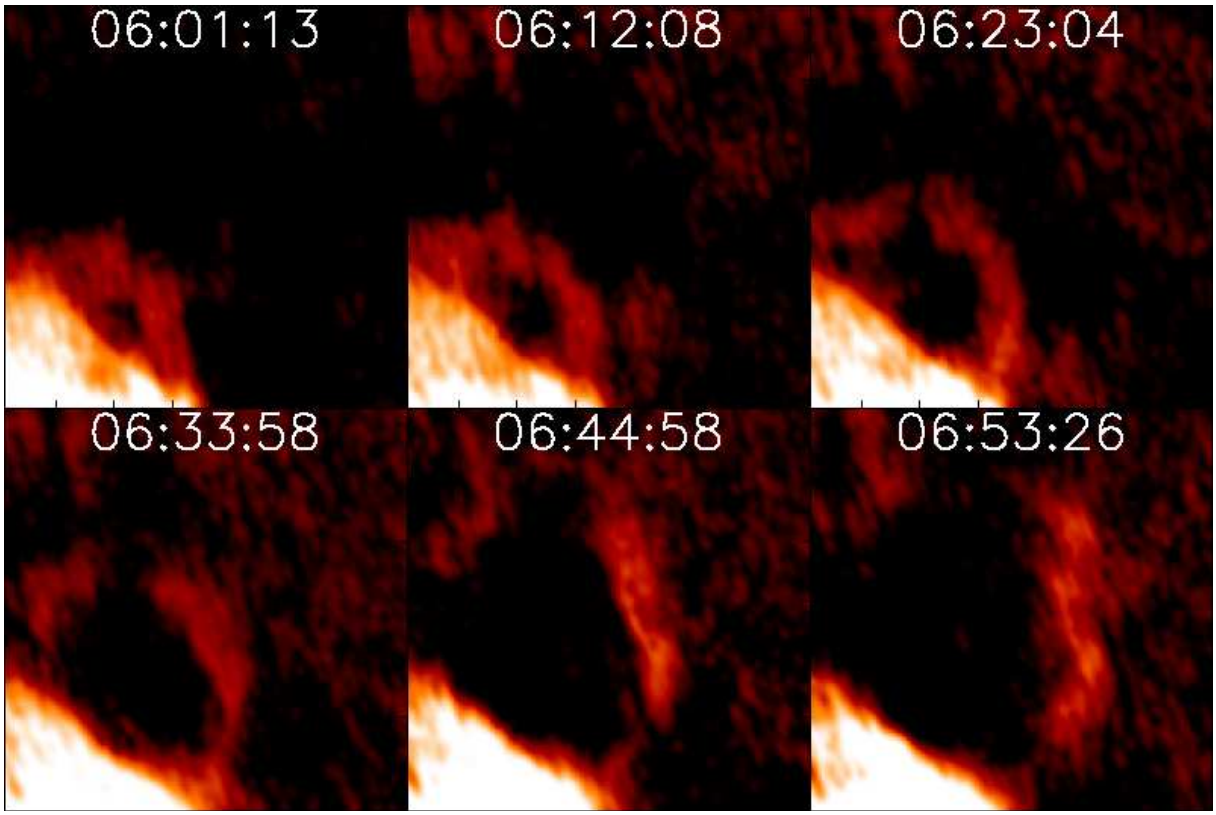

Fig. 1 - Snapshots of the Sun in microwaves obtained by the Siberian Solar Radio Telescope 5.7 GHz, similar to BDA. Northwest quadrant of the Sun is shown. The eruptive prominence can be seen to increase in height over a period of ~ 50 minutes. (Courtesy: V. V. Grechnev)

Filaments

The solar disk ("the microwave quiet Sun") has been estimated by Zirin et al. (1991) at various frequencies and found to follow the relation,

$$T_{b} = Af^{-2.1} + B, \qquad (2)$$

where A = 140077 and B = 10880 (the temperature of the chromosphere in K). At 5.6 GHz equation (2) gives a brightness temperature of ~14640 K. Therefore, the prominence when observed on the disk, appears as a depression (dark filament) with respect to the quiet Sun, by ~ 6640 K. The contrast is much better than what is observed by the Nobeyama radioheliograph, and hence will be very useful in tracking filaments, which are one of the best indicators source regions from where CMEs erupt. When the filament erupts, it can often get heated up and becomes indistinguishable from the quiet Sun ("disappears"). The radio disappearance is due to a different physical mechanism compared to the Hα disappearance; the latter happens when the filament ceases to absorb the Hα line radiation when its temperature increases. Since the prominence remains optically thick for a long time after eruption, the 5.6 GHz observation can track eruptive prominence for a longer time.

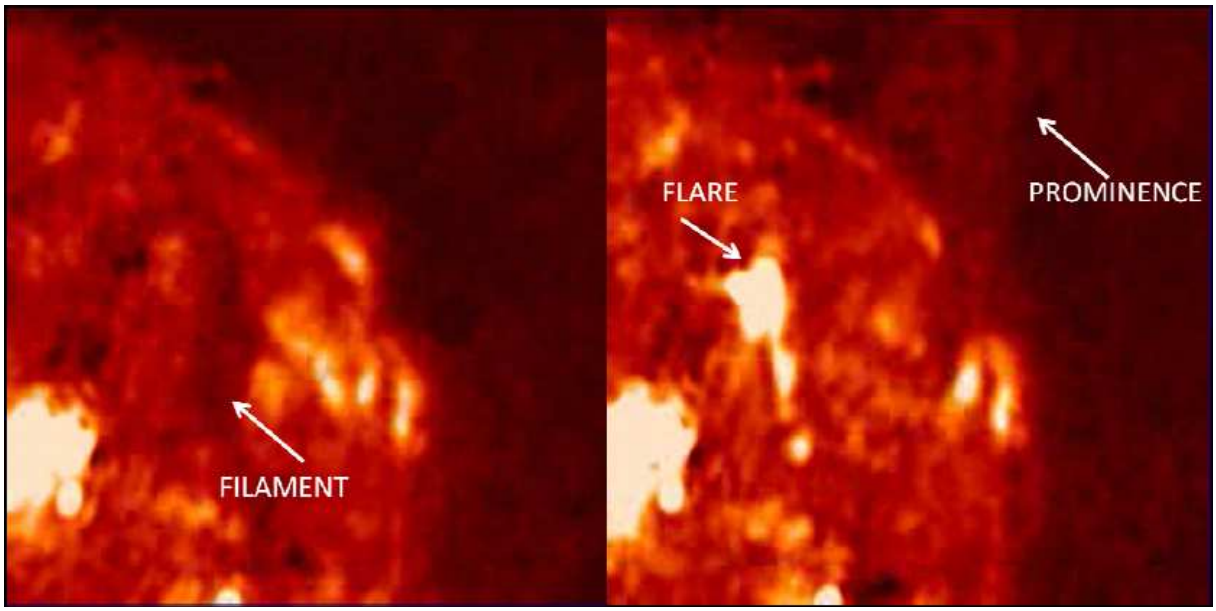

Fig. 2 - U-shaped dark filament on the disk (left) and the same filament becoming an eruptive prominence on the right. Post flare loops can be seen after the filament eruption. Locating the filament and flare using the same instrument provides a great advantage in identifying CME sources.

Post-eruption arcade (Flare)

Hanaoka et al (1994) imaged the arcade formation of the 1992 July 30–31 event in microwaves. The imaging was possible because the free-free emission from the arcade was high enough to be detected in microwaves. From *Yohkoh*/SXT images, the average temperature and density of the arcade were derived to be 3.5 MK and 2.4 × 109 cm−3 respectively. Using the measured size (28000 km) of the arcade at the brightest region as the line of sight depth, equation (1) gives an optical depth of 0.0017 and results in a brightness temperature of ~ 6000 K, similar to what was observed. After accounting for the difference in spatial resolution of radio and X-ray data, Hanaoka et al (1994) showed that the observed and computed brightness temperatures were in close agreement. For the same parameters, BDA will observe an order of magnitude higher brightness temperature because of the inverse-square dependence of the optical depth on frequency. The optical depth becomes 0.016 and

the brightness temperature is 55000 K. Figure 2 shown an actual observation from SSRT at 5.7 GHz showing the filament before and during eruption as well as the flare after the filament has lifted off.

The coronal cavity

The coronal cavity is typically at the same temperature as the frontal structure of the CME, but of lower density. If the density is an order of magnitude lower, one gets an optical depth of ~0.00016, so the brightness temperature becomes ~320 K. Thus, one should be able see the cavity as a dark feature between the prominence and the corona. It is possible that the cavity on the disk also will be observed as a depression as an extension of the prominence. It has been demonstrated by Gopalswamy et al. (1991) that the filament cavities are readily observed at 1.5 GHz. Multifrequency observations using the BDA should be able to readily observe the cavity on the disk as well as above the limb.

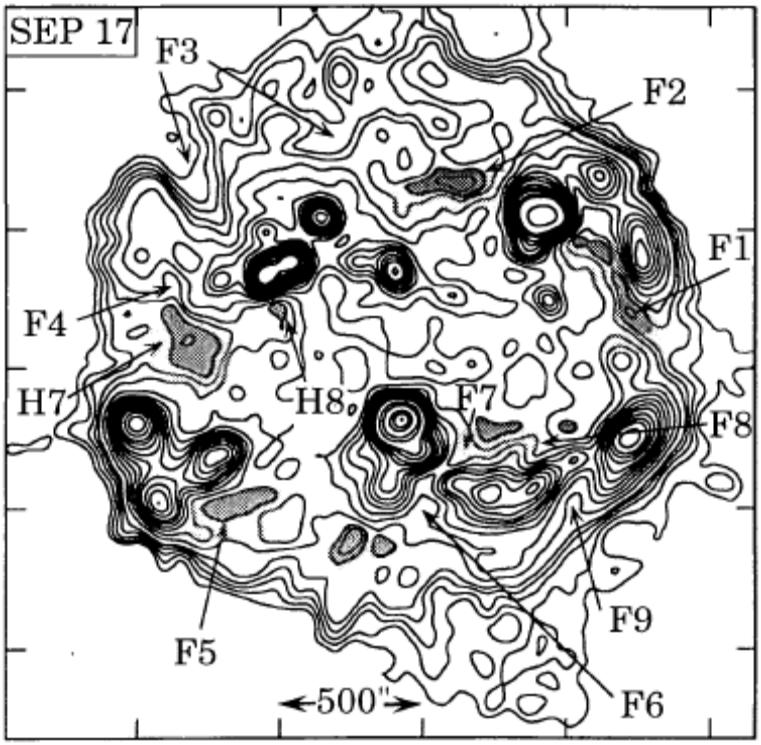

Fig. 3 - A quiet Sun image of the Sun at 1.5 GHz by the Very Large Array (VLA) on September 17, 1988. F and H denote filaments and coronal holes, respectively. Other compact bright regions are active regions. BDA will be able to image all these features in a dedicated manner.

CORONAL HOLES

Coronal holes are important large-scale structures on the Sun, which produce high-speed solar wind streams (HSS). When HSS collide with the neighboring slow solar wind, they produce large-scale magnetized plasma structures known as the corotating interaction regions (CIRs). CIRs are responsible for a different type of geomagnetic storms that are known for producing MeV electrons in Earth's magnetosphere. These electrons can be hazardous to satellites in the magnetosphere, and hence important for space weather prediction. Observing coronal holes in the equatorial region of the Sun is

thus very important. BDA can readily observe the coronal holes at all frequencies as depressions. Figure 3 shows an example of the quiet Sun showing filaments and coronal holes observed by the Very Large Array (VLA) at 1.5 GHz. This frequency will be used by the BDA, so coronal holes can be tracked and studied. In addition, coronal holes will appear as depressions at all the BDA frequencies, so the structure of coronal holes can also be studied.

SUMMARY

In summary, the Brazilian Decimetric Array (BDA) will make important contributions to the field of space weather by observing the solar sources of adverse weather in geospace. Coronal mass ejections and coronal holes are the two sources of mass emission from the Sun that result in geomagnetic storms and energetic particles. Coronal mass ejections on the solar disk are not well observed by coronagraphs. Radio telescopes like the BDA can readily observe the inner parts of CMEs (the prominence core and cavity) when they start on the Sun, thus providing advanced warning of impending adverse space weather at least one day ahead of time. Similarly, the BDA will be able to observe the presence of coronal holes on the disk and forecast high speed streams. We demonstrated the feasibility of making very useful radio measurements by considering the physical parameters of various coronal features applied to the BDA.

REFERENCES

Bastian, T. S., Gary, D. E., *J. Geophys. Res*., 102, 14031, 1997.

Fujiki, K., Proc. of the Nobeyama Symposium, Eds.: T. S. Bastian, N. Gopalswamy and K. Shibasaki, NRO Report No. 479, 249-254, 1999.

Gopalswamy, N., Proc. of the Nobeyama Symposium, Eds.: T. S. Bastian, N. Gopalswamy and K. Shibasaki, NRO Report No. 479, 141-152, 1999.

Gopalswamy, N., White, S. M., Kundu, M. R., *ApJ*, 379, 366, 1991.

Gopalswamy, N., Hanaoka, Y., *ApJ*, 498, L179, 1998.

Gopalswamy, N., Kundu, M. R., *ApJ*, 390, L37, 1992.

Gopalswamy, N., Kundu, M. R., *Adv Space Res.*, 13(9), 95, 1993a.

Gopalswamy, N., Kundu, M. R., *Solar Phys.*, 143, 327, 1993b.

Grechnev, V. V. et al., Proc. of Nobeyama Symposium 2004, 101-110, 2006.

Hanaoka, Y. and 19 co-authors, *PASJ*, 46, 205, 1994.

Hundahausen, A. J., in 'Coronal Mass Ejections', ed. N. Crooker et al, AGU Monograph 99, 1, 1997.

Irimajiri, Y., Takano, T., Nakajima, H., Shibasaki, K., Hanaoka, Y., Ichimoto, K., *Solar Phys.*, 156, 363, 1995.

Tousey, R., *Adv. Space Res*., 13, 713, 1973.

Zirin, H., Baumert, B. M., Hurford, G. J., *ApJ*, 370, 779, 1991.

MULTIFRACTAL ANALYSIS OF AN INTERMITTENT SOLAR BURST OBSERVED BY THE BRAZILIAN SOLAR SPECTROSCOPE

Reinaldo R. Rosa[1], Maurício J. A. Bolzan[2], Francisco C. R. Fernandes[2], Talita B. Veronese[1], Hanumant S. Sawant[3]

[1]Laboratório Associado de Computação e Matemática Aplicada (LAC), INPE
Av. dos Astronautas,1758 – 12201-970, São José dos Campos-SP, Brasil
(reinaldo@lac.inpe.br)
[2]Instituto de Pesquisa e Desenvolvimento - Universidade do vale do Paraíba - UNIVAP
Av. Shishima Hifumi, 2911 – 12244-000, São José dos Campos-SP, Brasil
(bolzan@univap.br; guga@univap.br)
[3]Divisão de Astrofísica - Instituto de Pesquisas Espaciais - INPE
Av. dos Astronautas,1758 – 12201-970, São José dos Campos-SP, Brasil
(sawant@das.inpe.br)

ABSTRACT

The solar radio emissions in the decimetric frequency range (above 1 GHz) are very rich in temporal and spectral fine structures due to nonlinear processes occurring in the magnetic structures on the corresponding active regions. In this paper we characterize the singularity spectrum, $f(\alpha)$, for a typical SFU profile coming from solar burst dynamical spectra observed at 1000-2500 MHz. We interpret our findings as evidence of inhomogeneous plasma turbulence driving the underlying plasma emission process and discuss the multifractal approach into the context of BDA data analysis.

INTRODUCTION

Today, several theoretical aspects of solar are related to the high resolution and high sensitivity data observed in the lowest microwave range (1-3 GHz), usually reported as the *decimetric range* (Aschwanden, 2005). It is known that the large amount of energy released during a solar are and the relatively short timescale in which all related events occur lead to the conclusion that a solar are is a magneto-hydrodynamic (MHD) instability taking place in strongly anisotropic turbulent plasma (Kuperus, 1976). The importance of this MHD scenario has been investigated, for example, from nonlinear analysis of decimetric bursts at 3 GHz observed during the June 6, 2000 flare (Rosa et al., 2008). It was found that the 3 GHz radio burst power spectrum exhibits a power-law which is an evidence of stochastic intermittency due to a self-affine dynamics as found in the MHD turbulence theory. Intermittent energetic process implies that the fluctuations are correlated without a dominant characteristic time scale, as predicted in the models for multi-loop interactions (Tajima et al., 1987). However, in order to characterize more precisely the nature of such self-affine turbulent process, a complementary analysis, based on the singularity spectrum technique, is required.

As known from the turbulence theory the intermittency leads to deviation from usual Kolmogorov energy structure functions and its main signature are the singularity spectra exponents,

$f(\alpha)$, which represent a power-law scaling- free dependence (Frisch, 1995). For inhomogeneous plasma turbulence, the so-called multi-fractal *p*-model describes how the energy can be distributed among scales following a multiplicative rescaling structure (Halsey et al., 1986). Although the variability pattern of the 3 GHz burst can be interpreted as a typical profile resulting from a turbulent process, data obtained through Brazilian Decimetric Spectrometer (BSS) (Sawant et al., 2001), in the range of 1-2.5 GHz, are richer in intermittency. Hence, in this paper, taking into account the *p*-model singularity spectra, we obtain the $f(\alpha)$ for a typical BBS burst, improving our search for a robust technique by which inhomogeneous plasma turbulence process might be identified. The importance of the singularity spectra approach is discussed in the context of the Brazilian Decimetric Array (BDA) high resolution data analysis (Sawant et al., 2007).

DATA AND METHODOLOGY

Data

The Brazilian Solar Spectroscope (BSS) is a digital spectroscope and its signal can be recorded up to 100 digital frequency channels. The BSS operates over the frequency range of 1000 - 2500 MHz, with high time (10 - 1000 ms) and frequency (3 MHz) resolutions, in conjunction with the polar mounted 9 meter diameter parabolic antenna. Absolute timing accuracy is 3 ms and the minimum detectable flux is (3 s.f.u. (Madsen et al., 2004).

Figure 1 shows a BSS dynamic spectrum from where we selected the 1890 MHz frequency channel in order to analyze a typical intermittent time series (Figure 2a). This time series was observed with time and frequency resolutions of 100ms and 10 MHz, respectively.

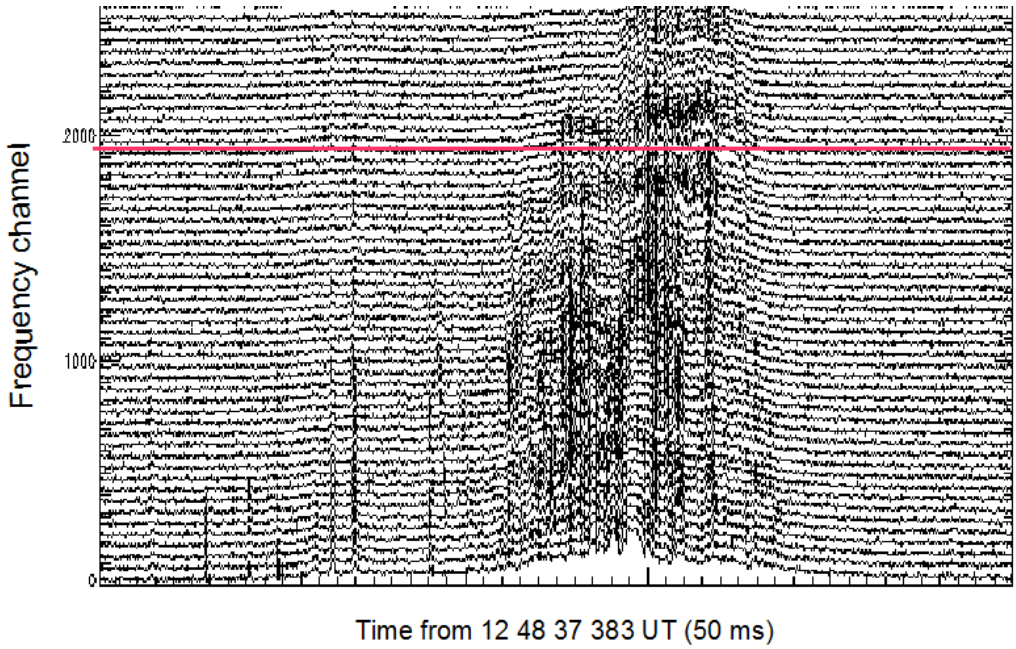

Fig. 1 - The 1000-2500 MHz dynamic spectrum for the solar burst observed from BSS. The red line identifies the 1890 MHz frequency channel.

Multifractal Analysis

Mathematical methods for multifractal analysis of intermittent patterns associated with multiplicative cascades provide a quantitative interpretation of a wide range of physical heterogeneous processes (e.g., Struzik, 2000). Here, we have considered, in order to obtain the singularity spectrum $f(\alpha)$ from the SFU-component time series, the Wavelet Transform Modulus Maxima (WTMM) (Mallat, 1989). The basic idea behind the WTMM method is to describe a partition function over only the modulus maxima of the wavelet transform of a signal SFU(t) (see Appendix). Recently, the robustness of this methodology has been tested for intermittent geomagnetic fluctuations using, as a reference pattern, the so-called *p*-model (Halsey et al., 1986).

In the theory of multifractal statistics the *p*-model is a canonical mathematical system that describes nonhomogeneous energy cascade processes in turbulent flows (e.g., Rodrigues Neto et al., 2001). Hence we performed the theoretical multiplicative cascade *p*-model as a canonical reference in our analysis. The *p*-model is given by

$$\alpha = \frac{\log_2 p_1 + (\omega - 1)\log_2 p_2}{\log_2 l_1 + (\omega - 1)\log_2 l_2} \tag{1}$$

and

$$f(\alpha) = \frac{(\omega - 1)\log_2(\omega - 1) - \omega \log_2 \omega}{\log_2 l_1 + (\omega - 1)\log_2 l_2} \tag{2}$$

where (is a free parameter and $l_1 = l_2 = 1/2$ if the eddies are equal as a two-scale Cantor set. In the *p*-model, the largest coherent structure is assumed to be built up by a specific energy flux per unit length and then a scale-independent space-averaged cascade rate occurs. In this process the flux density is transferred to the two smaller eddies with the same length but different flux probabilities p_1 and p_2 (p_1+p_2 = 1). The process is repeated several times with p_1 and p_2 randomly distributed, being the asymmetric breakdown in the fragmentation process driven by the parameter $p = p_1 = 1 - p_2$. The common value of p1 = p2 = 0.5 corresponds to the homogeneous energy transfer rate with no intermittency effects. The values of $p > 0.5$ correspond to an intermittent turbulence. In the present work, we use a maximum likelihood algorithm to fit the *p*-model in each characteristic scale.

RESULTS AND INTERPRETATION

In order to compute the characteristic $f(\alpha)$ for 1890 MHz SFU burst, it is necessary to choose a set of characteristic time scales in the SFU(t) time series to use in the Morlet wavelet transform. Upholding the daily variability component, we use the concept of scale (r) through the difference SFU(t, r) = SFU($t + r$) - SFU(t). As a representative set of MHD oscillations we choose three very close typical characteristics scales: 6, 10 and 15 seconds, observed in our 1.7 min duration time series (Figure 2a). For comparison, we show the respective singularity spectra obtained using the *p*-model. Choosing typical parameters values for the *p*-model (Bolzan et al., 2009) we use an algorithm to fit the experimental and theoretical data. The results are shown in Figure 2b from where the 1890 MHz SFU intermittency can be interpreted as the result of a possibly multifractal process related to the *p*-model nonhomogeneous asymmetric energy cascade. This result makes evident the importance of studying the presence of intermittent phenomena driving the solar decimetric fluctuations.

Table 1 - Singularity spectra parameters for each characteristic scale.

Increment (r)	Time scale (s)	p_1/p_2	l_1	$f_{max,p}$	$f_{max,SFU}$	$\Delta\alpha_p$	$\Delta\alpha_{SFU}$
60	6	0,70	0,23	1,16	1,14	0,67	0,89
100	10	0,75	0,30	1,14	1,15	0,74	0,95
150	15	0,72	0,28	1,16	1,14	0,81	0,99

CONCLUDING REMARKS

The multifractal signature for 1890 MHz decimetric solar burst was successfully detected by using the Wavelet Transform Modulus Maxima and these results are in agreement with multifractal process found for *p*-model inhomogeneous asymmetric energy cascade.

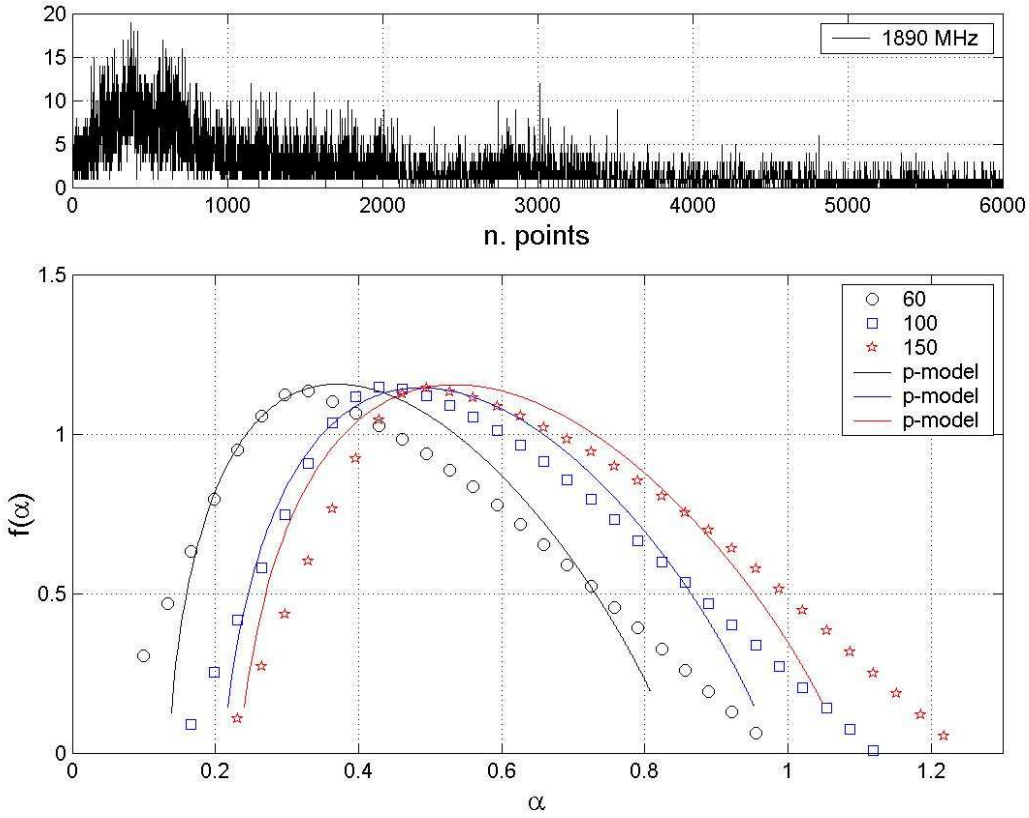

Fig. 2 - (a) The 1890 MHz time profile from the 1000-2500 MHz dynamic spectrum showed in Figure 1. (b) The corresponding singularity spectrum for tree characteristic time scales (60points_100ms = 6s, 10s and 15s) of the 1890 MHz profile and their corresponding *p*-model fitting.

At least for three characteristic scales, 6, 10 and 15 seconds, intermittency is strongly related to multifractal processes where the typical MHD oscillations can play an important role. Thus, 1890 MHz SFU time series can be interpreted as being the response of an out of equilibrium process, possibly related to the particle acceleration from a transversal MHD loop-loop nonlinear interaction

and/or to the turbulent interaction between electron beams and evaporation shocks from the optically thick sources of a single loop.

Despite the simplicity of our approach based on a single BSS data set, at least two relevant aspects related to the BDA project are addressed: (i) the need of complementary analysis using a large data set, including the future BDA data and (ii) the need of the high BDA spatial resolution data in order to have images of the related decimetric active regions and their respective energy sources.

ACKNOWLEDGEMENTS

The Brazilian agencies FAPESP, CAPES and CNPq.

APENDIX

A Singularity Spectrum from Wavelet Transform Modulus Maxima (WTMM)

The wavelet transform of the time series SFU(t) is written as

$$W_\phi\,[SFU(t)](a,b) = \frac{1}{a}\int SFU(t)\varphi^{*}\left[\frac{t-b}{a}\right]dt, \quad a>0 \tag{A.1}$$

where φ^* is the complex conjugate of a continuous wavelet function. This transformation gives the coefficient of the wavelet decomposition of the signal SFU(t) at time t = b for scale a (Enescu et al, 2006). For analysis where the variability pattern contains nonstationary power at many different scales, such as SFU(t), a wavelet analysis based on a plane wave modulated by a Gaussian is required.

Thus, it is then considered the Morlet wavelet, here taken in its form to satisfy the so-called admissibility condition (Farge, 1992)

$$\varphi(t) = \pi^{-1/4}\, e^{i6t}\, e^{-t2/2} \tag{A.2}$$

The scaling and translation of this mother wavelet function over the signal SFU(*t*) are performed by the parameters *a* and *b*. While the scale parameter a stretches (or compresses) the mother wavelet to the required resolution, the translation parameter *b* shifts the basis functions to the desired time location. It can be shown that the wavelet transform can reveal the local characteristics of SFU(*t*) at a point t_0. More precisely, we have the following power-law relation

$$W_\phi\,[H](a,t_0) \approx |\,s\,|^{\alpha(t0)} \tag{A.3}$$

where $\alpha(t_0)$ is the Hlder exponent (or singularity strength). Thus, the exponent $\alpha(t_0)$, for fixed location t0, can be obtained from a log-log plot of the wavelet transform amplitude versus the scale a. However, this power-law characterization is difficult when the process is governed by a hierarchical distribution of singularities compromising the exact determination of α on a finite range of scales. In such case any transformation of the signal SFU(*t*) may obey some renormalization operation involving multiplicative cascades and it has been demonstrated that the local maxima of $|W\varphi\,(a,b)|$ at a given scale *a*, are likely to contain all the hierarchical distribution of singularities in the signal.

At a given scale *a* each one of the WTMM bifurcates into new two maxima giving rise to a rich multiplicative cascade in the limit $a \rightarrow 0$. Thus, it is possible to identify a space-scale partitioning over

the maxima distribution and, consequently, a usual *thermodynamical* method of computing the multifractal spectrum of SFU(t) is to define a partition function which scales, in the limit $a \rightarrow 0$ as

$$Z(a, q) = \sum_n |W_\varphi H(a, t_n(a))|^q \approx a^{\tau(q)}, \quad \text{(A.4)}$$

where t_n is the position of all local maxima at a fixed scale s and q is the moment of the measure distributed on the WTMM hierarchy, used to define the power-law scaling of $Z(a,q)$. This power-law yields for small a the scaling exponents $\tau(q)$ - the multifractal spectrum (Muzy et al., 1991). Actually, there is hierarchy of the WTMM that has been used for defining the partition function $Z(a,q)$ based on the multifractal formalism (Arneodo et al., 1995).

The final step in the WTMM method used here is to examine, for a set of scales a, the correspondent singularity spectrum $f(\alpha)$. If one finds a single value _ for all singularities t_n, the signal has a monofractal structure. However, if the underlying process is multifractal, then different parts of the signal are characterized by different values of α (Oswiecimka et al., 2006). The singularity spectrum, approximately an upside-down parabola, peaks at $f_{\alpha,\max}$. The range $\Delta\alpha$ quantifies the fractal non-uniformity, while f_α characterizes how frequently burst components with scaling exponent α occur. The nonhomogeneous turbulent energy cascade is characterized comparing such singularity spectrum parameters for the correspondent turbulent *p*-model.

REFERENCES

Arneodo, A., Bacry, E., Muzy, J. F., *Physica A*, 213, 1-2, 232-275, 1995.

Aschwanden, A., Springer, Berlin, 2005.

Bolzan, M. J. A., Rosa, R. R., Sahai, Y., Annales Geophysicae 27(2), 569-576, 2009.

Enescu, B., Ito, K., Struzik, Z., *Geophysical Journal International*, 164(1), 63-74, 2006.

Farge, M., *Annual Review of Fluid Mechanics*, 24, 395-457, 1992.

Frisch, U., Cambridge University Press, New York, 1995.

Halsey, T. C., Jensen, M. H., Kadanoff, L. P., Procaccia, I., Shraiman, B. I., *Physical Review A*, 33, 1141, 1986.

Kuperus, M., *Sol. Phys*. 47(1), 7990, 1976.

Madsen, F. R. H., Sawant, H. S., Fernandes, F. C. R., Cecatto, J. R., *Braz. J. Phys.*, 34(4b), 2004.

Mallat, S., *EEE Trans. Pattern Analysis and Machine Intelligence* 11, 674-693, 1989.

Muzy, J. F., Bacry, E., Arneodo A., *Physical Review Letters*, 67, 25, 3515-3518, 1991.

Oswiecimka, P., Kwapien, J., Drozdz, S., *Physical Review E*, 74, 016103, 2006.

Rodrigues Neto, C., Zanandrea, A., Ramos, F. M., Rosa, R. R., Bolzan, M. J. A., S, L. D. A., *Physica A*, 295(1-2), 215-218, 2001.

Rosa, R. R., Karlicky, M., Veronese, T. B., Vijaykumar, N. L., Sawant, H. S., Borgazzi, A. I., Dantas, M. S., Barbosa, E. B. M., Sych, R. A., Mendes, O., *Adv. Space Res.*, 41(5), 844-851, 2008.

Sawant, H. S., Subramanian, K. R., Faria, C., Fernandes, F. C. R., Sobral, J. H. A., Cecatto. J. R., Rosa, R. R., Vats, H. O., Neri, J. A. C. F., Alonso, E. M. B., Mesquita, F. P. V., Portezani, V. A., Martinon, A. R. F., *Solar Phys.*, 200, 167, 2001.

Sawant, H.S. et al., *Solar Phys.*, 242, 213-220, 2007.

Struzik, Z. R., *Fractals* 8, 163-179, 2000.

Tajima, T., Sakai, J., Nakajima, N., Kosugi, T., Brunel, F., Kundu, M. R., *Astrophys. J*, 321, 1031, 1987.

Proceedings of the Brazilian Decimetric Array Workshop
São José dos Campos, Brazil - July 28 – August 1, 2008

SOLAR RADIUS MEASUREMENTS WITH THE BDA

Adriana B. M. Valio[1] and Joaquim E. R. Costa[2]

[1]CRAAM/Mackenzie,
São Paulo, SP
[2]Divisão de Astrofísica - Instituto de Pesquisas Espaciais - INPE
Av. dos Astronautas,1758 – 12201-970, São José dos Campos-SP, Brasil

ABSTRACT

Our goal is to study certain aspects of the decimetric emission produced in the solar corona. This study is basically composed of the quiet Sun emission. Therefore, we intend to use the data from the *Brazilian Decimetric Array* (BDA) at 1.2 and 1.7 GHz in order to determine the solar diameter at these frequencies and also to verify the existence, or not, of a brightening near the solar limb and characterize it. Both types of data will be used to test and improve the solar atmospheric model developed by Selhorst and collaborators.

INTRODUCTION

Solar Radius

Due to its importance in the structure determination of solar atmospheric models, the solar radius has been measured in several wavelengths from radio through the visible part of the electromagnetic spectra. During the last two decades, the optical observations failed in showing an 11 year periodic variation in the solar radius. The measured variation ranged from tens to miliarcsecond to 0.5 arcsec, both in phase and anticorrelated with the solar activity cycle.

Detection of the solar radius changes at radio frequencies indicate that the location in the atmosphere where the radio emission is produced is varying. Actually, these variations reflect changes in the local distribution of temperature and density of the solar atmosphere. Previous research (Bachurin, 1983) has shown an increase in the solar radius of 9.6 and 13.8 arcsec at 13 and 8 GHz, respectively, from 1976 to 1981. More recently, Costa et al. (1999) measured the solar radius at 48 GHz and found that it decreased in correlation with activity cycle between 1991 e 1993. An important aspect is that the radius measurements are very well correlated with the changes observed in the solar irradiance, which may produce climate variations at Earth.

In 2004, Selhorst et al. (2004) showed that the variation of the solar radius at 17 GHz depends of where and when it is measures. The average radius changes by 4 arcsec between solar minimum and the maximum, following very well the solar activity cycle. On the other hand, if the radius is measured only in the Polar Regions, the variations are smaller, only about 1 arcsec and are anticorrelated with the solar cycle. Their conclusion is that the solar radius is strongly influenced by the presence of active regions near the limb, which obviously follow the solar cycle, whereas the polar radius has a strong contribution from the polar brightening that varies inversely with the 11 year cycle. Moreover, a strong limb brightening of 10 to 15 % is observed at 17 GHz, being more intense (25-30%) in the Polar Regions. The average thickness of the limb brightening is of the order of 60 arcsec (Selhorst et al., 2003).

Solar Limb Brightening

The study of the temperature distribution with position on the solar disk, obtained from radio observations, have fundamental implication on the determination of the structures of the chromosphere and corona. These variations are observed as a brightening near the solar limb and either be caused by the positive temperature gradient in the chromosphere or by the presence of jets of matter called spicules. An important phenomenon observed in the 17 GHz solar maps is this brightening near the limb, which is seen all around the Sun forming a ring of non uniform distribution.

Despite the report of several authors (Shimabukuro et al., 1975; Lindsey and Hudson, 1976; Horne et al., 1981; Lindsey et al., 1981; Gomez-Gonzalez et al., 1983; Lindsey et al., 1984; Bastian et al., 1993) of limb brightening detection at several wavelengths from 33 to 1000 GHz, no systematic study has been performed searching for a variation with the solar cycle. Very little information exists about angular variations of this ring. On a previous work at 350 GHz (Bastian et al., 1993), a limb brightening of approximately 16 % above quiet Sun levels was found, appearing differently in the North-South direction from the East-West one. Efanov et al. (1980) identified that the polar limb brightening was anticorrelated with the solar activity cycle.

It is believed that the limb brightening is due to two factors: i) increase of the chromospheric temperature with height (opposite to the limb darkening observed at optical wavelengths) and ii) presence of spicules which appear more prominently at the solar limb.

Spicules are fundamental components of the solar chromosphere. At the limb they are seen as jets of matter and can be observed in chromospheric spectral lines, such as H-alpha. The spicules have a rising mass flux, approximately 100 times larger than that of the solar wind. These structures are a challenge to the theories which need to explain how the chromospheric material is dragged to such great heights without increasing the temperature by about 10000 K, the temperature of the chromosphere.

OBSERVATION

To determine the solar radius and study the limb brightening at 1.2 and 1.7 GHz we plan to use the data from the *Brazilian Decimetric Array* (BDA). It will be interesting to compare these results with simultaneous observations from the Rádio Observatório de Itapetinga (ROI), at 22 and 43 GHz.

METHODOLOGY

The solar limb is defined as the point where the quiet Sun intensity falls to half its most common value (the quiet Sun level). The set of points of all the limb positions form a circumference which will be fit by the least square method in order to obtain the solar radius. This measurement will determine the region in the solar atmosphere where the decimetric emission is being produced, and it will be possible to compare this result with the data obtained at other wavelengths (Costa, Homor and Kaufmann, 1986).

As for the solar limb brightening, its presence near the limb will be studies from the convolution of a flat disk, representing the Sun, with the real antenna beam (Costa et al., 2002). This model will then be subtracted from the observations, which result will then show, or not, the existence of the brightening. Once identified, it will possible to obtain its intensity, width, and angular distribution, possibly understanding its main causes. We will also analyze its temporal correlation with the solar activity cycle.

SOLAR ATMOSPHERE MODEL

We intend to test the quiet Sun characteristics at 1.2 and 1.7 GHz, such as radius and limb brightening, and compare these with the values derived from solar models. As a model of the solar atmosphere, we will use the bidimensional atmosphere developed to describe the quiet Sun atmosphere based on previous models and confronted with observational data at 17 GHz 17 GHz (Selhorst et al., 2005). Several authors (Vernazza et al., 1981; Fontenla et al., 1993) have developed models for the solar atmosphere, however these models were based on spectral line data from the photosphere and lower chromosphere, and these models do not agree with observation made at radio frequencies.

BIBLIOGRAPHY

Bachurin, A. F., *Bulletin of the Crimean Astrophysical Observatory*, 67, 113, 1983.
Bastian, T. S., Ewell, M. W., Zirin, H., *ApJ*, 415, 364, 1993.
Costa, J. E. R., Homor, J. L., Kaufmann, P., in *Solar Flares and Coronal Physics using P/OF as a Research Tool* (NASA-CP 2421), Huntsville, 201, 1985.
Costa, J. E. R., Silva, A. V. R., Makhmutov, V. S., Rolli, E., Kaufmann, P., Magun, A., *ApJ Letters*, 520, 63, 1999.
Gomez-Gonzalez, J., Barcia, A., Delgado, L., Planesas, P., *A&A*, 122, 219, 1983.
Horne, K., Hurford, G. J., Zirin, H., de Graauw, T., *ApJ*, 244, 340, 1981.
Lindsey, C., Hudson, H. S., *ApJ*, 203, 753, 1976.
Lindsey, C., Hildebrand, R. H., Keene, J., Whitcomb, S. E., *ApJ*, 248, 830, 1981.
Lindsey, C., de Graauw, T., de Vries, C., Lidholm, S., *ApJ*, 277, 424, 1984.
Selhorst, C. L., Silva, A. V. R., Costa, J. E. R., Shibasaki, K., *A&A*, 401, 1143, 2003.
Selhorst, C. L., Silva, A. V. R., Costa, J. E R., *A&A*, 420, 1117, 2004.
Selhorst, C..L., Silva, A. V. R., Costa, J. E. R., *A&A*, 433, 365, 2005.
Shimabukuro, F. I., Wilson, W. J., Mori, T. T., Smith, P. L., *Solar Phys.*, 40, 359, 1975.

Proceedings of the Brazilian Decimetric Array Workshop
São José dos Campos, Brazil - July 28 – August 1, 2008

SOLAR DECIMETRIC EMISSION

Koovapady R. Subramanian

Solar Radio Astronomy Group
Indian Institute of Astrophysics
Koramangala, Bangalore – 560034, India

ABSTRACT

The importance of solar observations at decimetric wavelengths is explained. Characteristics of various types of decimetric radio bursts during flares are described. Radio observations of solar active regions are also described.

INTRODUCTION

Radio observations of the Sun contribute to the understanding of many physical processes which occur on the Sun. From the thermal bremsstrahlung emission in the quiet Sun to thermal gyro - resonance in strongly magnetized solar active regions to the non thermal emission from Mev electrons accelerated in solar flares, observations of radio emission in the entire radio band provides additional means of understanding the myriad phenomena on the Sun from the base of the chromosphere to the outer Corona. The range of frequency in the band 300 – 3000 MHz roughly corresponds in height to the lower corona generally less than 1.2 solar radii. High frequency part of this spectrum is the operating frequency range of Brazilian decimetric array (BDA). In the solar corona, the characteristic frequency of the background plasma is: the plasma frequency and the electron gyro frequency that determine the observing radio frequency by fp = 9000 $\sqrt{}$ n Hz and fc = 2.8 B MHz where n is the electron density/cm^3 and B is the magnetic field in Gauss. Radio emission is produced at these frequencies (fundamental) and or second harmonic (and higher for some gyro magnetic emissions. The decimeter range of 300 – 3000 MHz corresponds to source densities of 1.2×10^9 to 1.3×10^{11} cm^{-3} assuming fundamental emission. This is the range of densities where the primary energy release of flares is expected to take place. The way in which different radio frequencies can be used to probe different levels of the atmosphere is shown in the Figure 1.

The solar radio emission in the decimeter band has been studied extensively using spectrographs and imaging instruments. From the diagnostic point of view that the radiation in the band 1 – 5 GHz allow direct measurement of temperature and magnetic field without the complications arising in the analysis at other wavelengths like the knowledge of the chemical abundance etc. The large resurgence of solar radio astronomy in the past decade is due to the use of large interferometers like VLA and WSRT for imaging and radio spectrographs in different parts of the world in particular the Phoenix (Benz, 1998) in Zurich and the BSS (Sawant, 2003) at INPE in Brazil.

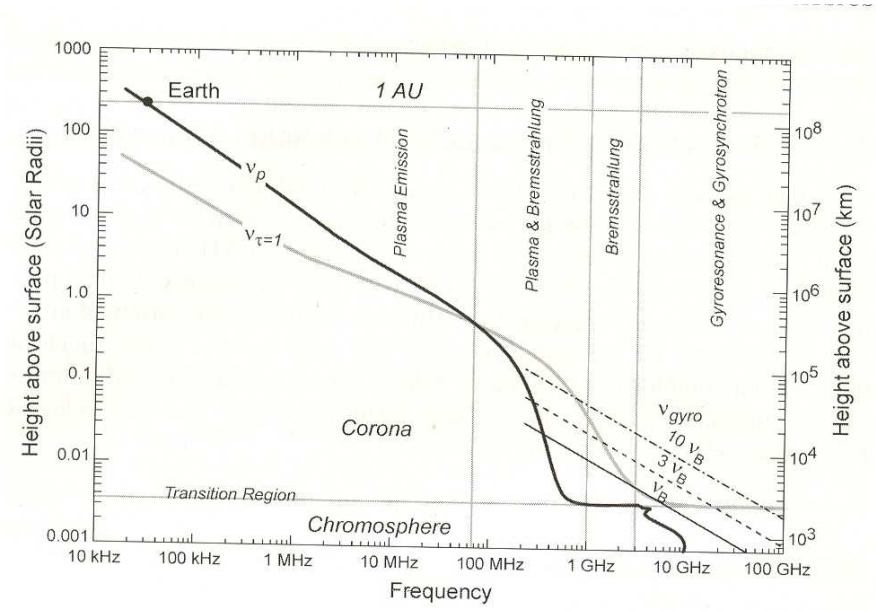

Fig. 1 - Characteristics radio frequencies in the solar atmosphere (Gary and Hurford, 1989).

For the past two decades imaging observations of solar active regions and flares with high spatial resolution (< 20 sec of arc) were made by VLA and WSRT. Also RATAN and SSRT have been used to study the SUN. In recent years GMRT has been used to observe the Sun few times in a year. The spatial resolution of VLA ranges from 3 arc min at 330 MHz to about 5 arc sec at 15 GHz. Radio spectrographs in the decimetric band used in recent years for solar observations is shown in the Table 1.

Table 1 - Broadband spectrographs in the decimeter range

	Range (MHz)	Time resolution (s)	Spectral resolution $\Delta f / f$ (%)
Artemis (Greece)	470- 110	0.01	0.8
Beijing (China)	3700 – 3100	0.001	-
Hirasiso	2500 – 25	3 - 4	0.2
Ondrejov (Czech Rep.)	4800 – 800	0.1	0.6
Porto (Portugal)	600 – 200	0.1 or 0.01	> 0.16
Tremsdorf (Germany)	800 – 40	0.1 or 0.001	0.46
Zurich (Switzerland)	4000 – 100	< 0.1	0.2

DECIMETRIC EMISSION FROM FLARES

The radio emission of flares at wavelengths from millimeter to decameter waves includes a large variety of radiation processes. They can be considered as different diagnostic tools particularly suited for the analysis of non thermal electron distribution, enhanced level of various kinds of plasma waves and dynamical plasma processes. From the study of solar flares using solar radio spectrographs it is

known that there is a variety of (flare related) bursts with distinctive morphologies in the frequency time domain. Situated in the spectrum between metric range (< 300 MHz well known for five types of bursts) and the centimetric synchrotron emission at frequencies > 3 GHz the decimetric emissions manifest a large variety of structures many of which are still unexplored. Figure 2 shows a typical example of broadband spectrum recorded by Phoenix 2 spectrograph. In addition to type III bursts many type III like burst were observed.

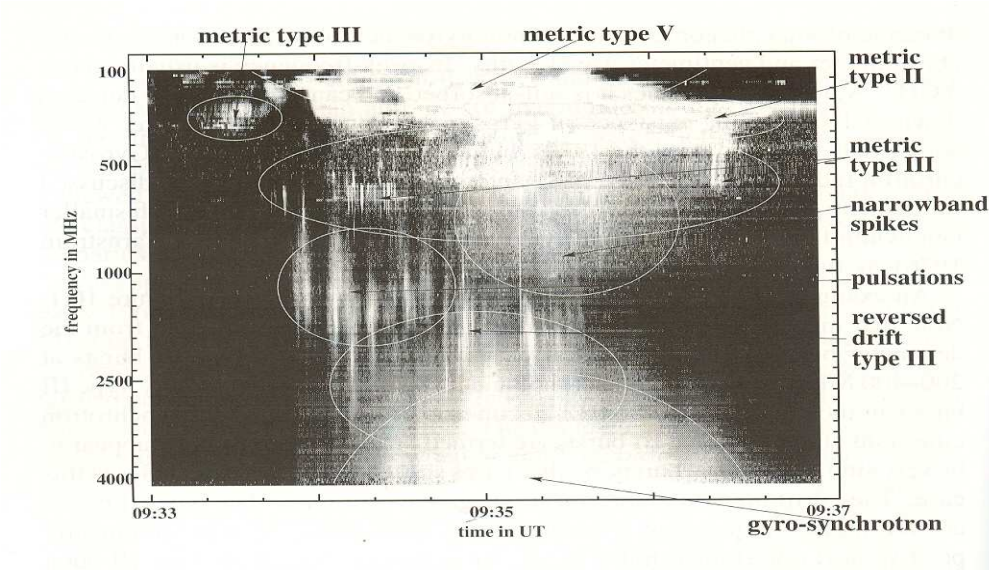

Fig. 2 - Broadband spectrum showing a rich variety of bursts in the meter – decimeter wavelengths (Benz, 1991).

The decimetric range has been systematically explored since 1980s with digital radio spectrographs with high spectral and temporal resolution (Benz, 1991). Most decimetric type III emissions are shaped similar to metric type III radio bursts. Their characteristics are:

a) impulsive onset;
b) occur in groups of some tens to hundreds;
c) similar to metric and IP type IIIs;
d) have short duration (0.5 – 1 sec);
e) high drift rates < 100 MHz;
f) occur in groups (tens to 100s);
g) reverse drift common as normal drift (above 1 GHz).

These bursts are interpreted on the basis of electron beams interacting with the ambient coronal plasma to excite a bump on tail instability of Langumir waves. This emission can occur at fundamental and harmonics. The electromagnetic emission is assumed to be produced at the local plasma frequency and /or it harmonics. Type III bursts are a diagnostics of the electron density of the plasma traversed by the beam. The recent interest in type III bursts is motivated by their use as diagnostics for location of the electron acceleration process, as traces of the magnetic field lines along which electron propagates and the density of the ambient corona they traverse. Imaging observations have shown that type III sources are often not single, but emerge simultaneously into different directions. Down

propagating branches of type III bursts are sometime double sources. Their simultaneous existence suggests a common origin. Figure 3 shows radio bursts in the frame work of flare scenario.

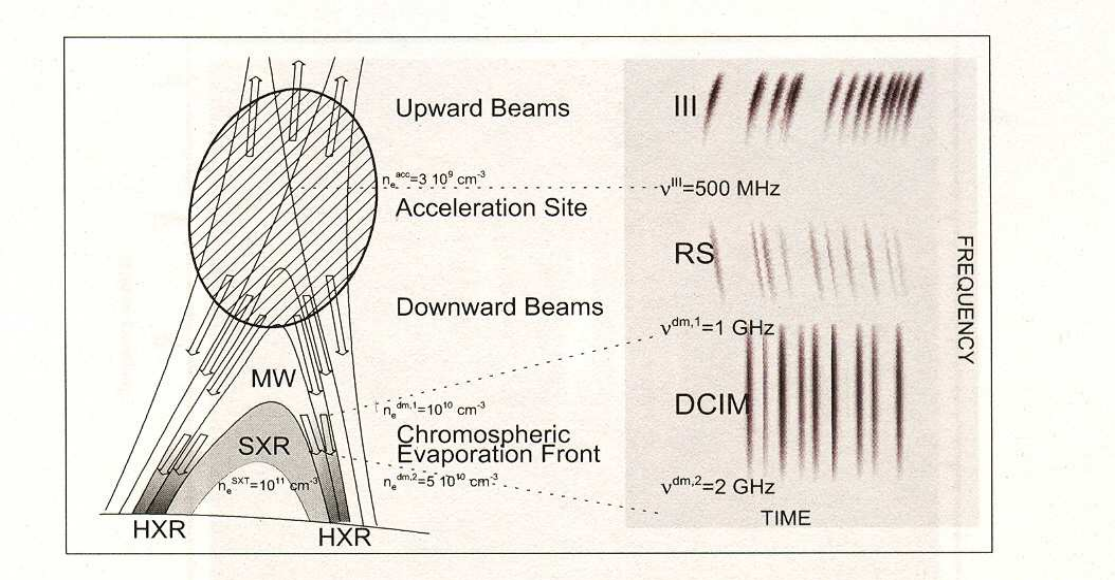

Fig. 3 - Acceleration region above the X-ray bright flare loop accelerating beams in the upward and downward direction is shown.

Spike bursts are seen very often in the decimetric band. Their characteristics are:

a) short duration (< 0.1 s);
b) narrow band ($\Delta f/f \sim 0.03$);
c) highly polarized;
d) short rise and decay times;
e) frequency of occurrence 300 MHz – 8 GHz;
f) occur in clusters;
g) correlated with flares.

The spike bursts are suggested due to Electron Cyclotron Maser Emission (ECME) generated by beams of electrons. They represent basic fragmentation of the energy release in flares.

Diffuse continua occur in the 1 – 3 GHz range than in other range of frequencies. Their characteristic duration ranges between one and some tens of seconds too long for type III burst and too short for a type IV burst. The circular polarization is found to be weak.

Stationary type IV events are continua of > 10 minutes duration occurring in the 0.1 – 3 GHz range. This emission is usually modulated in time scales of 10s or less and is strongly polarized. The emissions are due to electrons trapped in loop shaped magnetic field lines. These broad band emissions occur usually above 1 GHz.

The emission is suggested due to Gyro synchrotron emission of mildly relativistic electrons.

SOLAR ACTIVE REGIONS

Solar active regions are localized areas on the Sun where magnetic flux has erupted through the photosphere into the chromosphere and corona. They are characterized by the presence of sunspots in

white light, enhanced line emission (e.g., Hα, CaII), and greatly enhanced soft X-ray (SXR) and radio emission. As their name implies, solar active regions are the sites of solar flares, a variety of radio bursts, enhanced coronal heating, and play a role in various mass ejections. A key goal of solar physics is to understand their birth, evolution, and decay, and their production of transient, energetic activity.

Manifestation of solar activity is shown as solar active regions which are three dimensional plasma structures of high density, temperature and magnetic field located above sun spots. Radio observations of the solar active regions show multi structure components of the plasma structures generated by different mechanism thermal and non-thermal in origin. The classification of these components and their mechanism depend on the imaging observations at many frequencies. When observed at centimeter wavelengths, a typical solar active region consists of a bright compact source embedded in a diffuse component of low brightness. The Active regions in this Figure 4 show 2 bands symmetric about the equator. The compact source corresponds to the positions of strong magnetic fields.

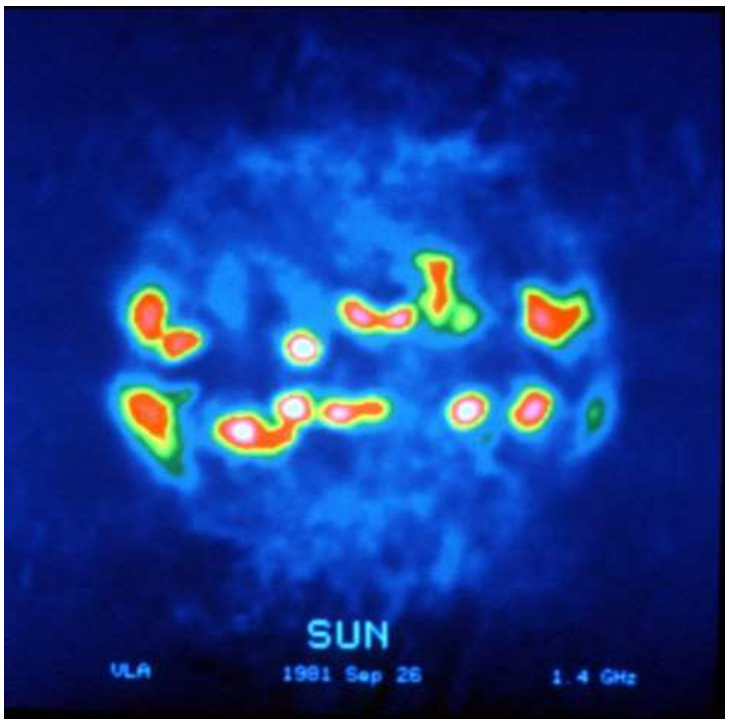

Fig. 4 - Brightness distribution of the Sun shows that the bright features, the solar active regions, form two bands symmetric about the solar equator (Dulk and Gary).

With brightness temperature of Tb ~ 10^6 K, the compact sources are due to gyro resonance emission at low harmonics of the local gyro frequency. The diffuse component which is very well correlated with the H-alpha plage is associated with weaker magnetic fields. The low brightness (Tb ~ 10^6 K) of the diffuse component is due to the optically thin thermal bremsstrahlung. The relative importance of the compact and diffuse sources is wavelength dependent. Diffuse components have spatial scale of the whole active regions of ~ 10^5 km. This component is especially typical for wavelength range of 8- 12 cm and longer. The size of active region at 1.5 GHz ~ 100 arc sec and their

sizes depend on the wavelength of observation (Lara et al., 1998). Study of Active Region Magnetic Field Structures Using VLA Radio, YOHKOH X-ray and MEES Optical Observations were made by Gopalswamy et al. (1994). Full disk VLA images at 20 cm wavelength revealed a number of compact (10" – 20") low brightness sources which were the radio counter parts of EUV bright points detected by EIT (Lang and Wilson, 1997). Statistical analysis of Active regions at 21 cm shows an electron temperature ~ 4.5 MK, Emission measure of 5×10^{28} cm^{-3} and density 1.2×10^{9} cm^{-3}. Observations at 91cm using VLA have showed large sale (5- 10 arc min) that appear to connect widely spaced active regions on the solar surface. VLA observations at 20 cm shows also shorter (1- 2 arc min) loops above individual active regions that evolve in time scales of minutes to hours. Radio observations with the VLA have given information on the size, locations and time evolution of active regions. It has been found that observation of the variation of the size of the gyro resonance source with frequency shows an exponential relationship between the area and wavelength.

CONCLUSIONS

The radio emissions at decimetric wavelengths originate in the upper chromosphere and base of the Corona. Their study is important since the acceleration of electrons takes place in these regions. Using spectrographs and imaging instruments, detailed investigations had been made to understand the physics of active regions.

ACKNOWLEDGEMENTS

I would like to thank the funding authorities, FAPSEP, for their financial support to attend the BDA workshop.

REFERENCES

Benz, A, O., Güdel, M., Isliker, H., Miszkowicz, S., Stehling, W., *Solar Phys.*, 133, 385, 1991.

Gary D. E., Hurford, G., *Proc. Waite*, 1989.

Gopalswamy, N., Schmahl, E. J., Kundu, M. R., Lemen, J. R., Strong, K. T., Canfield, R. C., de La Beaujardiere, J., *Kofu Symp.*, 1994.

Lang, K. R., Willson, R. F., Fifth SOHO Workshop: The Corona and Solar Wind Near Minimum Activity. Ed. A. Wilson, European Space Agency, 1997, p.505.

Sawant, H. S., Subramanian, K. R., Faria, C., Fernandes, F. C. R., Sobral, J. H. A., Cecatto, J. R., Rosa, R. R., Vats, H. O., Neri, J. A. C. F., Alonso, E. M. B., *Solar Phys.*, 200, 167, 2001.

Lara, A., Gopalswamy, N., Kundu, M. R., Perez-Enriquez, R., Koshiishi, H., Enome, S., *Solar Phys.*, 178, 353-378, 1998.

CALIBRATION OF BDA SOLAR OBSERVATIONS WITH GPS SATELLITES AS CALIBRATOR SOURCES

Felipe R. H. Madsen[1,2], Jorge F. V. Silva[2], José R. Cecatto[2] and Hanumant S. Sawant[2]

[1]Vale Soluções em Energia – VSE
Rod. Presidente Dutra, km 138 – 12247-004, São José dos Campos-SP, Brasil
(felipe.madsen@vsesa.com.br)
[2]Divisão de Astrofísica - Instituto Nacional de Pesquisas Espaciais - INPE
Av. dos Astronautas,1758 – 12201-970, São José dos Campos-SP, Brasil
(jorgeval@das.inpe.br; jrc@das.inpe.br; sawant@das.inpe.br)

ABSTRACT

A new technique for the calibration of BDA complex visibilities is proposed, making use of satellites of the Global Positioning System (GPS) as calibrator sources. The technique is based on the properties of the GPS signals, namely the strong flux, higher than that of the Quiet Sun at 1575 MHz, and the source dimensions which imply that the satellites can be regarded as point sources for the BDA. The present status of development of the technique is presented, as well as the results of its application to solar observations using the prototype of the Brazilian Decimetric Array (PBDA), during the period from May to September, 2007. The results indicate that the GPS signals are adequate for calibration of solar observations with the BDA.

Key-words: calibration, solar observations

INTRODUCTION

The solar observations made with interferometers are usually not completely calibrated due to the low brightness (~ 1 – 20 Jy) of most of the celestial calibrators. It is also impossible to observe these standard calibrators with the prototype of the Brazilian Decimetric Array (BDA – Sawant et al., 2007), due to their low brightness and the small number of antennas (5) of the array that implies very low sensitivity. These facts imply that the calibration of BDA solar data requires the use of very strong calibrators, and very few are available in the present catalogs.

A different calibration approach is the suggestion to use satellites of the Global Positioning System (GPS) as calibrator sources (Zhiwei et al., 2007). The GPS signal power on Earth's surface is well known, around -160 dBW at the frequency of the L1 carrier at 1.575 GHz (Rizos, 1999), that is inside the operation band of the PBDA, optimized to 1.6 GHz. Given the satellite orbits, at an approximate height of 20,000 km, it is also possible to consider them as point sources in the far field of the BDA synthesized beam. These properties led to the suggestion that GPS satellites might be appropriate as calibrators for solar observations with interferometers, motivating tests with the BDA.

A method was developed to test this hypothesis that is outlined as follows:

(i) Determine the variation of the position of the satellite in the sky, based on the TLE (two line elements) estimate, in a spherical coordinate system attached to the EW baseline.
(ii) Obtain a set of theoretical phases from the variation of the satellite's position as determined in (i).

(iii) Obtain the phase dispersion of the measured visibilities with respect to the model by subtracting the theoretical phases from the data set.
(iv) Obtain a set of antenna-based calibration solutions from the phase dispersion of the measured visibilities.
(v) Determine the baseline-based amplitude gains through normalization of the observed amplitudes according to the known flux of the satellite signal.
(vi) Determine the phase gains for each baseline, combining the antenna-based gains.
(vii) Apply the calibration solutions to the solar data, interpolating the solutions obtained.

OBSERVATIONS AND RESULTS

The test observations were done with the Prototype of the Brazilian Decimetric Array (PBDA) from May to September 2007. Shown in Figure 1 is a comparison between the theoretical synthesized beam of the PBDA in the EW direction and the one dimensional brightness profile of the GPS satellite after the calibration was applied to the data.

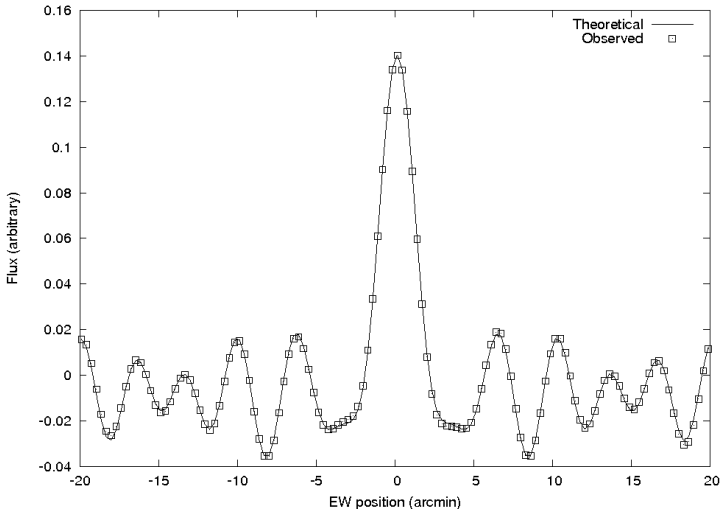

Fig. 1 – Comparison between the theoretical synthesized beam of the PBDA and the one dimensional profile of the GPS satellite GPS BIIA-22 (PRN 05) as observed on test observations on 07/13/2007.

The solar observations were carried out from 24 to 29 September 2007. Each scan on the Sun was preceded and succeeded by scans on a GPS satellite, so that the calibration solutions for the solar data could be obtained by interpolating the calibration solutions for the satellites. The map obtained on 27 September 2007 is shown in Figure 2, where a map of the Sun in EUV on the same day is shown for comparison.

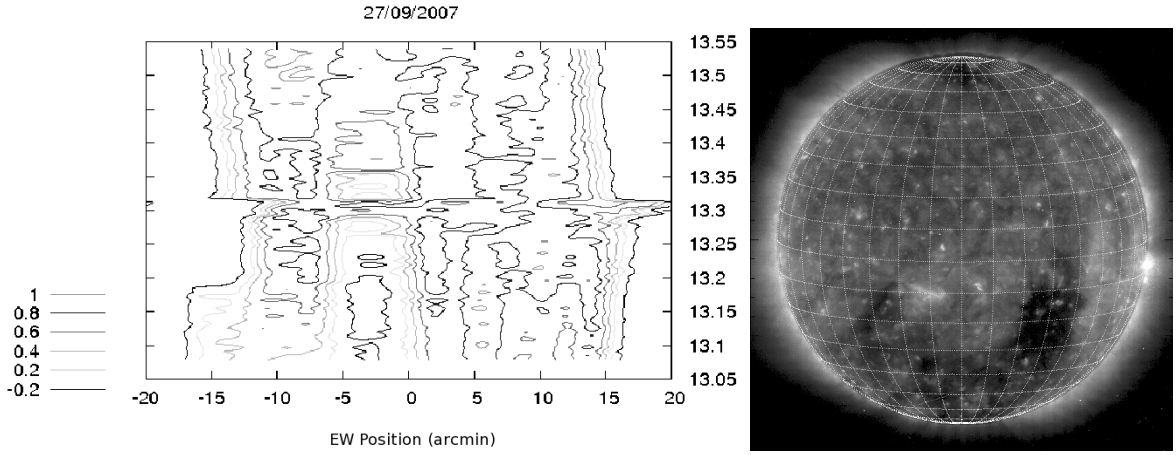

Fig. 2 – One dimensional brightness profile of the Sun obtained with the PBDA on 27 September 2007 (left), and map of the Sun at 195 A obtained with the Extreme Ultra-Violet Imaging Telescope (EIT/SoHO) on the same date. Note that a depression in brightness is seen in both maps, but it appears shifted eastward on the PBDA map with respect to the EIT map.

CONCLUSIONS

The results indicate that very high phase accuracy can be obtained on interferometric observations of GPS satellites, and that these sources are indeed adequate for the calibration of interferometric observations of strong sources like the Sun, particularly for solar observations with the BDA. However, the results also indicate that more tests and further technique development are required to ensure the reliability of the method.

At the present status, the implementation of this method still demands the inclusion of antenna-based calibration for amplitudes, as well as an absolute flux scale, based on the GPS signal power. Also, further solar observations with the BDA have to be carried out, specially after the installation of more antennas, aiming at improving the accuracy of the antenna-based solutions, which implies better calibration and better maps.

Finally, tests of calibration of solar observations with GPS signals should be done with other interferometers to allow the complete verification of the method proposed in this work.

REFERENCES

Rizos, C., http://www.gmat.unsw.edu.au/snap/gps/gps_survey/principles_gps.htm, 1999.

Sawant, H. S. et al., *Solar Phys.*, 242 (1-2), 213-220, 2007.

Zhiwei, L., Gary, D. E., Nita, G. M., White, S. M., Hurford, G. J., *Pub. Astronomical Soc. Pacific*, 119, 853, 303-317, 2007.

SESSION 4 - NON-SOLAR INVESTIGATIONS

Proceedings of the Brazilian Decimetric Array Workshop
São José dos Campos, Brazil - July 28 – August 1, 2008

ENIGMAS OF CENTAURUS A

Luiz C. L. Botti[1,2]

[1]CRAAM/Escola de Engenharia – Universidade Presbiteriana Mackenzie
Rua da Consolação 896 – 01302-907- São Paulo- SP- Brasil
[2]CEA – Instituto Nacional de Pesquisas Espaciais - INPE
Av. dos Astronautas,1758 – 12201-970, São José dos Campos- SP, Brasil
(botti@craam.mackenzie.br)

ABSTRACT

Centaurus A (NGC5128) is the powerful radio source associated with the massive elliptical galaxy NGC5128. It is to a distance of about 3.8 ± 0.4 Mpc (Rejkuba, 2004) and is the closest active galaxy. Note that at this distance 1' on the sky corresponds almost to 1 kpc. It is the largest extragalactic radio galaxy in the sky, with dimensions of about 5° × 9°. Centaurus A has strong emission at 1.4 GHz, about 215 Jy, from the central 30'of the radiosource. The morphology of NGC5128 is very complex and highly structured, it shows significant structure ranging over a factor of 10^8 in size from the largest scales down to less than a mili-arcsecond. Giant outer lobes are extending to about 250 kpc, the northern middle lobe extending to about 30 kpc, inner lobes and central jets extending to about 5.0 and 1.4 kpc. There is a jet which issues from the outer ridge of the northern inner lobe a further 7 kpc to a northern middle lobe. The northern middle lobe is strongly polarized on the ridge furthest from the outer jet which connects it to the inner lobe. The nature of the middle lobe remains unclear, but it is very likely that there is strong interaction between the radio source and the intergalactic medium. The inner jets and lobes have been studied in detail using VLBI and VLA. The proximity of Centaurus A means we have a better spatial resolution of the source, meaning we can see the more subtle interactions of the radio source with the intergalactic medium. The origin of the radio emission is relativistic plasma jets from the central black hole of NGC5128. Our scientific goal is to study the extent to which interactions with the intergalactic medium are shaping the morphology of Centaurus A (using the BDA, VLA, Chandra) and trying to associate approximately 26 knots observed by Chandra (0.85 keV to 2.5 keV) with possible features in BDA maps (1.2-1.7, 2.8 and 5.6 GHz). It will be possible (using X-rays and radio data) to extract spectra for a large number of jet regions. Another objective could be the study of the temporal behavior of Centaurus A at 22 and 43 GHz (Itapetinga antenna, Atibaia, Brazil), trying to associate the variability with the born of components in the jet. At 22 GHz we are observing parts of both internal lobes together with the central source, while at 43 GHz the northern lobe is well separated from the nucleus. But there is some contribution of the southern lobe. This inner jet at radio frequencies is also asymmetric, which the same sidedness as the middle lobe.

Key-words: galaxies: jets – galaxies: active – radio: galaxies: individual: NGC5128-CenA

INTRODUCTION

Centaurus A (J1950 α = 13h 22m 31.6 s δ = -42º 45' 33") is an active galactic nuclei (AGN) usually classified as a FR I type radio galaxy and as a Seyfert 2 object in the optical (Dermer and Gehrels, 1995). Centaurus A is sometimes called blazar at higher energies (Morganti et al., 1992). It contains an active galactic nucleus, having Marconi et al., 2001 estimated the mass of central black hole of about 10^8 M_π. Centaurus A possesses an inner jet close to the nucleus which is detected in the radio and X-ray regime. Centaurus A has a giant lobe with an extension of about 10° on the sky. It is detected from radio to MeV gamma-rays (Clay et al., 1994; Johnson et al., 1997; Israel, 1998). One characteristic of Cen A is its emission at gamma-rays, making it the only radio galaxy detected in MeV gamma-rays. All AGN detected at higher energies are blazars (Collmar et al., 1998). Blazars can be observed at several wavelenghts from radio to gamma-rays. Rapidly variable, blazar emit polarized nonthermal optical light and their total energy output is often dominated by their high-energy emission in X-rays and gamma-rays. Relativistic outflows are observed which and probably are powered by mass accretion onto black hole in the center. The jets are aligned almost parallel to the line-of-sight in blazars but we would like to point that there is other configuration to the jet in Centaurus A, perpendicular to the light-of-sight. This fact seems very controversial, but can be a representation of several active galaxies considered as normal, which are just too far away to be detected at gamma rays. The nucleus of Centaurus A is obscured by the dust lane. This core only can be visible at wavelengths longer than 0.8 µm (Marconi et al., 2000). Single telescope observations have not been able to resolve the nucleus at any wavelength. For example at 1 µm the maximum lengh that can be obtained is about 100 mas; radio interferometry (VLBI) reveals a central structure with 1 pc length (60 mas) at λ = 60 cm (500 MHz). Meisenheimer et al. (2007) carried out interferometric observations at mid-infrared (8.3 µm and 12.6 µm). The mid-infrared emission from the core of Centaurus A is dominated by an unresolved source with less than 10 mas. A counter jet also can be seen inside Centaurus A. At 43 GHz (with interferometric observations) an angular diameter about 0.5 mas or 0.01 pc can be observed. It is the remnant of catastrophic disturbance between two galaxies: a dusty spiral galaxy and a bright elliptical galaxy. In consequence of the interaction there are several outbursts inside this source.

BDA OBSERVATIONS

BDA phase I: five antennas with 4 meter-diameter parabolic dishes were operated using alt-azimuthal mount and operating frequency range between 1.2-1.7 GHz. The 5 antennas had been laid out over a distance of 216 meters in the west-east direction for a spatial resolution approximately 3' at 1.5 GHz. During this phase was impossible to map this radio source. BDA phase 2: it was planned to laid out 21 antennas over the distance of 400 meters in the east-west direction and another 10 antennas over a distance of 200 meters in the north-south direction forming a T-shaped array. The operating frequencies will include higher values: 1.2-1.7, 2.8 and 5.6 GHz. The spatial resolution will be 0.9' with a sensitivity of about 5 Jy (1.2-1.7 and 2.8 GHz). BDA phase 3: four antennas will be added in the east-west direction and two more antennas in the north-south direction. The baselines will be increased in both directions to 2.5 km and 1.25 km, respectively, to increase the spatial resolution of the array up to approximately 4.5 arc seconds at 5.6 GHz. BDA appears as a highly competitive instrument because it can detect low flux density radio sources (< 60 mJy). With this final array will be possible to map the complex structures of Centaurus A.

ASSOCIATED FEATURES IN CENTAURUS A

The whole radio source has been mapped with single-dish telescopes at linear resolutions no better than 4 kpc. The radio-bright inner lobes have been mapped with aperture synthesis telescopes at higher resolutions of about 40 pc and the inner jets and core have been mapped at (sub)parsec resolutions in VLBI experiments. Centaurus A possesses an inner jet close to the nucleus with a large inclination of about 70º (Tingay et al., 1998). In Figure 1 several structures can be observed in this peculiar galaxy: the outer lobes, the middle lobe, the inner lobes and the jet. A pair of inner jets each extend almost 1.4 kpc (80”) from the nucleus, a pair of radio lobes which each extend out 6 kpc (6'). The northern middle lobe has a scale size of about 14' (14 kpc).

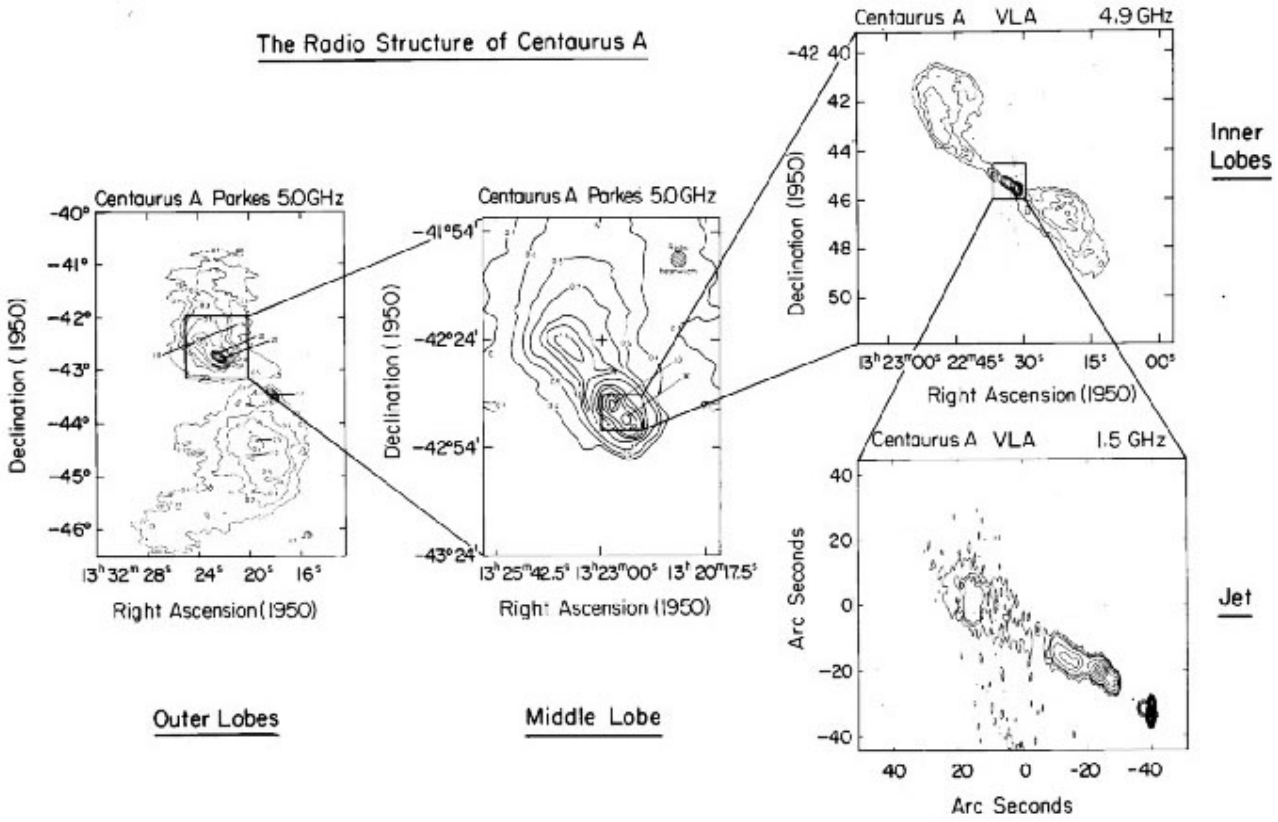

Fig. 1 - Components of the radio source CenA (Burns et al., 1983).

The nature of the middle lobe remains unclear. Maybe can be the interaction between radiosource and the intergalactic medium. The middle lobe is strongly polorised, with magnetic fields vectors almost orthogonal to the field lines of the connecting jets and inner lobes. This radiosource has been observed by Shain (1958), Sheridan (1958), Cooper et al. (1965), Haslam et al. (1981), Combi and Romero (1997), Junkes et al. (1993), Haynes et al. (1983), with angular resolution between 4.1’ and 48' and flux density between 28000Jy at 20 MHz and 681 Jy at 4.8 GHz. The internal lobes and core have been observed by Slee et al. (1983), Christiansen et al. (1977), Clarke et al. (1992),

Tateyama and Strauss (1992), with angular resolution between 4.2” and 258” and flux density between 31 Jy at 43 GHz and 734 Jy at 324 MHz. The nuclear jet has been observed by Slee et al. (1983), Schreier et al. (1981), Clark et al. (1992), Jones et al. (1994), Schreier et al. (1981), Botti and Abraham (1993), Fogarty and Schuch (1975), Kellerman (1974), Tateyama and Strauss (1992), with angular resolution between 0.1” and 252” and flux density between 2 Jy at 327 MHz and 18 Jy at 89 GHz.

In the figure 2 we can see the interaction between the several features of this galaxy and the ambient intergalactic medium (IGM) at 5 GHz. Centaurus A is to a distance of about 3.7 Mpc and is the closest active galaxy. The proximity of this radio galaxy make Centaurus A the ideal source to study the influence this galaxy in the IGM. Centaurus A shows a wide range of complex structures with two jets emerging from its nucleus which bend as they interact with the intergalactic medium (Figure 2).

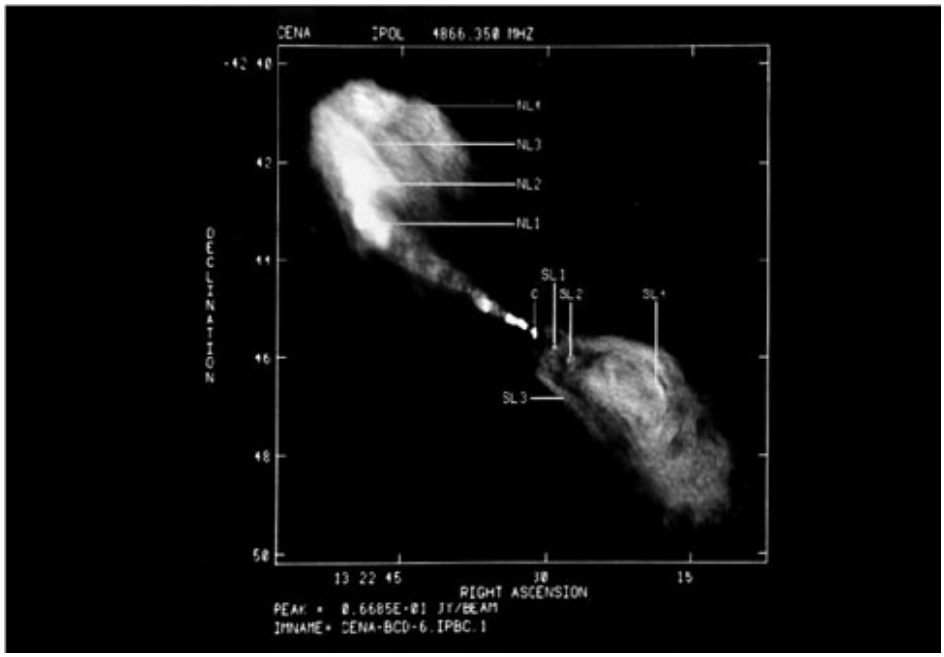

Fig. 2 - Inner lobes and jets at a resolution of 4.4 x 1.2 arcsec (Clarke et al., 1992).

The interstellar medium also can be very important in shaping the jets in Centaurus A (Graham, 1998). There is evidence that the galactic gas can be nice to the confinement of the jet in some Seyfert galaxies, in very distant quasars and in the knots of Centaurus A. It has been known for some time that shells of HI and molecular gas (CO), ionised optical filaments and young massive OB stars are all located well beyond the host galaxy and closely follow the inner and middle radio jets. These structures are the result of the interaction of existing intergalactic gas clouds shock-heated by the expanding jet-lobe. The shocks cause catastrophic cloud-collapse which eventually triggers star formation in northeast radio lobe (Graham, 1998).

VARIABILITY

Centaurus A is highly variable object in all wavelength bands (Kellermann et al., 1974; Davison

et al., 1975; Winkler and White, 1975; Kaufmann et al., 1977; Lawrence et al., 1977; Mushotzky et al., 1978; Delvaille et al., 1978; Beall et al., 1978; Schreier et al., 1979; Baity et al., 1981; Feigelson et al, 1981; Botti, 1983; Gehrels et al., 1984; Cunningham et al., 1984; Lepine et al., 1984; Terrell, 1986; Botti, 1990; Turner et al., 1992; Botti and Abraham, 1993; Jourdain et al., 1993; Hawarden et al., 1993; Kinzer et al., 1995; Steinle et al., 1998; Bond et al., 1996; Romero et al., 1997; Kellermann et al.,1997; Turner et al., 1997; Gastaldi, 2007).

Botti (1990) found correlations between radio (22 and 43 GHz) and X-rays (3-12 keV). The large beams used (approximately 4' at 22 GHz and approximately 2' at 43 GHz) include significant non-nuclear emission, but the radio variability shows to be correlated with that at 3-12 keV which must be associated with the nucleus.

In the figure 3 is shown a continuous monitoring of Centaurus A in X-rays between 1991 and 2008 using the BATSE (Burst and Transient Source Experiment: 20–200 keV) instrument on board CGRO (Compton Gamma Ray Observatory) and RXTE (Rossi X-ray Timing Explorer: 2-10 keV).

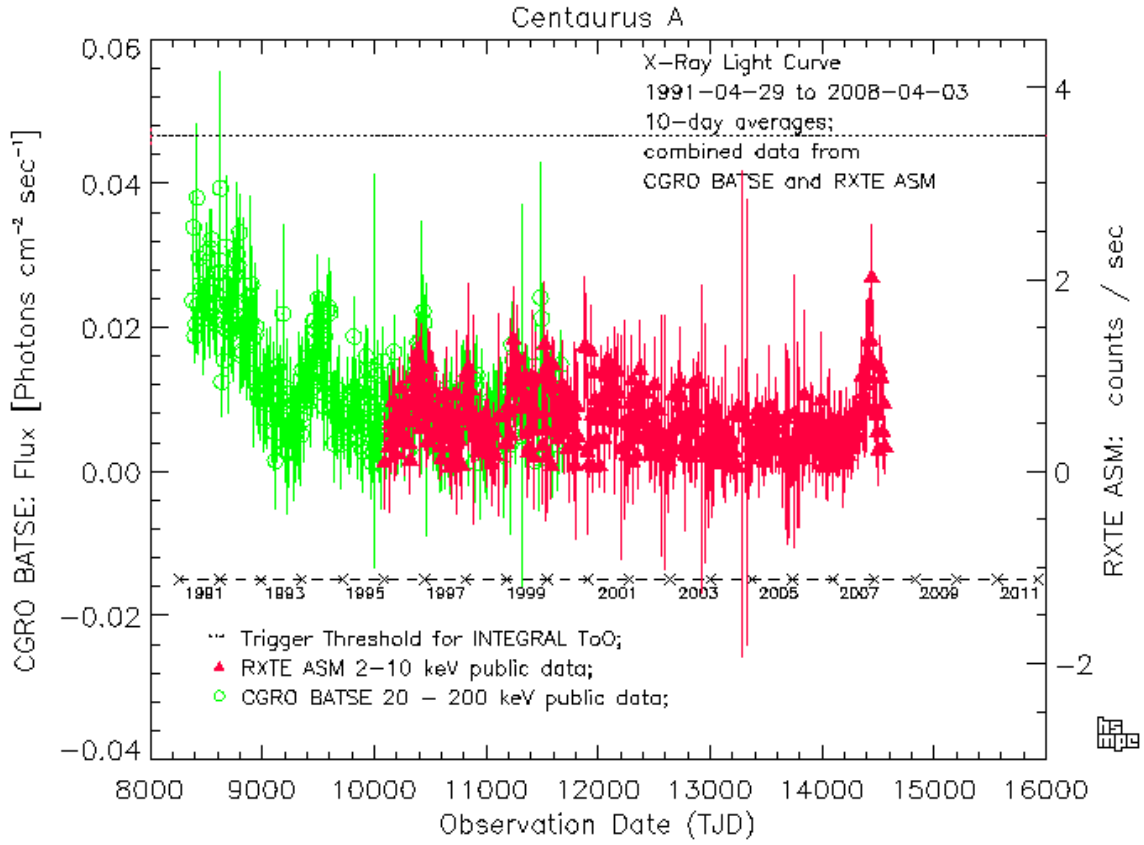

Fig. 3 - A continuous monitoring of Centaurus A (BATSE- Burst and Transient Source Experiment and RXTE-Rossi X-ray Timing Explorer).

DISCUSSION

There is evidence that an unknown distributed particle acceleration process operates in the jet of Centaurus A (Enigma 1). The inner part of the Cen A jet is dominated by shock-related knots. Farther

from the nucleus there is more diffuse X-ray emission in the jet. The cause of particle acceleration in this part of the jet is unknown. Knot is any compact feature in the jet that is clearly distinguished in surface brightness from its surroundings.

The nature of the middle lobe remains unclear. The inner VLBI jet is also asymmetric, with the same sidedness as the middle lobe. The asymmetry of the inner jet can be due to Doppler Boosting but the same explanation is not correct in case of the asymmetry of the middle lobe (Enigma 2).The middle lobe is associated with soft x-rays-emission (Feigelson et al., 1981). Radio observations using high resolution still does not exist for this region of the source. BDA will be able to be used for this finality.

To make competitive extragalactic observations with BDA we need to work with good dynamic range. Australia Telescope Compact Array - ATCA is using a high dynamic range (100000). Image processing algorithms to deal with the high dynamical range and large field-of-view must be improved by BDA team. Will it be possible have high dynamic range in BDA system?

Explore feedback between the polarized radio jets and the environment of the Centaurus group of galaxies can be one of BDA goals. Will it be possible to exploit the strong polarized continuum of Centaurus A using BDA system?

Interaction between the non-thermal plasma ejected from the active nucleus and the interstellar medium of Centaurus A is responsible for a variety of phenomena such as ionisation of the gas and AGN driven outflows.

A high-energy outflow close to the black hole may be producing the X-rays by the same synchrotron process that explains the knots in the jet. The knots near the nuclear component are much brighter in X-rays than the farthest knots. The reason for this dimming is unknown (Enigma 3). It is likely to be related to the slowing of the jet. High–energy electrons spiralling around magnetic fields lines produce the X-ray emission from the jet. The electrons must be continually reaccelerated or the X-ray will fade out. Knot-like features detected by Chandra (Hardcastle et al., 2007) show where the acceleration of particles to high energies is currently occurring. The inner part of the X-ray jet close to the black-hole is dominated by these knots of X-ray emission. The radio emission is produced by the synchrotron process in which high-energy electrons radiate as they spiral around the magnetic field of the galaxy.

CONCLUSION

Centaurus A will be an ideal source to make non-solar observations with BDA system. No other radio galaxy allows its lobe structures to be studied in so specific detail. At declinations which range from - 47º to -38º, Centaurus A is perfectly located for the BDA.

ACKNOWLEDGEMENTS

This work was partially supported by the Brazilian Agency FAPESP. I would like to thank the BDA workshop organizers for their essential support.

REFERENCES

Baity, W. A., Rothschild, R. E., Lingenfelter, R. E., Stein, W. A., Nolan, P. L., Gruber, D. E., Knight, F. K., Matteson, J. L., Peterson, L. E., Primini, F. A., Levine, A. M., Lewin, W. H. G., Mushotzky, R. F., Tennant, A. F., *ApJ*, 244 (1), 429, 1981.

Beall, J. H., Rose, W. K., Graf, W., Price, K. M., Dent, W. A., Hobbs, R. W., Conklin, E. K., Ulich, B. L., Dennis, B. R., Crannell, C. J., Dolan, J. F., Frost, K. J., Orwig, L. E., *ApJ*, 219 (1), 836, 1978.

Bond, L. A., Ballet, J., Denis, M., Vargas, M., Jourdain, E., Roques, J. P., Bouchet, L., Niel, M., Chernyakova, M., Churazov, E., Gilfanov, M., Sunyaev, R., Finoguenov, R., Dyachkov, A. A., Khavenson, N., Novikov, B., *A&A*, 307, 708, 1996.

Botti, L. C. L, Abraham, Z., *MNRAS*, 264, 807, 1993.

Botti, L. C. L, Dissertation of Master's Degree Instituto de Pesquisas Espaciais, São José dos Campos, no of pages: 114 (Publication no 2913-TDL/149), 1983.

Botti, L. C. L, Ph.D. Thesis Instituto de Pesquisas Espaciais São José dos Campos, no of pages: 258 (Publication no 5218-TDL/432, 1990.

Burns, J. O., Feigelson, E. D., Schreier, E. J., *ApJ*, 273, 128, 1983.

Christiansen, W. N., Frater, R. H., Watkinson, A., O'Sullivan, J. D., Lockhart, I. A., *MNRAS*, 181, 183, 1977.

Clarke, D. A., Burns, J. O, Norman, M. L., *ApJ*, 395, 444, 1992.

Clay, R. W., Dawson, B. R., Meyhandan, R., *Astropart. Phys.*, 2, 347, 1994.

Collmar, W., Bennett, K., Bloemen, H., Blom, J. J., Hermsen, W., Lichti, G. G., Ryan, J., Schomfelder, V., Stacy, J. G., Steinle, H., Williams, O. R., Winkler, C., *Astrophys. Lett. Commun*., 39, 57 (525), 1999.

Combi, J. A., Romero, G. E., *A&AS*, 121, 11, 1997.

Cooper, B. F. C., Price, R. M., Cole, D. J., *Aust. J. Phys*., 18, 589, 1965.

Meisenheimer, K., Tristam, K. R. W., Jaffe, W., Israel, F., Neumayer, N., Raban, D., Rottgering, H., Cotton, W. D, Graser, U., Henning, Th., Leinert, Ch., Lopez, B., Perrin, G., Prieto, A. *A&A*, 471, 453, 2007.

Cunningham, C. T., Ade, P. A. R., Robson, E. I., Radostitz, J. V., *MNRAS*, 211, 543, 1984.

Davison, P. J. N., Culhane, J. L., Mitchell, R. J., Fabian, A. C., *ApJ*, 195 (1), L23, 1975.

Delvaille, J. P., Epstein, A., Schnopper, H. W., *ApJ*, 219 (2), L81, 1978.

Dermer, C. D., Gehrels, N., *ApJ*, 447,103, erratum in April, 456, 412, 1995.

Feigelson, E. D., Schreier, E. J., Delvaille, J.P., Giacconi, R., Grindlay, J. E., Lightman, A. P., *ApJ*, 251, 31, 1981.

Fogarty, G., Schuch N. J., *Nature*, 254, 124, 1975.

Gastaldi, Dissertation of Master's Degree Universidade Presbiteriana Mackenzie São Paulo, 2007.

Gehrels, N., Cline, T. L., Teegarden, B. I., Paciesas, W. S., Tueller, J., Durouchoux, P. H., Hameuryj, J. M., *ApJ*, 278,112, 1994.

Graham, J. A., *ApJ*, 502, 245, 1998.

Hardcastle, M. J., Kraft, R. P., Sivakoff, G. R., Goodger, J. L., Croston, J. H., Jordan, A., Evans, D. A., Worral, D. M., Birkinshaw, S., Brassington, N. J., Forman, W. R., Harris, W. E., Jones, C., Juett, A. M., Murray, S. S., Nulsen, P. E. J., Sarazin, C. L., Woodley, K. A., *ApJ*, 670 (2), L81, 2007.

Haslam, C. G. T., Klein, U., Salter, C. J., et al., *A&A*, 100, 209, 1981.

Haynes, R. F., Cannon, R. D., Ekers, R. D., *Proc. ASA*, 5, 241, 1983.

Hawarden, T. G., Sandell G.., Matthews, H. E., Friberg, P., Watt, G. D., Smith, P. A., *MNRAS*, 260, 844, 1993.

Israel, F. P. *Astron. Astrophys. Review*, 8, 237, 1998.

Johnston, W. N.; Zdziarki, A. A.; Madejski, G. M. et al., In: C. D. Dermer, M. S. Strickman, J. D. Knafess, eds., AIP Conf. Proc. 410, 4th Compton Symposium: Seyferts and Radio Galaxies, p. 283, 1997.

Jones, P. A., McAdam, W. B., Reynolds, J. E., *MNRAS*, 268, 602, 1994.
Jourdain, E., Bassani, L., Roques, J. -P., *ApJ*, 412, 586, 1993.
Junkes, N., Haynes, R. F., Harnett, J. I ., Jauncey, D. L., *A&A*, 269, 29, 1993.
Kaufmann, P., Santos, P. M., Raffaelli, J. C., Scalise Jr, E., *Nature*, 259 (5626), 311, 1977.
Kellerman, K. I., *ApJL*, 194, L135, 1974.
Kellerman, K. I., Zensus, J. A., Cohen, M. H., *ApJL*, 475, L93, 1997.
Kinzer, R. L., Johnson, W. N., Dermer, C. D., Kurfess, J. D., Strickman, M. S., Grove, J. E., Kroeger, R.A., Grabelsky, D. A., Purcell, W. R., Ulmer, M. P., Jung, G. W., Mcnaron-Brown, K., *ApJ*, 449, 105, 1995.
Lawrence, A., Pye, J. P., Elvis, M., *MNRAS Short Communication*, 181(3), 93, 1977.
Lépine, J. R. D., Braz ,M. A., Epchtein, N., *A&A*, 131,72, 1994.
Marconi, A, Schreier, E. J., Ethan, J., Koekmoer, A., Capetti, A. Axon, D., Machetto, D., Caon, N., *ApJ*, 528 (1), 276, 2000.
Marconi, A, Schreier, E. J., Koekmoer, A, Capetti, A. Axon, D., Machetto, D., Caon, N., *ApJ*, 549 (2), 915, 2001.
Morganti, R., Fosbury, R. A. E., Hook, R. N., Robinson, A., Tsvetanovy, Z., *MNRAS*, 256, 1p, 1992.
Mushotzky, R. F., Serlemitsos, P. J., Becker, R. H., Boldt, E. A., Holt, S. S., *ApJ*, 220, 790, 1978.
Rejkuba, M., *A&A*, 413, 903, 2004.
Romero, G. E., Benaglia, P., Combi, J. A., *A&AS*, 124, 307, 1997.
Schreier, E. J., Burns, J. O, Feigelson, E. D., *ApJ*, 251, 523, 1981.
Shain, C. A., *Aust. J. Phys*, 11, 517, 1958.
Schreier, E. J., Feigelson, E., Delvaille, J., Giacconi, R., Grindlay, J., Schwartz, D., Fabian, A., *ApJL*, 234, L39, 1979.
Sheridan, K. V., *Aust. J. Phys*. 11, 400, 1958.
Slee, O. B., Sheridan K. V., Dulk G. A., Little A. G., *Proc. ASA*, 5, 247, 1983.
Steinle, H., Bennett K., Bloemen H., Collmar W., Diehl R., Hermsen W., Lichti, G. G., Morris D., Schoenfelder V., Strong A. W., Williams O. R., *A&A*, 330, 97, 1998.
Tateyama, C. E., Strauss F. M., *MNRAS*, 256, 8, 1992.
Terrell, J., *ApJ*, 300, 669, 1986.
Tingay, S. J., Jauncey, D. L., Reynolds, J. E., Tzioumis, A. K., King, E. A., Preston, R. A., Jones, D. L., Murphy, D. W., Meier, D. L., van Ommen, T. D., McCulloch, P. M., Ellingsen, S. P., Costa, M. E., Edwards, P. G., Lovell, J. E. J., Nicolson, G. D., Quick, J. F. H., Kemball, A. J., Migenes, V., Harbison, P., Jones, P. A., White, G. L., Gough, R. G., Ferris, R. H., Sinclair, M. W., Clay, R. W., *ApJ*, 115, 960, 1998.
Turner, P. C., Forrest, W. J., Pipher, J. L., Shure, M. A., *ApJ*, 393, 648, 1992.
Turner, T. J., George, I. M., Mushotzky, R. F., Nandra, K., *ApJ*, 475, 118, 1997.
Winkler, P. F., White, A. E., *ApJ*, 199(3), L139, 1975.

Proceedings of the Brazilian Decimetric Array Workshop
São José dos Campos, Brazil - July 28 – August 1, 2008

25 YEARS OF COSMIC MICROWAVE BACKGROUND RESEARCH AT INPE

Carlos Alexandre Wuensche and Thyrso Villela

Divisão de Astrofísica - Instituto de Pesquisas Espaciais - INPE
Av. dos Astronautas,1758 – 12201-970, São José dos Campos-SP, Brasil

ABSTRACT

This article is a report of 25 years of Cosmic Microwave Background activities at INPE. Starting from balloon flights to measure the dipole anisotropy caused by the Earth's motion inside the CMB radiation field, whose radiometer was a prototype of the DMR radiometer on board COBE satellite, member of the group cross the 90s working both on CMB anisotropy and foreground measurements. In the 2000s, there was a shift to polarization measurements and to data analysis, mostly focusing on map cleaning, non-gaussianity studies and foreground characterization.

INTRODUCTION

The cosmic microwave background radiation (CMB) is one of the most important cosmological observables presently available to cosmologists. Its properties can unveil information, among others, about the inflationary period, the overall composition of the Universe (Ω_0), the existence of gravitational waves, the age of the Universe and other parameters related to the recombination and decoupling era (Hu and Dodelson, 2002). These observables are critical to understand the physical processes accounting for the formation and evolution of the Universe. The CMB is observed from a few GHz to a few hundreds of GHz. It also observed in various angular scales, varying from less than 1 arcmin to many degrees, each range of scales encoding information about specific physical processes from the early (or not so early) Universe. Its properties (intensity, anisotropies and polarization) can be studied from the ground, on board stratospheric balloons and satellites and are strongly hampered by the so-called foreground contaminants, constituted by radio point sources and Galactic emission.

It is expected that the next space missions to measure the anisotropy and the polarization of CMB will mostly deal with foreground systematics, since the sensitivity obtained from years in space can only increase by a $(t)^{-1/2}$ factor and the technology used for detectors are quickly approaching the quantum limit efficiency (see, e.g., CMB Task Force 2006, hereafter CMBTF2006). Also, most detectors used in the present generation of instruments and projected for the next one are in the 10 - 1 microK.sqrt(Hz) sensitivity (ref). On the other hand, foreground emission is arguably the last frontier to CMB studies, since the details of synchrotron, free-free and dust emission, as well as their spectral and spatial distributions are still poorly understood. Presently, the foreground emission from the abovementioned processes accounted for in many different CMB missions (see, e.g., CMB F2006) between 30 and 600 GHz can contribute at the same intensity level or above, than the E and B polarization modes of CMB.

INPE's Cosmology Group (hereafter CG) has contributed to many aspects of CMB studies in the last 25 years and is presently devoted to foreground emission and total intensity measurements in the experimental side (see, e.g., Tello et al., 2007; Levy et al., 2008; Kogut et al., 2009; Fixsen et al., 2009; Seiffert et al., 2009). On the phenomenological and data analysis aspects, the group has contributed in the CMB anomalies and asymmetries aspects, as well as in the search of global isotropy of the Universe (see, e.g., Abramo et al. 2006; Abramo, Sodré and Wuensche, 2006; Bernui and Villela, 2006; Bernui et al., 2007; Bernui, Tsallis and Villela, 2007; Bernui, Ferreira and Wuensche, 2008; Bernui 2008).

This paper will describe briefly the contributions of the CG to CMB studies, including only the most significant results from the 80s, 90s and 2000s. Section 2 presents the CMB history and INPE's CG participation. Section 3 includes our contribution to foreground studies. Section 4 contains our data analysis and phenomenology contributions and the technological contributions are in Sec. 5. We summarize this article in Section 6.

INPE AND CMB HISTORY

In the early 80's, three issues were attacked by CMB researchers: the expected blackbody characteristics, of CMB, the expected dipole signal from our movement though CMB photons and the temperature fluctuations left on CMB as a result of the primordial density fluctuation,s due to the coupling between photon and matter before the recombination era, at z ~ 1400 - 1100.

The era pre-COBE

A series of balloon flights were performed in the USA and in Brazil to nail down the dipole characteristics, which was not a cosmological signal, and to search for the cosmological CMB quadrupole signal. The combined result from these two flights were reported by Lubin and Villela (1986) and Lubin et al (1985), with a dipole intensity of 3.44 ± 0.17 mK and a direction of RA = 11.2 h, Dec = -6^{o}. The reported quadrupole upper limit was 7×10^{-5} microK. The instrument used in these flights was a prototype of one of the DMR (Differential Microwave Radiometer) used onboard COBE satellite, which was launched in 1989.

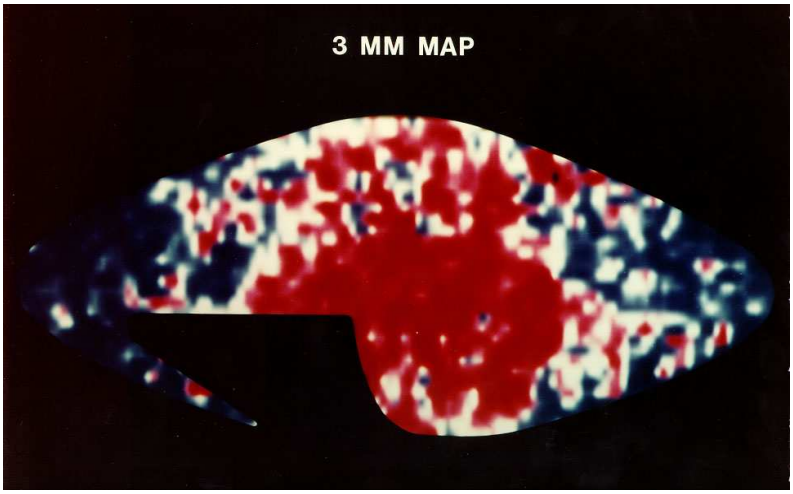

Fig. 1 - Dipole anisotropy map (in celestial coordinates) covering 85% of the sky. The black region in

the lower left part of the map was not covered during the two observation campaigns.

The COBE times

COBE was launched in 1989 and was the first NASA satellite fully dedicated to measure the CMB. It carried three experiments onboard: the FIRAS (Far InfraRed Absolute Spectrophotometer) to measure the CMB spectrum, operating from 60 to 600 GHz, The DMRs (Differential Microwave Radiometers) were designed to measure the angular distribution and operated in 31, 53 and 90 GHz. DIRBE (Diffuse InfraRed Background Explorer) was designed to measure mostly the dust emission in the far infrared band of the eletromagnetic spectrum (from 240 μm to 1.25 μm). The COBE mission ended in 1994 and was very successful, setting milestones for the next generation of balloon and ground experiments during the 90s.

The blackbody shape of CMB temperature spectrum was reported weeks after launch (Mather et al., 1990, Figure 2), showing an almost perfect blackbody shape. The expected large-scale temperature fluctuations were reported a little later by Smoot et al. (1992). The COBE maps, from a full sky map to clean, CMB only map, can be seen in Figure 3. The interpretation of COBE results were discussed in a companion paper by Wright et al. (1992). However, the DMR observed the sky with a large horn (about 7 degrees FWHM) and did not probe intermediate and small angular scales ($\theta < 2°$), where the signature of the density fluctuations in the form of acoustic peaks should be found.

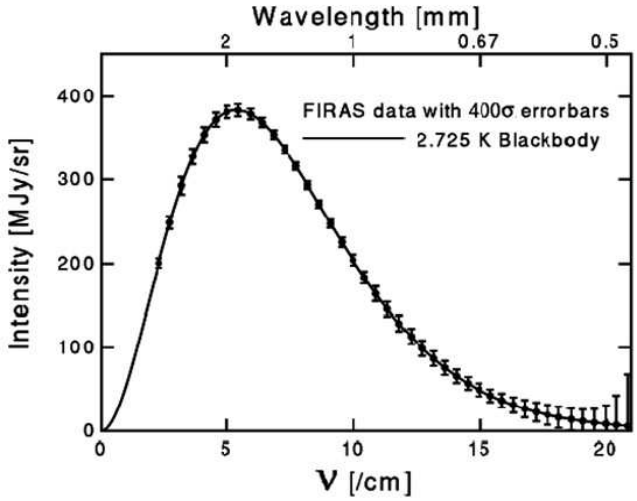

Fig. 2 - The FIRAS measurements on top a theoretical blackbody curve. Note the amplification of the error bars in order to be noticed in the graph.

One of the COBE science team members, Philip Lubin, then at University of California Santa Barbara, proposed a series of experiments in the late 80s, to measure these medium scales. Together with Paul Richards, at the University of California, Berkeley, they started a series of experiments to search for CMB anisotropy in medium angular scales. The result were 4 balloon flights with bolometers as their detectors (the ACME-MAX series: Alsop et al., 1992; Gundersen et al., 1993; Meinhold et al., 1993; Clapp et al., 1994; Devlin et al., 1994; Tanaka et al., 1996; Lim et al., 1996), and 4 campaigns at the South Pole, using HEMT detectors (the ACME-SP series: Meinhold and

Lubin, 1990; Gaier et al., 1992; Schuster et al., 1993; Gundersen et al., 1995). Some of their results, detecting medium-scale temperature fluctuations, can be seen in Figures 4, 5 and 6.

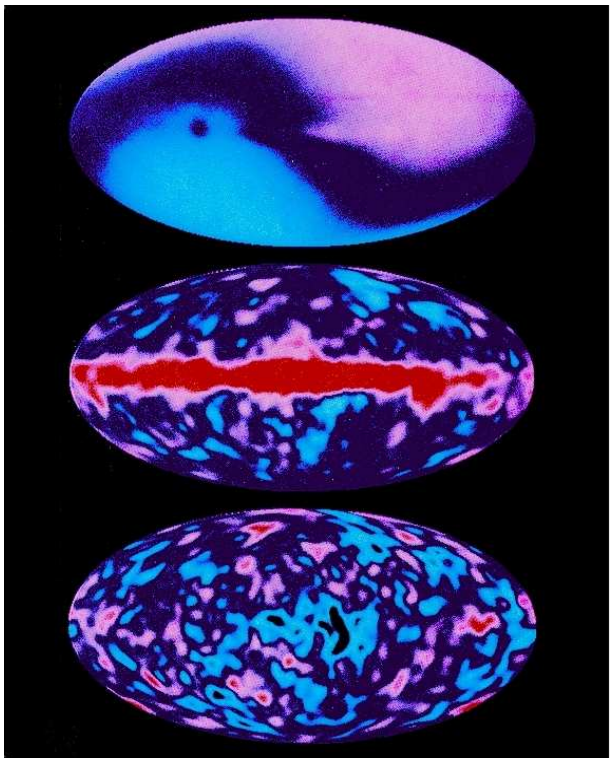

Fig. 3 - COBE anisotropy maps. The top map contains the dipole and the Galaxy emission on top of the CMB anistropies; the center map had the dipole removed, containing CMB and Galaxy; the bottom map contains CMB fluctuations only.

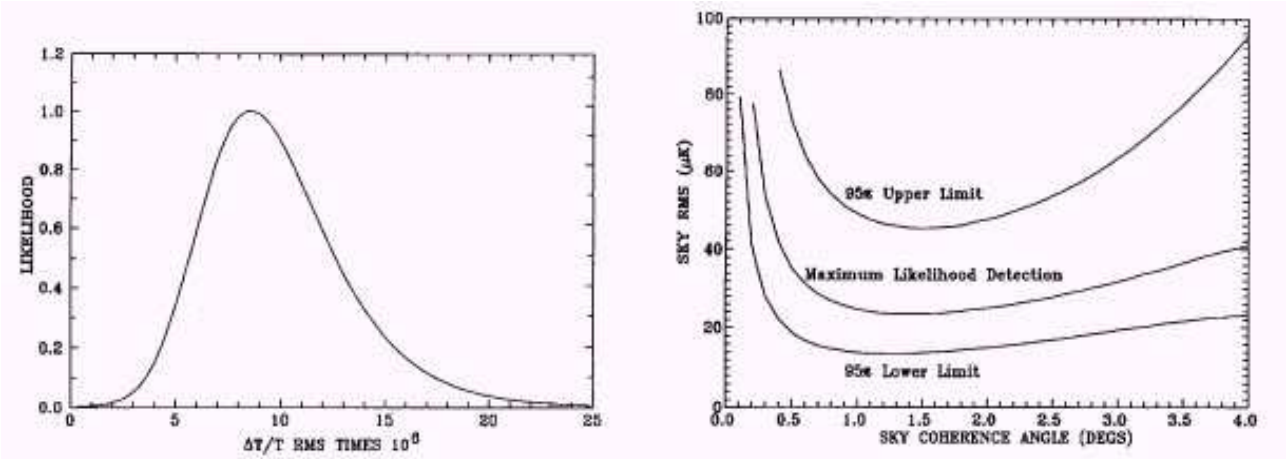

FIG. 3.—95% confidence upper limit, maximum to the likelihood, and 95% confidence lower limit, for an assumed Gaussian sky autocorrelation function

Fig. 4 - Results from Schuster et al (1993). Note the picture in the right, with the autocorrelation function results used to verify the results and claim the detection as done in this work.

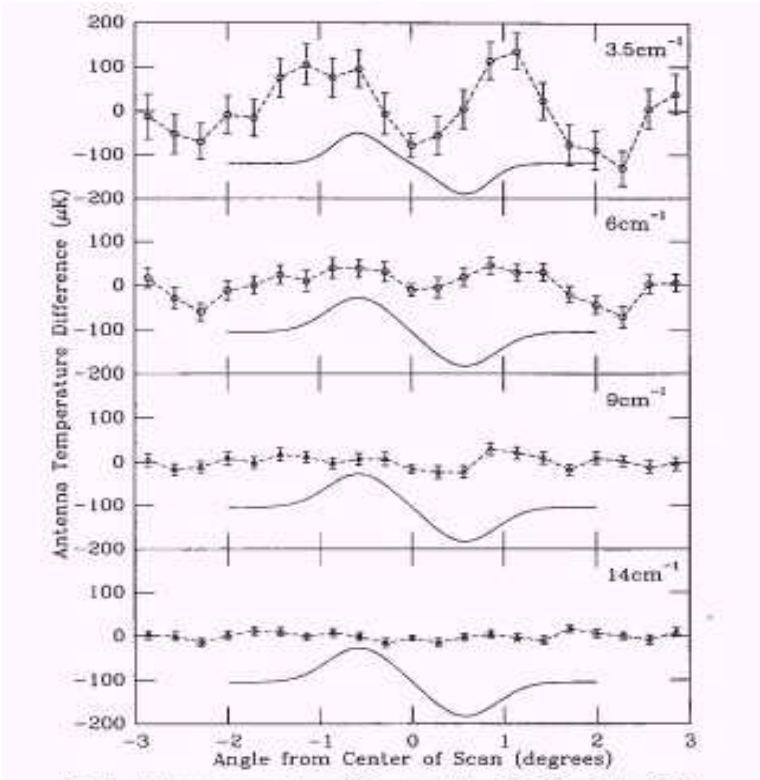

Fig. 5 - Results from Devlin et al. The CMB excess claimed as a detection can be noticed in the upper part of the figure.

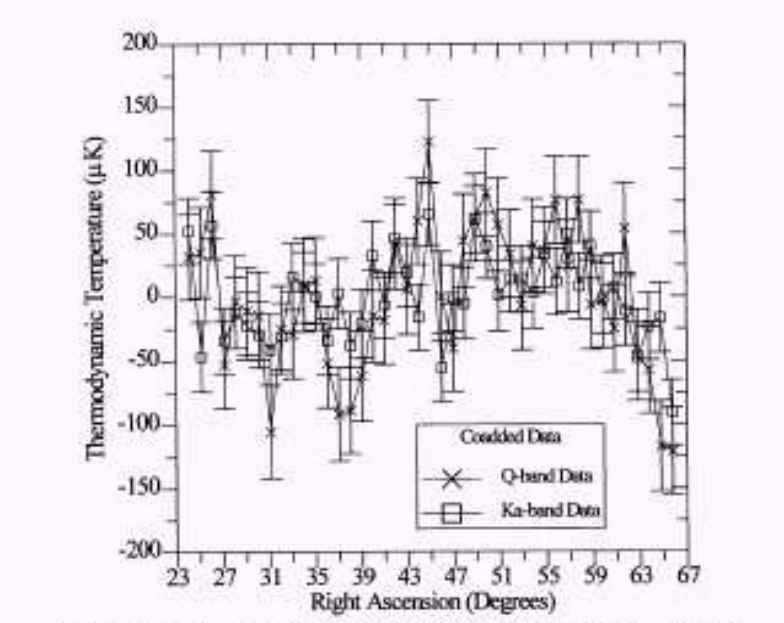

Fig. 6 - The ACME-SP 1995 from Gundersen et al. These data points were one of the first to be used to delimit the acoustic CMB peak.

In the late 90s, the UCSB group developed a new telescope concept, using a large (2.6 m diameter), flat rotating mirror as a tool to quickly cover large regions of the sky, and flew this instrument on a balloon. Since it carried HEMT detectors but flying onboard a stratospheric balloon, it was named HACME, standing for Hemts on ACME (Staren et al. 2000; Tegmark et al., 2000, Figure 7). HACME made one of the first maps of CMB anisotropy in medium angular scales and was a prototype for another new telescope: BEAST (Background Emission Anisotropy Scanning Telescope), to be described in the next section.

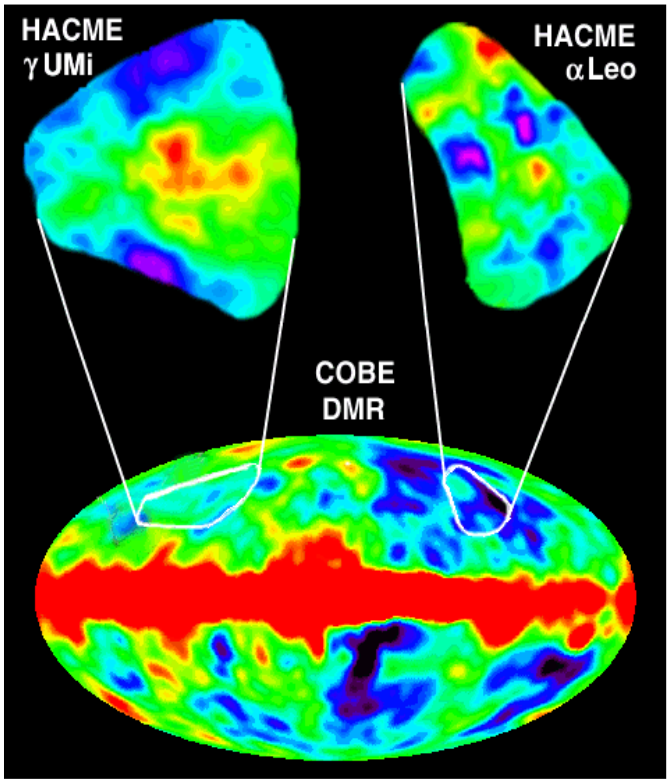

Fig. 7 - A high resolution CMB map, made by the HACME experiment, compared to the COBE all-sky map.

The 2000s

The BEAST telescope operated on the ground, in the White Mountain Research Station (USA) and incorporated two carbon fiber large mirrors (paraboloid of 2.2 m and ellipsoid of 0.8 m in the semi-major axes) on board a gregorian mounting with an off-axis optic (Figure 8). It also featured a new optical design to minimize sidelobe contributions (Figueiredo et al., 2005; Childers et al., 2005), building on the experience of its predecessors. BEAST measured the CMB anisotropies and the Galaxy contribution around the north celestial pole (Meinhold et al. 2005; Mejia et al. 2005) and was the first instrument of the group to measure the CMB power spectrum and put limits in the cosmological parameters (O'Dwyer et al., 2005). Figure 9 shows the area covered by BEAST (about 4% of the sky) compared to a full sky WMAP map.

Fig. 8 - BEAST in its dome in White Mountain. The size of the instrument and components can be figured out by comparing with investigators in front of the gondola. They are about 1,80 m tall.

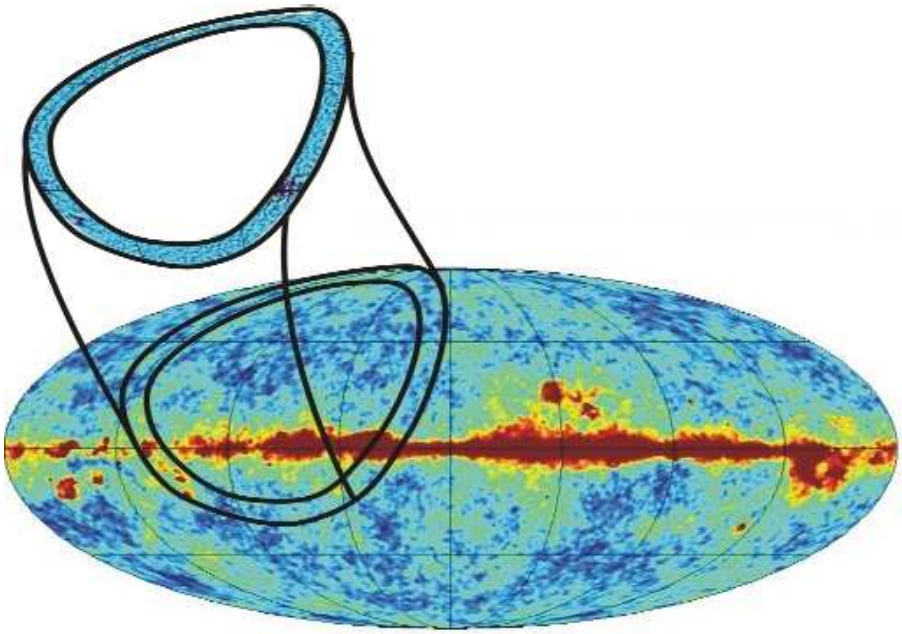

Fig. 9 - Superposition of BEAST on top a combined WMAP map including the Galaxy.

The natural extension of BEAST would be an instrument with polarization measurement capabilities and this came with the WMPol (White Mountain Polarimeter), also operating at White Mountain Research Station. The results were not as good as the previous one, due to instrumental and sensitivity limitations. The instrument took data at 42 GHz and reported upper limits for CMB E-mode polarization of 14 microK (Levy et al. 2008). It was intended as a prototype for a more sofisticated "foreground-cleaner" instrument, setup to measure CMB foregrounds between 10 and 20 GHz, and also to be sensitive to B-mode polarization. This experiment, called COFE (COsmic Foreground Explorer), is described by Leonardi et al. (2006).

FOREGROUND STUDIES

INPE's CG has been involved in foreground studies since the early 90's, when the GEM (Galactic Emission Mapping) project started. Its goal: to map synchrotron radiation at 408 MHz, 1,465 MHz, 2.3 GHz, 5 GHz and 10 GHz along 60-deg wide declination bands from several locations with a single dish. Using the 408 MHz measurements as a cross-check with the Haslam survey (Haslam et al 1982) and the novel observational strategy of a rotating dish, the GEM experiment began its search for the spatial and spectral distribution of foreground templates without the baseline inhomegeneities that plagued combinations of earlier low frequency surveys. Another checks could be done against the 1420 MHz Reich and Reich survey (1986) and the Jonas 2.3 Gz survey (2003), In addition, Stokes U and Q polarization components have been implemented for the 5 and 10 GHz experiments, which avoid Faraday rotation to a cosmological level of interest for CMB studies.

GEM started its operations at 408 and 1,465 MHz in Bishop, California (USA) in 1993 and it spent a brief, but intense, campaign in Villa de Leyva, Colombia, (Torres et al 1996) where 2.3 GHz observations were added. Mapping of the Southern Sky began after its arrival in Brazil in 1998 (Tello et al 2000, 2007) and recently polarization measurements at 5 GHz became a very welcome reality (Ferreira 2008).

INPE's CG participation in the development of the GEM project has been crucial since its early stages, from the construction of receivers at 1,465 MHz (Tello 1997) and 5 GHz (Ferreira 2008) to a more efficient design of the ground screen and shield (Tello et al 1999, 2000) and the adaptation of a cryogenic system for the 5 and 10 GHz receivers. Understanding ground contamination has been one of GEM's main assets in producing a reliable baseline for maps of the radio continuum at low ferquencies (Tello et al 1999). Polarization measurements will also benefit of newly implemented control and cryogenic systems.

In 2009 the CG will completely refurbish the optical design of the GEM dish to accomodate the challenging requirements of polarization measurements at 10 GHz, as well as the design and fabrication of the 10 GHz receiver, which will be completely fabricated in Brazil.

CMB DATA ANALYSIS

Additionally, the group has devoted some time to do some phenomenology and worked in CMB data analysis as well, both to produce science results and to propose new analysis tools. In the early 2000's there were some efforts to search for non-gaussianity in the CMB anisotropies, addressed in a series of papers by Andrade, Wuensche and Ribeiro (2004, 2005, 2006). This deviation from gaussianity can be tested with a non-extensive statistics approach proposed by Tsallis (1988). Bernui, Tsallis and Villela (2006, 2007) did such test and reported a very small degree of non-extensivity in the CMB data using 1- and 3-year WMAP data.

After the WMAP results were released (Bennett et al. 2003, Hinshaw et al. 2007), the questions about the isotropy and asymmetry of CMB angular distribution was studied using a statistical tool, the PASH, proposed by Bernui and Villela (2006). These papers examined both the isotropy and the symmetries of CMB anisotropies (Bernui, Ferreira and Villela 2004; Bernui 2005; Bernui et al 2006; Abramo et al. 2006, Abramo, Sodré and Wuensche 2006).

Using the same idea, Bernui, Ferreira and Wuensche (2008) explored the isotropy of the GRB distribution in the Universe, showing no major evidence of anisotropy in the data.

TECHNOLOGICAL DEVELOPMENTS

INPE's CG has taken part in a large number of CMB missions, contributing, in many of them, towards the technological side of the instrument, besides data analysis and science discussions. Table 1 shows some of CG contributions since 1990, and in which stage there was a major involvement.

Table 1 - CG contributions since 1990.

Part	Study	Design	Fabr.	Test	Oper.	Year
BEAST Horns			X	X		2001
Waveguides and transitions		X	X			2001
ARCADE horns and transitions		X	X	X		2005
GEM Dewar	X	X	X	X	X	2006
GEM fences	X	X	X	X	X	2001
1.465 and 5 GHz receivers	X	X	X	X	X	
Optical project for HACME and BEAST	X	X	X			1996
Microwave simulations for WMPOL and GEM	X	X	X	X		2005-2007
5 GHz OMT	X	X	X	X		2006

CONCLUSIONS

Since its creation, in the late 80s, the CG at INPE has been deeply involved in all aspects of CMB measurements and CMB foregrounds, particularly synchrotron emission. There were collaborations covering ground, balloon and satellite missions, mostly with groups from Berkeley and Santa Barbara (USA) and a deep involvement of all the scientists and students from the group.There also efforts devoted to CMB data analysis and phenomenology addressing issues in datasets produced

by instruments in which the CG was involved. These efforts attacked mostly non-gaussianity aspects of CMB distribution and its global isotropy and asymmetry.

Summing up all contributions, INPE's CG produced a total of 54 papers in about 25 years of existence, including a major gap, from 1987 to 1997, where most of the PhD degrees produced in the group were concluded. The group produced, as of December 2008, a total of 9 PhD theses and 9 MSc dissertations, some of which now hold permanent positions at universities and research centers in Brazil and abroad, and still keep some level of contact with the science scene at INPE.

Presently the group is mostly involved in the development of a 10 GHz receiver for the GEM instrument and is working on the data analysis of the ARCADE instrument, a collaboration between Goddard Space Flight Center/NASA, Jet Propulsion Lab/NASA, University of California Santa Barbara, University of Maryland, all in USA, and INPE.

REFERENCES

Abramo, L. R. W., Sodré Jr., L., Wuensche, C. A. *Anomalies in the low CMB multipoles and extended foregrounds*. Physical Review D, 74, 083515, 2006.

Abramo, L. R. W.; et al. *Alignment Tests for low CMB multipoles*. Physical Review D, 74, id. 063506, 2006.

Andrade, A. P. A., Wuensche, C. A., Ribeiro, A.L.B.. *Correlated mixture between adiaba tic and isocurvature fluctuations and recent CMB observations*. Physical Review D, 71, 043501, 2005.

Andrade, A. P.; Wuensche, C. A.; Ribeiro, A.L.B. *Contribution of a mixed mixture model to the anisotropies of the CMBR*. The Astrophysical Journal, 602, pp. 555, 2004.

Andrade, A.P.A.; Ribeiro, A.L.B.; Wuensche, C.A. *The Peak-Peak Correlation Function in Nearly-Gaussian Models*. Astronomy and Astrophysics, 457, pp.385-391, 2006.

Bennett, C. et al. *First year Wilkinson Microwave Anisotropy Probe (WMAP) observations: preliminary maps and basic results*. The Astrophysical Journal Supplement Series, 148, 1, 2003.

Bernui, A. *The large-scale angular correlations in CMB temperature maps*. Brazilian Journal of Physics, vol. 35, p.1185-1190, 2005.

Bernui, A. et al. *On the cosmic microwave background large-scale angular correlations.* Astronomy and Astrophysics, 454, 409-414, 2006.

Bernui, A.; Tsallis, C.; Villela, T. *Temperature fluctuations of the cosmic microwave background radiation: A case of non-extensivity?*Physics Letters A, 356, 426 - 430, 2006.

Bernui, A.; Tsallis, C.; Villela, T. *Deviation from Gaussianity in the cosmic microwave background temperature fluctuations*. Europhysics Letters, 78, 19001, 2007.

Bernui, A.; Ferreira, I.S.; Wuensche, C.A. *On the Large-Scale Angular Distribution of Short Gamma-Ray Bursts*. The Astrophysical Journal Letters, 673, 968-971, 2008.

Childers, J. et al. *The Background Emission Anisotropy Scanning Telescope (BEAST): Instrument Description and Performance*. The Astrophysical Journal Supplement Series, 158, 124-138, 2005.

Clapp, A. C. et al. *Measurements of anisotropy in the cosmic microwave background radiation at degree angular scales near the stars Sigma Herculis and Iota Draconis*. The Astrophysical Journal Letters, 433, L57-L60, 1994.

Devlin, M. et al. *Measurements of anisotropy in the cosmic microwave background radiation at 0.5 deg angular scales near the star Gamma Ursae Minoris.* The Astrophysical Journal Letters, 430, L1-L4, 1994.

Ferreira, I. S. *Polarização da Emissão Síncrotron da Galáxia: Instrumentação e Medidas.* PhD Thesis, 2008.

Figueiredo, N. et al. *The optical design of the Background Emission Anisotropy Scanning Telescope*. The Astrophysical Journal Supplement Series, 158, 118-123, 2005.

Gundersen, J. O.; et al. A degree scale anisotropy measurement of the cosmic microwave background near the star Gamma Ursae Minoris. The Astrophysical Journal Letters, 413, L1-L5, 1993.

Gundersen, J. O. et al. *Degree-scale anisotropy in the cosmic microwave background: SP94 results*. The Astrophysical Journal Letters, 443, L57-L60, 1995.

Haslam, C. G. T. et al. *A 408 MHz all-sky continuum survey. II - The atlas of contour maps*. Astronomy and Astrophysics Supplement Series, 47, p. 1, 2, 4-51, 53-142, 1982

Hinshaw, G. et al. *Three-Year Wilkinson Microwave Anisotropy Probe (WMAP) Observations: Temperature Analysis*. The Astrophysical Journal Supplement Series, 170, 288-334, 2007.

,Jonas, J.L.; Baart, E.E.; Nicolson, G.D. *The Rhodes/HartRAO 2326-MHz radio continuum survey*. Monthly Notices of the Royal Astronomical Society, 297, 977-989, 1998.

Leonardi, R., et al. *The Cosmic Foreground Explorer: a balloon-borne microwave polarimeter to characterize large-scale CMB polarized foregrounds*. New Astronomy Reviews, 50, pags. 977-983, 2006.

Levy, A.; et al.*The White Mountain Polarimeter Telescope and an Upper Limit on Cosmic Microwave Background Polarization*. The Astrophysical Journal Supplement Series, 177, 419-430, 2008.

Lim, M. et al. T*he Second Measurement of Anistropy in the Cosmic Microwave Background Radiation at 05 Scales near the Star MU Pegasi*. The Astrophysical Journal Letters, v.469, p.L69, 1996

Lubin, P. et al. *A map of the cosmic background radiation at 3 millimeters*. The Astrophysical Journal Letters, vol. 298, L1-L5, 1985.

Lubin, P.; Villela, T. *Measurements of the Cosmic Background Radiation*, in "Galaxies Distances and Deviations from Universal Expansion", Eds. B.F. Madore and R.B. Tully, Reidel, vol. 180, 169-175, 1986.

Marvil, J.;.et al. *An astronomical site survey of the barcroft facility at the white mountain research station*. New Astronomy, 11, pp. 218-225, 2006.

Meinhold, P.; et al. *Measurements of the anisotropy of the cosmic background radiation at 0.5 deg scale near the star MU Pegasi*. The Astrophysical Journal Letters, 409, L1-L4, 1993

Meinhold, P. et al. *The advanced cosmic microwave explorer - A millimeter-wave telescope and stabilized platform*. The Astrophysical Journal, vol. 406, p. 12-25, 1993

Meinhold, Peter; et al.*A Map of the Cosmic Microwave Background from the BEAST experiment*. The Astrophysical Journal Supplement Series, 158, 101-108, 2005.

Mejia, J.; et al. *Galactic foreground contribution to the BEAST CMB Anisotropy Maps*. The Astrophysical Journal Supplement Series, 158, 109-117, 2005.

O´Dwier, I., et al. *The angular power spectrum of the BEAST experiment*. The Astrophysical Journal Supplement Series, 158, pp. 93-100, 2005.

Reich, P.; Reich, W. *A radio continuum survey of the northern sky at 1420 MHz - II*. Astronomy and Astrophysics Supplement Series, vol. 63, no. 2, p. 205-288, 1986.

Schuster, J. et al. *Cosmic background radiation anisotropies at degree scales: further results from the South Pole*. The Astrophysical Journal Letters, 412, L47-L50, 1993.

Staren, J., et al. *A Spin Modulated Telescope to Make Two Dimensional CMB Maps*. The Astrophysical Journal, 539, 52-56, 2000.

Souza, R. R. *Um mapa da emissão galáctica em 408 MHz*. M.Sc. Dissertation, INPE, 2000

Tanaka, S. et al. *Measurements of Anisotropy in the Cosmic Microwave Background Radiation at 0 degrees -8.5 Scales near the Stars HR 5127 and Phi Herculis*. The Astrophysical Journal Letters, v.468, p.L81, 1996

Tegmark, M. et al. *Cosmic Microwave Background Maps from the HACME Experiment.* The Astrophysical Journal, 541, 535-541, 2000.

Tello, C. *Um experimento para medir o brilho total do céu em comprimentos de onda centimétricos*. PhD Thesis, 1997.

Tello, C.; et al. *Diffraction analysis of a double-shielded antenna in the Fraunhofer and Fresnel regimes: Model predictions.* Radio Science, 34, p. 575-586, 1999

Tello, C.; et al. *Spillover and diffraction sidelobe contamination in a double-shielded experiment for mapping Galactic synchrotron emission*. Astronomy and Astrophysics Supplement, 145, p.495-508, 2000

Tello, C.; et al. *The 2.3 GHz continuum survey of the GEM project*. arXiv e-print: astro-ph/0712.3141, 2007.

Torres, S. et al. *The GEM project: An international collaboration to survey galactic* radia*tion emission.* Astrophysics and Space Science, 240, 225 - 234, 1996.

Wright, E.L. et al. *Interpretation of the cosmic microwave background radiation anisotropy detected by the COBE Differential Microwave Radiometer*. The Astrophysical Journal Letters, vol. 396, L13-L18, 1992.

Wuensche, C. A.; Lubin, P. M.; Villela, T. *An Alternative Algorithm for Cosmic Microwave Background Radiation Sky Harmonic Analysis*. Astronomical Data Analysis Software and Systems III, A.S.P. Conference Series, Vol. 61, p. 269, 1994.

SESSION 5 - SPACE WEATHER

THE FIRST LANDMARK OF THE BRAZILIAN SPACE WEATHER PROGRAM

H. Takahashi, Antônio L. Padilha, Hanumant S. Sawant, Joaquim E. R. Costa, José R. Cecatto, Walter D. Gonzalez, Eurico de Paula, Icaro Vitorello, Haroldo de Campos Velho, José D. S. da Silva, M. A. Abdu, Odim Mendes Jr, Alisson D. Lago, Clésio M. D. Nardin, N. SantAnna, Maria V. Alves, Jonas R. Souza

Instituto de Pesquisas Espaciais - INPE
Av. dos Astronautas,1758 – 12201-970, São José dos Campos-SP, Brasil

ABSTRACT

The Brazilian Space weather program started at INPE in 2007 under support of Ministry of Science and Technology. Main purpose of the program is to monitor the space climate and weather, from sun, interplanetary space, magnetosphere and ionosphere-atmosphere by satellite and ground based observations, and to provide useful information to space related communities, technological, industrial and academic areas. It is aimed to monitor sun-earth environment physical parameters: the solar radiation and CME event by using radio telescope (BSS, BDA and SPUA), interplanetary environment by muon cosmic ray telescope, equatorial ionosphere scintillation occurrence by GPS receiver net work and ground induced current (GIC) variability by magnetometer net work. Data transmission via internet, construction of data bank system, data assimilation and modeling for future forecasting service and space weather daily bulletin services are under development. Our goal is to establish the whole system to be in operation in 2011.

INTRODUCTION AND OBJECTIVES

A space weather and climate program is being initiated at the Brazilian National Institute for Space Research (INPE) to study events from their initiation on the sun to their impacts on the earth, including their effects on space-based and ground-based technological systems. The program is built on existing capabilities at INPE, which include scientists with a long tradition and excellence in the observation, analysis and modeling of solar and solar-terrestrial phenomena and an array of geophysical instruments that spans all over Brazil from the north to south of the magnetic dip equator. Available sensors include solar radio frequency receivers and telescopes, optical instruments and solar imagers, GNSS receivers, ionosondes, VHF radars, all-sky imagers, magnetometers and cosmic ray detectors.

In the equatorial region, ionosphere and thermosphere constitute a coupled system with electrodynamical and plasma physical processes being responsible for a variety of peculiar phenomena. The most important of them are the equatorial electrojet current system and its instabilities, the equatorial ionization anomaly, and the plasma instabilities/irregularities of the night-time ionosphere (associated with the plasma bubble events). In addition, space weather events modify

the equatorial ionosphere in a complex form and up to now unpredictable manner. Consequently, a main focus of the program will be on monitoring the low, middle and upper atmosphere phenomena and developing a predictive model of the equatorial ionosphere through data assimilation, that could help to mitigate against the deleterious effects on radio communications and navigation systems.

The technological, economic and social importance of such activities was recognized by the Brazilian government and a proposal for funding was approved for the period 2008-2011. New ground instruments will be installed during this period allowing us to extend our current capability to provide space weather observations, accurate forecasts of space weather conditions, and timely hazard alert warnings. The program is expected to be fully operational for the peak activity of the next solar maximum in 2011-2012.

ACTIVITY PLAN IN PRIORITY

The program will take three frontiers, Group 1 covers data collection of Sun-interplanetary space and magnetosphere, Group 2 covers data collection of ionosphere upper atmosphere and geomagnetic field, and Group 3 works on generation of data bank, simulation model and to operate information center. The group 1 is responsible for generation of real time data of the solar radio frequency radiation map, CME event, cosmic ray (muon) variability, in addition to the satellite data (SOHO, ACE, STEREO). The group 2 will take responsibility for real time ionospheric scintillation map, equatorial anomaly map, and plasma bubble activity map. The group 3 collects all of these data and to construct a data center, data assimilation and simulation model operation. Daily publication of bulletin through website is also a task of this group.

Solar CME and Solar wind monitoring

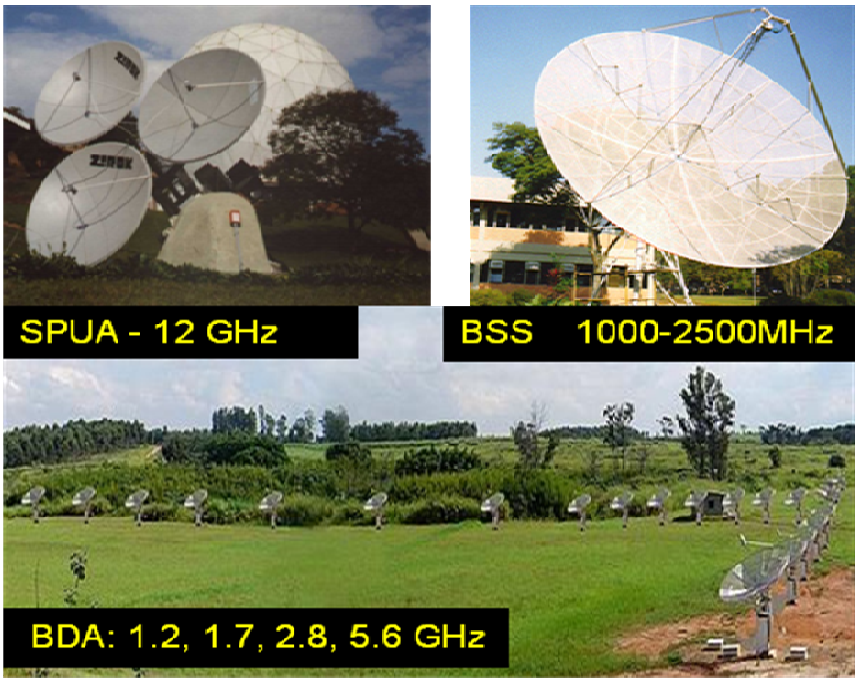

Fig. 1 - Solar radio telescopes for Space weather and climate mission of INPE.

Solar CME event will be monitored by several different type of radio telescope in operation at Itapetinga and in fure at Cachoeira Paulista. SPUA observes the solar surface with 12 GHz frequency. BSS covers 1.0 – 2.5 GHz radiation. BDA(Brazilian decimetric array) antennas map the solar surface with 1.2, 1.7, 2.8, 5.6 GHz frequencies. It will be capable to localize the radiation source region in the solar disc, which is important to predict CME event in the direction of the earth (Sawant et al., 2009). Figure 1 shows BDA, BSS and SPUA antenna view.

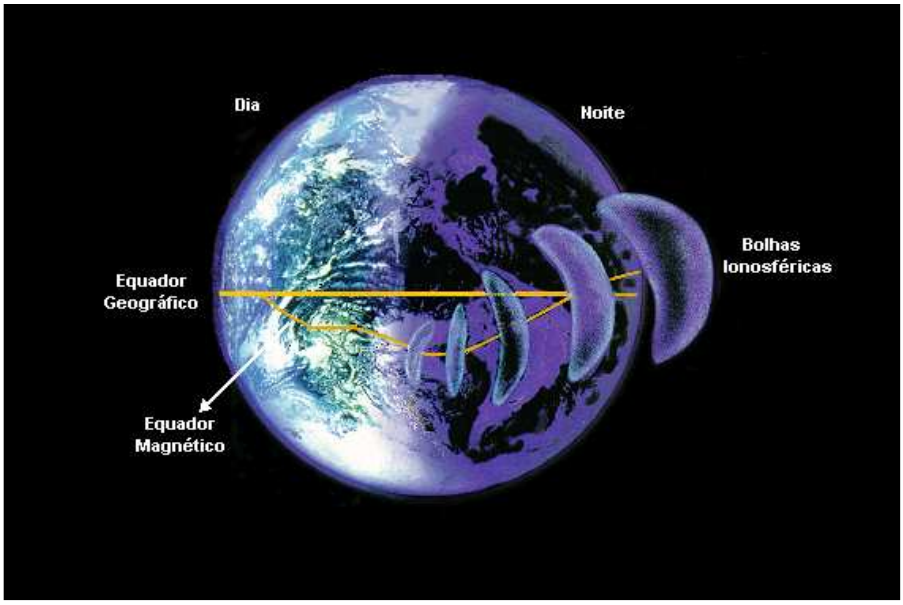

Fig. 2 - Ionospheric plasma bubble generation mechanism in the equatorial region.

Cosmic ray monitoring by muon detector at São Matino da Serra (30°W, 50°W) will be enable us to monitor interplanetary environment. An Increase or decrease of the cosmic ray flux near the earth environment indicates variability of solar flux and CME event (Okazaki et al., 2008).

Equatorial Ionosphere monitoring

In the equatorial and low latitude region, there are regional ionospheric phenomena, equatorial ionospheric (Appleton) anomaly and ionospheric irregularities (plasma bubbles). In Figure 2 generation of the plasma bubble in the local evening side is shown. The ionospheric disturbance causes radio wave scintillation that affects satellite to ground communication and GPS satellite applications. Figure 3 shows scintillation area caused by the plasma bubble activity. Today it is well known that the equatorial ionospheric disturbances are caused by magnetospheric origin from top and also by meteorological activity from below (Abdu et al., 2009).

The present program focuses the subject to ionospheric scintillation effect as the first step. GPS receiver net work deployed in the equatorial region maps the scintillation area. In addition to it, a couple of ionosonde, GPS receiver and magnetometer will be installed at magnetic conjugate points away from the magnetic equator, one at Boa Vista and the other at Campo Grande. The two observation sites monitor ionospheric F-layer uplifting and to predict occurrence of plasma bubbles.

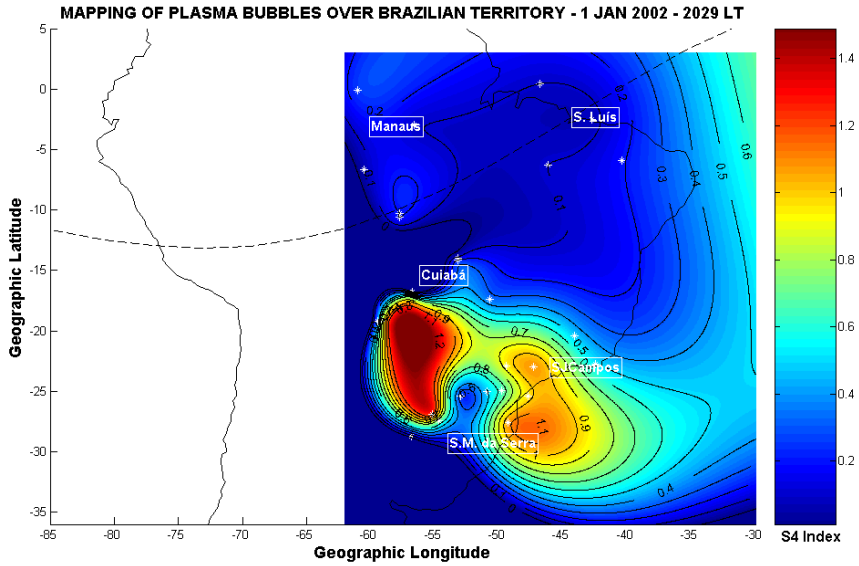

Fig. 3 - Ionospheric scintillation map generated by ground based GPS receiver network.

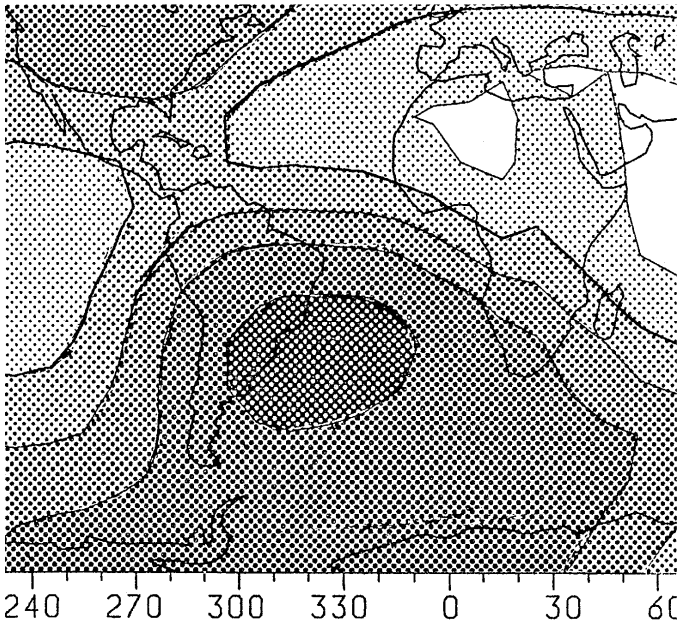

Fig. 4 - Energetic particle precipitation map (in gray scale) in the south Atlantic and American continent region observed by satellite OHZORA (Kohno et al., 1990).

Geomagnetic storm and the South American Geomagnetic Anomaly (SAGA)

The effect of solar flare and solar wind (mass and velocity) are severe in the earth's polar regions. Also important is the region of South American magnetic anomaly region where the magnetic

field is almost a half compared to the other regions. Due to the lower mirror height, energetic particle flux penetrates in the ionosphere. Figure 4 shows particle flux in the SAGA region observed by satellite (Kohno et al., 1990). An increase of malfunction of the satellite in this region has been reported by several previous works. Therefore information of the energetic particle flux is important for satellite operation. The present program plans to provide the magnetic storm information to Brazilian satellite operation center.

BRAZILIAN SPACE WEATHER PROGRAM IN 2008 - 2011

The present program is aimed to create a center for investigation and prediction of the space weather and climate, and to provide the information to space related human activities. Our special interest is, however, rather regional focusing our mission in the equatorial ionosphere weather condition and South American Geomagnetic Anomaly (SAGA) effect.

The space weather and climate program plans to establish following items during the period of 4 years from 2008 to 2011:

(1) To establish a space weather and climate center, and to publish daily bulletin of the space weather information,
(2) To establish ground based space weather monitoring stations, GPS receiver net work, magnetometer net work, ionospheric sounder network, Solar radio frequency telescopes and cosmic ray telescopes.
(3) To establish data bank system for space weather related data from ground-based and satellites.
(4) To establish ionosphere weather map and solar radio frequency radiation map.

ACKNOWLEDGEMENTS

The Space weather and climate program is supported by Ministry of Science and Technology of Brazil. One of the authors thanks to CNPq who supported the present project under contract 301876/2007-0.

REFERENCES

Abdu, M. A., Kherani, E. A., Batista, I. S., de Paula, E. R., Fritts, D. C., Sobral, J. H. A., *Ann. Goephys.*, in press, 2009.

Kohno, T., Munakata, K., Nagata, K., *Planet. Space Sci*,. 38(4): 483-490, 1990.

Okazaki, Y., Fushishita, A. Narumi, T., Kato, C., Yasue, S., Kuwabara, T., Bieber, J.W., Evenson, P., Da Silva, M.R., Dal Lago, A., Schuch, N., Fijii, Z., Duldig, M.L., Humble, J.E., Sabbah, I., Kota, J., Munakata, K., *ApJ*, 681, 693-707, 2008.

Sawant, H. S., Cecatto, J. R., Meszarosova, H., Faria, C., Fernandes, F. C. R., Karlicky, M., Andrade, M. C., *Adv. Space Res*., DOI: 10.1016/j.asr.2009.03.019, 2009.

Proceedings of the Brazilian Decimetric Array Workshop
São José dos Campos, Brazil - July 28 – August 1, 2008

PRELIMINARY RESULTS WITH NEURAL NETWORK FOR DATA ASSIMILATION TO THE SPACE WEATHER

Haroldo F. de Campos Velho[1] and Fabrício P. Härter[2]

[1]*Laboratory for Computing and Applied Mathematics (LAC)*
National Institute for Space Research (INPE) – São José dos Campos-SP, Brazil
(haroldo@lac.inpe.br)
[2]*National Institute of Meteorology (INMet)*
(fabricio.harter@inmet.gov.br)

ABSTRACT

Data assimilation is an essential step for improving space weather operational forecasting by means of an appropriated combination between observational data and data from a mathematical model. In the present work data assimilation methods based on Kalman filter and artificial neural networks are applied to a three-wave model of auroral radio emissions. A novel data assimilation method is presented, whereby a multilayer perceptron neural network is trained to emulate a Kalman filter for data assimilation by using cross validation. The results obtained render support for the use of neural networks as an assimilation technique for space weather prediction.

INTRODUCTION

Space weather research is the study of the disturbances in the space environment, usually caused by the solar activity and/or interactions of interstellar medium and galactic cosmic rays with the heliosphere. Due to the potential impact of space weather on technological systems on Earth, as well as on human health, space weather forecasting is today an essential task. Nonlinear and chaotic phenomena represented by mathematical models have an intrinsic relationship with the initial conditions (IC). Therefore, from very small discrepancies between two similar ICs, after some time-steps, a disagreement could occur for some systems. In other words, sensitive dependence on the IC could cause the forecasting error to grow exponentially fast with the integration time (Grebogi et al., 1987).

This implies that a better representation for the initial condition will produce a better prediction. The problem for estimating the initial condition is so complex and important for operational prediction system, which it constitutes a science called *Data Assimilation* (Daley, 1993; Kalnay, 2003). Nowadays data assimilation is a research topic in some of the areas of applied physics, such as meteorology, oceanography, and ionospheric weather (for last issue see: Schunk et al., 2004; Scherliess et al., 2004; Hajj et al., 2004).

Many methods have been developed for data assimilation. They have different strategies to combine numerical forecasting and observations, using Kalman filter or variational approaches, for example.

The use of artificial neural network (ANN) for data assimilation is a very recent issue.

The first implementation of the ANNs as a new approach for data assimilation was employed by Nowosad et al. (2000). There are applications in chaotic systems, as well as 1D shallow water equations. An artificial neural network is an arrangement of units characterized by a large number of very simple neuron-like processing units; a large number of weighted connections between the units, where the knowledge of a network is stored; and highly parallel distributed control. Two distinct phases can be devised while using an ANN: the training phase (learning process) and the run phase (activation). The training phase consists of an iterative process for adjusting the weights for the best performance of the network in establishing the mapping of many input/target vector pairs. Once trained, the weights are fixed and new inputs can be presented to the network, which calculates the corresponding outputs based on what had been learned.

In the worked example here, a multilayer Perceptron neural network (MLP-NN) (Haykin, 1994; Nowosad et al.,2000) is trained to emulate a Kalman filter-based data assimilation system. This novel data assimilation strategy is applied to a three-wave model of auroral radio emissions near the electron plasma frequency involving resonant interactions of Langmuir, Alfvén and whistler waves (Chian et al., 1994; Lopes and Chian et al., 2002). Observational evidence of auroral radio emission and nonlinear coupling between Langmuir, Alfvén and whistler waves have been obtained in rocket experiments in the Earth's auroral plasmas (Boehm et al., 1990). These auroral whistler waves may explain the leaked AKR (auroral kilometric radiation), providing the radio signatures of solar-terrestrial connection, and may be used for monitoring space weather from the ground.

Data assimilation is a specialized field of data analysis. The amount of data available today, with the observation system enhancing in quality and quantitative, becomes data analysis a challenge for the science of this new century. Actually, many people are addressing such challenge as *data science*.

NONLINEAR COUPLED WAVE EQUATIONS

A nonlinear analysis of auroral Langmuir, whistler and Alfvén (LAW) events in the planetary magnetosphere was carried out by Lopes and Chian (1996), under the assumption that all three interacting waves are linearly damped. The simplest model for describing the temporal dynamics of resonant nonlinear coupling of three waves can be obtained assuming terms in the wave amplitudes. Moreover, the waves may be assumed monochromatic, with the electric fields $E_\alpha(x,t)$ written in the form: $E_\alpha(x,t) = \left[A_\alpha(x,t)/2\right]\exp\{i(k_\alpha x - \omega_\alpha t)\}$, where $\alpha = 1,2,3$ and the time scale of the nonlinear interactions is much longer than the periods of the linear (uncoupled) waves.

In order for three-wave interactions to occur, the wave frequencies ω_α and wave vectors k_α must satisfy the resonant conditions: (i) $\omega_3 \approx \omega_1 - \omega_2$; (ii) $k_3 \approx k_1 - k_2$. Under these circumstances, the nonlinear temporal dynamics of the system can be governed by the following set of three first-order autonomous differential equations written in terms of the complex slowly varying wave amplitude (Meunier et al., 1982):

$$\frac{dA_1}{d\tau} = \nu_1 A_1 + A_2 A_3 \tag{1a}$$

$$\frac{dA_2}{d\tau} = i\delta A_2 + \bar{\nu}_2 A_2 - A_1 A_3^* \tag{1b}$$

$$\frac{dA_3}{d\tau} = \bar{v}_3 A_3 - A_1 A_2^* \qquad (1b)$$

where the variable $\tau = \chi t$, with χ is a characteristic frequency; $\delta = (\omega_1 - \omega_2 - \omega_3)/\chi$ is the normalized linear frequency mismatch, and $\bar{v}_\alpha = v_\alpha / \chi$ gives the linear wave behaviors on the long time scale. The wave A_1 is assumed linearly unstable ($v_1 > 0$) and the other two waves, A_2 and A_3, are linearly damped ($\bar{v}_2 = \bar{v}_3 \equiv -v < 0$), and it is set $\chi = v_1$ (Meunier et al., 1982; Lopes and Chian, 1996). The system admits both periodic and chaotic waves. Figure 1 shows the strange attractor.

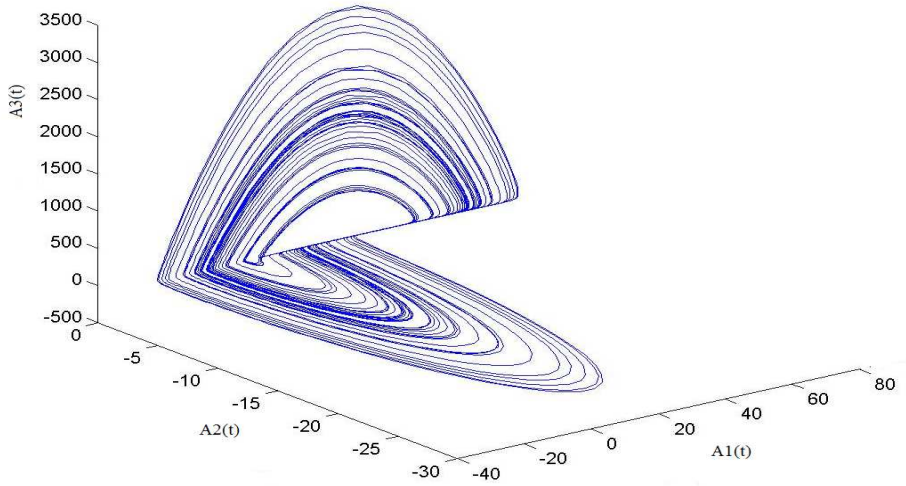

Fig. 1 - The strange attractor for the three-waves: Eqs. (1a)–(1c).

DATA ASSIMILATION EXPERIMENT

Process is illustrated using synthetic experimental data, where synthetic observations are generated by addition of random small level noise on the exact value: $A_\alpha^{Obs}(t_n) = A_\alpha(t_n) + \lambda r_n$, where $\lambda = 10^{-5}$, and r_n is a random value at time t_n. Figure 2 shows observed data inserted after each 5 time-steps on the mathematical model data without any assimilation technique under chaotic regime. The black and blue lines represent the reference model ("model") and the dynamical system evolution after the data insertion ("corrupted model"), respectively. Clearly, it is noted that the dynamics of the system is lost, even with a small difference in the IC.

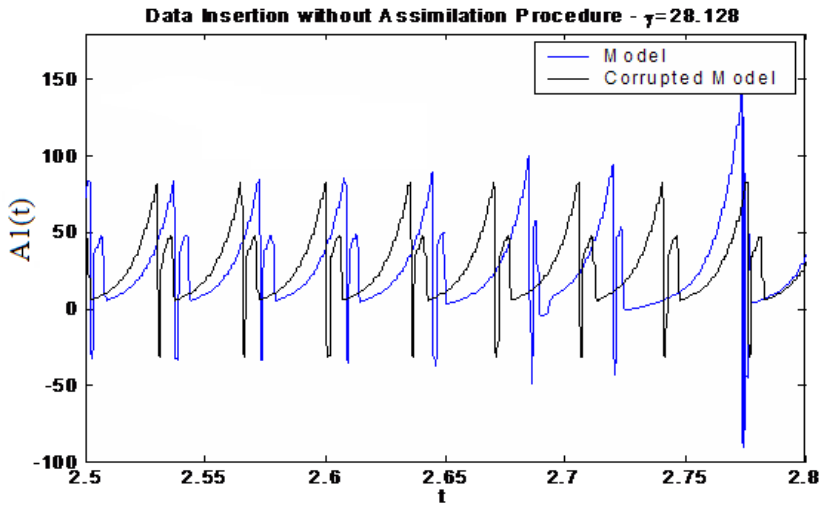

Fig. 2 - Data insertion without assimilation technique with frequency of $5\Delta t$.

Here, the assimilation process will perform by two methods: Kalman filter and neural networks. Denoting the vector $Z^o=[A_1 \quad A_2 \quad A_3]^T$ for the observed data, the extended Kalman filter can be summarized as:

1. Forecasting: $Z_{n+1}^f = F\left(Z_n^f\right)+\mu_n$
2. Evaluation by observation system: $Z_{n+1}^f = H\left(Z_n^f\right)+\nu_n$;
3. Compute the covariance error matrix: $P_{n+1}^f = F_n P_n^a F_n^{-1} + Q_n$;
4. Kalman gain (G): $G_{n+1} = P_{n+1}^f H_n^T \left[R_n + H_n P_{n+1}^f H_n^T\right]^{-1}$;
5. Analysis: $Z_{n+1}^a = Z_{n+1}^f + G_{n+1}[Z_{n+1}^o - H(Z_{n+1}^f)]$;
6. Up date the error covariance matrix: $P_{n+1}^a = \left[I - G_{n+1}H_n\right]P_{n+1}^f$.

The mathematical model is represented by $F(.)$, μ_n is the stochastic forcing (random modeling noise error) and its covariance matrix is expressed by Q_n. The observation system is modeled by operator (or just a matrix, for linear systems) H_n, and ν_n is the noise associated to the observation (covariance matrix denoted by R_n). The typical Gaussian probability density function and zero-mean hypotheses for the noises are adopted. For non-linear dynamical systems, the extended Kalman filter is used (the operator $F(.)$ is expanded into Taylor series, and only linear expansion components are considered). One problem for this approach is to estimate the matrix Q_n. Jazswinski (1970) has proposed an adaptive Kalman filter, where the matrix Q_n is parameterized with these parameters estimated by a secondary Kalman filter. We have applied the Jazswinski's proposal to the data assimilation with good results (Nowosad et al., 2000). The goal here is to design an artificial neural network for emulating a Kalman filter, reducing the computational effort of the assimilation process.

The assimilation procedure using neural network is a non-linear mapping between analysis and data from observation and prediction model:

$$Z^{a}_{n+1} = f_{NN,W}\left[Z^{o}_{n+1}, Z^{f}_{n+1}\right] \tag{2}$$

where $f_{NN,W}$ is the neural network, and W is the matrix of the connection weights. A multilayer perceptron neural network (MLP-NN) was trained with the backpropagation algorithms (Haykin, 1994). The training or learning process is a procedure to identify the best values for the matrix W: the output from the neural network should similar a previous analysis – more details see Härter and Campos Velho (2008a), for a higher dimension system see Härter and Campos Velho (2008b). This target analysis could be the observation, or other acceptable analysis obtained by other method. We follow the second option, and the neural network is designed to emulate the analysis from the Kalman filter.

Numerical example

For simplicity, we assume that all error covariance matrices are diagonal ones. The numerical values for these are given as following:

$$Q_n = 0.1I; \quad R_n = 2I; \quad P_0^f = \begin{cases} 10Z_0^f & (i = j) \\ 0 & (i \neq j) \end{cases}. \tag{3}$$

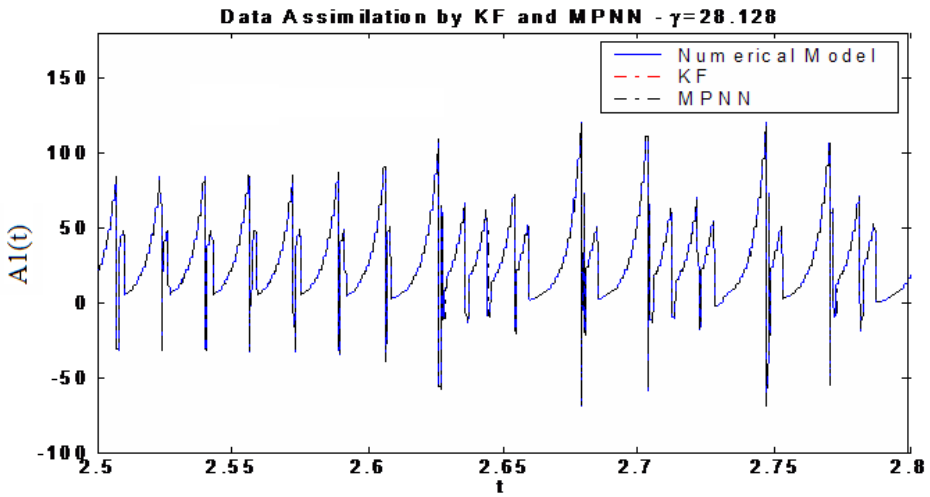

Fig. 3 - Data assimilation using Kalman filter and neural.

The three-wave system is integrated using a fourth-order Runge Kutta scheme, with $\Delta t = 10^{-2}$. After the choice of the best weight set, the 3-wave system is integrated considering data assimilation at each 5 time-steps. Figure 3 depicts the last 10^3 time-steps of a time series of A_α: it is not possible to distinguish the true dynamics, and assimilation obtained with Kalman filter and neural network.

The MLP-NN and KF are effective to carry out the assimilation. Figure 4 shows the mean errors of KF and MLP-NN. Small errors are verified for both schemes.

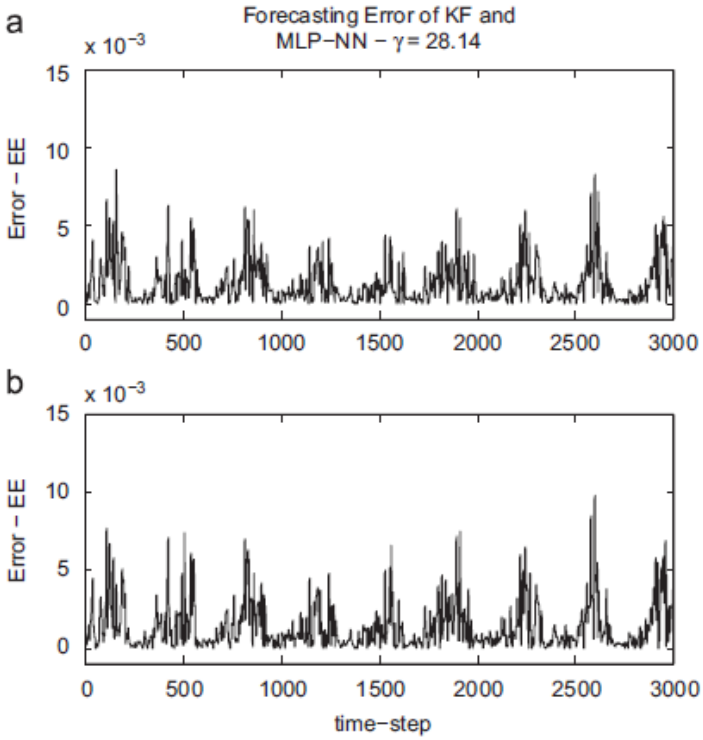

Fig. 4 - Error for data assimilation: (a) Kalman filter, (b) neural network.

REFERENCES

Boehm, M. H., Carlson, C. W., McFadden, J. P., Clemmons, J. H., Mozer, F. S., *Journal of Geophysical Research*, 95, 12157-12171, 1990.

Chian, A. C. -L., Lopes, S. R., Alves, M. V., *Astron. Astrophy.s*, 290, L13-L16, 1994.

Daley, R., *Atmospheric Data Analysis*, Cambridge University Press, 1991.

Garner, T. W., Wolf, R. A., Spiro, R. W., Thomsen, M. F., *Journal of Geophysical Research*, 104, 25145-25152, 1999.

Grebogi, C., Ott, E., Yorke, J. A., *Science*, 238, 585-718, 1987.

Guo, J. S., Shang, S. P., Shi, J. K., Zhang, M. L., Luo, X. G., Zheng, H., *Space Science Reviews*, 107, 229-250, 2003.

Hajj, G. A., Wilson, B. D., Wang, C., Pi, X., Rosen, I. G., *Radio Science*, 1, RS1S05, 2004.

Härter, F. P., Rempel, E. L., Campos Velho, H. F., Chian, A., *Journal of Atmospheric and Solar-Terrestrial Physics*, 70, 1243-1250, 2008.

Härter, F. P., Campos Velho, H. F., *Applied Mathematical Modelling*, 32, 2621-2633, 2008.

Haykin, S., *Neural Networks: A Comprehensive Foundation*. Mcmillan, 1994.

Jazswinski, A. H., *Stochastic Processes and Filtering Theory*. Academic Press, 1970.

Kalnay, E., *Atmospheric Modeling, Data Assimilation and Predictability*, Cambridge University Press, 2002.

Lopes, S. L., Chian, A.C.-L., *Astronomy and Astrophysics*, 305, 669-676, 1996.

Meunier, C., Bussac, M. N., Laval, G., *Physica*, D4, 236-243, 1982.

Nowosad, A. G., Rios Neto, A., Campos Velho, H. F., *Hybrid Methods in Engineering*, 2(3), 291-310, 2000.

Scherliess, L., Schunk, R. W., Sojka, J. J., Thompson, D. C., *Radio Science*, 1, RS1S04, 2004.

Schunk, R. W., Scherliess, L., Sojka, J. J., Thompson, D. C., Anderson, D. N., Codrescu, M., Minter, C., Fuller-Rowell, T. J., Heelis, R. A., Hairston, M., Howe, B. M., *Radio Science*, 1, RS1S02, 2004.

AUTHOR INDEX